Republic of Iraq

Ministry of Higher Education and Scientific Research

University of Technology

Machines and equipment Engineering Department

Enhancement of Film Cooling Performance by Using Ramped- Holes Injection

A Thesis Submitted to the
Machines and Equipment Engineering Department
University of Technology
in partial fulfillment of the requirements for the degree of Doctor of Philosophy in Mechanical Engineering

BY

Falah Fakher Hatem AL-Jabery
(B.Sc. 1981, M.Sc. 1987)

Supervised by

Prof. Dr. Assim H. Yousif AL-Darajee

Assit. Prof. Dr. Kutaeba J. AL-Khishali

January 2014 **ربيع الأول 1435**

BAGHDAD - IRAQ

(الرَّحْمَنُ (١) عَلَّمَ الْقُرْآن (٢) خَلَقَ الإِنسَانَ (٣) عَلَّمَهُ الْبَيَانَ (٤)
الشَّمْسُ وَالْقَمَرُ بِحُسْبَانٍ (٥) وَالنَّجْمُ وَالشَّجَرُ يَسْجُدَان (٦)
وَالسَّمَاءَ رَفَعَهَا وَوَضَعَ الْمِيزَانَ (٧) الا تطغوا في الْمِيزَانَ (٨))

صدق الله العلي العظيم
(سورة الرحمن)

Linguistic Certification

I certify that this thesis entitled: **"*Enhancement of Film Cooling Performance by Using Ramped-Holes Injection*",** was prepared by "***Falah Fakher Hatem AL-Jabery***" under my linguistic supervision. Its language was amended to meet the English style.

Dr. Samir Ali Amin
Assist. Professor

Name: **Dr. Samir A. Amin**

Title: **Linguistic Supervisor (Asst. Prof.)**

Date: 2 / 2 / 2014

Supervisors Certification

We certify that the preparation of this thesis entitled "***Enhancement of Film Cooling Performance by Using Ramped-Holes Injection***" was prepared by "***Falah Fakher Hatem AL-Jabery***" under our supervision in the Machines and equipment Engineering Department of the University of Technology in a partial fulfillment of the requirements for the degree of Doctor of Philosophy in Mechanical Engineering.

Signature:
Name: **Dr. Assim H. AL-Darajee**
Title: Prof.
Date: 3 / 4/2014

Signature:
Name: **Dr. Kutaeba J. AL-Khishali**
Title: Asst. Prof.
Date: 2 / 2 /2014

EXAMINATION COMMITEE CIRTIFICATE

We, the examining committee, certify that we have read this thesis entitled ***"Enhancement of Film Cooling Performance by Using Ramped-Holes Injection"*** and we have examined the student ***"Falah Fakher Hatem Al-Jabery"*** in its contents and in what is related to it, and that in our opinion, its adequate as a thesis for the Degree of Doctor of Philosophy in Mechanical Engineering.

Signature:
Name: Dr. **Sabah T. Ahmed**
Prof.-Member
Date: 2/ 2/2014

Signature:
Name: Dr. **Mohammed I. Mohsin**
Assist. Prof.-Member
Date: 2/ 2/2014

Signature:
Name: Dr. **Fouad A. Saleh**
Assist. Prof.-Member
Date: 2/2 /2014

Signature:
Name: Dr. **Karima E. Amori**
Assist. Prof.-Member
Date: 2/ 2/2014

Signature:
Name: Dr. **Assim. H. Yousif**
Prof.- Supervisor
Date: 3 / 2 /2014

Signature:
Name: Dr.**Kutaeba J. Al-khishali**
Assist. Prof.-Supervisor
Date: 2 / 2/2014

Signature
Name: Dr. **Ihsan Y. Hussain**
Prof.-Chairman
Date: 5 /2 /2014

Approved by the Machines and Equipment Engineering Department

Signature:
Name: Dr. **Jafar M. Hassan**
Prof.-Dean of Machines and Equipment Engineering Department
Date: / /2014

Dedication

TO THE SPIRIT OF MY FATHER

TO MY MOTHER

TO MY BELOVED FAMILY

MY WIFE,

ESLAM,

HASSAN,

ALI,

MARWA,

SHAMS,

AND

MOHAMMED

I DEDICATE THIS WORK

Falah

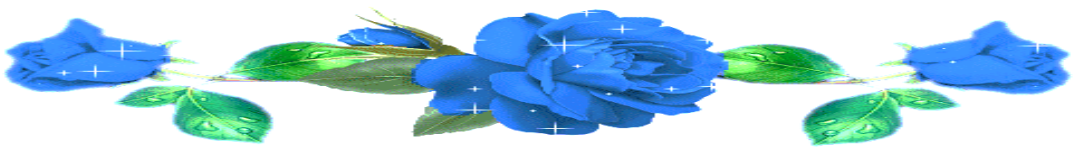

Acknowledgement

First and foremost, praise is to GOD who has sustained me throughout this work and for all the blessings bestowed upon me. This study would not have been done without the help of ALLAH and then many people.

I would like to express my deepest thanks and sincere gratitude to my supervisors **Prof. Dr. Assim H. AL-Darajee** and **Asst. prof. Dr. Kutaeba J. AL-Khishali.,** for their assistance, guidance, encouragement and endless help throughout the steps of this work.

My sincere thanks and great appreciation are also expressed to the former department dean **Prof. Dr. Sabah T. Ahmed, Prof. Dr. Abdulhassan A. Karamallah**, **Dr. Moayed R. Hassan, Dr. Amer AL-Dabagh, Dr. Muwafaq S. Alwan, Dr. Haider Sabah, Sinan Abdalghafar, Humam K. Jalghaf, Zainab Hassan,** and all my friends for their assistance in providing me with all experimental facilities.

I would like also to submit my thanks to all staff members of the Mechanical Engineering Department.

Gratitude is extended to those whom contributed in one way or another in the preparation of this effort.

Falah Al-jabery

Abstract

The effect of introducing ramps with cylindrical and conical holes on the film cooling performance has been investigated numerically and experimentally in the present study. A computational fluid dynamic code **(FLUENT)** has been used to predict the flow behavior at the ramped-holes regionand create simulation that mimicked the experiments. Six models with different holes arrangements of ramped-holes are introduced in the experimental test program; these models are selected depending upon the numerical simulation analysis. One of these models, which is a single row of cylindrical holes, works as a baseline model. For all three cylindrical hole models, the diameter of the cylindrical hole is 4mm, and the hole length to diameter ratio is 3.5 with a central pitch distance between each two neighboring holes of 4D. Three conical hole models consist a one row holes of 4 mm diameter at inlet, diverged by 6^{o} to the exit, and the forward injection angle (θ) is 35^{o} for all models. The heat transfer coefficient and heat flux ratio are determined experimentally by using a single test transient IR thermography technique. The study is performed at a single Reynolds number of 5100 based on mainstream velocity and hole diameter at three different blowing ratios of 0.5, 1.0 and 1.5.

The present experimental results of the baseline model are well in agreement with previous experimental results at blowing ratios of 0.5 and 1. The numerical approach verification of the current CFD is made by comparison with present experimental results, it is fair to say that the CFD results shows approximately similar trend and behaviour with slight difference in local adiabatic film cooling effectiveness levels.

The experimental results showed that the adiabatic film cooling effectiveness is greatly enhanced when introducing ramps. The distribution of spanwise averaged film cooling effectiveness along the x-axis exhibited that the double ramped-holes model provides promising film cooling performance, particularly at blowing ratios of 1 and 1.5. For all ramped-holes models, the heat transfer coefficient ratio and the heat flux ratio are slightly increased. The adiabatic film cooling effectiveness for single-ramped cylindrical hole model improved by 40.2%, 175.8%, and 234.9% over that of standard cylindrical hole model, while for double-ramped cylindrical hole model, it is enhanced by 45.3%, 185.8%, and 369% more than that of standard cylindrical hole model for blowing ratios of 0.5,1 and 1.5, respectively. Regarding to the single-ramped conical hole model , the improvement of adiabatic film cooling effectiveness is 134%, 292.6%, and 554.6% over that of standard cylindrical hole model, whereas the double-ramped conical hole model enhanced the adiabatic film cooling effectiveness by 130.3%, 343.7%, and 679.4% more than that of standard cylindrical hole model for blowing ratios of 0.5,1, and 1.5, respectively. The ramped-conical holes models show a promising solution to enhance the film cooling effectiveness, particularly for the gas turbine combustor film cooling.

Table of Contents

Nomenclature

Latin Characters		
Character	**Description**	**Units**
C	Constants	-
D	Film hole diameter	m
h	Heat transfer coefficient with film cooling	$W/m^2.K$
h_d	Hydraulic diameter	m
h_o	Heat transfer coefficient without film cooling	$W/m^2.K$
$\bar{h}/h_o$	Spanwise averaged heat transfer coefficient ratio	-
K	Thermal conductivity	W/m.K
k	Turbulent kinetic energy	m^2/s^2
q	Heat flux to the surface with film cooling	W/m^2
$\bar{q}/q_o$	Spanwise averaged heat flux ratio	-
$\bar{\bar{q}}/q_o$	Total area-averaged heat flux ratio	-
S	Spanwise hole spacing	m
T	Temperature	^oC
t	Time	s
U	velocity	m/s
X/D	Normalized streamwise distance	-
x	coordinate of streamwise	-
y	coordinate normal to surface	-
z	coordinate of spanwise	-
Greek Symbols		
Character	**Description**	**Units**
β	Distance between the backward-facing ramp step and the row of film-cooling holes	m
γ	Ramp angle	Degree
ε	Dissipation rate of turbulent kinetic energy	m^2/s^3
η	Film cooling effectiveness	-
$\bar{\eta}$	Spanwise averaged film cooling effectiveness	-
$\bar{\eta}_c$	Streamwise averaged film cooling effectiveness	-
$\bar{\bar{\eta}}$	Total area-averaged film cooling effectiveness	-
θ	Injection angle	Degree
μ	Viscosity of air	$N.s/m^2$
ϑ	Kinematic viscosity	m^2/s
ρ	Density	kg/m^3

Ø	Overall film cooling effectiveness	-
ω	Specific dissipation rate	1/s
Superscripts		
+	Parameter scaled with viscous length or time scale	-
subscripts		
aw	Adiabatic wall	-
c	Coolant air	-
f	Film	-
i	Initial	-
m	Mainstream hot air	-
w	Wall	-
Abbreviations		
BR	Blowing ratio ($BR = \frac{\rho_c u_c}{\rho_m u_m}$)	-
CFD	Computational Fluid Dynamic	-
DR	Density ratio ($DR = \frac{\rho_c}{\rho_m}$)	-
CVP	Counter Rotating Vortex Pair	-
TBC	Thermal Barrier Coatings	-

Chapter One

Introduction

Chapter One
Introduction

1.1 General

A gas turbine is an engine designed to convert the energy of the fuel into some form of useful power, such as mechanical power or high-speed thrust of a jet. Today, the gas turbine is widely used, and it has been developed into a very reliable, versatile engine with a high power to weight ratio. It is used exclusively to power all new military and commercial aircraft by one form or another of a gas turbine, also gas turbine has been widely used to power gas plants, boats, trains, trucks, cars, and many other applications. The basis gas turbine engine and its components are shown in figure (1-1) [1], the cycle consists of a compressor where air is compressed adiabatically, a combustion chamber where the fuel is burned with air, resulting in the maximum cycle temperature, the combustion products then expand adiabatically in the turbine. From a thermodynamics cycle analysis, it is found that the thermal efficiency and specific power of gas turbines can be improved by increasing the turbine inlet temperature (maximum cycle temperature); however, a major problem associated in achieving the performance improvement of a gas turbine unit is the availability of materials that withstand such high temperatures and combined stresses. One solution has been the use of turbine cooling which allowed the turbine designer to increase the turbine inlet temperature while maintaining a constant material temperature.

Turbine cooling was considered in German designs in 1935, with concentrated efforts during World War II [1]. The development of turbine maximum temperature over the past 50 years is shown in figure (1-2), improvements in parts materials have allowed an increase of melting point

around 200°C, and the use of turbine cooling has allowed an increase of approximately another 250°C, which allows the turbine inlet temperature above the melting points of the materials used [2]. Raising the turbine inlet temperature can significantly increase the performance of a gas turbine engine. The performance of a gas turbine engine is usually measured in terms of overall efficiency, specific thrust, and specific fuel consumption. It is clear from figure (1-3) that the increase in turbine inlet temperature increases specific thrust [3].

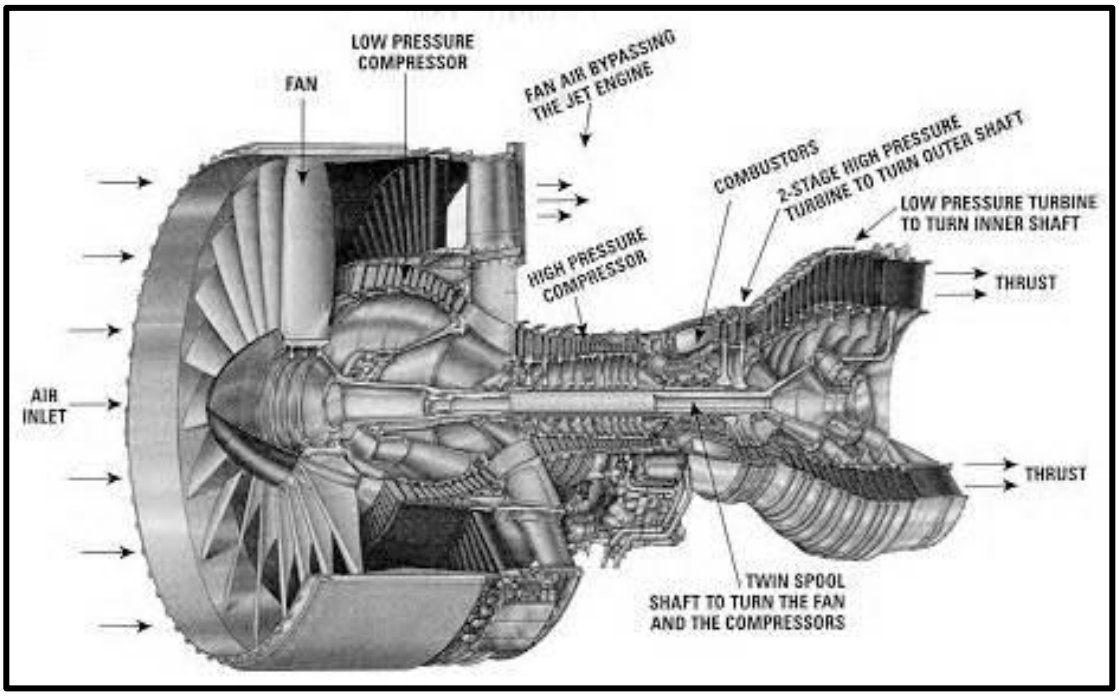

Figure (1-1): Components of gas turbine engine [2]

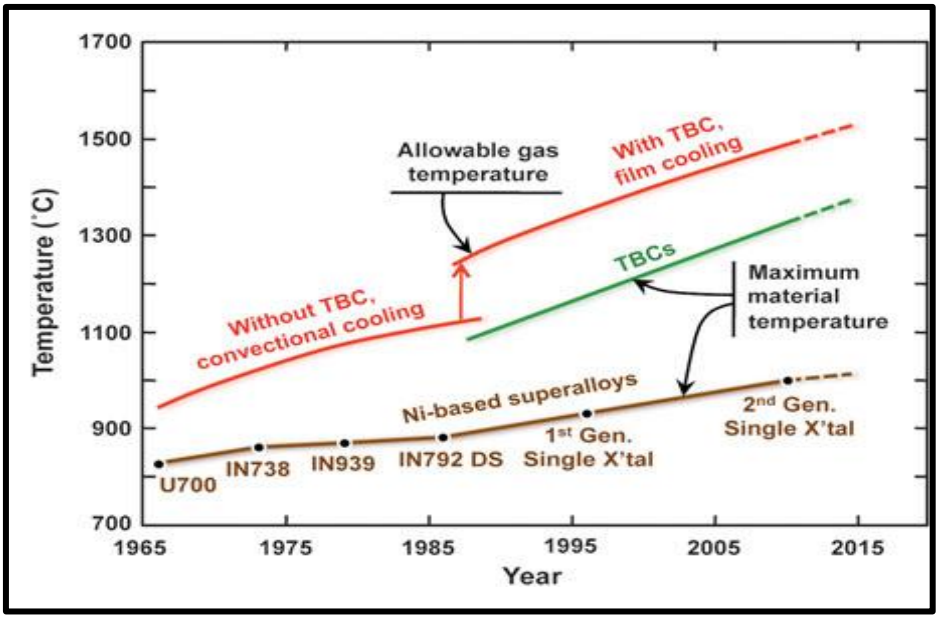

Figure (1-2): Development of turbine maximum temperature over the past 50 years [4]

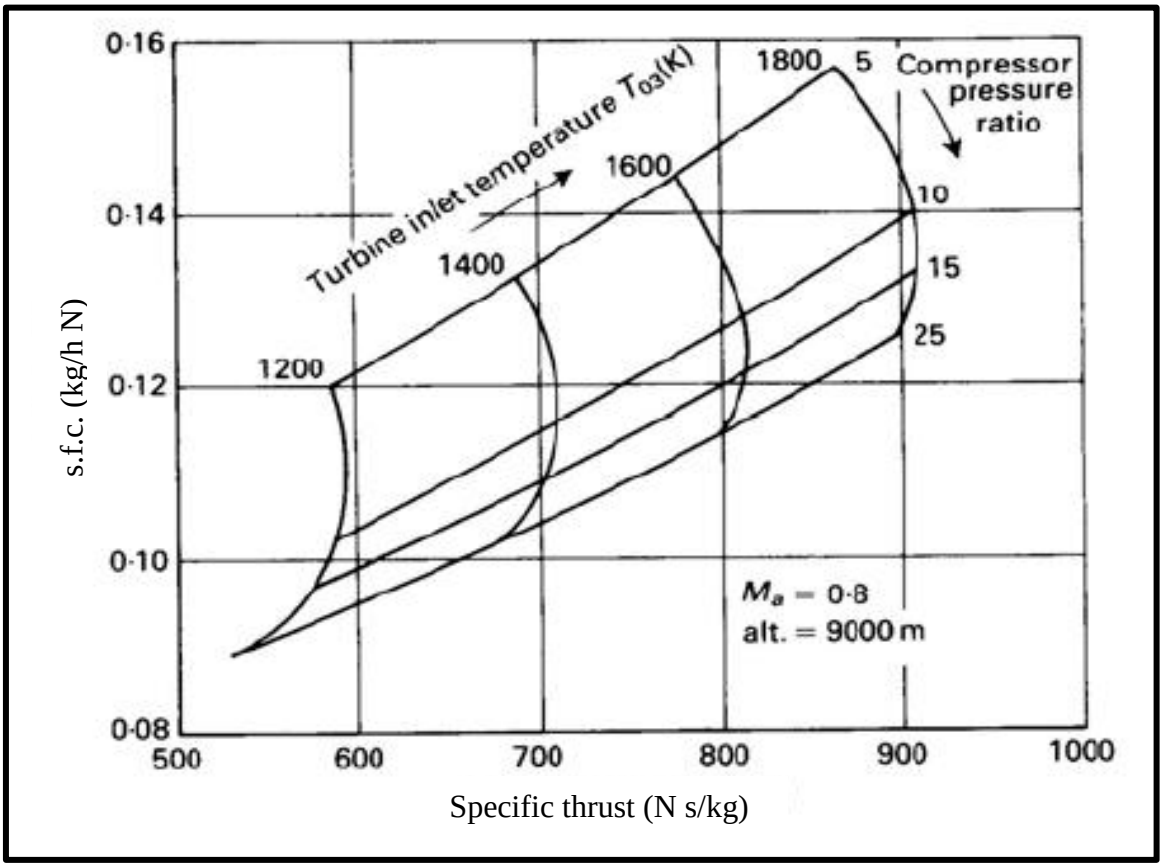

Figure (1-3): Typical turbo-jet cycle performance [3]

1.2 Gas Turbine Cooling Techniques

Air (from compressor) is the main coolant that has been used with surfaces exposed to high-temperature gas streams. The surfaces cooling can be classified as, internal and external cooling; internal cooling involves convection and impingement cooling methods. The external cooling involves film and transpiration cooling method. The comparison of these cooling techniques is shown in figure (1-4).

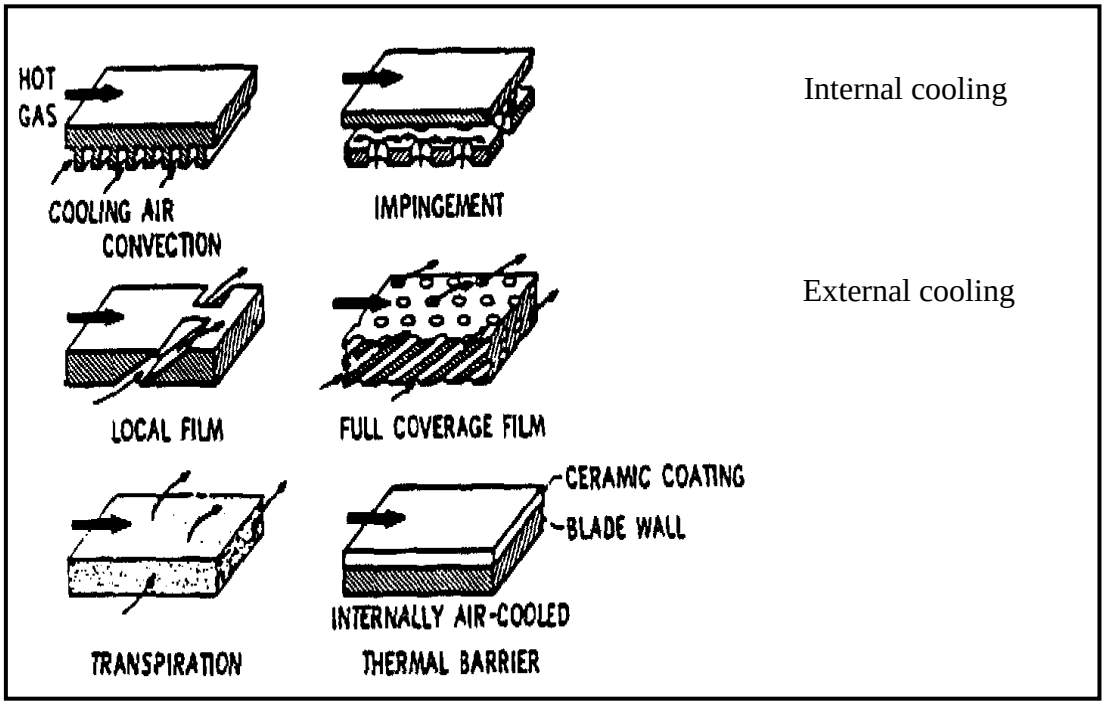

Figure (1-4): Internal and external cooling systems [5]

1.3 Cooling Strategies: Film Cooling

Film cooling is a technique used in many systems to protect the component surfaces exposed to high-temperature gas streams. Applications have been widespread, particularly in gas turbines, where combustor liners, turbine shrouds, blades and other hot parts of the engine have used air bled off from the compressor outlet as the coolant film. Such techniques reduce

the thermal stresses that tend to occur with an increase of inlet temperature to the first-stage turbine of high-performance gas turbine systems.

Film cooling involves the injection of a secondary fluid (air) into the boundary layer of the primary fluid (hot gas mainstream) at one or more discrete location along a surface exposed to high-temperature gas streams to protect that surface not only in the immediate region injection, but also in the downstream region. Film cooling protects the surface directly by formation of a relatively cool insulation film of cooled air as compared to internal cooling, where surface is cooled by extracting heat by convection. Film cooling is more effective than internal cooling, because the cooling air absorbs energy as it passes inside the body and through the holes, and then further reduces the body temperature by reducing the amount of heat energy transferred from the gases to the surface material [5]. The injection of the coolant air into the boundary layer causes mainly pressure losses which tend to reduce some of advantages of using higher turbine inlet temperature, also if too much air is injected into boundary layer or the velocity is too high, the cooling air may penetrate the boundary layer defeating the purpose of using film cooling. If holes are placed too close together, stress concentrations, which could be detrimental to engine performance and reliability, may occur. On the other hand, a large number of small holes are required in the body, because the cooling effect of film is quickly dissipated by downstream mixing of the film air with mainstream hot gases and the heating of the film air by the hot gases. Film cooling research on flat surface is common, flat surface models can be used to study the effects of individual parameters with relative ease and less expensive. The effects of geometric parameters (hole geometry shape, size and spacing of the holes) and flow parameters (blowing

ratio, density ratio, mainstream Reynolds number ...etc.) have been also studied on flat surfaces.

1.3.1 Film Cooling Performance

The performance of film cooling is usually characterized by the non-dimensional adiabatic wall temperature (effectiveness) and heat transfer coefficient. The heat transfer coefficient, (h), and the adiabatic wall temperature, (T_{aw}), are the two parameters that define the performance of a particular film cooling configuration. While (h) is a function of the fluid mechanics of the film cooling configuration, T_{aw} is also dependent on the temperature of the coolant and mainstream flows, and is intermediate between them. In order to remove the temperature dependence, the dimensionless adiabatic wall temperature, called the adiabatic film cooling effectiveness, is defined [6]:

$$\eta = \frac{T_m - T_{aw}}{T_m - T_c} \tag{1-1}$$

Where: T_m is the mainstream temperature.

T_c is the coolant temperature.

The value of (η) varies from unity, at the point of injection, to zero at large downstream distances.

Heat transfer coefficient can be described using some important variables. In general, convective heat transfer is described by:

$$q = h(T_{aw} - T_m) \tag{1-2}$$

The first of the important variables in this equation is the heat transfer coefficient (h). The heat transfer coefficient is for the most part dictated by the external flow field. (h) is a factor that relates the driving

temperature difference, ($T_{aw} - T_m$), to absorbed heat flux energy (q). In order to keep surface temperatures low, it is the best interest of the turbine designer to attempt to minimize heat transfer coefficient (h). In general, the injection of film cooling changes the fluid flow profile around the surface and usually increases the heat transfer coefficient. This increase in (h) is undesirable as it promotes heat transfer from the hot mainstream flow, and good designs of film cooling should attempt to minimize this increase. Obviously, an understanding of exactly how film coolant schemes affect the heat transfer coefficient is important. While the introduction of film cooling has the effect of increasing (h) slightly, the technique's advantage is realized by a large decrease of the adiabatic wall temperature (T_{aw}).

In general, the film cooling performance is a function of many parameters in an engine environment. The most influential parameters can be grouped into two categories:

1- Cooling geometry which includes:

a) Hole geometry and its position, orientation, and inclination angle.
b) Tabs, struts or vortex generators in each hole.
c) Creating a trench or crater about holes.
d) Upstream geometry modification by using ramps to modify the approaching boundary layer flow, and its interaction will the film cooling jets.

2- Aerodynamics which includes:

a) Local freestream Mach number, M_a.
b) Freestream turbulence.
c) Film cooling momentum ratio.
d) The film cooling blowing or mass flux ratio (BR).
e) Film cooling density ratio (DR).

1.4 Strategies to Control the Formation of Kidney Vortices

The studies in the field of interaction between coolant jet from inclined holes and the mainstream flow show formation of kidney vortices, i.e., a counter rotating vortices pairs (CVP) [7]. Figure (1-5) shows the formation of the (CVP); these vortices are detrimental to film cooling, because it brings about two undesirable effects. Firstly, the hot mainstream air is forced to enter beneath the jet, thus heating the wall surface. Secondly, the mutual interaction between the vortex pair tends to lift the jet off the wall surface which diminishes the film cooling. The formation of these counter rotating vortices is dictated by the shear layer between the mainstream flow and the coolant jet and not due to the viscous wall effect in the film cooling hole or plenum. The lateral expansion of the conical or shaped holes exit produces two major benefits [8], the first is that each counter rotating vortex tends to remain near the edge of the hole, so increasing the width of the hole exit increases the distance between the pairs, hence decreasing the interaction and delaying the jet lift off. In addition to this, a properly shaped hole will generate a pair of anti-kidney vortices which are opposite to the kidney vortices vortices in the sense of rotation. These two pair cancels each other and prevents the jet from lifting off.

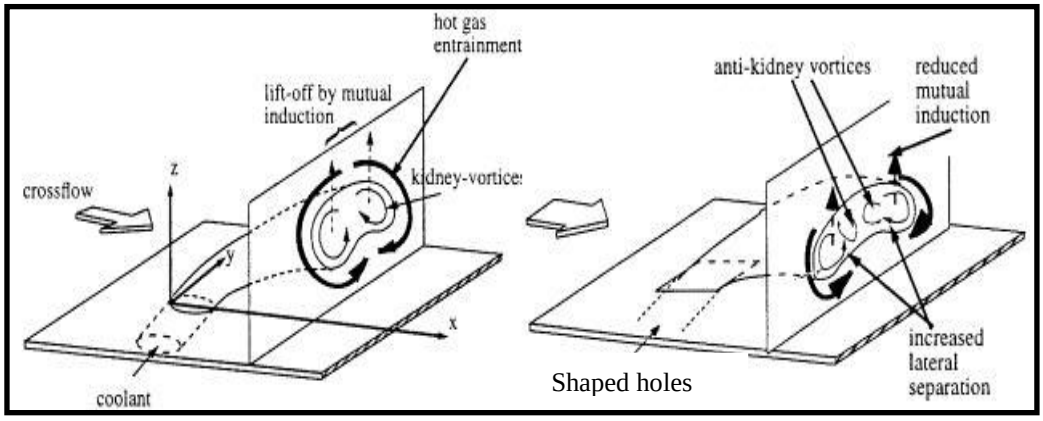

Figure (1-5) Kidney and anti-kidney shaped vortices and the advantages of shaped holes

1.5 Thesis Objectives

This work is a numerical and experimental investigation of some parameters affecting the film cooling thermal performance of ramped-holes. The effect of using double ramped-hole on the film cooling performance has been experimentally investigated for the first time.

The objectives of this work are to predict the film cooling performance for different novel combinations models. This goal is to be accomplished through the following steps:

1- Caring out a numerical simulation for a baseline model and the novel combinations of ramped-holes (cylindrical and conical) models, in order to determine the jet-mainstream interactions and for better understanding these interactions and the deformation and strength of vortices to investigate the effects of using ramped-hole on the adiabatic film cooling effectiveness before choosing suitable models for experimental work. It will be done through simulations of the governing equations which include the continuity, momentum, and energy equations and the transport equations for the turbulent kinetic energy, and dissipation, these equations will be solved numerically by using the package FLUENT version (12.1).

2- Experimental work will provide an evaluation of the film cooling effectiveness, heat transfer coefficient ratios, and heat flux ratios for five selective models in addition to baseline model (cylindrical hole without ramp) in order to compare the film cooling performance of the novel combinations models with the baseline model.

3- Analysis and discussion of results for final conclusions and recommendations.

Chapter Two

Literature Survey

Chapter Two
Literature Survey

Flat surface is commonly used in film cooling researches. Flat surface models can be used to study the effects of individual parameters with relative ease and are less expensive. Studies have proved that the results obtained on simple flat surface models can be applied to real engine designs with slight corrections [9]. The effects of geometrical parameters, like hole geometry, shape, size and spacing of the holes and flow parameters, like coolant to mainstream blowing ratio, temperature ratio, mainstream Reynolds number, velocity, etc. have been studied on flat surfaces. Also, the effects of pressure gradient and curved surface have also been studied. Some studies have focused only on the film cooling effectiveness results, and others have presented both film cooling effectiveness and heat transfer coefficient variation.

2.1 Experimental Work

Experiments done at the University of Minnesota by **Goldstein et al. (1970) [10]** are some of the most basic flat plate discrete hole film cooling experiments. These experiments were performed on both a single coolant hole and one row of coolant holes with flat plate geometry. Also, these experiments were performed at low speeds rather than at high speeds which are more representative of an engine environment. The thrust of their research was to vary the injection angles and blowing ratios to investigate the film cooling effectiveness. These experiments generally showed that the cooling effectiveness was optimized for the hole inclined at 35^{o} to the streamwise direction, and that the centreline effectiveness decayed monotonically with distance from the coolant hole. Also, this study showed that at a blowing ratio of approximately 0.5, the centreline

cooling effectiveness reached a maximum value. The researchers suggested the decline of effectiveness at higher blowing ratios was due to the coolant film lifting off the surface and allowing the hot stream to penetrate to the surface.

Goldstein et al. (1974) [11] studied the effect of the use of shaped injection hole for improving the film cooling performance. They used a 10^o spanwise diffused hole and found that the shaped hole provide better film cooling characteristics than the cylindrical hole, because the reduced momentum of the jet attenuated coolant lift-off from the blade surface, and thus less penetration of the coolant into the mainstream.

Brown and Saluja (1978) [12] measured the film cooling effectiveness on a flat plate in a wind tunnel. Tests were done using a single cylindrical hole and, in three cases, a row of cylindrical holes. The holes were inclined at an angle of 30° from the test surface, and pitch-to-diameter ratios of 8.0, 5.33, and 2.67 were used. It was found that as the pitch was decreased, the spanwise-averaged film cooling effectiveness increased. Also, the maximum effectiveness was found to occur at a blowing ratio of around 0.5 for all cases. Finally, it was found that the free-stream turbulence had the effect of decreasing the film cooling effectiveness.

Foster and Lampard (1980) [13] presented spanwise-averaged film cooling effectiveness results over a flat plat with 35^o, 55^o and 90^o streamwise angles for long injection tubes spaced 3-diameters apart. They used foreign gas injection to simulate a density ratio of 2.0. They, however, measured only the film cooling effectiveness at blowing ratios of 0.5 and 1.4, they suggested that the film cooling effectiveness is independent of the density ratio.

Makki and Jakubowski (1986) [14] presented the downstream heat transfer results for a film hole with a trapezoidal shaped expansion.

They showed that the shaped film hole consistently provided better heat transfer characteristics than simple cylindrical holes with the same metering section. Also, they reported that the shaped holes offered up to 23% better film cooling performance than the corresponding cylindrical hole.

Honami et al. (1994) [15] described the behaviour of the injected jet over a flat surface with 90^o orientation angle holes. They measured streamwise mean velocity, boundary layer temperature fields, and effectiveness distributions using liquid crystal. Their results showed that the 90^o orientation angle injection formed an asymmetric structure with a large-scale vortex motion on one side caused by the interaction with the mainstream. In addition, they concluded that the asymmetry was promoted with increased mass flux ratio, resulting in low film cooling effectiveness.

Sen et al. (1996) [16] and Schmidt et al. (1996) [17] presented two companion papers, in which the effect of adding a 15° forward diffusion exit to a streamwise oriented hole was investigated. They found that the exit diffused film hole demonstrated better spread of adiabatic film cooling effectiveness than the cylindrical counterpart. From the heat transfer coefficient standpoint, the forward expanded hole performed poorly, presumably because of the increased interaction between the jet and mainstream.

Kohli and Bogard (1997) [18] examined the film cooling effectiveness of the shaped holes on a flat plate using 35^o and 55^o injection angles, the result showed that the shaped holes with a large injection angle had better cooling performance than cylindrical holes. They also reported on the thermal and velocity fields in the region around the injection holes**.**

Ekkad et al. (1997) [19] provided the film cooling effectiveness results for two different density ratios. The adopted orientation angles

were 0^o, 45^o, and 90^o using the transient liquid crystal technique, they reported that the compound angle injection produced higher film effectiveness than the simple angle injection for both density ratios. They concluded that the highest film cooling effectiveness was obtained at a blowing ratio of 1.0 for compound angle injection.

In Sung Jung and **Joon Sik Lee (2000) [20]** studied experimentally the effect of orientation angles and velocity ratios of a cylindrical hole on the boundary layer temperature distribution and film cooling effectiveness. The results showed that the increased lateral momentum in the case of large orientation angle injection strongly affected boundary layer temperature distribution.

Baldauf et al. (2001) [21] conducted experiments to measure film cooling effectiveness on a flat plate with a single row of cylindrical film cooling holes in a wind tunnel for different values of blowing ratio, injection angle, pitch, density ratio, and turbulence intensity. A correction for the test plate, not being perfectly adiabatic, was made using FEA. It was found that the overall effectiveness was optimized for a blowing ratio of 1.0. At steep injection angles, the coolant jet separated from the test plate surface earlier. For small pitches, there was more interaction between the adjacent jets, which caused them to merge earlier. The surface effectiveness was optimized at lower blowing ratios for lower values of density ratio. Finally, it was observed that increasing the turbulence also increased the interaction between the coolant and the hot gas, resulting in less extension of the effect of the coolant in the streamwise direction.

Takahashi et al. (2001) [22] performed experiments on a flat plate with a single row of film cooling holes. Measurements of the film cooling effectiveness were taken for seven different types of holes. It was found that since the film cooling jet through the cylindrical hole did not

spread out over the downstream portion of the wall, the film cooling effectiveness of the cylindrical holes was lower than that of the rectangular holes having the same width. For rectangular holes, the highest film cooling effectiveness was seen for the widest slot. The optimum mass flux ratio which gives the highest effectiveness increased to 1.0 as the hole geometry approached a "slit". Finally, they showed that the films cooling jets through the oval holes adhered to the wall better and spread out earlier than those through the rectangular slots and were thus more effective.

Lee et al. (2002) [23] investigated the flow visualization and film cooling effectiveness used a round shaped holes with compound angle orientations on a flat plate. The shaped holes have a 15^{o} forward expansion with a fixed inclination angle of 35^{o}. The orientation angles are 0^{o}, 30^{o}, and 60^{o}, and the blowing ratios are 0.5, 1.0, and 2.0. Flow in the injectant exit plane was visualized using oil aerosol particles, and the adiabatic film cooling effectiveness was measured using the thermochromic liquid crystal technique. They concluded that the shaped holes with simple angle injection did not provide substantial improvement in the film cooling performance compared to cylindrical holes. However, shaped holes with compound angle injection exhibit improved film cooling effectiveness up to 55% in comparison with round hole data at high blowing ratios.

Yu et al. (2003) [24] conducted transient liquid crystal experiments to measure the film cooling effectiveness and heat transfer coefficients on a film-cooled flat plate. Three different types of cooling holes were tested: 30° cylindrical hole (Shape A), 30° cylindrical hole with 10° forward diffusion (Shape B), and 30° cylindrical hole with 10° forward diffusion and 10° lateral diffusion (Shape C). Blowing ratios of 0.5 and 1.0 were used. The results showed that Shape (C) gave 30-50%

improvement in the film cooling effectiveness over Shape (A). Shape (B) also gave improvement, but the results were closer to those of Shape (A) than those of Shape (C). Flow visualization showed significant lift-off of the coolant from the wall for Shapes (A) and (B), whereas the coolant out of Shape (C) flowed much closer to the wall.

Rhee et al. (2003) [25] conducted an experimental study to investigate the film cooling effectiveness for one, two, and three rows of four different types of film cooling holes: two sizes of cylindrical holes, a rectangular hole, and a rectangular hole with an expanded exit. For multiple rows of holes, the coolant injected through upstream rows prevented the downstream coolant from lifting off and prevented entrainment of main flow into the coolant, increasing the film cooling effectiveness downstream. For cylindrical holes, local peak values were observed due to separation and reattachment of the coolant. Due to the Coanda effect, the coolant flow through the rectangular holes spreaded widely and sticked close to the surface, resulting in higher effectiveness than for the cylindrical hole case. The rectangular holes with expanded exits resulted in film cooling effectiveness similar to that of slot film cooling. For three rows of holes, the hole type was seen to have less effect on the film cooling effectiveness.

Yuen and Botas (2003) [26] presented an experimental investigation of film cooling effectiveness for a cylindrical hole with a streamwise angle of 30º, 60º and 90º, in a flat plate test facility with zero pressure gradient. The free-stream Reynolds number based on the free-stream velocity and hole diameter was 8563, a hole length of L/D=4 was used, and the blowing ratio was varied from 0.33 to 2. The wide band crystals of temperature with a steady-state heat transfer method were used to obtain the film cooling effectiveness. For a single 30° hole, in the region immediately downstream of the hole the maximum effectiveness

occurred for a blowing ratio less than 0.5. Downstream of this immediate region, centreline effectiveness and lateral spread increased up to a blowing ratio of 0.5, then decreased with increasing blowing ratio due to jet penetration into the free stream. Also, the region with film cooling effectiveness greater than 0.2 did not extend beyond an X/D of 13.

Hasan et al. (2003) [27] investigate experimentally the effect of discrete triangular-shaped tabs with different orientations on the film cooling performance from a row of cylindrical holes inclined at 35^{o} along the streamwise direction. The taps were located along the upstream edge of the holes, three blowing ratios were tested. The results showed that the tabs oriented downwards provide the highest film cooling effectiveness at a blowing ratio of 0.56 while the tabs oriented horizontally provided the highest film cooling effectiveness at blowing ratios of 1.13 and 1.7. The higher film cooling effectiveness with the tabs was due to the generation of secondary eddies counter-rotating with respect to the kidney pair; these eddies reduced the jet penetration and thus increased film cooling effectiveness.

Barigozzi et al. (2007) [28] investigated experimentally the effect of using an upstream ramp on discrete hole film cooling. The analysis was carried out on a flat plate model, using both a cylindrical and fan-shaped hole configuration. To compare different cooling schemes, a combined aero-thermal analysis was performed. Tests have been carried out at low speed and low inlet turbulence intensity level, with blowing ratios varied in the range 0.3–1.0, the upstream ramp provided a moderate improvement in the case of cylindrical holes, as it allows the coolant to diffuse someway, before interacting with the mainstream, but it produced also a significant increase of aerodynamic losses. The fan shaped hole geometry without the ramp resulted to be the best solution, as it provides a

coolant injection with a good lateral spreading and a low turbulence level (low blowing ratio).

Mohamad and Mansoor (2011) [29] investigated experimentally the film cooling performance of cylindrical holes, cylindrical holes embedded in transverse trench and semi-cylindrical holes. The adiabatic film cooling effectiveness was determined on a flat plate downstream of a row of inclined geometries; the hot wire anemometer has been used for velocity measurements and thermocouple for temperature measurements. It was observed that at low turbulence intensity (low blowing ratio), the trench shape showed better results but for higher values, the angled trench shape is much better. Also, up to X/D=8, the performance is highly favorable.

Shuping et al. (2011) [30] presented an experimental study on a concept for enhancing the film cooling performance by placing an upstream ramp in front of a row of cylindrical film cooling holes. Parameters studied include upstream ramp angle (8.5°, 15°, and 24°) and blowing ratio of (0.3, 0.4, 0.6, 0.9, and 1.4). The results indicated that the film cooling characteristics in the region downstream of the film cooling holes are sensitive to the combination of ramp angle (height) and blowing ratio. In general, a large ramp angle with a high blowing ratio leads to more effective film protection.

Yousif et al. (2013) [31] investigated experimentally the film cooling performance for two rows of staggered holes with opposite orientation angles on a flat plate by using a single test transient IR thermograph technique at different blowing ratios. The attitude of the downstream row holes was fixed at inclination angle of 30° and orientation angle of zero, while the upstream row holes was fixed with opposite orientation angle of 180° and the inclination angles were changed three times as (20°, 30°, and 40°). Three different blowing ratios

(0.5, 1.0, and 1.5) were used in experimental program at each case. Enhancements were observed, in which as the blowing ratio increased and the inclination angle of upstream row decreased, the film cooling effectiveness and heat transfer coefficient were increased.

2.2 Numerical and Experimental Work

Hyams et al. (1996) [32] studied the effects of slot jet shaping on the heat transfer downstream of a slot jet. They found that shaping of the slot inlet and exit provided significant gains in the film cooling performance due to the suppression of separation at the slot inlet, and a spreading of the region over which the leeward side of the jet must accelerate at the hole exit, reducing the turbulence and shear stress in this region. These designs are not applicable to blade and vane film cooling, because of the lack of structural strength.

Hyung et al. (2001) [33] conducted a study to investigate experimentally and numerically film cooling performance around a conical-shaped film cooling hole with compound angle orientations. The result showed that the shaped holes reduced the penetration of jet, and more uniform cooling performance was obtained even at relatively high blowing ratios, because the conically expanded hole exit reduced the momentum of the lateral spreading. The better cooling performance is obtained with shaped holes expands 4^{o} in all directions from the hole middle to the exit.

Bunker (2002) [34] investigated the film cooling effectiveness for geometries wherein the coolant from discrete holes enters a slot before mixing with the main stream. Basically, the angled holes were entrenched in a shallow trench. The holes embedded in the trench provided higher film cooling effectiveness distributions than the ones on the plane surface.

However, Bunker provided only film effectiveness distributions, and also the hole had a compound angle (radial injection) in the lateral direction.

Sargison et al. (2002) [35] studied a converging slot-hole geometry (console), in which the hole transitions from circular to slot convergence in the axial direction and divergence laterally. The attempt was to make the three-dimensional nature of the jet into a two-dimensional slot film. The results were aimed at improving the film cooling effectiveness.

Lu et al. (2005) [36] studied the effect of trench exit area and edge shape on the film cooling performance using an IR thermography method. Their results showed that the film cooling holes provided higher film cooling effectiveness when embedded in a trench. However, in some geometry, when the trench began at the upstream edge of the hole, the film cooling effectiveness diminished. The heat transfer coefficient enhancement due to the embedding was not significantly higher compared to the typical unembedded cylindrical hole. The overall heat flux ratio comparing the film cooling with the embedded holes to unembedded holes showed that the full trench and downstream trench spacing after the hole exit produced the highest heat flux reduction**.**

Lu et al. (2007) [37] presented an experimental and numerical investigation of film cooling performance for a row of cylindrical holes embedded in transverse trenches. The heat transfer coefficients and film cooling effectiveness were obtained simultaneously using a single test transient IR thermography technique at four blowing ratios of 0.5, 1.0, 1.5 and 2.0. Six trench cases with different widths and depths were tested. The results showed that the trench of holes in a slot reduced the jet momentum at exit and also provided significantly higher film cooling effectiveness with some increase in heat transfer coefficients. They also

presented the CFD simulation using FLUENT to better understand the film cooling performance.

2.3 Numerical Work

Walters and Leylek (2000) [38] performed a computational analysis of film cooling from a single row of cylindrical holes in a flat plate. Solutions were obtained using the standard (k-ε) turbulence model. Two types of near-wall treatments (wall functions and a two-layer approach) were used, and the results were compared. It was found that the coolant jet was moved away from the wall by the counter-rotating vortex structure (due to induction lift), and that these vortices strengthened as the blowing ratio was increased. The significance of the hole geometry in vortex generation was also noted, since the geometry affected the distance between vortex centres. It was further noted that the turbulence in the near field had a significant effect on the film cooling performance, and that whether the turbulence generated in the hole or in the interaction between the coolant and the main flow was the dominant source depended on the blowing ratio. In addition to causing the coolant to lift off of the wall, the counter-rotating vortex structure also had the effect of "pinching" the coolant flow near the wall, that is, preventing the lateral diffusion of coolant in that region. The use of a two-layer model allowed the resolution of a small reverse flow zone immediately downstream of the hole exit trailing edge, whereas the use of wall functions did not. The temperature contours predicted with the wall functions differed significantly from those predicted with the two-layer model in the near-field region within a few hole diameters downstream of the hole but not in the far-field region.

Hyams and Leylek (2000) [39] examined the film cooling process for a shaped, streamwise injected, inclined jet for a blowing ratio

of 1.25 and 1.88. Detailed field results as well as surface phenomena involving adiabatic film cooling effectiveness and heat transfer coefficient were presented. They found that the laterally diffused, simple angle holes provided the best coverage and highest surface film cooling effectiveness magnitudes**.**

Heidmann and Hunter (2001) [40] performed detailed computations of film cooling effectiveness on a three-dimensional grid with a single row of cylindrical holes at various combinations of blowing ratio and density ratio. The results were used to compute the source terms to be used in two-dimensional calculations of the film cooling effectiveness that would give the same result as the three-dimensional calculation. The correct source terms did indeed produce the desired result, but this method is still impractical, since it can only be done by first performing the detailed calculation. A near-wall correction model over predicted the film cooling effectiveness due to under prediction of vertical flow and hot mainstream gas entrainment. A model that distributed the source terms over a thicker layer (on the order of the hole diameter) provided a better prediction of film cooling effectiveness downstream of the film hole. This model performed best for lower blowing ratios at which the jet did not detach since the detachment of the jet was not explicitly modelled.

Abbe` s Azzi and Bassam (2007) [41] presented a numerical prediction for console geometry by using anisotropic eddy-viscosity/diffusivity model to predict the film cooling performance from consoles. The result showed that this model can correctly predict the spanwise spreading of the temperature field and reduce the strength of the secondary vortices. Also the result indicated that the new console hole suggested by **Sargison et al. [35]** is definitely superior to the other geometries as shown by the uniform spanwise spreading of the film

cooling effectiveness with a slight enhancement downstream of the intersection of the two consoles.

Sangkwon and Shih (2007) [42] presented, by using commercial CFD software FLUENT, a new design concept to increase the adiabatic film cooling effectiveness from a row of film cooling holes. They proposed a geometry modification upstream of the holes to modify the approaching boundary layer flow and its interaction with the film cooling jets, this was done by making the surface just upstream of a row of holes into a ramp with a backward-facing step. The results obtained showed that an upstream ramp with a backward-facing step can greatly increase the adiabatic film cooling effectiveness. The spanwise averaged adiabatic film cooling effectiveness with a ramp can be two or more times higher than that without the ramp.

Kanani et al. (2008) [43] investigated numerically the film cooling effectiveness at a flat plate. Three-dimensional geometry was generated and the effects of blowing ratio and geometrical shape were studied. A cylindrical round, simple angle (CYSA) and laterally diffused, simple angle (LDSA) hole with a streamwise angle of 30° and spanwise angle of 0° were used. Hole length to diameter ratio (L/D=4) is constant for all geometries. Also the diameter of film cooling hole for different cooling holes at the entrance surface (D=10 mm) is constant. The blowing ratio ranges from 0.5 to 1.67, and the mainstream Reynolds number based on the mainstream velocity and hole diameter was 8563. Results have a good correspondence with experimental data obtained by **Yuen and Botas [26]**. The simulation results showed that cooling hole shape affects film cooling effectiveness significantly. The vortex in the region near the hole of (LDSA) was very weak compared with this vortex for the (CYSA). The (LDSA) hole decreases the momentum of jet flow at the exit area of the hole and avoids lift-off phenomenon, and secondary flow is not

powerful enough to disturb the jet flow structure next to the wall. Also the results showed that the (LDSA) hole has a better lateral coverage due to the diffused shape of the hole and has a higher effectiveness value in a wider region on the wall.

Baheri et al. (2008) [44] presented a comparative-numerical investigation on film cooling from a row of simple and compound angle holes injected at 35º on a flat plat with four film cooling configurations: (a) cylindrical hole; (b) 15º forward diffused hole; (c) trenched cylindrical hole; (d) trenched 15º forward diffused hole. All simulations were at fixed blowing ratio of 1.25 and pitch to diameter ratio of 3. The mathematical film cooling model consists of the RANS, the energy equation and the standard (k-ε) model using a finite volume method. They found that the trenched compound angle injection shaped hole produced much higher film cooling protection than the other configurations.

Silieti et al. (2009) [45] studied numerically the ability of three turbulence models to predict the film cooling effectiveness from a fan-shaped cooling hole: the (k-ε) model, the SST (k-ω) model, and the (v^2-f) turbulence model. The flow and temperature fields were discussed in addition to local, two-dimensional distribution of film cooling effectiveness for the adiabatic and conjugate cases. The results were compared to experimental data in terms of centreline film cooling effectiveness downstream fan-shaped cooling hole. They showed that the (k-ε) model performed better than the other models in predicting the surface temperature distribution and hence the film cooling effectiveness.

Fayyaz and Muhammad (2010) [46] compared computationally, using commercial CFD software FLUENT, the film cooling effectiveness of cylindrical, square and two types of equilateral triangular holes with an inclination of 30^o with streamwise direction at Reynolds number of 10364, (L/D=4), density ratio of 0.92. The

theoretical results compared with the experimental ones of **Yuen and Botas [26]** showed well agreement even for a high blowing ratio. It was observed that the triangular hole having a lateral straight edge on leeward side showed much higher film cooling effectiveness values than the cylindrical film cooling hole case in the near hole region and almost similar coolant jet height as that in case of cylindrical film cooling. Also, it was observed that the triangular hole having lateral straight edge on windward side and converging corner on leeward side revealed lesser coolant jet height and higher film cooling effectiveness in the region X/D>10, especially at blowing ratios greater than 1.0.

Dia and Lin (2011) [47] investigated numerically three film cooling configurations, (cylindrical hole, shaped hole, and crescent hole). All holes were inclined at 35^{o} on a flat plate. All simulations were conducted at blowing ratio of 0.6 and 1.25, length to diameter ratio of 4 and pitch-to-diameter ratio of 3. They used (RANS) equations, the energy equation, and two-layer (k-ε) turbulence models. For the numerical investigation, the commercial CFD software FLUENT with standard (k-ε) turbulent models was applied. They found that the crescent hole exhibited the highest film cooling effectiveness among the three configurations both in spanwise and streamwise, especially downstream of the interaction of the two holes.

Lee and Kim (2011) [48] evaluated the effect of geometric variables of a laidback fan-shaped hole on the film cooling effectiveness using a Reynolds-averaged Navier-stokes analysis. The shape of the laidback fan-shaped hole is defined by four geometric design variables: the injection angle of the hole, the lateral expansion angle of the diffuser, the forward expansion angle of the hole, and the ratio of the length to diameter of the hole. They concluded that the increase of the forward expansion angle made a reduction of film cooling effectiveness, and the

lateral expansion angle had the biggest impact among the four geometric variables on the spatially averaged film cooling effectiveness.

2.4 Summary of Previous Works

Most of the above literature were considered with different hole configurations such as standard cylindrical holes, shaped hole, holes embedded in the trench, tabs placed at hole exit, and ramped holes have been investigated, focused either on reducing the upward momentum of the jets or on the deformation of the flow filed at the interaction zone. The effect of different types of turbulence promoters upstream of the film cooling holes has also been a focus of recent film cooling research. Some authors have performed experimental investigations of the film cooling effectiveness of holes embedded in a slot or trench, while others have presented a computational analysis of trench film cooling effectiveness as well. These studies concluded that the film cooling effectiveness around the holes is significantly improved when the holes are set in a trench due to a lateral spreading of the coolant and reduced coolant jet separation. The disadvantage of all slot or trench film cooling designs is that they are not suitable for application to blades and vanes except at the trailing edge, because of the lack of mechanical strength. The effect of using ramped holes though is not well defined but has potential to greatly increase the film cooling effectiveness in the same way by creating a vortex at the point where the coolant enters. The scope of the present work is to modify the approaching boundary-layer flow and its interaction with the film cooling jets by using ramped holes and to investigate the thermal performance of film cooling for two types of ramped holes rows (cylindrical and conical). The ramps can be applied and constructed in the thermal-barrier coating (TBC) system by using the ceramic top coat, which has very low thermal conductivity [42]. The applications of ramps

were found to be useful and suitable in combustors as shown in Figure (2-1), after burner, trailing edge and many other applications.

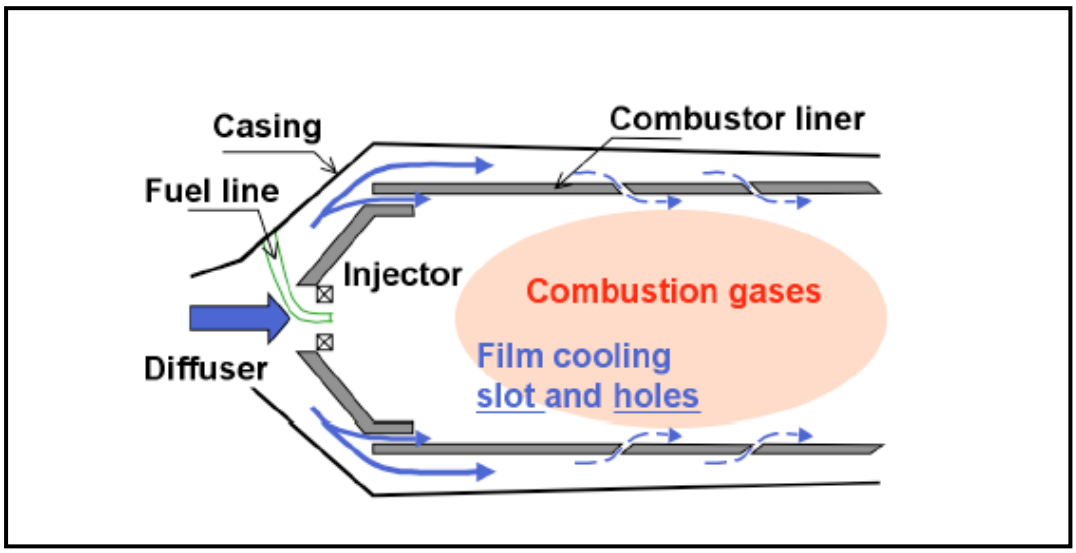

Figure (2-1) Film cooling schematics of a gas turbine combustor

Chapter Three

Numerical Simulation

Chapter Three
Numerical Simulation

3.1 Introduction

This chapter presents a description of the mathematical basis for a comprehensive general purpose model of fluid flow and heat transfer from the basic principles of conservation of mass, momentum, and energy. The computational fluid dynamics (CFD) becomes one of the most useful tools for complex phenomena without resorting to expensive prototype and difficult experimental measurement. Numerical prediction using FLUENT can be performed to determine the jet mainstream interactions and for better understanding the interaction of the injected coolant and the hot mainstream flow before choosing cases for experimental work.

The assumptions are:

1) Three dimensional steady flow.
2) Turbulent flow due to jet in a cross flow has a high turbulence intensity.
3) Incompressible fluids as velocities tend to be low (Mach number less than 0.3).
4) Newtonian fluid, like many common fluids such as water and air, displaying a linear relationship between shear and strain.

There are three main steps in any CFD analysis:

1) Pre-Processing
2) Solver Execution
3) Post-Processing

Pre-Processing is the step where the modelling goals are determined and computational grid is created. In the second step,

numerical models and boundary conditions are set to start up the solver. Solver runs until the convergence is reached.

When solver is terminated, the results are examined, and this is the post processing part. In present work, the pre-processing program used was Gambit 2.4.6 to create and grid the system geometry and then simulate the film cooling for different cases, and the solver and post-processing used were FLUENT version (12.1) by (ANSYS) [49].

3.2 Pre-Processing (The Geometry)

Pre-Processing is the step where the modelling goals are determined and computational grid is created. A schematic of the (side view) of the computational domain for a cylindrical-hole case is shown in figure (3-1). The Cartesian coordinate system with its origin is placed at the downstream edge of the film hole on the top surface of the test plate, and its *x*, *y* and *z* axes are aligned with the streamwise, vertical and lateral direction, as seen in figure (3-1).

The solid model of the whole assembly and hole intersection grid close-up are shown in figure (3-2). The computational domain included the coolant supply channel (plenum), the cooling hole, and the main channel (cross hot flow).

The cross flow test section was 16 mm in width, 50 mm in height, and 230 mm in long and the plenum cross section was 16 mm in width, 50 mm in height, and 50 mm in long. Two types of holes are considered; standard cylindrical shape hole and conical shape hole as seen in figure (3-3). For cylindrical shape, the hole diameter is 4 mm, the hole length is 3.5D, and for conical shape, the hole diameter is 4 mm at inlet and diverged by 6^{o} to the exit. Injection angle (θ) is 35^{o} for all cases, and

the exit plane located at X/D=40 downstream of cooling hole.

The ramps configurations used in the present investigation are shown schematically in figure (3-4), they have different dimension for each cases, as given in Table (3-1).

Table (3-1): Illustrated geometry for all models.

Model Number	**Ramp specification**	
	γ	β
Model 1 Baseline case	-	-
Model 2 Single ramped-cylindrical hole	11.3^o	0
Model 3 Single ramped-cylindrical hole	16.7^o	0
Model 4 Double ramped-cylindrical hole	16.7^o	0
Model 5 conical hole without ramp	-	-
Model 6 Single ramped-conical hole	11.3^o	0
Model 7 Single ramped-conical hole	16.7^o	0
Model 8 Single ramped-conical hole	16.7^o	0.5D
Model 9 Single ramped-conical hole	16.7^o	D
Model 10 Double ramped-conical hole	16.7^o	0

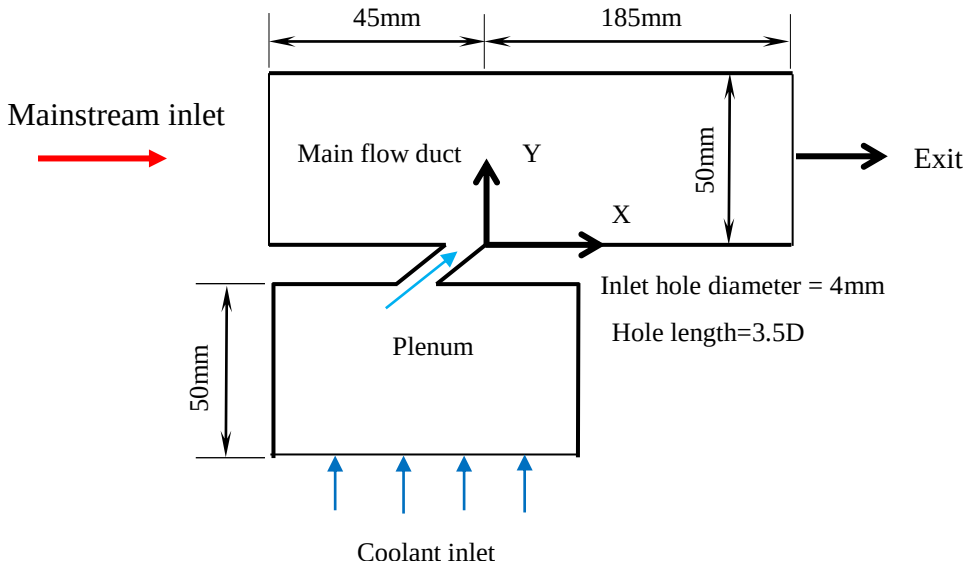

Figure (3-1) Schematic of the film-cooling configuration studied

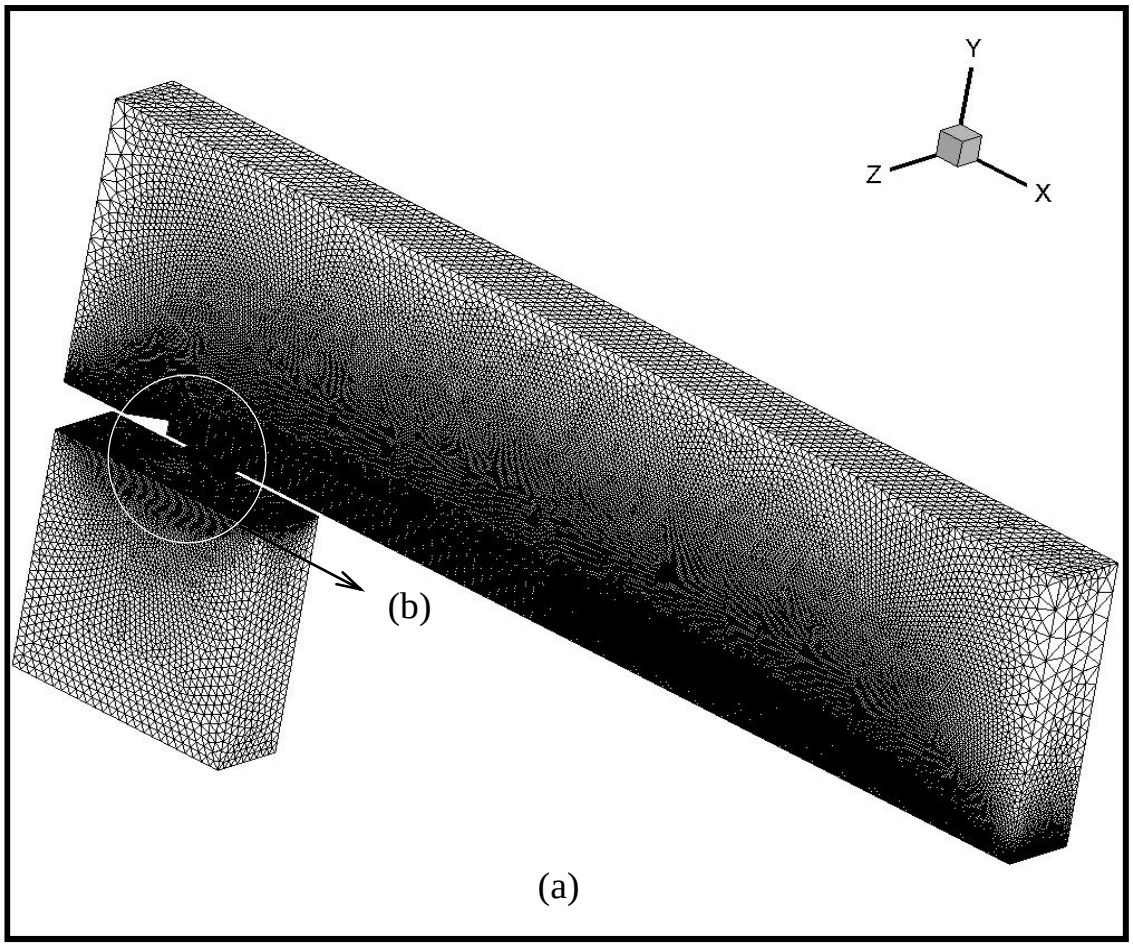

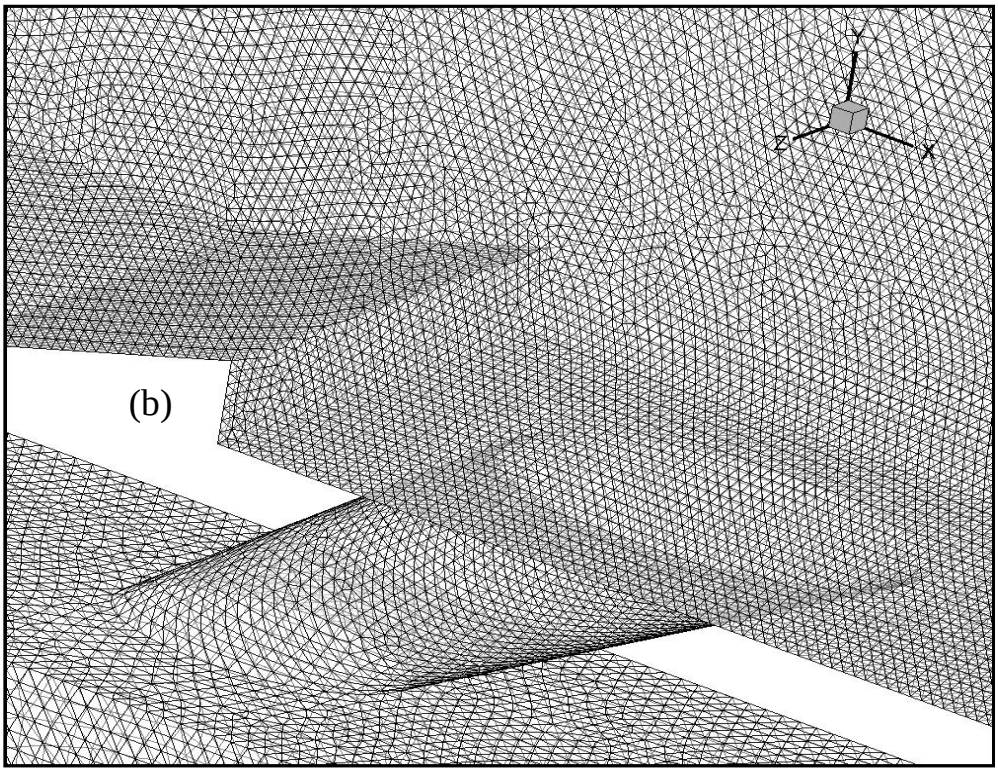

Figure (3-2): Computational grid for a case of conical hole with ramp (a) whole assembly (b) hole intersection close-up

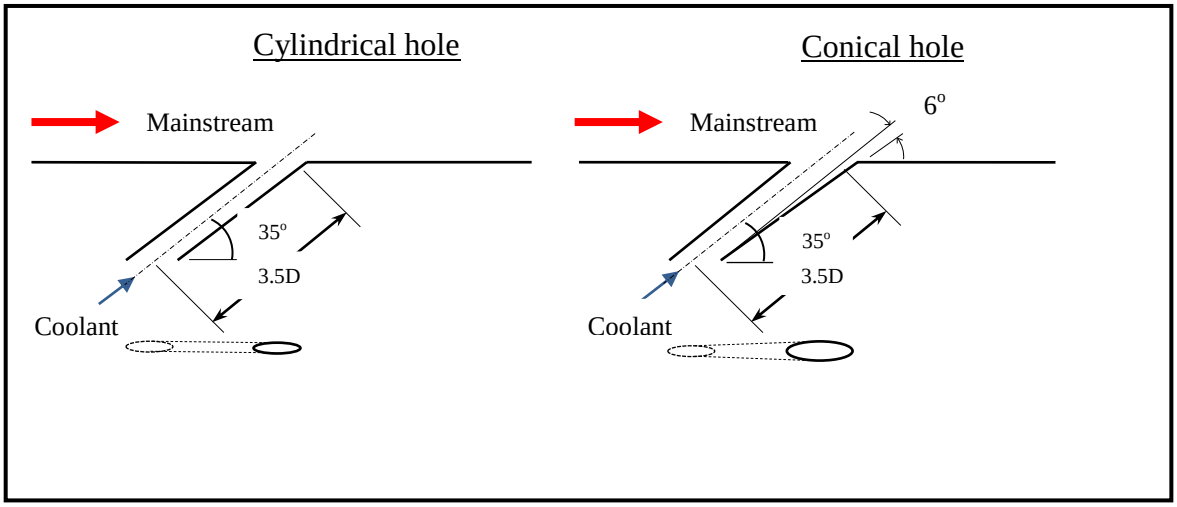

Figure (3-3) Film cooling hole configurations

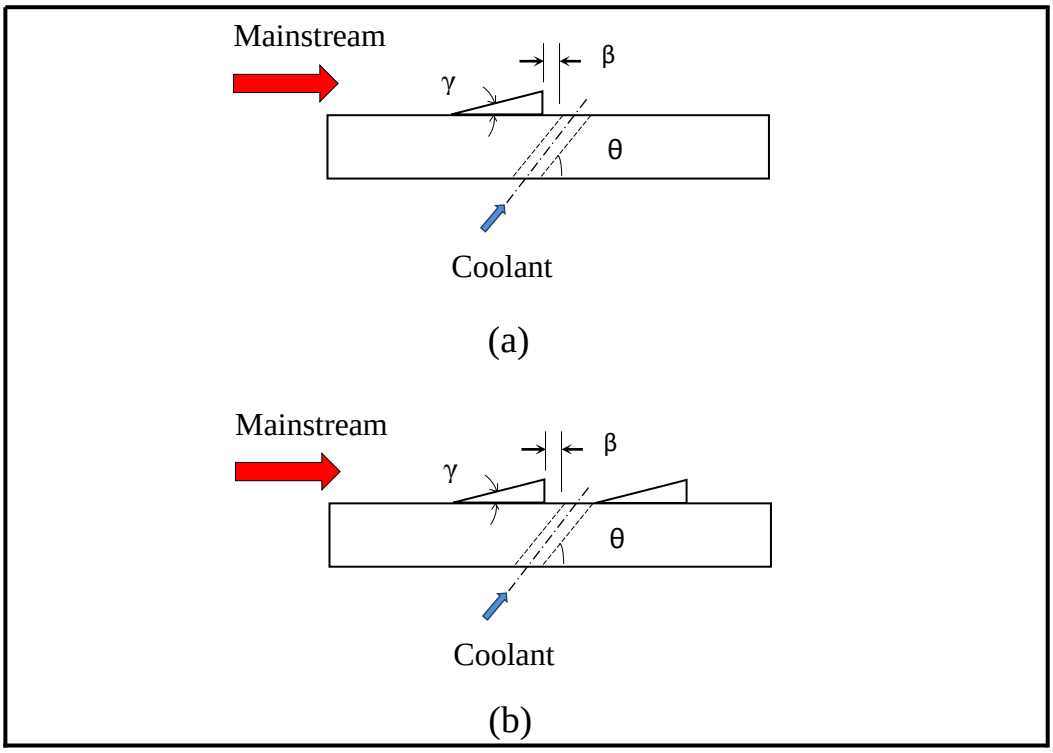

Figure (3-4): Schematic ramps studied (a) single ramp (b) double ramp

3.3 Governing Equations and Turbulence Model

The governing equations to be solved are the incompressible continuity, momentum, and energy equations and the transport equations for the turbulent kinetic energy, and dissipation is added through the turbulence models. The steady state governing equations for conservation of mass, momentum, and energy are given as [50],[51]:

$$\frac{\partial U_i}{\partial x_i} = 0 \tag{3-1}$$

$$\frac{\partial U_i U_j}{\partial x_j} = -\frac{1}{\rho}\frac{\partial p}{\partial x_i} + \frac{\partial}{\partial x_i}\left(\vartheta \tau_{ij} - \overline{\acute{u}_\iota \acute{u}_\jmath}\right) \tag{3-2}$$

$$\frac{\partial(U_j T)}{\partial x_j} = \frac{\partial}{\partial x_j}\left(\frac{\vartheta}{Pr}\frac{\partial T}{\partial x_j} - c_p\overline{\acute{u}_\iota \acute{T}}\right) \quad (3\text{-}3)$$

Where, (τ_{ij}) is the symmetric stress tensor defined as:

$$\tau_{ij} = \mu_t\left(\frac{\partial u_i}{\partial x_j} + \frac{\partial u_j}{\partial x_i} - \frac{2}{3}\delta_{ij}\frac{\partial u_k}{\partial x_k}\right) \quad (3\text{-}4)$$

The terms of ($\overline{\acute{u}_\iota \acute{u}_j}$) and ($c_p\overline{\acute{u}_\iota \acute{T}}$) represent the specific Reynolds stresses and specific turbulent heat fluxes, which should be modelled properly for a turbulent flow.

Two additional transport equations for the turbulence kinetic energy (*k*) and the turbulence dissipation rate (ε) are solved. The standard (*k*-ε) model [52] is a semi-empirical model based on model transport equations for the turbulent kinetic energy (*k*) and its dissipation rate (ε). Assumed that the flow is fully turbulent and the effects of molecular viscosity are negligible, the turbulence kinetic energy (*k)* and its dissipation rate (ε) are obtained from the following equations [53]:

$$\frac{\partial}{\partial x_i}\rho k u_i = \frac{\partial}{\partial x_j}\left[\left(\mu + \frac{\mu_t}{\sigma_k}\right)\frac{\partial k}{\partial x_j}\right] + G_k + G_b - \rho\varepsilon + Y_M + S_k \quad (3\text{-}5)$$

$$\frac{\partial}{\partial x_i}\rho\varepsilon u_i = \frac{\partial}{\partial x_j}\left[\left(\mu + \frac{\mu_t}{\sigma_\varepsilon}\right)\frac{\partial \varepsilon}{\partial x_j}\right] + C_{1\varepsilon}\frac{\varepsilon}{k}(G_k + C_{3\epsilon}G_b) - C_{2\varepsilon}\rho\frac{\varepsilon^2}{k} + S_\varepsilon \quad (3\text{-}6)$$

Turbulent viscosity (μ_t) is computed as a function of (*k*) and (ε) [53]:

$$\mu_t = \rho C_\mu \frac{k^2}{\varepsilon} \quad (3\text{-}7)$$

The generation of turbulence kinetic energy due to the mean velocity gradients (G_k) is computed by:

$$G_k = -\rho \acute{u}_i \acute{u}_J \frac{\partial u_j}{\partial x_i} \quad (3\text{-}8)$$

The generation of turbulence kinetic energy due to the buoyancy (G_b) can be neglected. (Y_M) represents the contribution of the fluctuating dilatation in compressible turbulence to the overall dissipation rate, $C_{1\varepsilon}$, $C_{2\varepsilon}$, and C_μ are taken as the default values ($C_{1\varepsilon}$ =1.44, $C_{2\varepsilon}$=1.92, and C_μ=0.09), σ_k and σ_ε are the turbulent Prandtl numbers for (k) and (ε) are taken as 1 & 1.3, respectively. These constants are recommended by Launder [53]. The above set of constants has been applied successfully for many three-dimensional flows [54]. S_k and S_ε are user-defined source terms [49].

3.3.1 Gambit Code

To solve any problem by using FLUENT code, a secondary program is used to create the geometry and grid. It is called GAMBIT. The grids have many kinds, such as hexahedron and T-Grid used to generate a tetrahedron, which are existing boundary mesh.

3.3.1.1 Choosing the Appropriate Grid Type

FLUENT can use grids comprising of tetrahedron or hexahedron cells in 3D, as shown in figure (3-5). The choice of which mesh type to use will depend on the application. For the problems which involve complex geometries, the creation of structured or block-structured grids (consisting of hexahedron cells) can be extremely time-consuming; if not impossible, the setup time is therefore the major motivation for using unstructured grids employing tetrahedron cells. The range of length scales of the flow is large, and a tetrahedron mesh can often be created

with far fewer cells than the equivalent mesh consisting of hexahedron cells [49]. This is because a tetrahedron mesh allows cells to be clustered in selected regions of the flow domain. Whereas, structured hexahedron meshes will generally force cells to be placed in regions where they are not needed. This is the reason behind this case in the current study of unstructured tetrahedron meshes chosen, as shown in figure (3-5), the Gambit grid generator with approximately 1.3 million computational cells for each case.

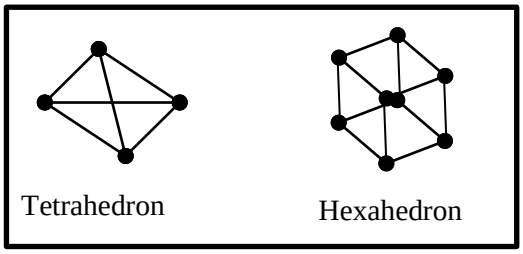

Figure (3-5): Tetrahedron and hexahedron cells

3.3.2 Fluent Code

FLUENT version (12.1) solves the governing integral equations for the conservation of mass, momentum, energy, and other scalars, such as turbulence. FLUENT is an ultimate useful computer program for modelling fluid flow and heat transfer in complex geometries. It provides complete mesh flexibility to solve flow problems with unstructured meshes that can be generated about complex geometries with relative ease.

There are two processors used to solve the flow and heat transfer equations. The first pre-processor is the program structure which creates the geometry and grid by using GAMBIT.

The second post processor is solving Navier-Stokes equations which include continuity, momentum and energy equations, while (k-ε) model drop the viscosity term by using finite volume technique, and by using the initialization described with some details about the

implementation of the boundary condition. Two methods are used in the solver, explicitly or implicitly. Explicit methods are generally easy to code but require very small time steps to satisfy stability restrictions. Therefore, many iterations and large computer times require reaching a steady-state solution. The implicit scheme simultaneously solves several equations. The maximum time step is much larger than that allowed for the explicit, so that fewer iterations and lower computer times are required [49].

3.3.3 Boundary Conditions

At all boundaries except those denoted as "main inlet," "coolant inlet," and "exit" in figure (3-1), are considered as an adiabatic wall boundary condition was used. At the "main inlet," a velocity-inlet boundary condition was specified with x-velocity equal to 20 m/s, and all other components equal to zero. The temperature was given as 323 K (50^{o}C). The turbulence intensity and calculated hydraulic diameter (which is used to determine turbulence length scales) were specified as 2% and 0.024 m, respectively. At the "coolant inlet," a velocity-inlet boundary condition was specified with y-velocity equal to the values calculated from the blowing ratio definition, then fed to the FLUENT, and all other components equal to zero. The coolant temperature was given as 293 K (20^{o}C) to give a temperature ratio of 0.4, as recommended by Chi Zhang [55]. The turbulence intensity and hydraulic diameter were specified as 3% and 0.023 m, respectively.

The Reynolds number based on mainstream velocity and hole hydraulic diameters is 5100.

The adiabatic film cooling effectiveness given in equation (1-1) and the downstream dimensionless distance (X/D) were introduced to the FLUENT as custom field function.

3.3.3.1 Initial Condition

The flow filed is unknown unless iteration is started; therefore, an initial guess is needed to start the solution. The initialization of the model is important for convergence. If the initial conditions are poor, then they take longer to converge or they may even result divergence. For the present work, all variables are initiated from the inlet boundary conditions.

3.3.4 Solvers

3D segregated, steady state solver is used for linearization of governing equations, and implicit method is used. For turbulence modelling (k-ε) model with standard wall functions is used [52, 53]. It has been shown in figure (3-6) that the averaged value of parameter scaled with viscous length or time scale (y^+) for the surface is less than 10 which is within the range of Ref.[56] to avoid the use of enhanced wall treatment mesh. Discretization scheme used is second order upwind for momentum, turbulence kinetic energy, turbulence dissipation rate and energy [57], whereas for pressure, standard discretization scheme is used [58]. For pressure-velocity coupling, simple algorithm is used [59]. Converged results are obtained after the specified residual sate met, as shown in figures (3-7) and (3-8); a converged result renders a mass residual of 10^{-5}, an energy residual of 10^{-7}, and momentum and turbulence kinetic energy residuals of 10^{-5}. These residuals are the summation of the imbalance for each cell, scaled by a representative of the flow rate.

Typically, more than 1500 iterations are needed to obtain a converged result which takes about 15 hours on a computer cluster consisting of eight nodes of 2.4 GHz Pentium COREi3 personal computers.

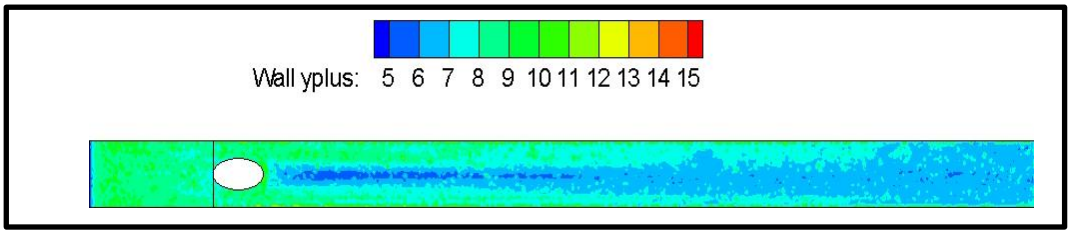

Figure (3-6): Plot for (y^+) for film cooling system

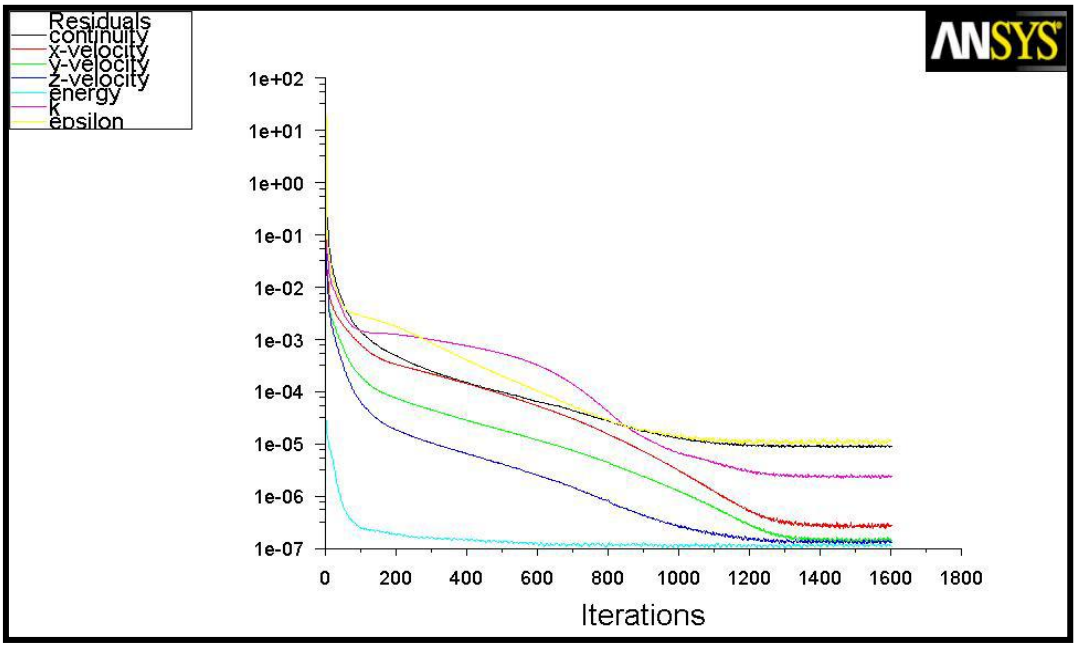

Figure (3-7): Convergence history for continuity, momentum, energy, and turbulence equation

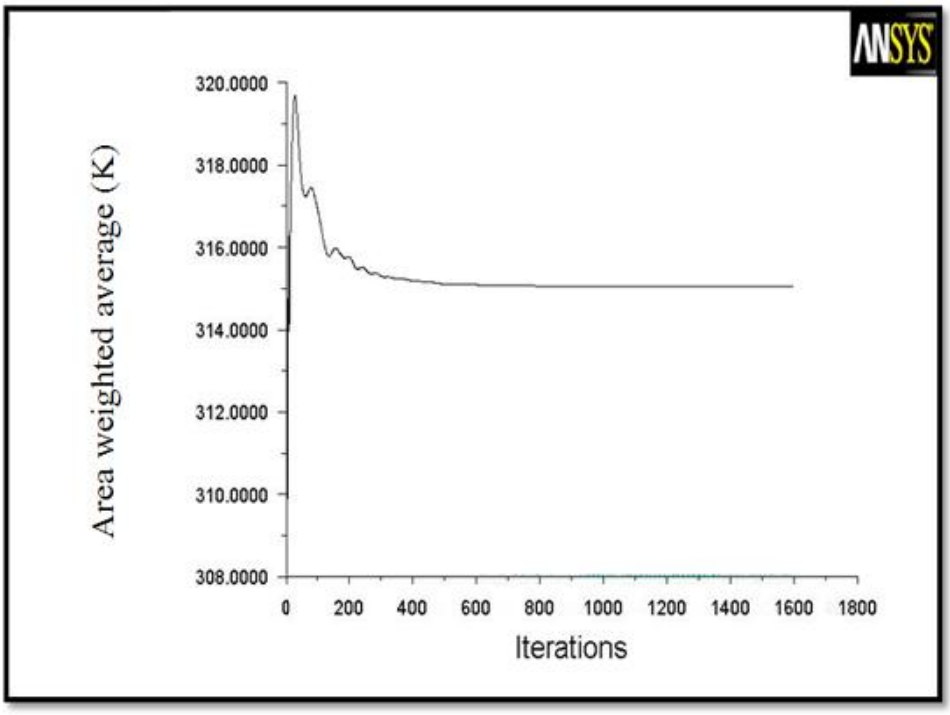

Figure (3-8): Average static temperature on test surface history for film cooling system

3.4 Film Cooling Configurations

Ten models are considered in the present study, each of different hole arrangements is shown in Table (3-1). Each model is provided with one hole to solve by FLUENT. Seven of these models are arranged with ramp. All models are solved for three blowing ratios of 0.5, 1, and 1.5.

Chapter Four

Experimental Work

Chapter Four
Experimental work

A description of the experimental facility used for thermal analysis is presented in this chapter. The low speed test rig and the instrumentations facilities are described. The six models geometry to be tested is also presented, and finally the general arrangement of the experimental set-up and computing procedure are discussed.

4.1 Experimental Apparatus

4.1.1 Test Rig

All experiments were carried out in a low-speed hot air supplier system with attached cold jet in the test section. The test rig is modified and rebuilt at University Of Technology-Equipment and machines Engineering Department. Figure (4-1) shows the sketch and photography of the test rig which has been designed by Assim et al. [60] and constructed by Muwafaq [61].

The mainstream air supply is the ambient air drawn by a blower, the blower is of 2.5 kW motor running with 2800 rpm. Air speed in the test section is controlled by using a manual open gate. The blower exit area having a rectangular shape with dimensions of (6.3x13.1) cm. The blower is supplied with a bend having the same dimensions of the blower exist and then connected to a diffuser having rectangular cross-sectional area of inlet and outlet dimensions as (6.3x13.1) cm and (35x50) cm, respectively and length of 82 cm. Air flow diffuses over a splitter plates into a constant area rectangular settling chamber of cross-sectional area (35x50) cm and length of 70 cm. The settling chamber contains a series of three electrical heaters, each of 4 kW power are used, honeycomb, and four grid screens. The test rig is modified by Humam [62] by adding grid screens and the

honeycomb which fitted the settling chamber cross-sectional area. The honeycomb and screens ensure adequate mixing of hot air and uniform temperature distribution throughout the test section. Figure (4-2) shows the honeycomb which has a depth of 20 cm; it's made from galvanized steel. After the settling chamber, hot air routed through a convergent-divergent contraction, to reduce the discharge losses, having a rectangular cross-sectional area at inlet and outlet as (35x50 cm) and (5x10 cm), respectively, and a length of 70 cm. In order to allow the air to reach the desired temperature, the air is initially routed out away from the test section by using a by-bass gate passage. The temperature of the air is continuously monitored at the exit of the gate, and when the desired temperature is reached by achieving temperature ratio of 0.4, the gate manually is fully opened. To minimize the heat losses to the surrounding, the settling chamber and the test section duct are insulated completely by glass wool insulator. The operating velocity of the hot air kept constant at 20 m/s through the experimental program, while the blowing ratios are controlled by changing the coolant velocity. More details about the design and construction of the low speed hot air supplier rig are given by Assim et al. and Muwafaq [60 and 61]

At the present experimental program, the mainstream hot air temperature (T_m) adjusted with a laboratory temperature (coolant air drawn by a blower) (T_c) (to give the highest limit of $T_c / T_m = 0.4$).

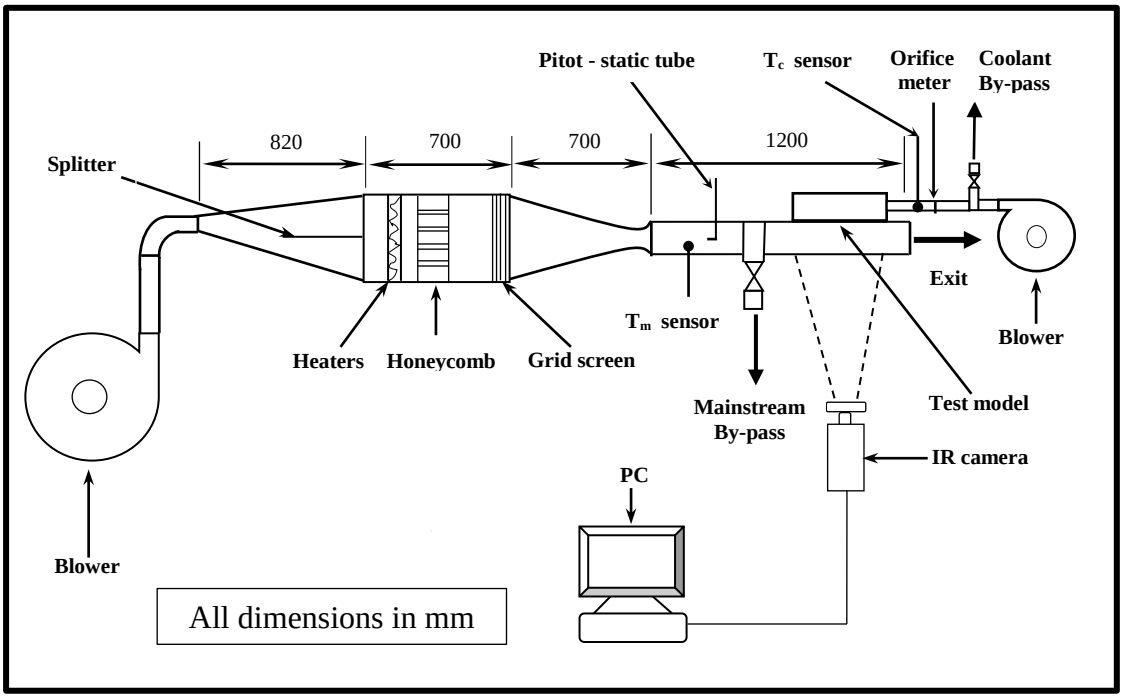

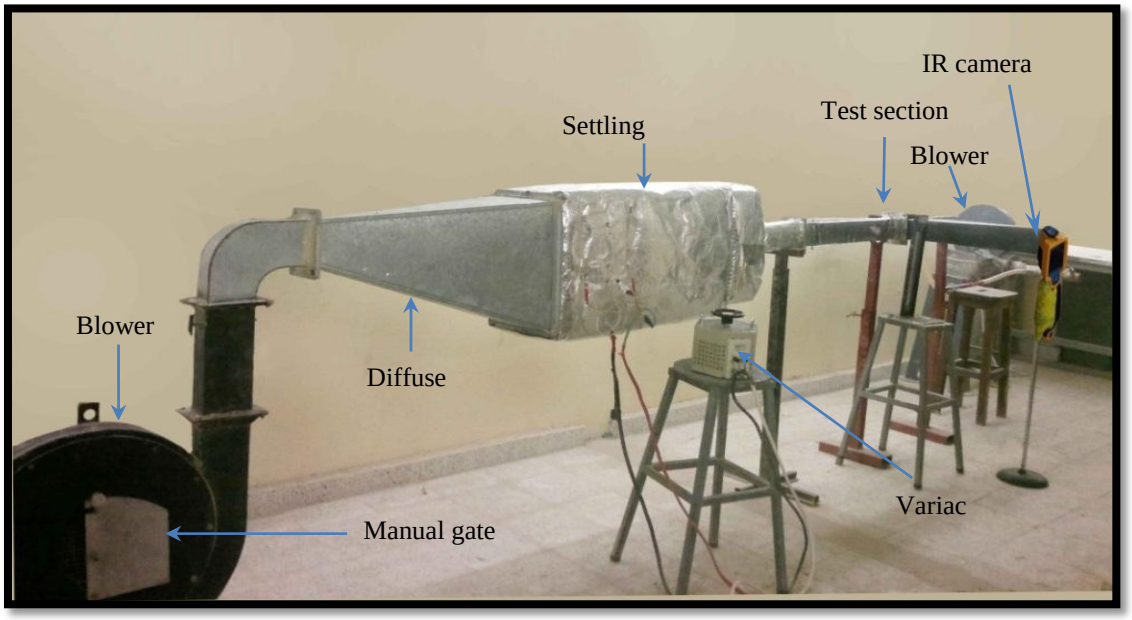

Figure (4-1): Schematic and photography of the experimental test rig

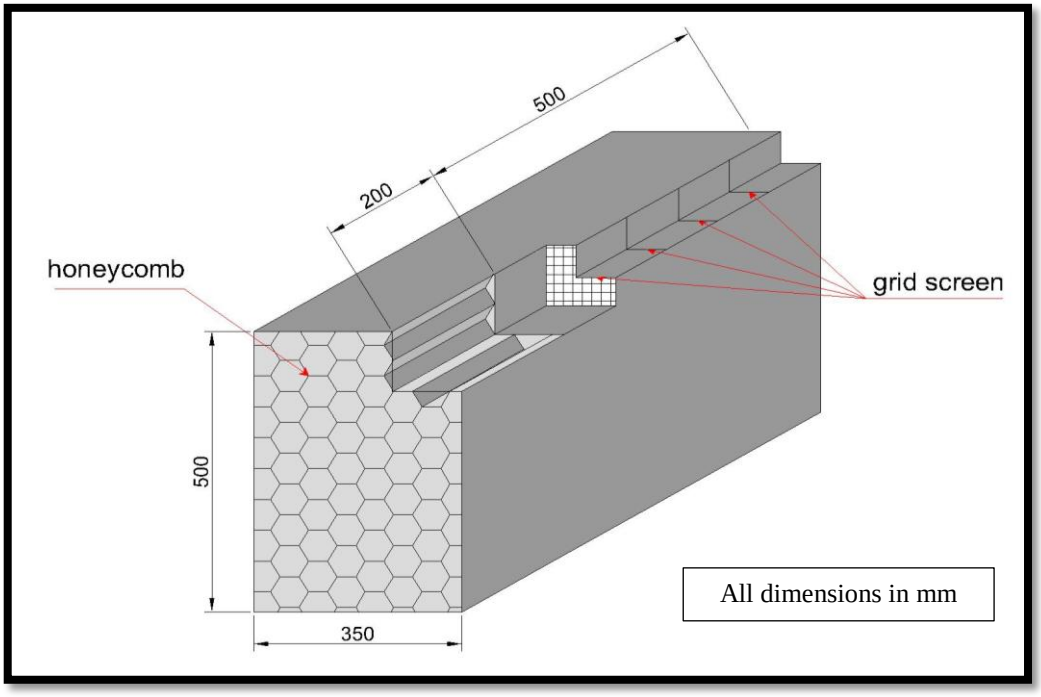

Figure (4-2): The honeycomb and grid screen

4.1.2 Coolant Supply

A centrifugal air blower of blowing capacity of 22.17m^3/min is used to supply the coolant air to the plenum. The coolant air passes through a pipe of 5 cm diameter, and then to ball valve controlling the volumetric flow rate injected throughout the coolant jet holes. The coolant air flow rate is measured by using orifice meter. The coolant air enters a plenum, and then injects through the film cooling holes into the test section to mix with hot mainstream forming film cooling layer.

4.1.3 Test Section and Observation Window

The coolant air injected from the holes is mixed with the hot mainstream in the test section. The test section has 5 cm width, 12.3 cm height and 23.4 cm length, as shown in figure (4-3).

The bottom wall of the test section works as a test model, six models are prepared, each model made of (12.3×23.4cm) Perspex plate of 0.8 cm thickness. The bottom model plate can be removed easily to be replaced by another model at each test.

A special design for the observation window is made and fixed in front the test section to enable the IR camera to view the test surface without interrupting the condition of flow and to keep the flowing air stagnation condition unaffected. The observation window shape is a rectangular diffuser, as shown in figure (4-4), with two opened ends, at the camera side (6×12 cm), and at the test section side (12.3×23.4 cm), the diffuser length is of 70 cm.

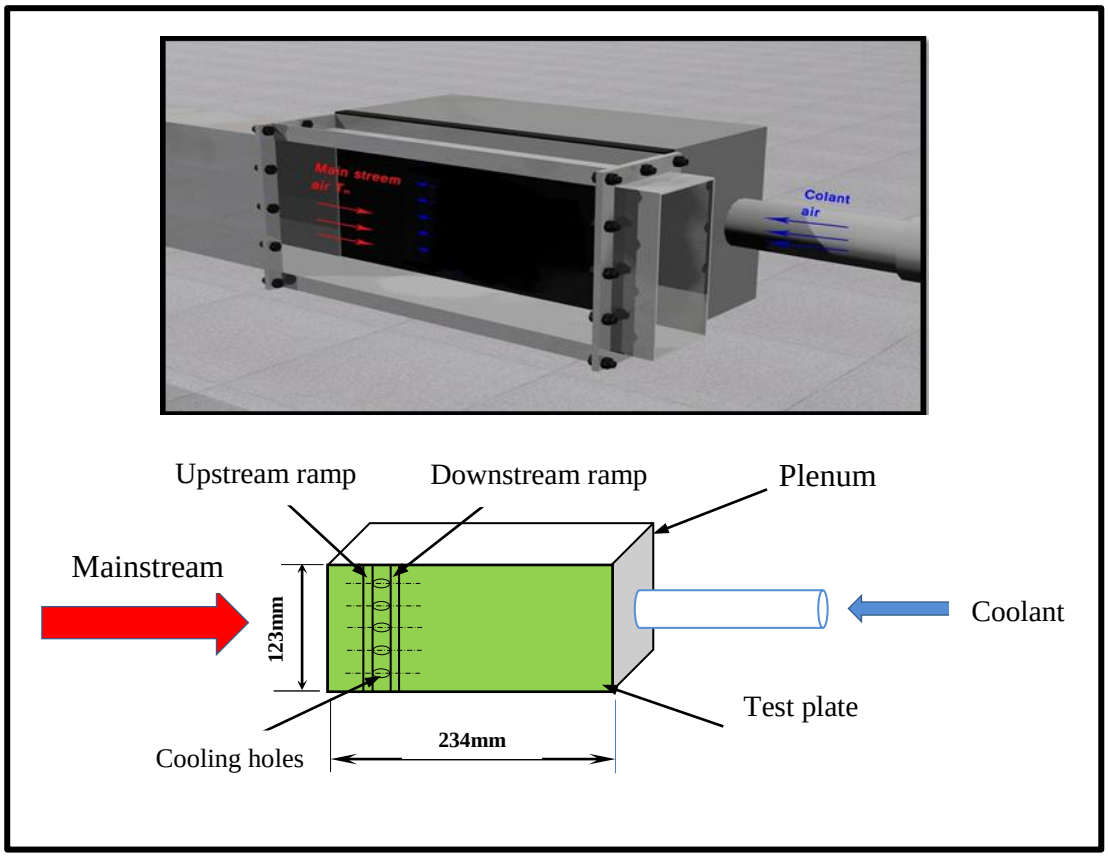

Figure (4-3): 3-D Schematic diagram of test section

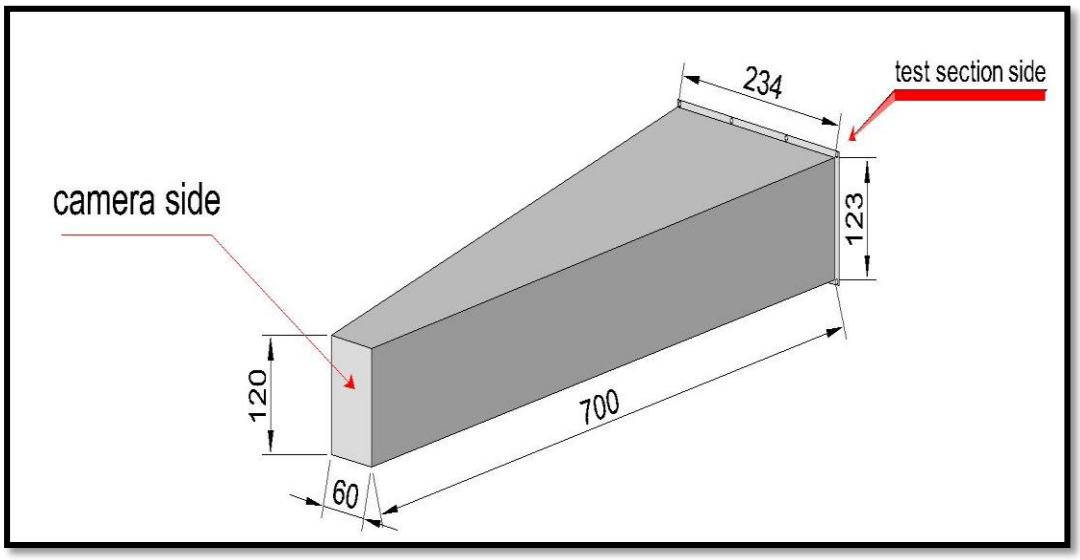

Figure (4-4): Observation window

4.2 Instrumentations

4.2.1 Thermocouples

The hot mainstream and injected coolant air temperatures were measured by using a digital electronic thermometer type (TM-914c) with the aid of thermocouples type-K. The coolant temperature is measured inside one chosen hole, since pre-testing showed that all film holes had the same flow rate and temperature conditions. The measuring system is calibrated by C.O.S.Q.C., and its certificate in Appendix (A).

4.2.2 Orifice Meter

Coolant air flow rate is measured by using 1.4 cm diameter orifice plate meter. The orifice plate is made according to BS1042 [63], and precise geometry is achieved to meet the maximum possible accuracy. The orifice plate is with D and D/2 tapping of 1.1 mm inside diameter which is less than 0.08D according to BS1042 Standard [63]. The thickness of orifice is 0.7 mm, and the orifice shape angle is 45º, rinsing angle from the downstream face of the orifice plate. The calculation of the flow rate is presented in details in Appendix (B).

4.2.3 Pitot-Static Tube

The main stream velocity is measured by using standard ellipsoidal nosed Pitot- static tube with curved junction (N.P.L Standard). It has an external diameter (d) of 7.98 mm, a stem of 45.8 cm long, a nosed total pressure inner diameter of 1.32 mm, and seven static holes of 0.97 mm diameter. The stem-static holes distance equals (8.02 d). The correction to the reading of the Pitot-static tube is determined according to BS1042 Standard [64], it was given in Appendix (C).

4.3 Thermography Measurement Technique

Thermograph is the use of an infrared imaging and measurement, camera to see and measure the thermal energy emitted from an object.

Thermal, or infrared radiation, is electromagnetic radiation that is not visible, because its wavelength is longer than that of visible light. Unlike visible light, in the infrared world, everything with a temperature above zero emits heat. It is observed that the higher the object's temperature, the greater the IR radiation emitted. Infrared allows us to see what our eyes cannot. Infrared thermography cameras produce images of invisible infrared or heat radiation and provide precise non-contact temperature measurement capabilities.

Thermograph technique is presented in details in Appendix (D). It is necessary to compensate for the effect of a number of different radiation sources to obtain the temperature accurately. This is done on-line automatically by the camera. However, the following object parameters must be supplied to the camera:

- The emissivity.
- The transmissivity of the atmosphere, (If the atmosphere is air like the present case, it is equal to 1).

- The temperature of the atmosphere.
- Object distance.

The test surface was coated with mat black paint to increase the emissivity of the test surface. When the paint dried, the test plate was heated up for one and a half hours so that the Perspex reaches the steady state temperature. During heating, the surface temperature was checked every fifteen minutes. Then, a reference point was selected, and its temperature was measured using a thermocouple. Until the temperature of the camera agrees with the thermocouple reading, then this is the emissivity value of the reference object.

4.3.1 IR Camera

The test flat plate surface temperature is measured by using infrared thermography technique. The infrared system used in this study is a Fluke Ti32 shown as photograph in figure (4-5). The calibrated temperature measurement range starts at -10 ºC to +80 ºC, which is the range of this work. The thermal image can be displayed using standard color palettes or Ultra Contrast ™ color palettes. Fluke Ti32 utilizes uncooled micro bolometer long wave detectors to sense IR radiation [65].

The IR camera is designed for general thermal measurement application. It has the following specifications [65]:

1. The field of view and minimum focus distance (with standard lens) are 23ºx17º and 15 cm, respectively.
2. The infrared spectral band range is 8.0 to 14 μm (long wave) and accuracy ±2 ºC or 2%.
3. The pixel detector is 320x240.

Thermal and visual images are displayed on the imager Liquid Crystal Display (LCD) and can be saved to a removable SD memory card with capacity of 2GB. Transferring images to a PC is accomplished by

removing the SD memory card and connecting it to a PC through the included multi-format USB card reader. Smart View software is used for image analysis and report generation from these saved images [65]. For more centrally, the system is calibrated by measuring the temperature of the test surface using a thermocouple type (K) fixed in test surface, at same time the temperature is measured by the IR camera, the test surface is heated by hot mainstream, the temperatures obtained by both measuring method is recorded during the heating process until achieving a steady-state condition. Due to the emissivity of the test surface, the temperature recorded by the IR camera is differed from the temperature obtained by the thermocouple, and then IR camera is adjusted until both reading temperatures are matched.

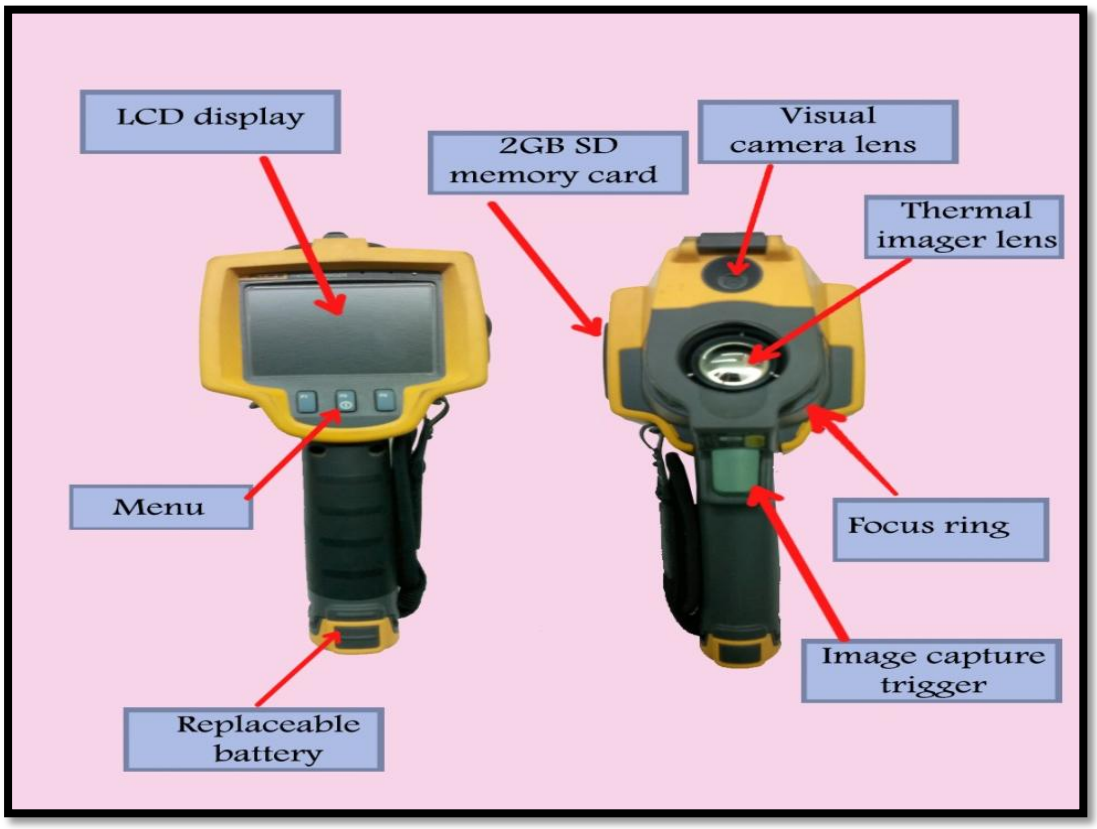

Figure (4-5): Photograph of the IR camera

4.4 The Models to be Tested Experimentally

The preliminary numerical results of ramped-holes are encouraging for using this technique for film cooling. To validate the idea of using ramped-holes and according to the results conducted from the CFD prediction, the following categories will be introduced:-

A. Model 1 consists of one row of film cooling standard cylindrical holes acting as the baseline case, and this model will be considered as a reference model for comparison with other models taken into account in the present investigation program, figure (4-6, a).
B. Model 2 consists of one row of single ramped- cylindrical holes (upstream ramp with a backward-facing step), figure (4-6, b).
C. Model 3 consists of one row of double ramped- cylindrical holes (upstream and downstream ramped-holes both with a backward-facing step), figure (4-6, c).
D. Model 4 consists of one row of film cooling conical holes acting as the baseline case for ramped- conical holes cases, figure (4-6, d).
E. Model 5 consists of one row of single ramped- conical holes (upstream ramp with a backward-facing step), figure (4-6, e).
F. Model 6 consists of one row of double ramped- conical holes (upstream and downstream ramped-holes both with a backward-facing step), figure (4-6, f).

Cylindrical hole models consist of one row of five holes of 4 mm diameter each hole is made with a hole length of 3.5D and with a central pitch distance between each two neighbouring holes of 3.5D. Conical hole models also consist of one row of five holes of 4 mm diameter each at inlet, diverged by 6^{o} to the exit, and the forward injection angle (θ) is 35^{o} for all cases.

Figure (4-7) shows the top view schematic diagram of such test plate. Models (1, 2, and 3) having conventional cylindrical cooling holes, while models (4, 5, and 6) having conical cooling holes.

Figure (4-8) depicts a sample of solid model for the test plate with double- ramped conical holes (upstream and downstream ramped-holes both with a backward-facing step)

The ramps geometries considered in models (2, 3, 5, and 6) are made with the length of 2.5D, located at (β) upstream the film cooling hole and make an angle of γ with the flat plate surface. According to the numerical results, all ramps angle and locations are taken as $\gamma=16.7^{o}$ and $\beta=0$ respectively.

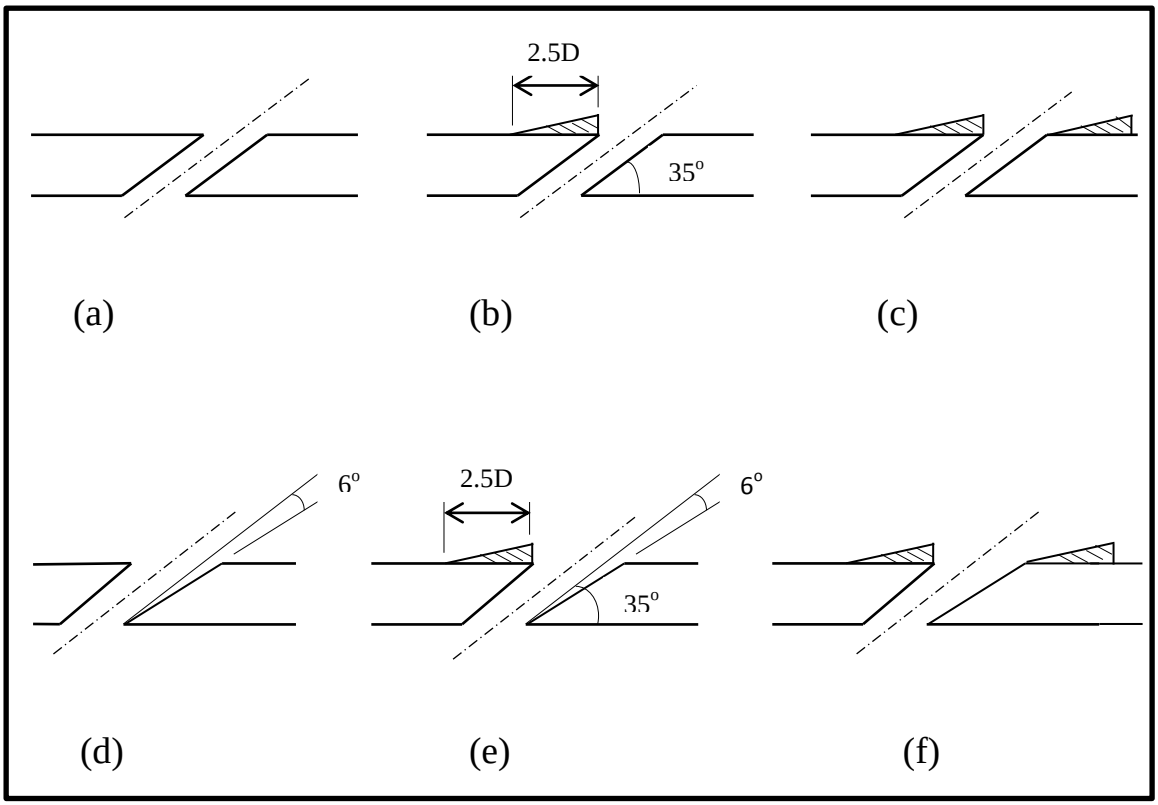

Figure (4-6): Tested models configuration

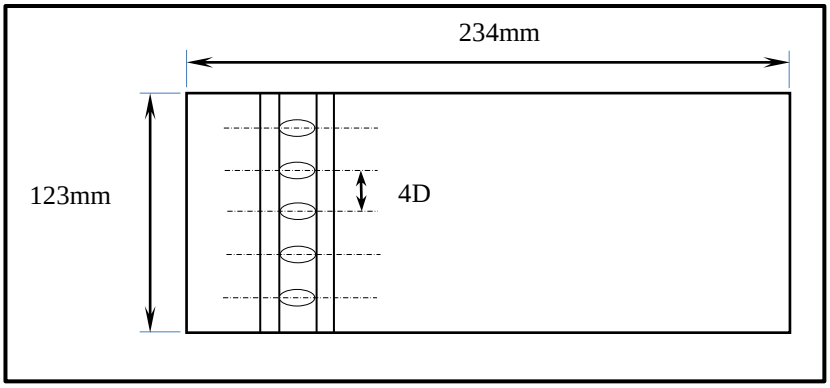

Figure (4-7): Test plate with film hole geometry

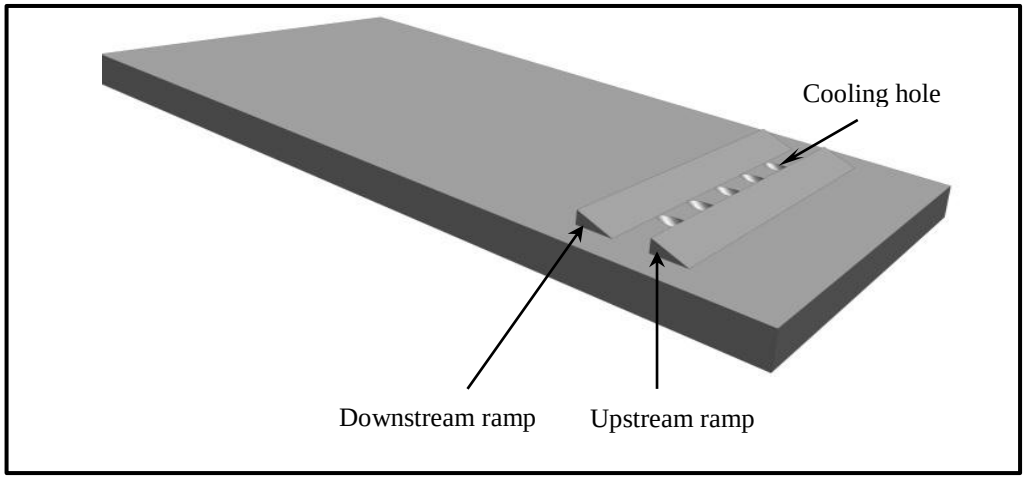

Figure (4-8): Solid model for double-ramped film hole configuration

4.5 Experimental Procedures

The experimental procedures were carried out according to the following steps:

a) Connecting the sample model to the test section.
b) Connecting the flexible pipe to provide the coolant to the test section.
c) Adjusting the velocity of the hot air by using the manual gate meter.

d) Pitot-static tube and U tube water manometer were used to measure the mainstream air velocity.
e) The mainstream air was routed out away from the tunnel by using a by-pass gate.
f) When the temperature of the mainstream air is reached to the desired temperature, the gate is fully opened to pass the air to the test section.
g) Running the blower to drive the coolant, and by using the manual gate, the orifice meter and U-tube water manometer were used to adjust the velocity according to blowing ratio (when BR=0.5, U_c = 9.41m/s).
h) Measuring the coolant temperature inside the plenum by using a digital thermometer.
i) Preparing the IR camera for capturing the image in return for the test section.
j) Running the blower of the coolant at the same time when opening the gate of the mainstream.
k) Images were captured and stored in the SD of the IR camera every 10 seconds, and capturing the images was kept until reaching the case of steady state.
l) Recording the U-tube manometers reading.
m) Recording the mainstream, coolant, and ambient temperatures.
n) Transferring images from a removable SD memory card to a PC by removing the SD memory card and connecting it to a PC through the included multi-format USB card reader.
o) Repeating the above steps again but by changing the velocity of the coolant two times (18.83 and 28.245 m/s).

4.6 The Adiabatic Film Cooling Effectiveness Estimation

The IR images for models surface at each investigated test was captured and stored by a thermal camera at steady-state condition. These images are transferred to PC. Smart View Software program supplied with camera can be used to limit the selected area to avoid the effect of the test section walls. The IR images converted to corresponding temperature digital values and then saved as Excel sheet data. Finally, the values of the adiabatic film cooling effectiveness (η) are computed, tabulated in the Excel sheet by using the adiabatic film cooling effectiveness definition.

4.7 The Heat Transfer Coefficient Estimation

The test plate is modeled as an infinitely thick flat plate under a transient heat transfer phenomenon.

Figure (4-9) shows a schematic diagram of flow over a flat plate.

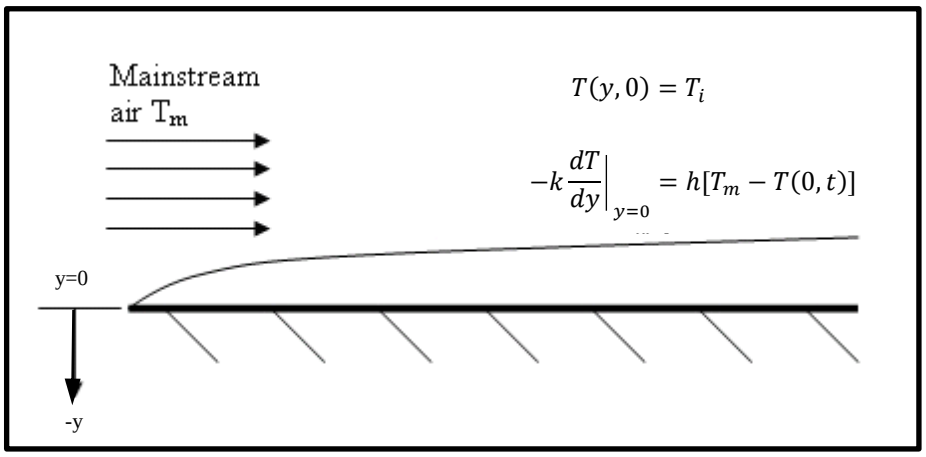

Figure (4-9): Flow over a flat plate

The test plate is initially at a uniform temperature (T_i), and the convective boundary condition is suddenly applied on the plate at time, (t >0), (the hot stream of air provides a heat flux to the surface of the plate

and convective heat transfer phenomena occurs). The 2-D transient conduction equation is given by:

$$\frac{\partial^2 T}{\partial y^2} + \frac{\partial^2 T}{\partial z^2} = \frac{1}{\alpha}\frac{\partial T}{\partial t} \quad (4\text{-}1)$$

Neglecting the lateral conduction, equation (4-1) becomes:

$$\frac{\partial^2 T}{\partial y^2} = \frac{1}{\alpha}\frac{\partial T}{\partial t} \quad (4\text{-}2)$$

Solving equation (4-2) need two boundary conditions, and an initial condition:

The initial condition at $t = 0 \quad T = T_i$ (4-3)

At $y = 0$ and $t \geq 0$, $-K\frac{\partial T}{\partial y} = h(T_w - T_m)$ (4-4)

At $y = \infty$ and $t \geq 0$, $T = T_i$ (4-5)

The main approximation often applied to analyze the transient conduction, shown in figure (4-9), is the semi-infinite approximation. Semi-infinite solids can be visualized as very thick walls with one side exposed to some fluid, the other side remains unaffected by the fluid temperature since the wall is very thick. Solving the partial equation (4-2) with the prescribed initial condition and boundary conditions at y = 0 gives the transient response of the test plate wall due to the convective heat load applied by the hot mainstream air. The solution is given by the flowing equation Incropera and DeWitt [66]:

$$\frac{T_w - T_i}{T_m - T_i} = 1 - \exp\left[\frac{h^2 \alpha t}{K^2}\right] erfc\left[\frac{h\sqrt{\alpha t}}{K}\right] \quad (4\text{-}6)$$

The function (erf) is the Gaussian error function defined as Incropera and DeWitt [66]:

$$\text{erf}\, w = \frac{2}{\pi} \int_0^w e^{-v^2} dv \quad (4\text{-}7)$$

The complementary error function, erfc*w* is defined as:

$$\text{erfc}\, w = 1 - \text{erf}\, w \quad (4\text{-}8)$$

In the above equations, all the test plate properties are known. Thus, recording (T_w) at different times (*t*), the value of heat transfer coefficient (*h*) can be found out. This might not be the case when the plate is being cooled by film injection.

The assumptions of semi-infinite solid are valid for this work because the transient test duration is small, usually less than 60 seconds, and also because of the test surface is made of Perspex which has low thermal conductivity, low thermal diffusivity and low lateral conduction, combinations of the above facts make sure that heat is conducted only in the x-direction and it does not reach the bottom of the test surface.

Considerations are taken for the present case, where the coolant air is being injected from the bottom of the plate surface, as shown in figure (4-10).

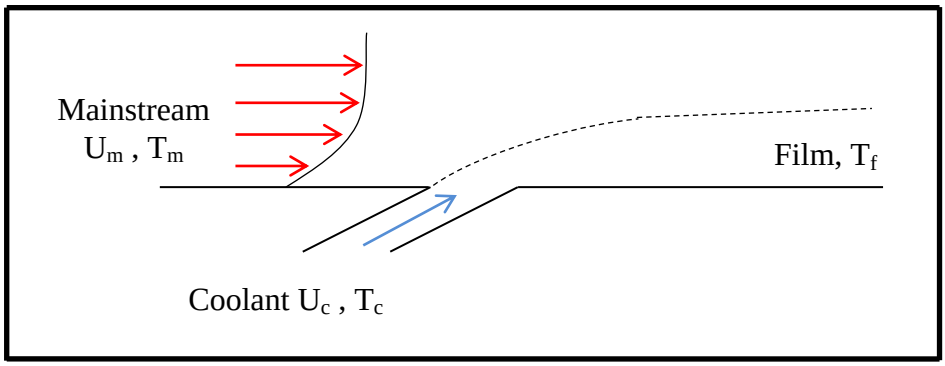

Figure (4-10): Film cooling over a flat plate

Now, in addition to the mainstream flow, secondary flow is also presented. In this case, three different temperatures are to be considered, such as the mainstream temperature (T_m), the coolant temperature (T_c), and the wall temperature (T_w). In film cooling situations, the mainstream temperature in equation (4-6) has to be replaced by a film temperature (T_f)

$$\frac{T_w - T_i}{T_f - T_i} = 1 - \exp\left[\frac{h^2 \alpha t}{K^2}\right] erfc\left[\frac{h\sqrt{\alpha t}}{K}\right] \qquad (4\text{-}9)$$

A non-dimensional temperature is defined as the film cooling effectiveness (η):

$$\eta = \frac{T_m - T_f}{T_m - T_c} \qquad (4\text{-}10)$$

The maximum value of this term could take unity, and that it is when the film temperature is equal to the coolant temperature. If the film temperature is equal to the hot mainstream temperature (without film cooling), the value of (η) is zero. From equations (4-9) and (4-10), the following equation can be obtained:

$$T_w - T_i = \left[1 - exp\left(\frac{h^2 \alpha t}{K^2}\right) erfc\left(\frac{h\sqrt{\alpha t}}{K}\right)\right][\eta T_c - (1-\eta)T_m - T_i] \quad (4\text{-}11)$$

This equation has two unknowns, the film cooling effectiveness (η) and the heat transfer coefficient (h) or if we refer to equation (4-10), the two unknowns are (h) and (T_f). We need two sets of data points to solve for the unknowns. Noting the temperature of the wall (T_w) at two different times, the value of unknowns can be determined. Thus, in the transient test, if at time (t_1), the surface is at temperature (T_{w1}) and at time (t_2), the surface is at temperature (T_{w2}), then the two events are represented by the equations (4-12) and (4-13):

$$\frac{T_{w1}-T_i}{T_f-T_i} = 1 - \exp\left[\frac{{h_f}^2 \alpha t_1}{K^2}\right] erfc\left[\frac{h_f\sqrt{\alpha t_1}}{K}\right] \quad (4\text{-}12)$$

$$\frac{T_{w2}-T_i}{T_f-T_i} = 1 - \exp\left[\frac{{h_f}^2 \alpha t_2}{K^2}\right] erfc\left[\frac{h_f\sqrt{\alpha t_2}}{K}\right] \quad (4\text{-}13)$$

Basically, two events are measured at every point leading to the solution of both (h) and (T_f) from the simultaneous solution of the equations (4-12) and (4-13). Measuring these two events at every point and solving above equations, the value of (h) and (T_f) can be found out. This method is presented by Vedula and Metzger [67] and Ekkad et al. [68]. In the transient test, the mainstream will be heated, and the coolant supply will be near room temperature. Two IR images at the same location of the surface temperature distributions are captured at the transient test, then (T_f) and (h) and hence (η) can be found out from a single test.

New parameter known as the net heat flux ratio, defined by Sen et al. and Ekkad [16, 69], is used to study the combined effect of film cooling effectiveness and heat transfer coefficient.

Net heat flux ratio is the ratio of heat flux to the surface with film cooling to the heat flux without film cooling. Its definition is given by the following equation:

$$\frac{q}{q_o} = \frac{h}{h_o}\left(1 - \frac{\eta}{\emptyset}\right) \quad (4\text{-}14)$$

Where $\emptyset$ is the overall cooling effectiveness given by [16]:

$$\emptyset = \frac{T_f - T_c}{T_m - T_c} \quad (4\text{-}15)$$

This heat flux ratio indicates the reduction in heat flux on the test surface from the film injection. If the value of this net heat flux ratio is less than 1.0, then the introduction of film cooling has beneficial effect. If the value is greater than 1.0, it can be said that the film cooling did not serve its purpose of cooling.

MATLAB program Software is prepared using a semi-infinite solid assumption presented to solve the above equations; program flow chart is presented in Appendix (E).

The experiment data used to introduce the local heat transfer coefficient ratio and the local net heat flux ratio for the selected area then saved as Excel table.

4.8 Uncertainty Analysis

In order to determine the accuracy of this study, an error analysis is performed using the methodology given by Kline and McClintock [70], this method is the standard procedure to measure uncertainty of the result from a single test. First, a conservative error estimate of the measured quantities was done. Then, the relative uncertainties in measured quantities were calculated. Finally, the average uncertainties of the results were calculated by taking the square root of the summation of the square of all the relative uncertainties.

Heat transfer coefficient for flow over flat surface was calculated using the following equation:

$$\frac{T_w - T_i}{T_m - T_i} = 1 - \exp\left[\frac{h^2 \alpha t}{k^2}\right] erfc\left[\frac{h\sqrt{\alpha t}}{k}\right] \quad (4\text{-}16)$$

Or

$h = f\,(T_w, T_i, T_m, \alpha, k, t)$

Error estimates of each variable are as follows:

$\Delta T_w = 0.5\ ^{o}\text{C}$ (IR camera specification)

$\Delta T_i = 0.5\ ^{o}\text{C}$ (IR camera specification)

$\Delta T_m = -1.35\ ^{o}\text{C}$ (from calibration certificate)

$\Delta t = 1\ \text{s}$

(α) and (*k*) are tabulated values from Incropera and DeWitt [66]. As a custom, 3% relative uncertainty is assumed for both variables. The relative uncertainties of the rest variables are;

$$UT_w = \frac{\Delta T_w}{T_w} \quad (4\text{-}17)$$

$$UT_i = \frac{\Delta T_i}{T_i} \quad (4\text{-}18)$$

$$UT_m = \frac{\Delta T_m}{T_m} \quad (4\text{-}19)$$

$$Ut = \frac{\Delta t}{t} \quad (4\text{-}20)$$

$U\alpha = Uk = 0.03$

The root mean square uncertainty in calculating heat transfer coefficient over flat plate (h) is:

$$Uh = \sqrt{(UT_w)^2 + (UT_i)^2 + (UT_m)^2 + (Ut)^2 + (U\alpha)^2 + (Uk)^2} \quad (4\text{-}21)$$

In calculating heat transfer coefficient for film cooling case, the relative uncertainty related to the coolant temperature will also be added.

$\Delta T_c = 0.3\ ^{o}\text{C}$ (from calibration certificate)

$$UT_c = \frac{\Delta T_c}{T_c} \quad (4\text{-}22)$$

So, the root mean square uncertainty in calculating heat transfer coefficient for film cooling case is:

$$Uh = \sqrt{(UT_w)^2 + (UT_i)^2 + (UT_m)^2 + (UT_c)^2 + (Ut)^2 + (U\alpha)^2 + (Uk)^2} \quad (4\text{-}23)$$

The value of Uh was found out to be $\pm$8.7%.

The value of Uh_{film} was found out to be $\pm$8.9%.

Chapter Five

Results and Discussion

Chapter Five
Results and Discussion

5.1 Introduction:

In this chapter, the numerical and experimental results are presented and discussed. The film cooling effectiveness and the local heat transfer coefficient for a single row of different jet holes arrangement, and the effect of using single and double ramped hole arrangement, have been investigated at different blowing ratios. The numerical simulations for ten different models which described in chapter three have been introduced in order to predict the flow behaviour, vortex type, and vortex generated at holes and holes downstream area, and the interaction between hot mainstream and coolant jet, then to select the best models, that give best fluid flow and thermal performance, to be considered in the experimental test program.

According to the numerical simulation results, six models are selected to introduce in the test program. A single test transient IR thermograph technique is made to evaluate the heat transfer coefficient, heat flux ratio and steady-state test to estimate the adiabatic film cooling effectiveness at three different coolant-to-mainstream blowing ratios 0.5, 1.0, and 1.5.

5-2 Numerical Results

5.2.1 Verification of Numerical Simulation

The numerical approach verification of the current CFD is made by comparison with the experimental results.

The spanwise averaged film cooling effectiveness ($\bar{\eta}$) is used as the main verification parameter between the numerical and experimental results of the baseline case (model 1) for blowing ratios of 0.5 and 1.

Sample of numerical results of spanwise averaged film cooling effectiveness ($\bar{\eta}$) distribution along the normalized streamwise distance (X/D) together with some preliminary tests results and results given by Yuen et al. [26] are presented in figure (5-1). It is fair to say that the present numerical results show approximately similar trend and behaviour with slight difference in local film cooling effectiveness (η) levels for both present and Yuen et al. [26] experimental results.

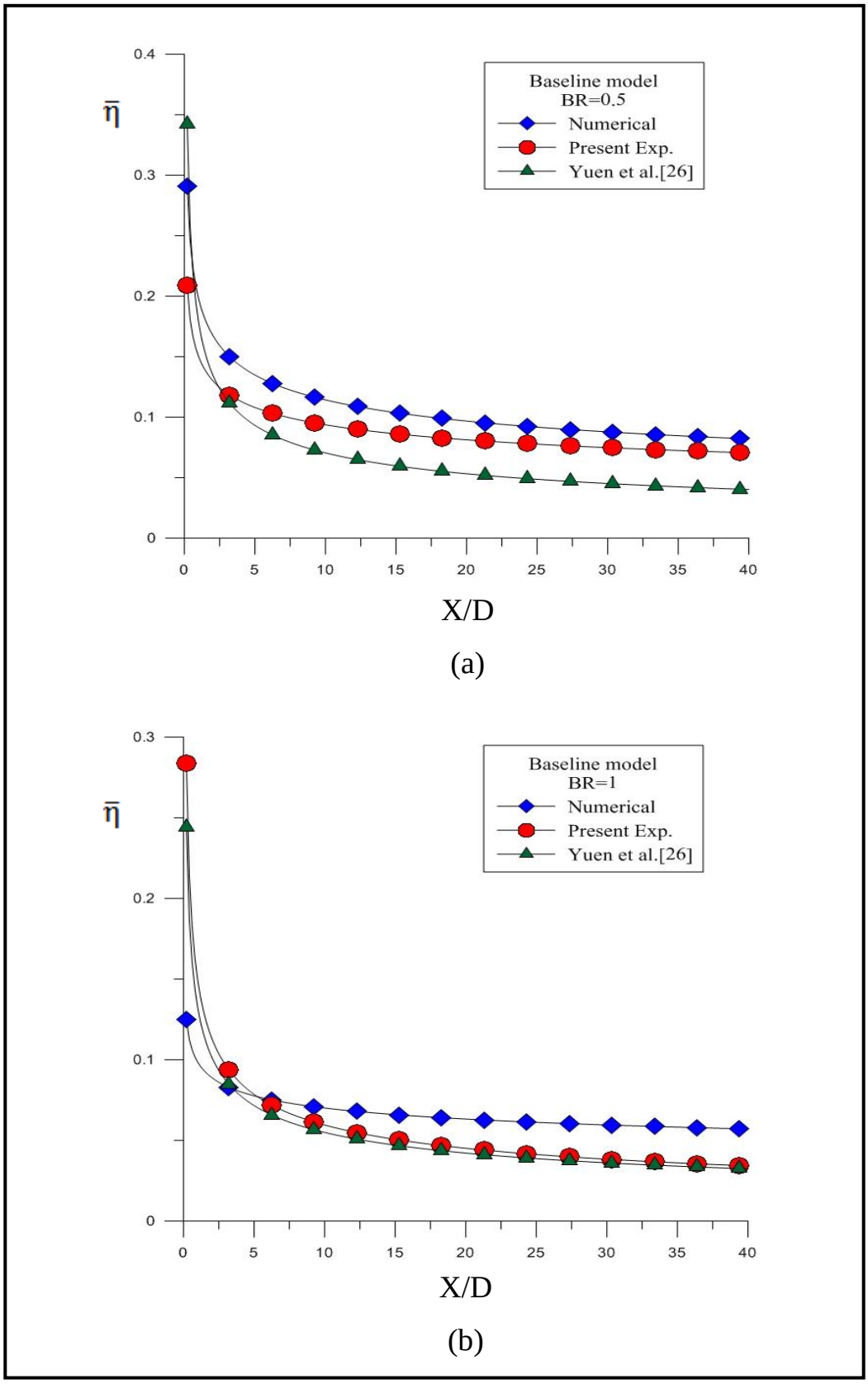

Figure (5-1): Verification of numerical results of ($\bar{\eta}$) with the experimental results (a) BR=0.5 (b) BR=1

5.2.2 Comparison of Computational Results for Conical Holes (model 5) with Cylindrical Holes Baseline (model 1)

In film cooling, the coolant is introduced to the hot stream section as cross flow jets. Different injection angles were proposed by many researchers, the optimum injection angles are found to be (30º-35º) according to Goldstein et al. and Bunker [10 and 71]. The behaviour of the flow structure is generated as a result of two flows interaction affected the performance of film cooling; therefore details of flow structure associated with this interaction should be highlighted and discussed in details. The interaction of the coolant jets with hot mainstream in three dimensional domains is a very complex flow regime, for simplicity and to make the flow recognizable and readable, the flow will be presented in two dimensions in a plane perpendicular and parallel to the cross flow at different plane location. These planes are captured from the computation approach using computer code Tec plot (360).

Figure (5-2) presents the main flow features of a single cylindrical hole (model 1) and conical hole (model 5), both holes are at injected angle 35^{o} in the direction of hot mainstream, at three blowing ratios of 0.5,1, and 1.5. The jet cross flow interaction generates a turbulent flow, which is dominated by coherent motion. In general, multiple vortex structures are produced where two large vortex structures have been detected, counter rotating vortex pair (CVP), i.e., kidney vortices and horseshoe vortices. The vortex main structures are originated from the holes rims at (X/D=0), as shown in a figure (5-3). This is agree with most literature as Friedrichs and Haven et al. [4 and 8], while some literature claimed that these kidneys vortex may be generated within the hole core according to the magnitude of the momentum ratio. Immediately downstream the hole, the vortices generation has an effect on the distribution of film coolant over the surface being protected. The

aerodynamics of these vortices depends upon the shape of the film cooling holes and blowing ratio. In both models, the (CVP) is the largest vortex appeared in the flow structure, which occurs at the interaction of coolant jet and hot mainstream, as shown in figure (5-3). This figure shows clearly the differences between the counter rotating vortices that generated in (model 1) and (model 5). The distance between the center of (CVP) generated by conical hole is wider than that of cylindrical hole, this causes wide coolant penetration in spanwise direction, so the spanwise (lateral) averaged adiabatic film cooling effectiveness ($\bar{\eta}$) may be improved.

The jet lift-off phenomenon caused by kidney vortices typically occurs at moderate and high blowing ratios, i.e., BR more than 0.5. For low blowing ratio, the momentum ratio is also very low; the hot mainstream flow departs the upward flow pushing the coolant jet towards the surface. This occurs in the cylindrical and conical hole producing low jet vortices levels, and the coolant stays attached to the surface providing good film cooling effectiveness. But at high blowing ratio, the coolant jet has high vortices levels in the cylindrical hole, and then the coolant lifted-off from the surface providing poor film cooling effectiveness. But in the conical hole case and due to the divergent passage, the coolant jet does not have high vortices levels as shown in figure (5-4), so in this case it's providing a good film cooling effectiveness. These results agree well with the results of Yuen et al. [26].

As the vortex propagates downstream the hole, the vortex grows continually downstream, the cooling jet is mixed and entrained with the hot mainstream and the coolant jet has been lifted off from the surface. This may indicate rapid dissipation of the film cooling downstream, especially at high blowing ratio, as shown in figures (5-5) and (5-6). And this is confirmed by figures (5-2) and (5-7), in which figure (5-7) presents a comparison of film cooling effectiveness contours between model 1 and

model 5 downstream the test surface of the holes for all blowing ratios, the overall area-averaged film cooling effectiveness ($\bar{\bar{\eta}}$) values are also given and labeled in this figure. It is clear from this figure that the film cooling effectiveness of model 5 is higher than that given by model 1, particularly at moderate and high blowing ratios of 1and 1.5.

For comparison purposes, the streamwise (centerline) averaged adiabatic film cooling effectiveness ($\bar{\eta}_c$) , the spanwise (lateral) averaged adiabatic film cooling effectiveness ($\bar{\eta}$), and the total area-averaged film cooling effectiveness ($\bar{\bar{\eta}}$) are used as the main comparison parameters between the numerical results of model 1 and model 5, at blowing ratios of 0.5, 1, and 1.5. This comparison is given in figures (5-8 to 5-13), the immediate decreasing of streamwise film cooling effectiveness is due to either hot stream penetration into coolant jet (at low blowing ratio) or due to cooling jet lift-off from surface (at high blowing ratio). For model 1, the effectiveness rapidly decreased at blowing ratio of 1.5 due to high lifting-off, as shown in figures (5-12) and (5-13), this behaviour not appears in model 5.

Figures (5-14) and (5-15) present the effect of blowing ratio on the adiabatic film cooling effectiveness for model 1 and model 5 respectively, model 5 showed higher film cooling effectiveness than model 1 in all blowing ratios; both models showed a droop behavior of film cooling effectiveness with increasing the blowing ratio, as shown in figure (5-16).

As a summery, model 1 provided a very weak cooling effectiveness, particularly at high blowing ratio. At blowing ratio of 0.5, model 1 provided a streamwise averaged film cooling effectiveness ($\bar{\eta}_c$) of 0.3224 and a total area-averaged film cooling effectiveness ($\bar{\bar{\eta}}$) of 0.0934, while model 5 provided 0.5055 for the ($\bar{\eta}_c$) and 0.1992 for the ($\bar{\bar{\eta}}$), here

the enhancement for ($\bar{\eta}_c$) is 56.8%, and 113.3 % for the ($\bar{\bar{\eta}}$). At blowing ratio of 1, model 1 provided a streamwise averaged film cooling effectiveness ($\bar{\eta}_c$) of 0.228 and a total area-averaged film cooling effectiveness ($\bar{\bar{\eta}}$) of 0.0632, while model 5 provided 0.4623 for ($\bar{\eta}_c$), and 0.1602 for ($\bar{\bar{\eta}}$), the enhancement for ($\bar{\eta}_c$) is 102.3% and 153.5.9% for the ($\bar{\bar{\eta}}$). At blowing ratio of 1.5, the enhancements in the film cooling effectiveness when using a conical hole compared with a cylindrical hole increased to 175.5% for ($\bar{\eta}_c$) and 227.1% for the ($\bar{\bar{\eta}}$). All details of the above comparisons are tabulated in Table (5-1).

Table (5-1): Summery of numerical results

Model	BR	$\bar{\eta}_c$	% enhancement in $\bar{\eta}_c$	$\bar{\bar{\eta}}$	% enhancement in $\bar{\bar{\eta}}$
Model 1	0.5	0.3224	-	0.0934	-
	1	0.2281	-	0.0632	-
	1.5	0.1154	-	0.0366	-
Model 2	0.5	0.2155	-33.2	0.1512	61.9
	1	0.2633	15.4	0.1288	103.8
	1.5	0.1741	50.8	0.0741	102.5
Model 3	0.5	0.1347	-58.2	0.1361	45.7
	1	0.2622	14.9	0.1785	182.5
	1.5	0.2221	92.4	0.1212	231.1
Model 4	0.5	0.1508	-53.2	0.1348	44.3
	1	0.2813	23.3	0.195	208.5
	1.5	0.2794	142.1	0.1712	367.8
Model 5	0.5	0.5055	56.8	0.1992	113.3
	1	0.4623	102.7	0.1602	157.1
	1.5	0.318	175.5	0.1197	227.1
Model 6	0.5	0.3414	5.9	0.2374	154.2
	1	0.443	94.0	0.2246	255.4
	1.5	0.3402	194.7	0.1692	362.3
Model 7	0.5	0.2474	-23.3	0.227	143.0
	1	0.3823	67.6	0.2626	321.5
	1.5	0.3446	198.6	0.2294	526.8
Model 8	0.5	0.2492	-22.7	0.2313	147.6
	1	0.3907	21.2	0.2473	291.3
	1.5	0.3411	195.6	0.2006	448.1
Model 9	0.5	0.3505	8.7	0.2257	141.7
	1	0.3895	20.8	0.2299	263.8
	1.5	0.3488	202.3	0.1879	413.4
Model 10	0.5	0.2425	-24.8	0.2268	142.8
	1	0.3719	63.0	0.2947	373.0
	1.5	0.3855	234.1	0.2809	667.5

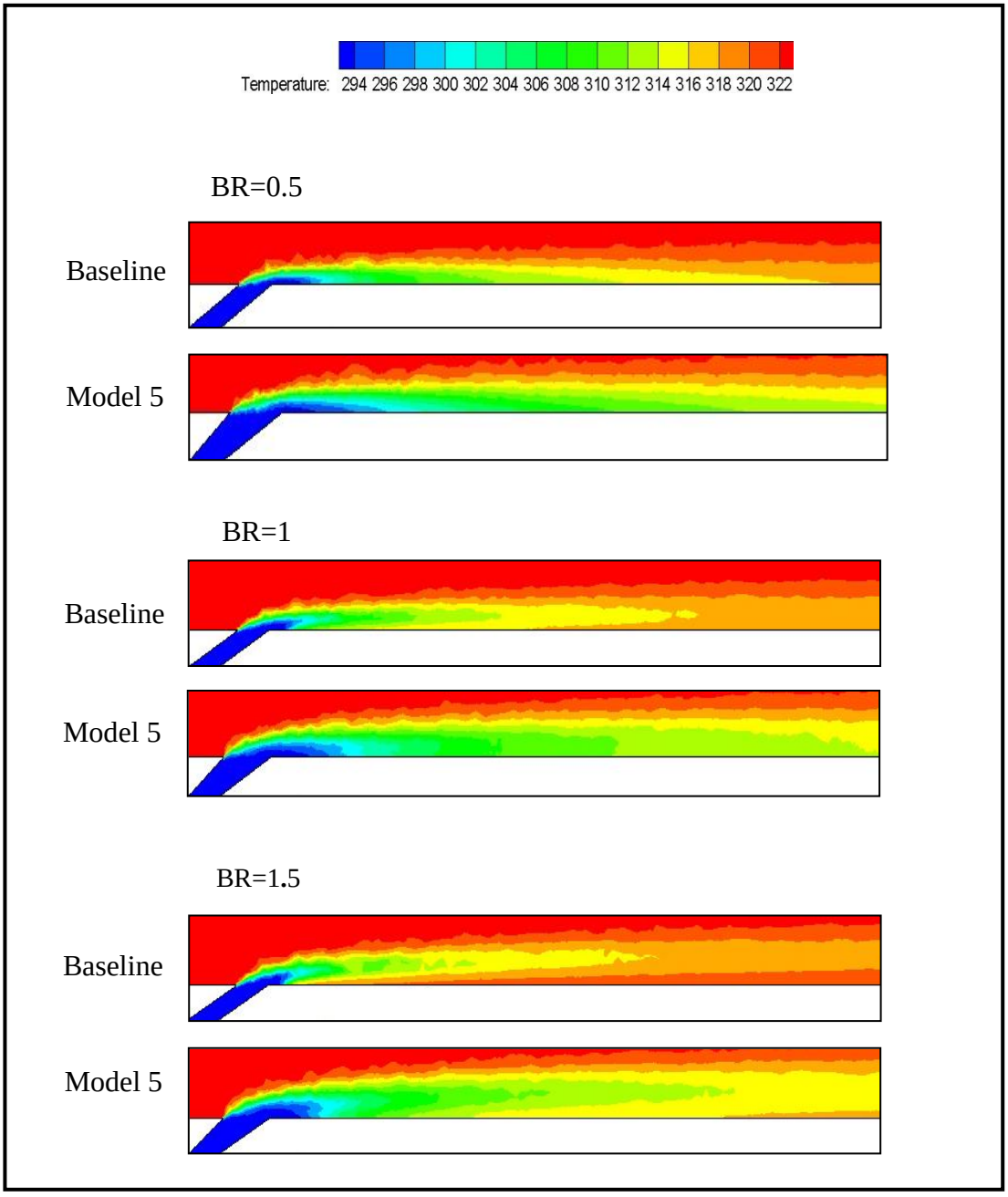

Figure (5-2): Mainstream and coolant jet interaction contour distribution at centre (X-Y) plane of a single hole injection at different BRs

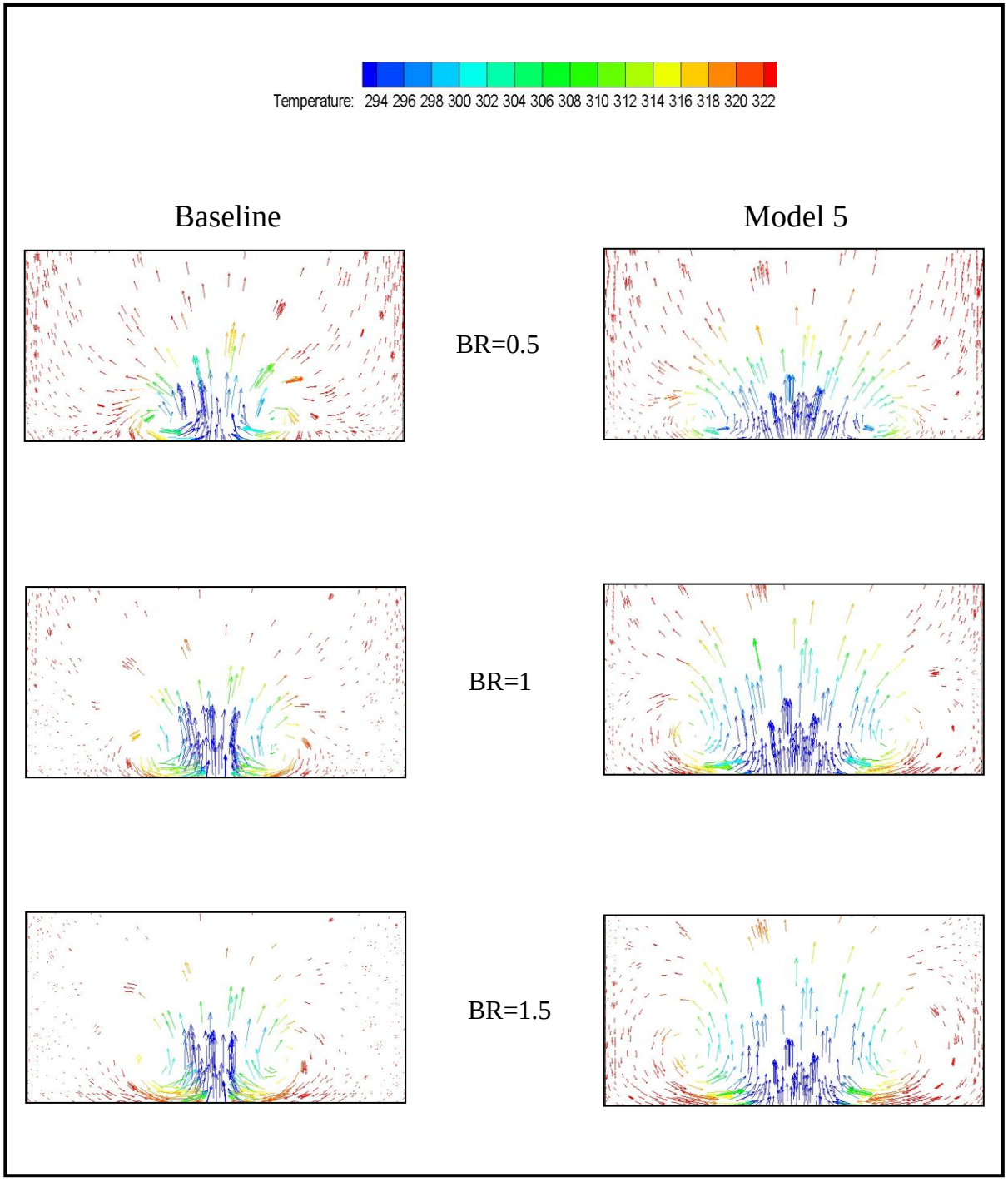

Figure (5-3): Comparison of flow vectors coloured by temperature at X/D=0 (Y-Z plane) for model 1 (baseline) and model 5 at different BRs.

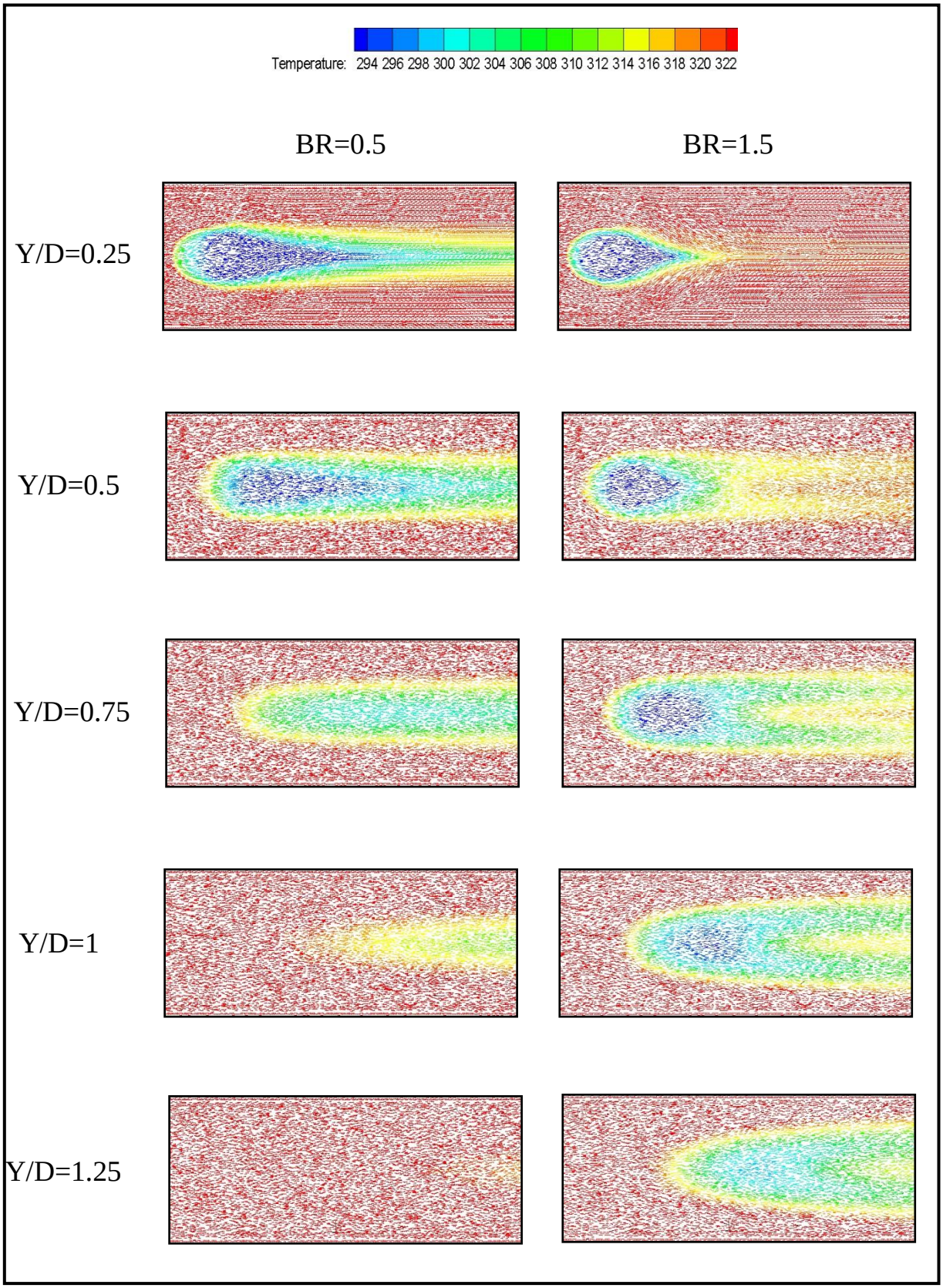

Figure (5-4): Flow vectors colored by temperature at different planes parallel to test surface (X-Z plane) for single hole injection at BR=0.5 and BR=1.5

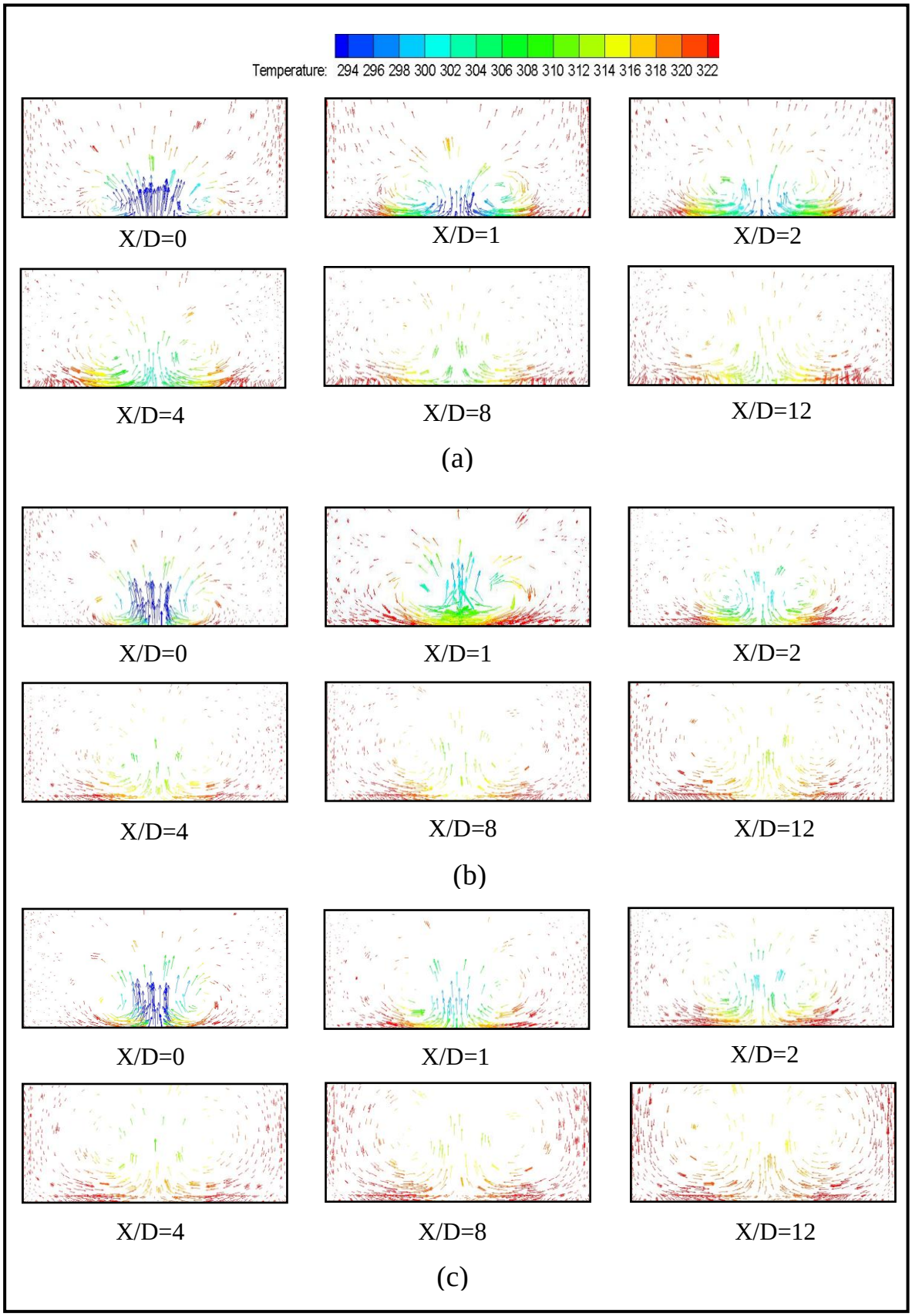

Figure (5-5): Vortex propagation coloured by temperature downstream the hole for model 1 at (Y-Z) planes (a) BR=0.5 (b) BR=1(c) BR=1.5

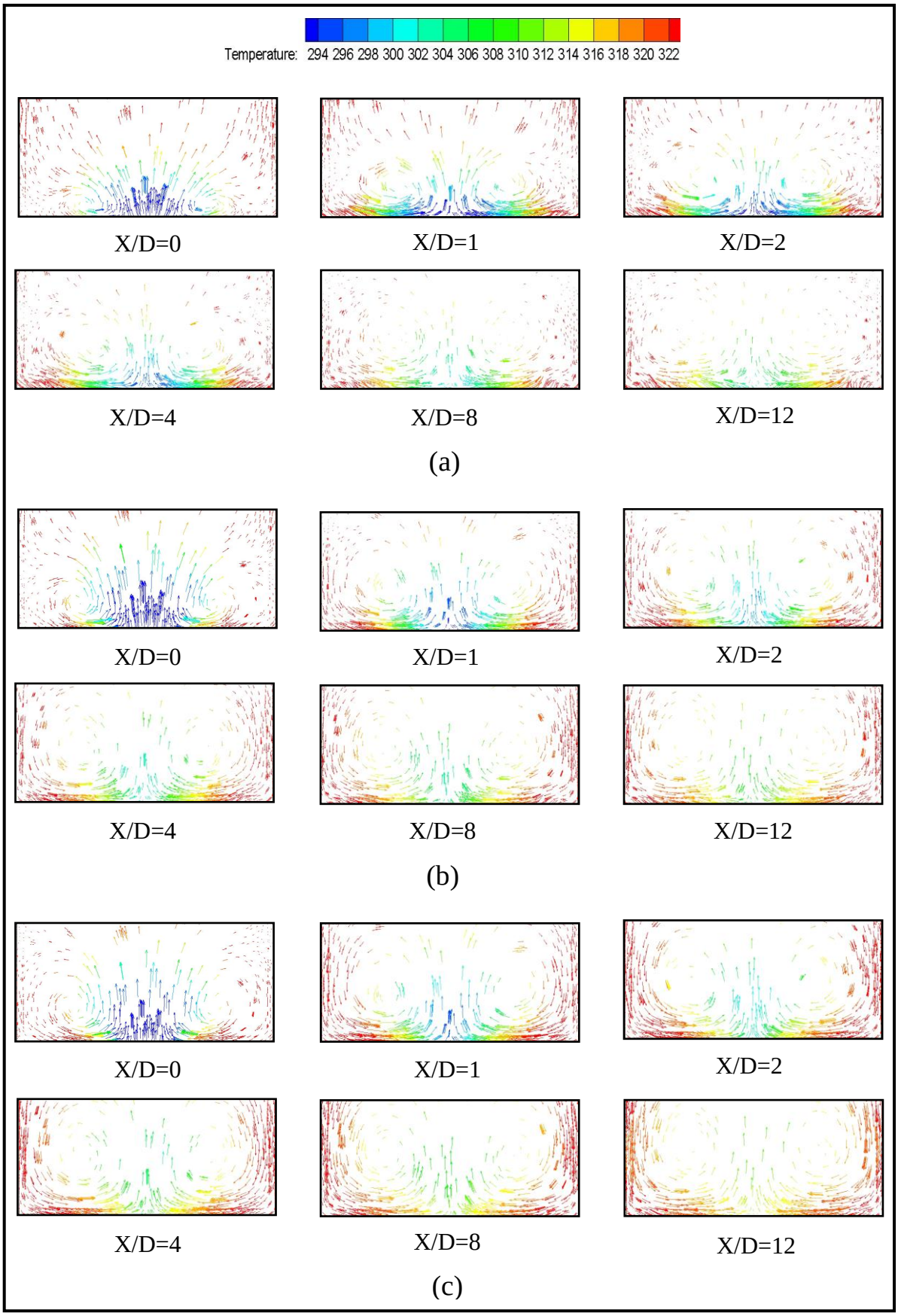

Figure (5-6): Vortex propagation coloured by temperature downstream the hole for model 5 at (Y-Z) planes (a) BR=0.5 (b) BR=1(c) BR=1.5

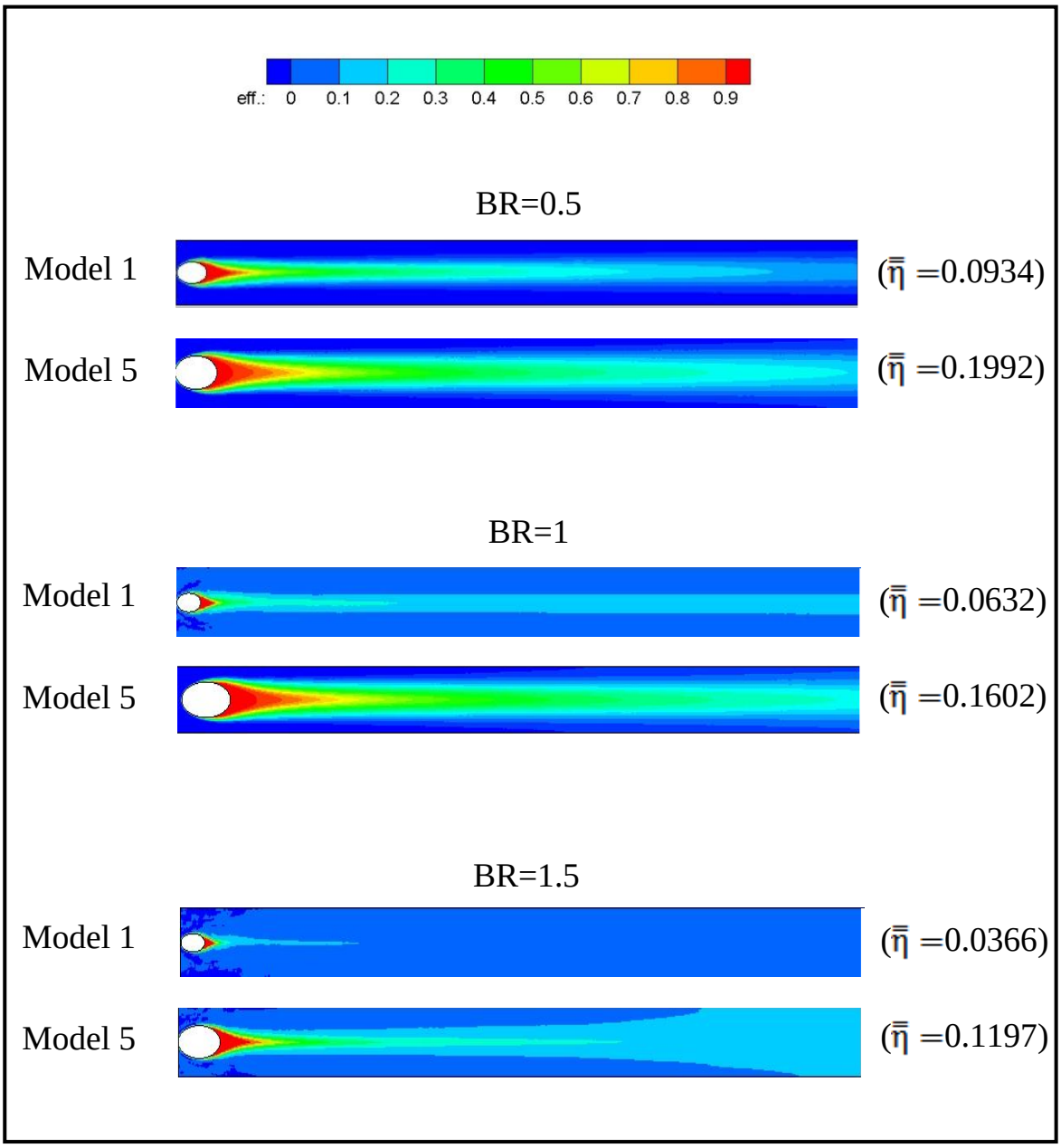

Figure (5-7): Comparison of film effectiveness distribution and ($\bar{\bar{\eta}}$) between model 5 and model 1 at different BRs

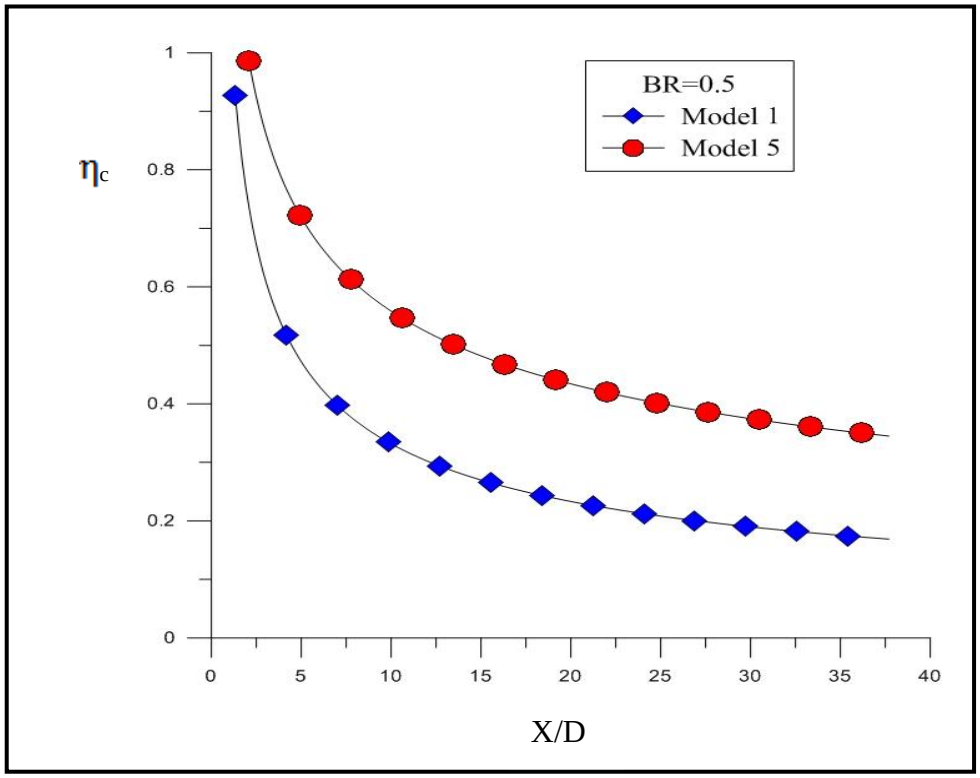

Figure (5-8): Comparison of (η_c) versus (X/D) between model 1 and model 5 at BR=0.5

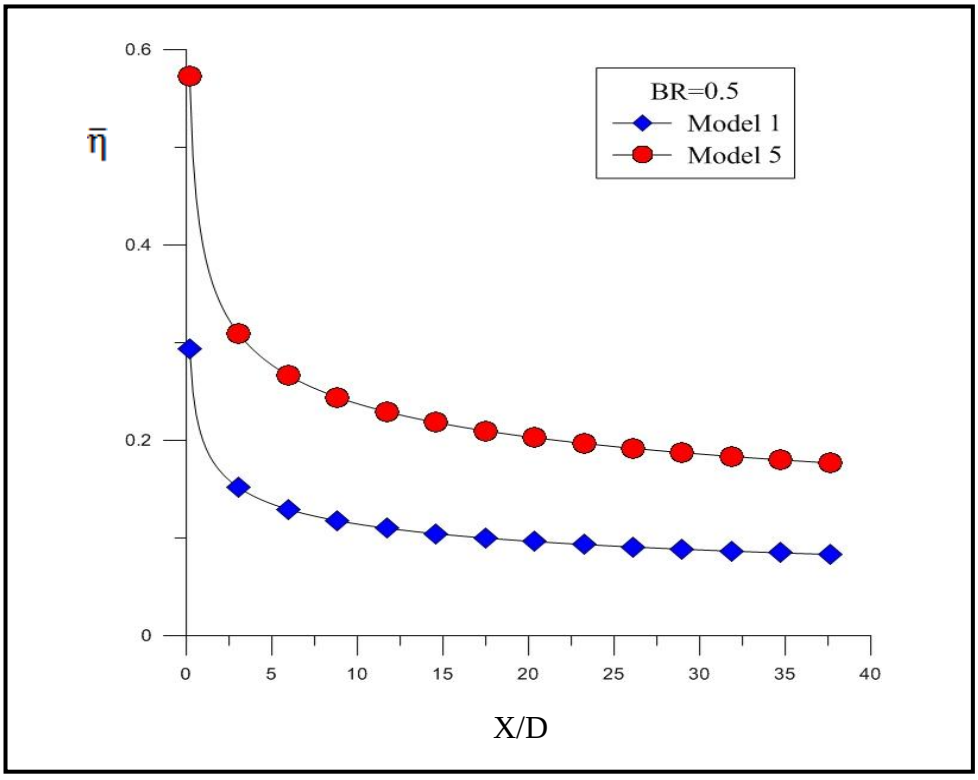

Figure (5-9): Comparison of ($\bar{\eta}$) versus (X/D) between model 1 and model 5 at BR=0.5

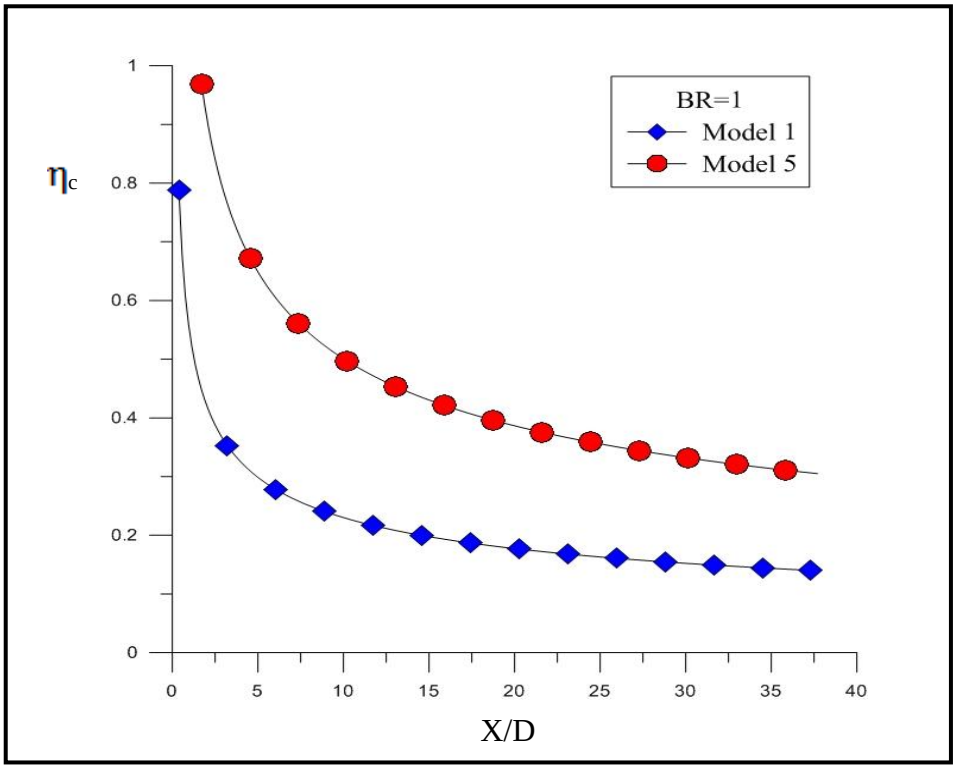

Figure (5-10): Comparison of (η_c) versus (X/D) between model 1 and model 5 at BR=1

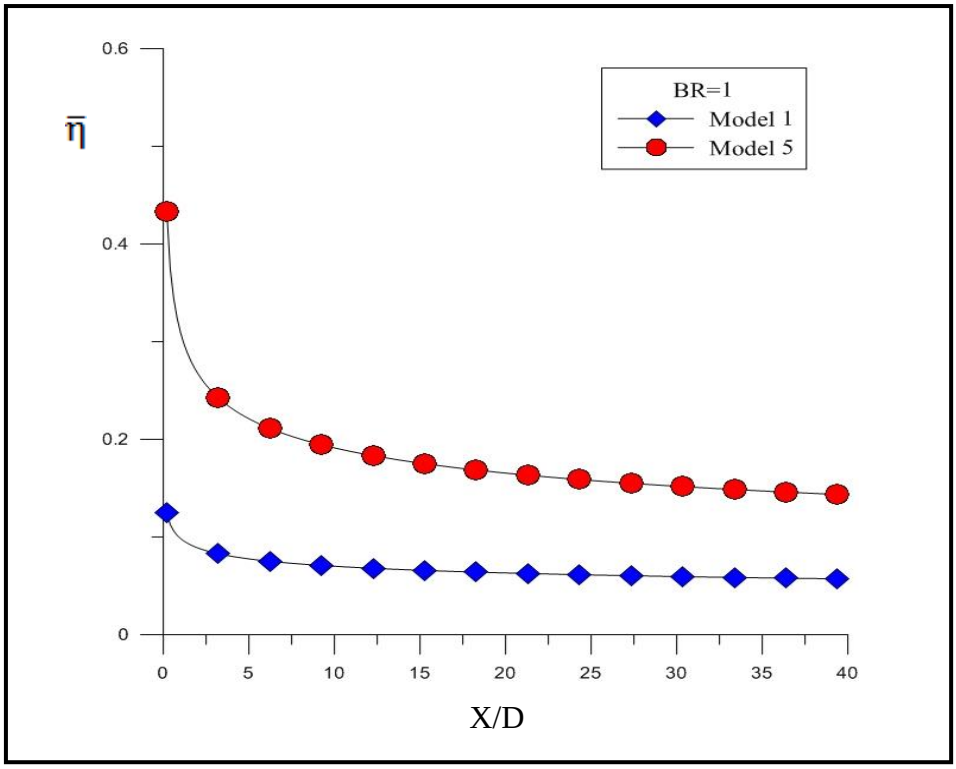

Figure (5-11): Comparison of ($\bar{\eta}$) versus (X/D) between model 1 and model 5 at BR=1

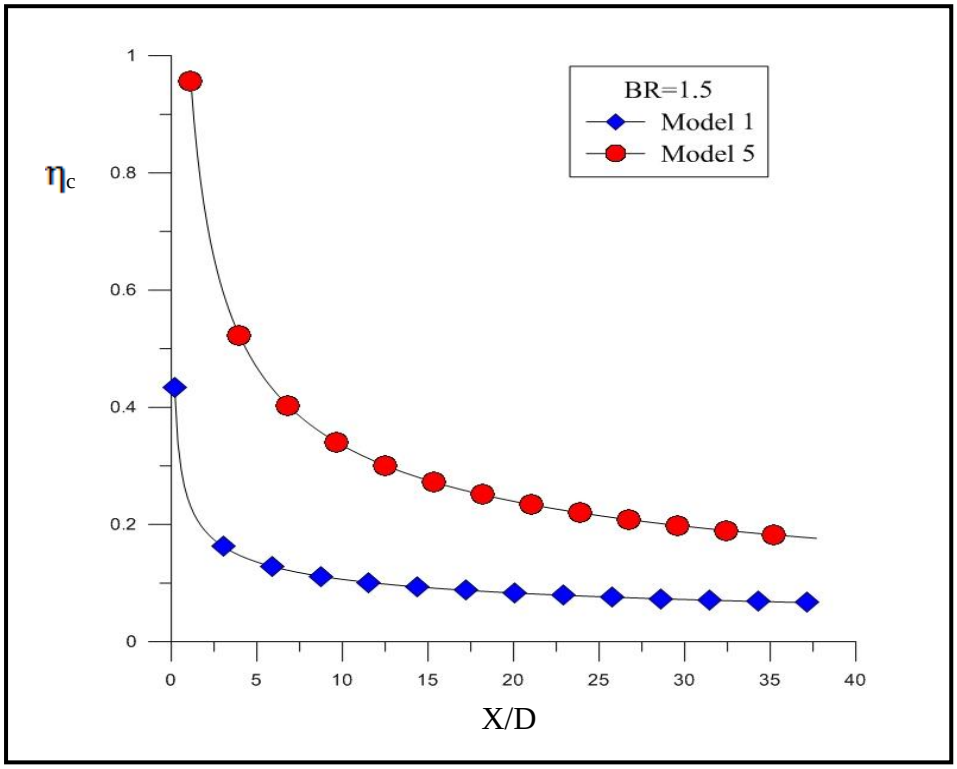

Figure (5-12): Comparison of (η_c) versus (X/D) between model 1 and model 5 at BR=1.5

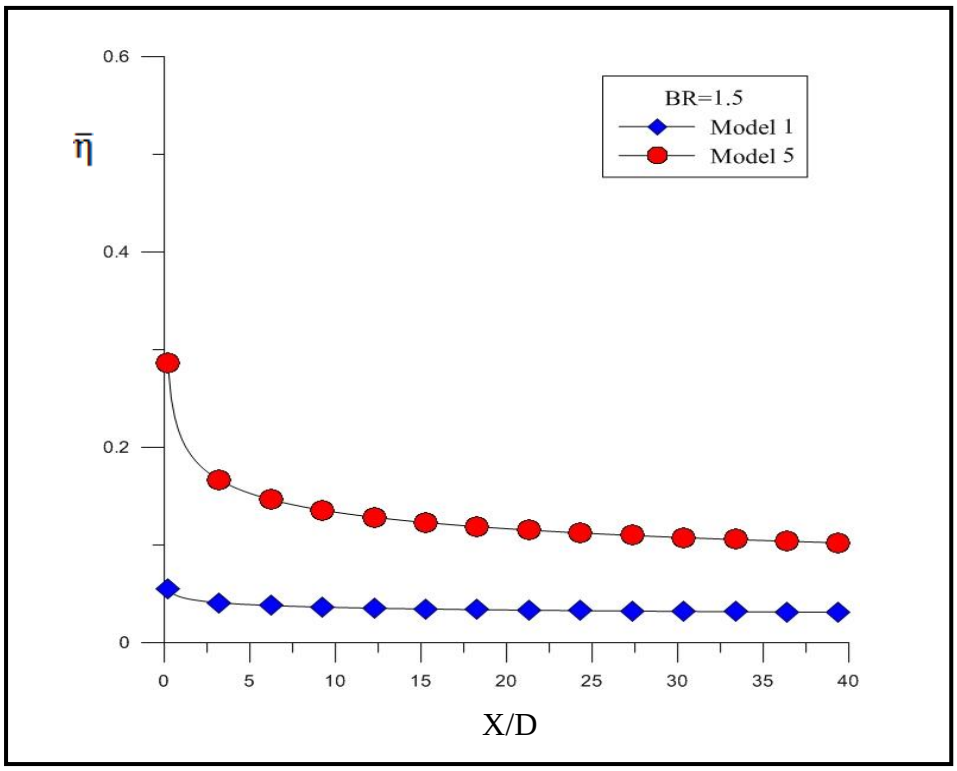

Figure (5-13): Comparison of ($\bar{\eta}$) versus (X/D) between model 1 and model 5 at BR=1.5

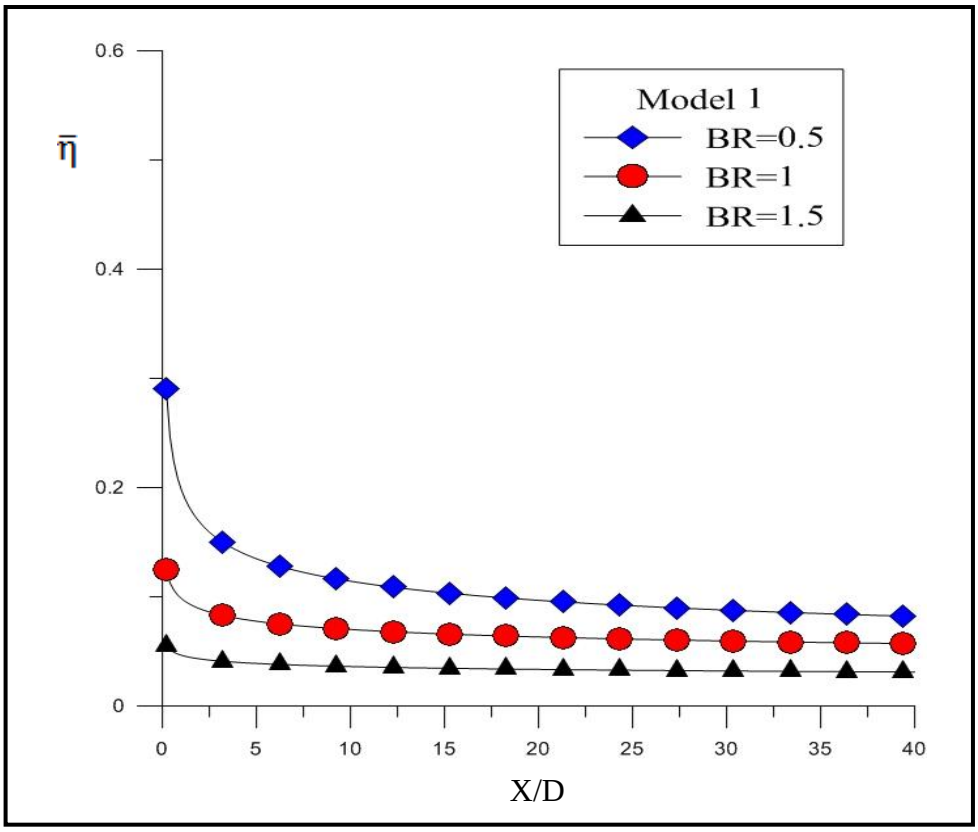

Figure (5-14): Effect of blowing ratio on the ($\bar{\eta}$) for model 1

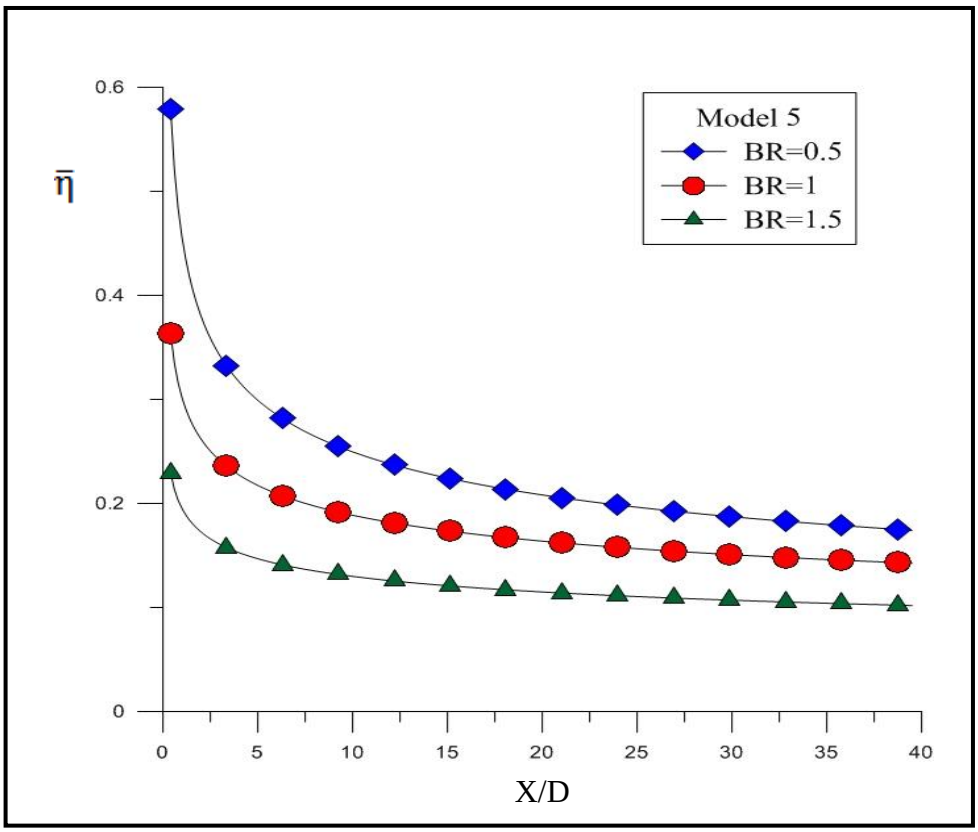

Figure (5-15): Effect of blowing ratio on the ($\bar{\eta}$) for model 5

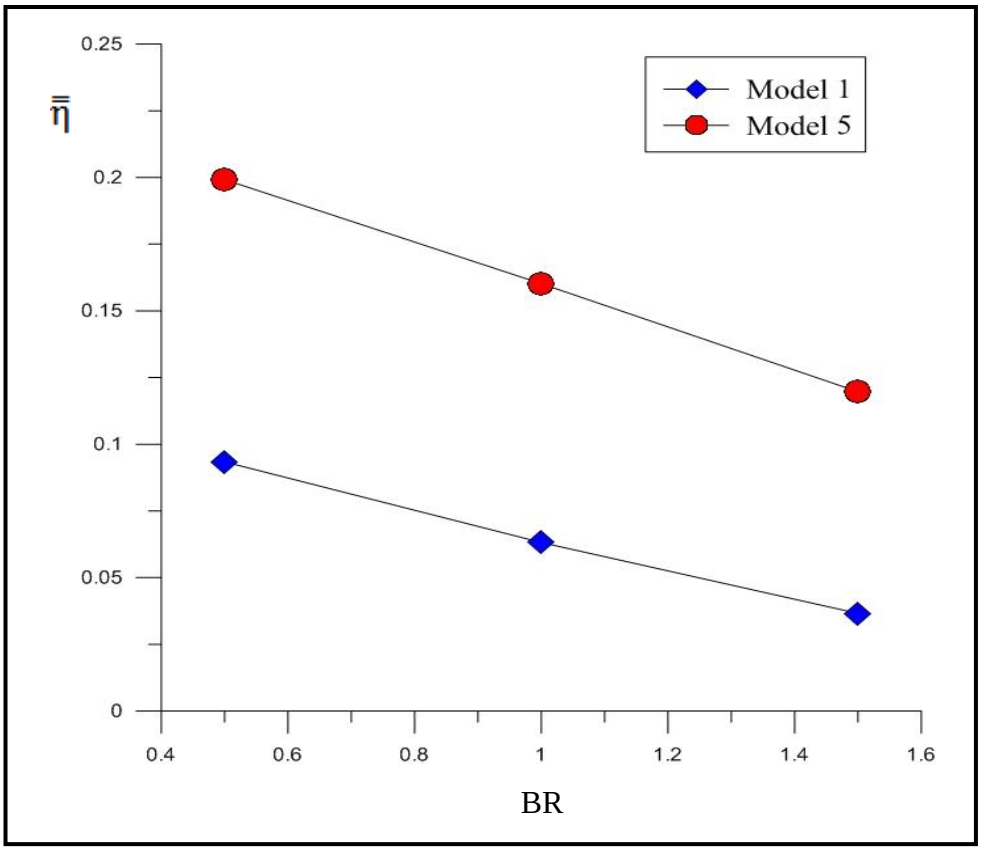

Figure (5-16): Effect of blowing ratio on the ($\bar{\bar{\eta}}$) for model 1 and model 5

5.2.3 The Effect of Using Single and Double Ramps on the Film Cooling Effectiveness

The effects of using ramps with cylindrical or conical holes were studied and compared with the baseline case. In this section, the nature of the flow induced by an upstream and downstream ramp is described first. Afterwards, its effects on the film cooling effectiveness are presented.

5.2.3.1 Effect of Using Single Upstream Ramp with Cylindrical and Conical Holes

Figure (5-17) shows the pressure distribution over the plate surface for all models under consideration, it can be observed that when there is no ramp, a significant pressure rise occurs just upstream the hole leading edge at the mainstream-cooling jet interaction. While with presence of ramps, the pressure around the hole is significantly reduced,

particularly at the cylindrical hole leading edge, the reduction in pressure is due to that the mainstream flow being diverted upward by the ramp. The interaction between the mainstream and the film-cooling jets occurred at a distance far away from the downstream of the leading edge. Also, it can be seen that the ramp increases the pressure upstream the ramp step, and the pressure is decreased downstream at the backward-facing step. The coolant therefore penetrated laterally around the hole and at the ramp backward-facing area at the low pressure zone.

A sample of numerical results of the velocity vector on the (Y-Z) plane is presented in figure (5-18) at BR=1. At X/D=0 plane, the velocity vector shows clearly the difference between the counter rotating vortex that generated between model 2 and model 6. The vortex generated at the ramped hole moves up from the surface causing a wide coolant penetration in spanwise direction as compared with baseline model, especially for conical ramped-holes case (model 6).

Figure (5-19) shows the effect of the presence of ramp on the velocity vectors created at the hole, it can be seen that there is a separated region (i. e., low pressure zone) that extends from the backward-facing step ramp. When the mainstream deflected upwards by ramp, the cooling jet flows easily through the cooling hole, as shown in figure (5-19). The large separated region at the film cooling hole for model 1 essentially disappears with presence of ramp according to Sangkwon and Shih [42]. For model 1, the net pressure force on the cooling jet is high, which bends the jet toward the plate surface, creating a large separated region in the film cooling hole area and thereby reducing the effective flow cross-sectional area. With presence of upstream ramp, the cooling jet does not deflect by the mainstream flow until a further distance, so that the effective cross-sectional area for flow is higher, which reduces the speed of coolant flow and the effective blowing ratio. Thus, lateral spreading of

each cooling jet increased as a longer length that covered by the film cooling, as shown in figure (5-20).

Figure (5-21) shows the temperature contours at different streamwise locations (Y-Z) planes (X/D=0, 2, 4, 6, 8, and 10), where the majority of the variation occurs for (model 2 and model 6). It is clear that with increasing the downstream distance, the vortices are such that they lift the jets from the surface, and lesser coolant flows under the jet core which results in higher temperature along the surface and leads to lower film cooling effectiveness with increasing the distance downstream of the hole injection specially, for model 1. This can be explained by the non-dimensional temperature distributions (effectiveness) as shown in figure (5-24).

Figure (5-22) depicts the comparison of ($\bar{\eta}$) versus (X/D) for models 1, 2 and 6 at different blowing ratios, it can be seen that model 6 improved the adiabatic film cooling effectiveness better than other models, and that much greater surface about the film-cooling hole is now protected laterally by the cooling jet.

Figure (5-23) shows the effect of blowing ratio on the overall area- averaged adiabatic film cooling effectiveness ($\bar{\bar{\eta}}$), it is seen clearly from the plot that model 6 shows a higher overall area-averaged effectiveness than other models, there is slight decreasing in film cooling effectiveness at blowing ratio of 1, and slight decreasing occurred at blowing ratios of 1.5 .At blowing ratio of 0.5 the ramped-holes give the best overall area- averaged adiabatic film cooling effectiveness.

Figure (5-24) gives the comparison of film cooling effectiveness contours and overall area-averaged film cooling effectiveness ($\bar{\bar{\eta}}$) of models 1, 2, and 6 at different blowing ratios. The overall area-averaged film cooling effectiveness ($\bar{\bar{\eta}}$) for model 2 enhanced by (61.9%, 103.8%,

and 102.5%), and for model 6 enhanced by (154.2%, 255.4%, and 362.3%) over that of the baseline at (BR= 0.5, 1.0, and 1.5), respectively. All details of the above results are given in Table (5-1).

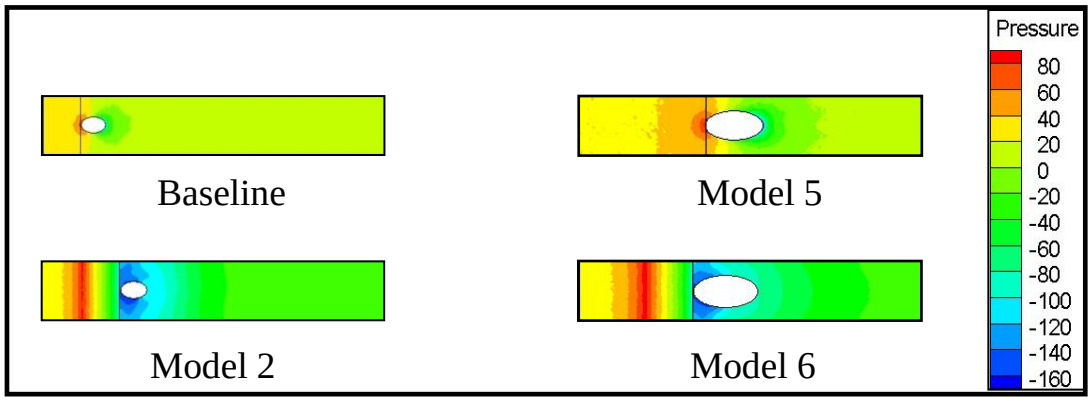

Figure (5-17): Pressure distribution on flat plate surface for different models (X-Z plane)

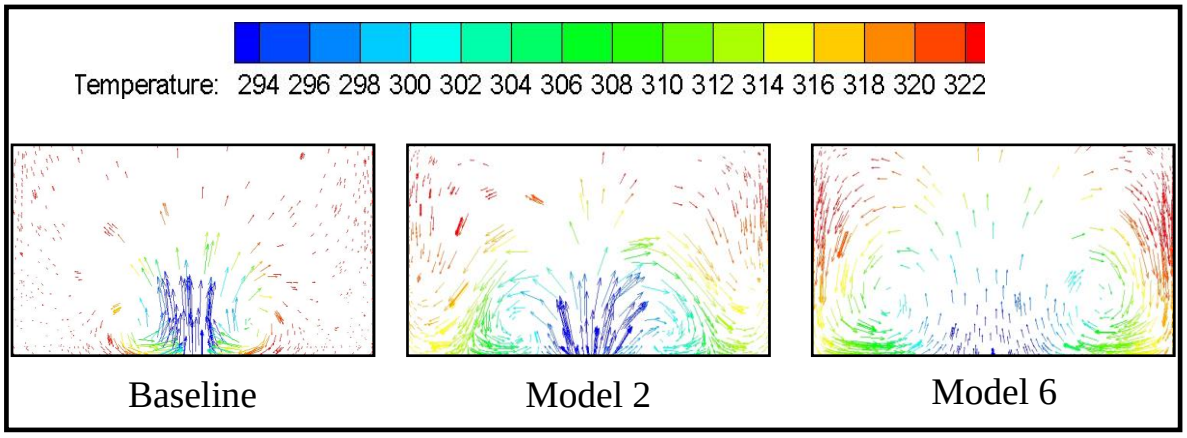

Figure (5-18): Flow vectors colored by temperature at X/D=0 (Y-Z plane) for model 1 (baseline), model 2, and model 6

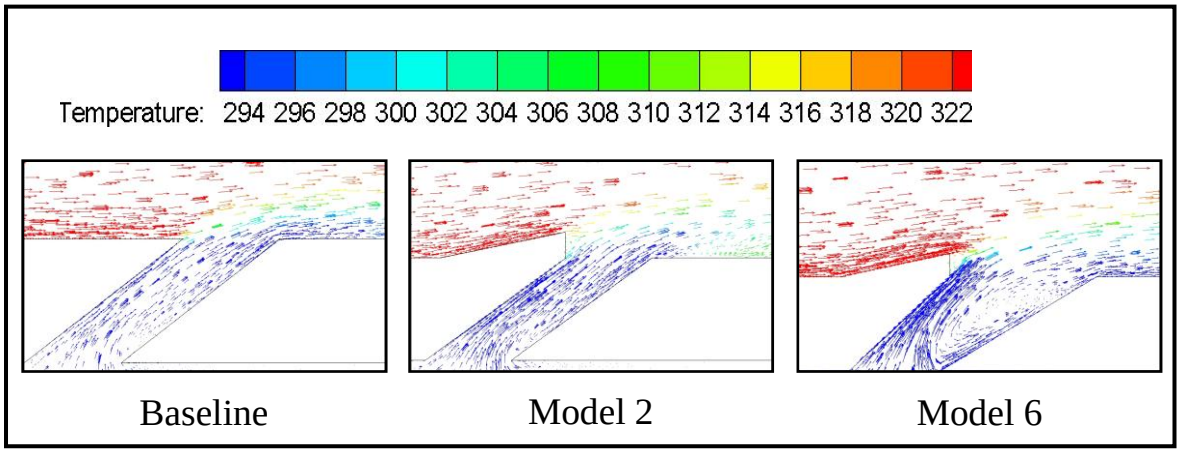

Figure (5-19): Flow vectors colored by temperature at centre (X-Y) plane for model 1 (baseline), model 2, and model 6 and at BR=1

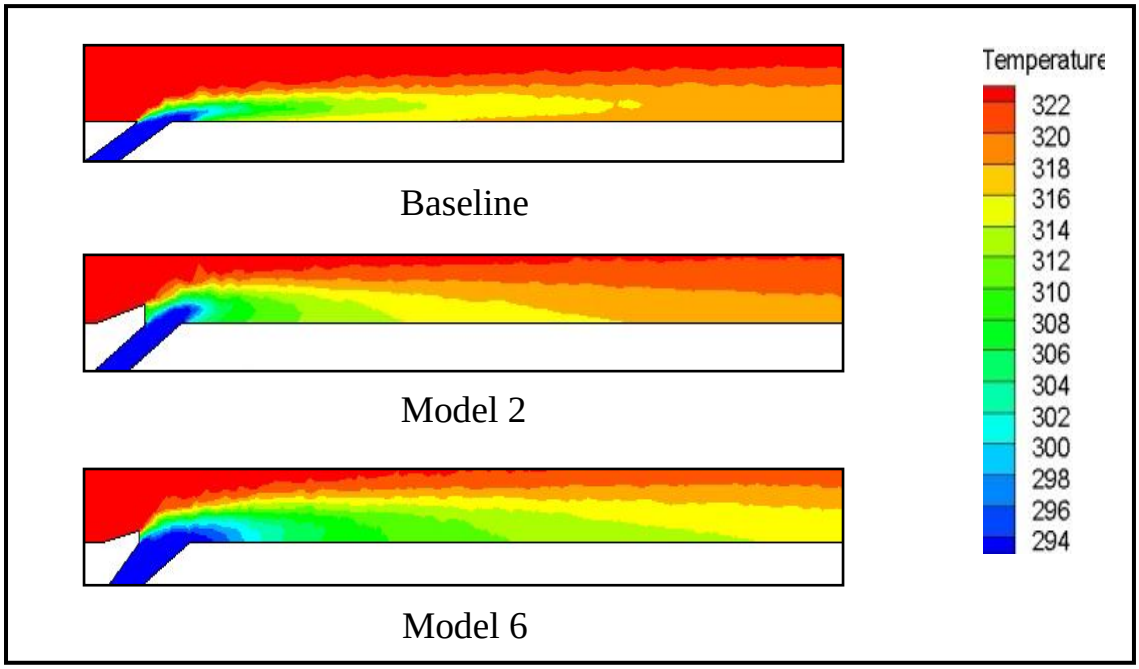

Figure (5-20): Mainstream and coolant jet interaction contour colored by temperature distribution at center (X-Y) plane of model 2 and model 6 compared with baseline at BR=1

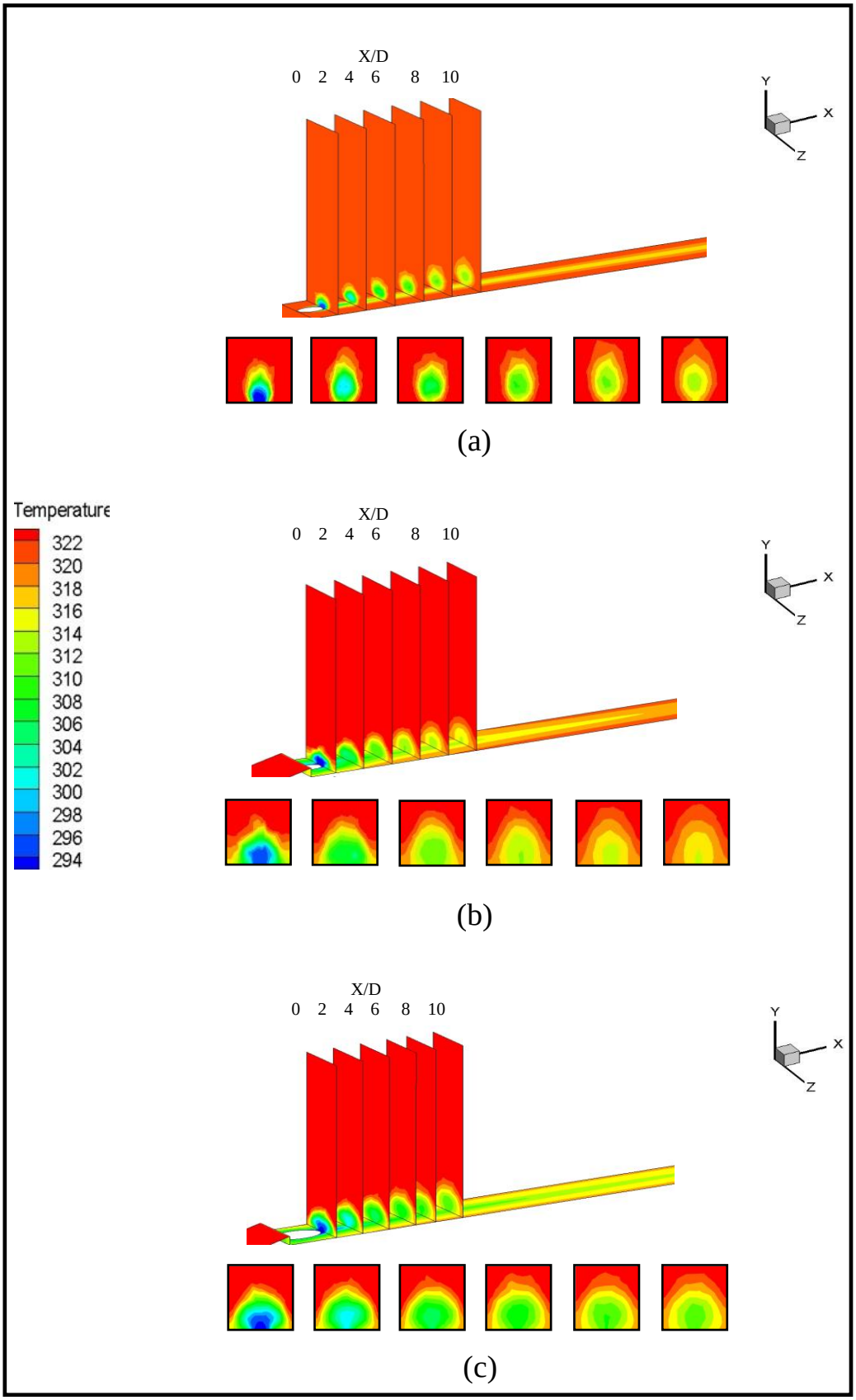

Figure (5-21): Temperature contours at different (Y-Z) planes (X/D=0, 2, 4, 6, 8, and 10) for (a) model 1 (baseline) (b) model 2 (c) model 6

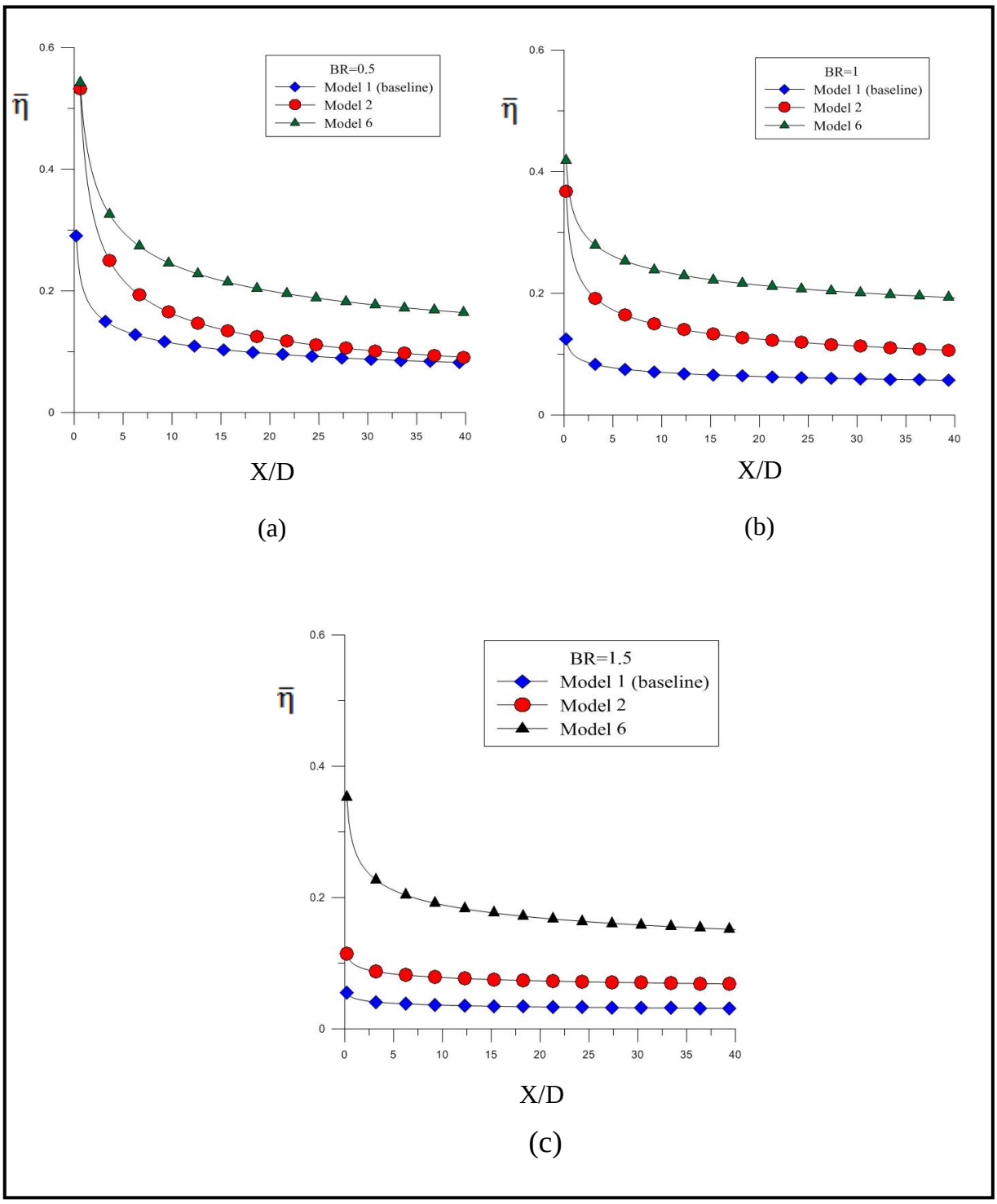

Figure (5-22) Comparison of ($\bar{\eta}$) versus (X/D) for model 1, model 2 and model 6 at (a) BR=0.5 (b) BR=1 (c) BR=1.5

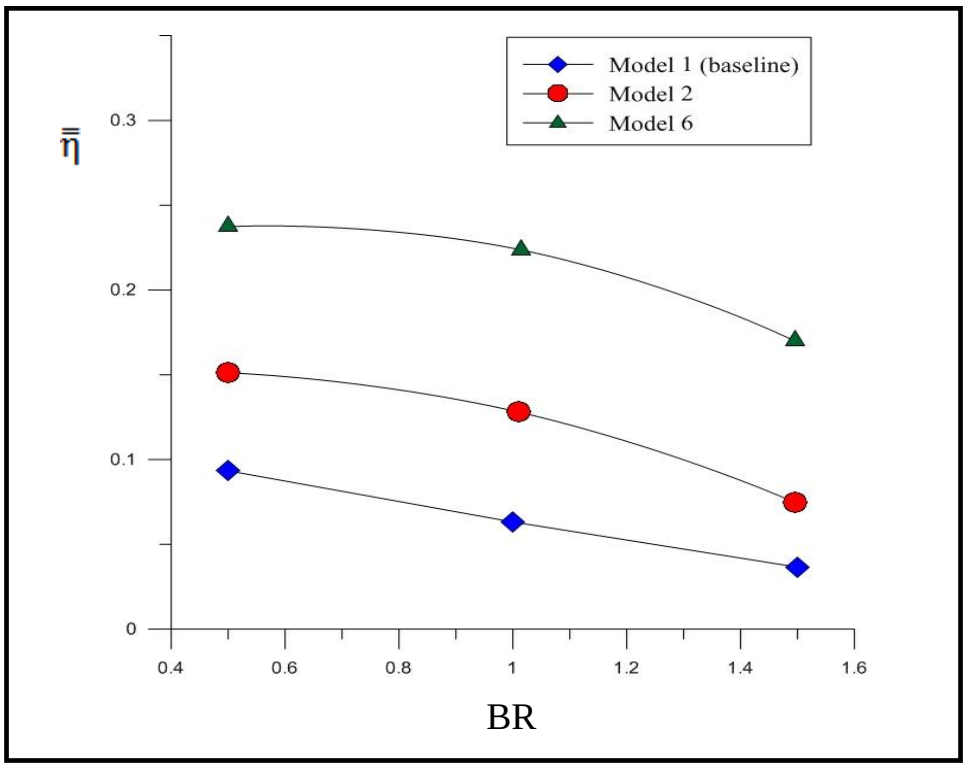

Figure (5-23): Effect of blowing ratio on the overall area-averaged film cooling effectiveness ($\bar{\bar{\eta}}$) for model 1, model 2, and model 6

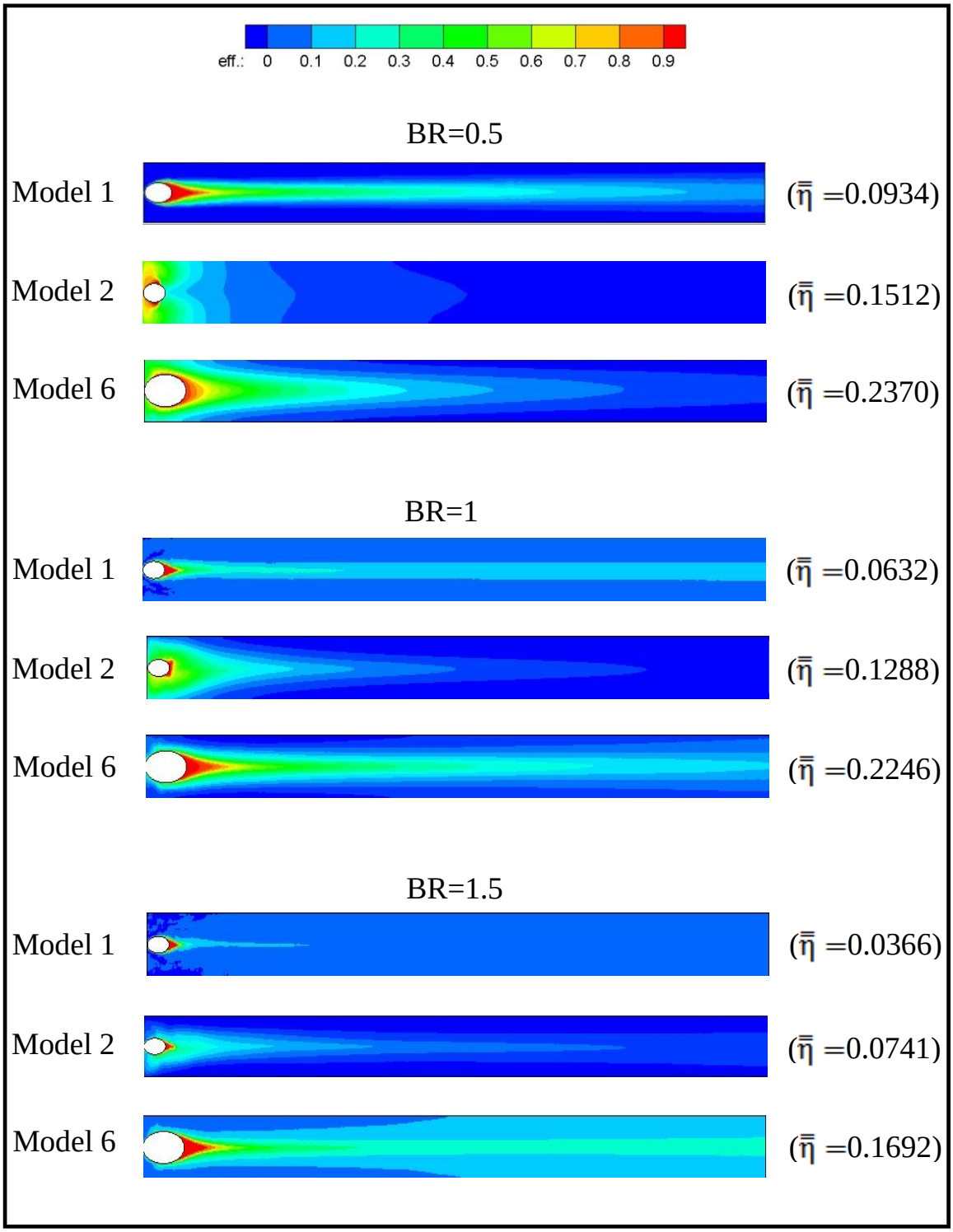

Figure (5-24): Comparison of film effectiveness contours and ($\overline{\overline{\eta}}$) between model 2 and model 6 with model 1 (baseline) at different BRs

5.2.3.2 The Effect of Ramp Angle

Figure (5-25) shows the results obtained for the spanwise averaged film-cooling effectiveness for two models at different ramp angles compared with the baseline model. It can be seen that with an upstream ramp, the adiabatic film cooling effectiveness is improved, and a wide range about the film-cooling hole is now protected by the cooling jet, including the region around the film-cooling hole area. This is consistent with the nature of the fluid flow described earlier (e.g., entrainment of coolant downstream of the ramps of backward-facing step by the recirculating flow in the separated region and the increased lateral spreading of the coolant upon exiting the film cooling hole).

Figure (5-26) reveals the effect of blowing ratio on the overall area- averaged film cooling effectiveness ($\bar{\bar{\eta}}$), the overall area-averaged film cooling effectiveness of models 1 and 2 is decrease as the blowing ratio increased. At blowing ratios of 1 and 1.5, model 3 provides higher overall area-averaged film cooling effectiveness than models 1 and 2, there is slight increase in film cooling effectiveness at blowing ratio of (1) and a slight decreasing occurred at blowing ratio of (1.5).

Figure (5-27) gives summary of the film cooling effectiveness contours and the overall area-averaged effectiveness ($\bar{\bar{\eta}}$) for different cases.

At blowing ratio of (0.5), model 2 (ramp angle of 11.3^{o}) provides the best effectiveness as compared with baseline and model 3 (ramp angle of 16.7^{o}), therefore the effectiveness enhanced by 61.9%.

At blowing ratios of 1 and 1.5, model 3 is better than others models, also ($\bar{\bar{\eta}}$) enhanced by 182.4% and 231.1% at blowing ratios of 1 and 1.5, respectively. Except at BR=0.5, model 3 of large ramp angle provided the best ($\bar{\bar{\eta}}$) values than others cases, so large ramp angle gave

high film cooling effectiveness, these results agree well with numerical results of Shuping et al. and Sangkwon and Shih[30 and 42], they observed that the higher spanwise averaged adiabatic film cooling effectiveness occurred at high ramps backward-facing step.

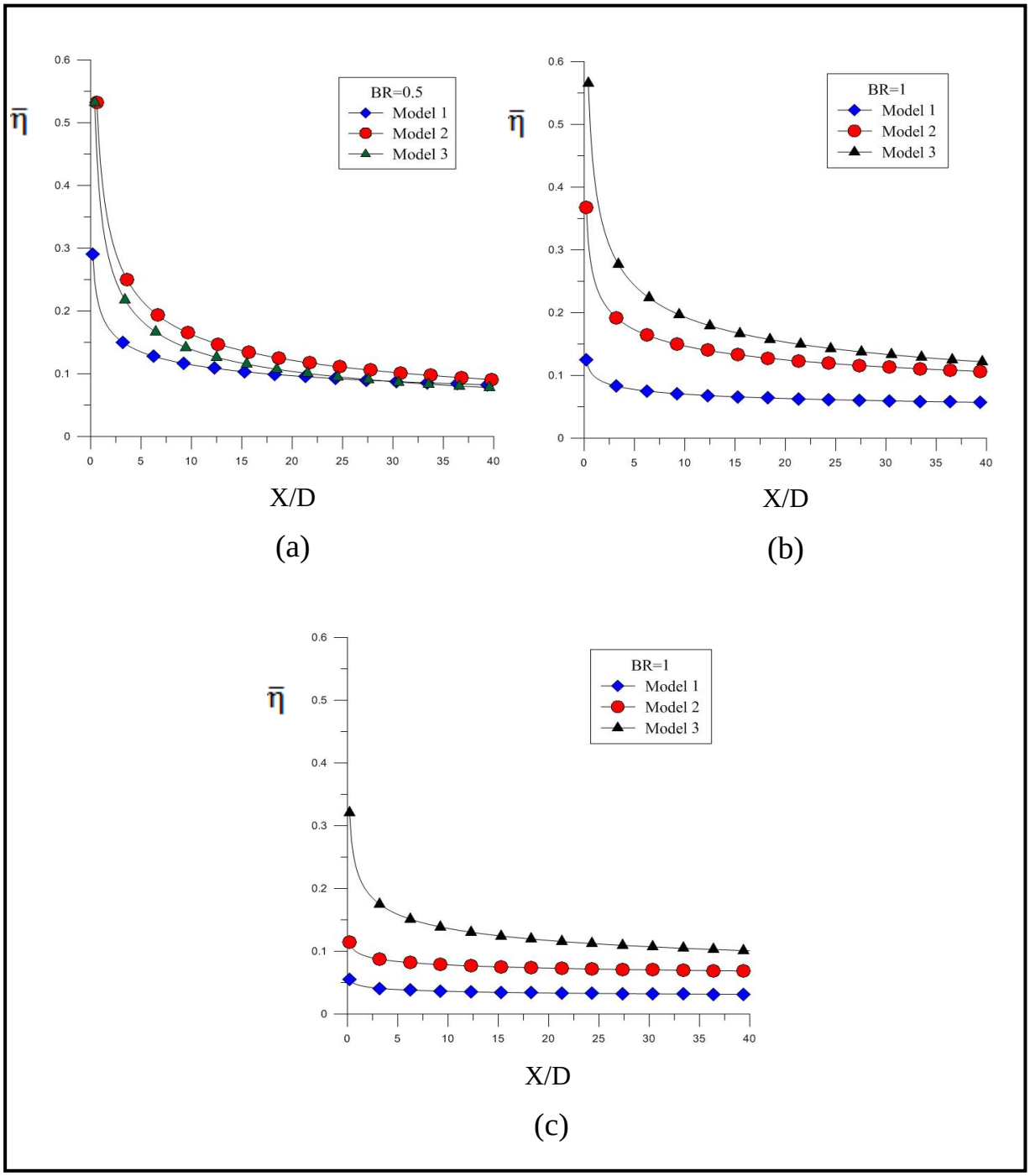

Figure (5-25): Comparison of ($\bar{\eta}$) versus (X/D) for model 1, model 2 and model 3 at (a) BR=0.5 (b) BR=1 (c) BR=1.5

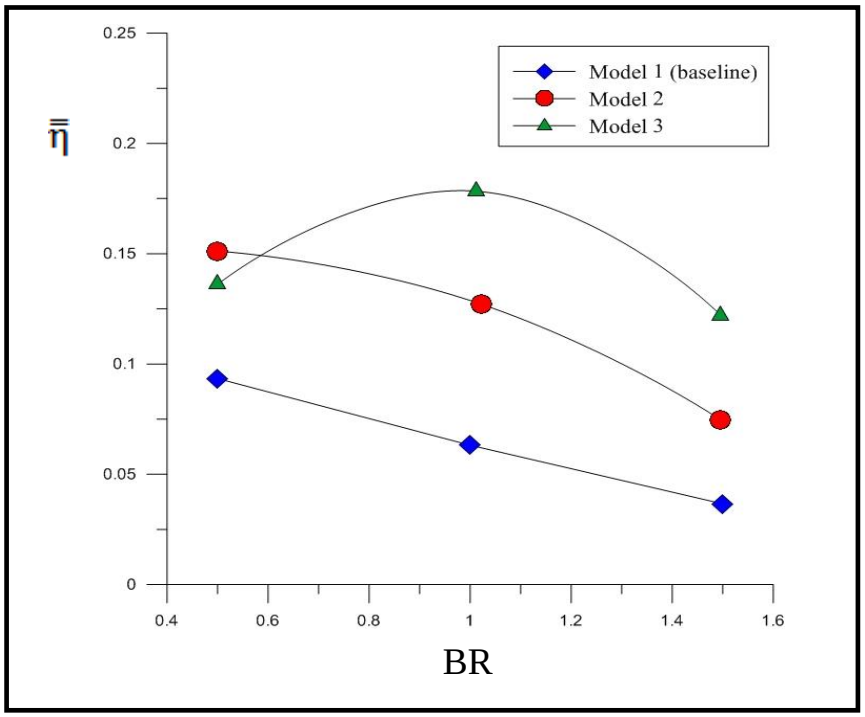

Figure (5-26): Effect of blowing ratio on the overall area-averaged film cooling effectiveness ($\bar{\bar{\eta}}$) for model 1, model 2, and model 3

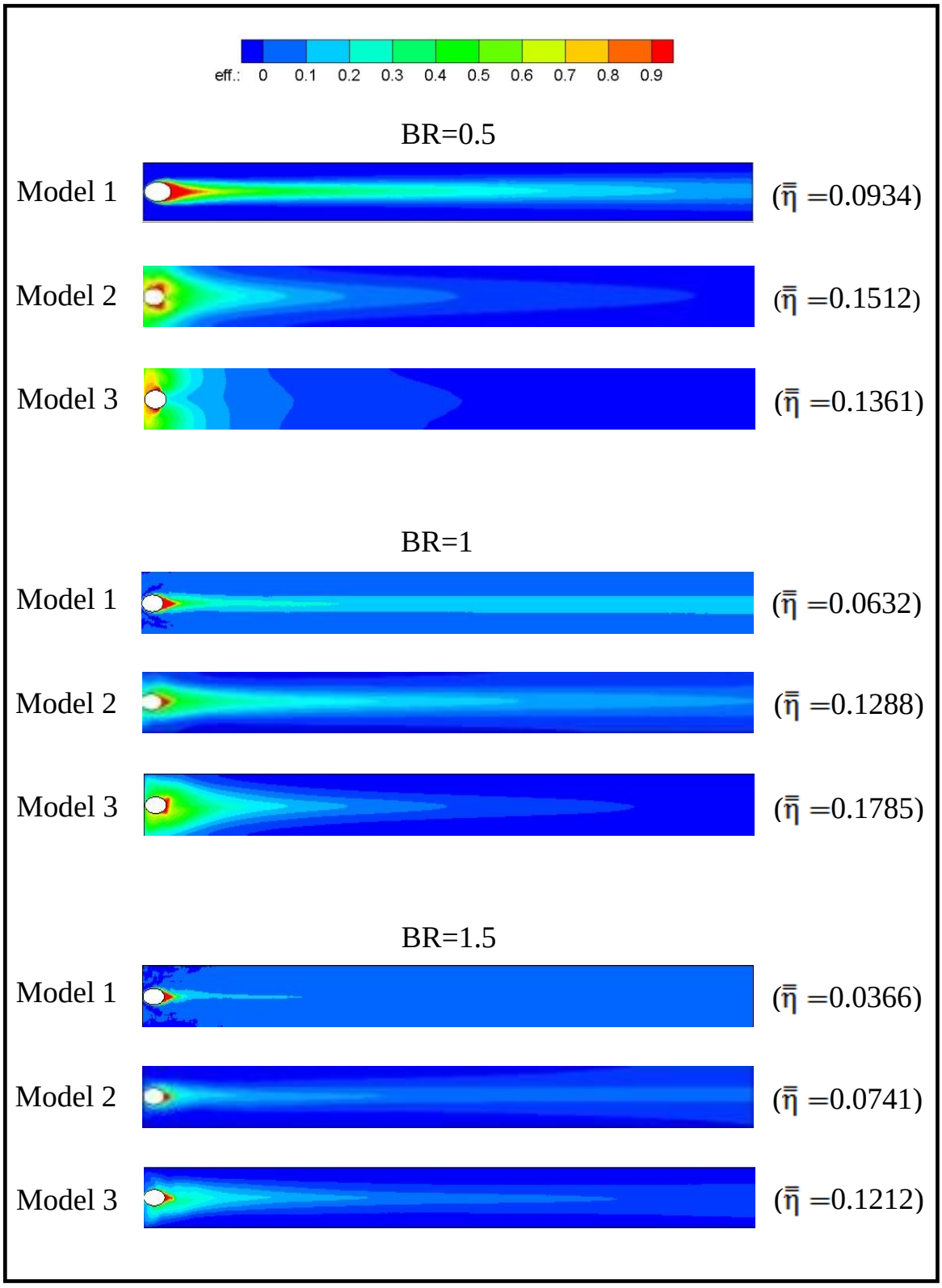

Figure (5-27): Comparison of film effectiveness contour and ($\bar{\bar{\eta}}$) between model 2 and model 3 with model 1 (baseline) at different BRs

5.2.3.3 Effect of Ramp Position on the Film Cooling Effectiveness

Figure (5-28) shows the effects of the conical ramped-holes distance of backward-facing step (β) at BR=1 upon the ($\bar{\eta}$). The main point rose from figure (5-28) is that for (model 8), upstream ramp at β=0.5D gives higher spanwise averaged adiabatic effectiveness than (model 9) of β=1.0D. Also there is no significant effect in the spanwise averaged adiabatic film effectiveness for all different ramp positions, therefore placing ramp at the hole edge (β=0) (model 7) gives the best averaged film cooling effectiveness.

Figure (5-29) illustrates the effect of blowing ratio on the overall area-averaged film cooling effectiveness ($\bar{\bar{\eta}}$), it seen clearly from this figure that models 7 provides higher overall area-averaged film cooling effectiveness than models 8 and 9 at blowing ratios of 1 and 1.5, for all models, there is no significant difference in the overall area-averaged film cooling effectiveness at blowing ratio of (0.5).

Figure (5-30) gives the comparison of film cooling effectiveness contours and overall area-averaged film cooling effectiveness ($\bar{\bar{\eta}}$) of models 7, 8 and 9 at different blowing ratios.

The overall area-averaged film cooling effectiveness ($\bar{\bar{\eta}}$) for model 7 enhanced by (143%, 315.5%, and 526.8%), for model 8 enhanced by (147.6%, 291.3%, and 448.1%), and for model 9 enhanced by (141.7%, 263.8%, and 413.4%) over that of the baseline at (BR= 0.5, 1.0, and 1.5), respectively. All details of the above results are given in Table (5-1).

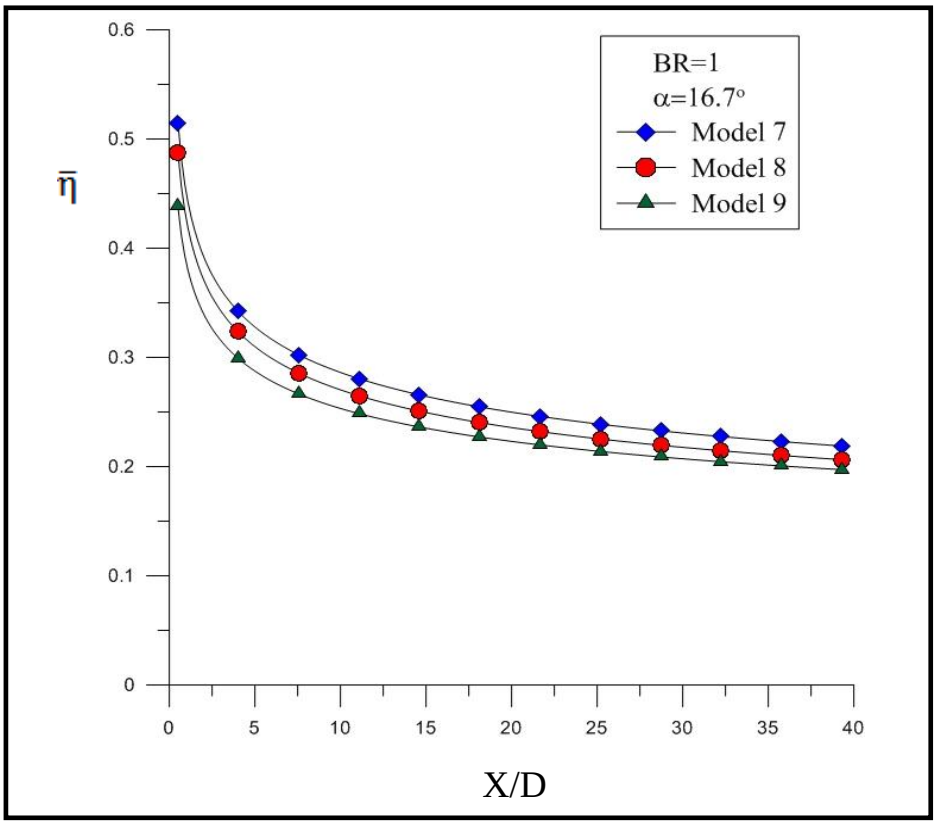

Figure (5-28): Effect of ramp position (β) on ($\bar{\eta}$) along (X/D) at BR=1

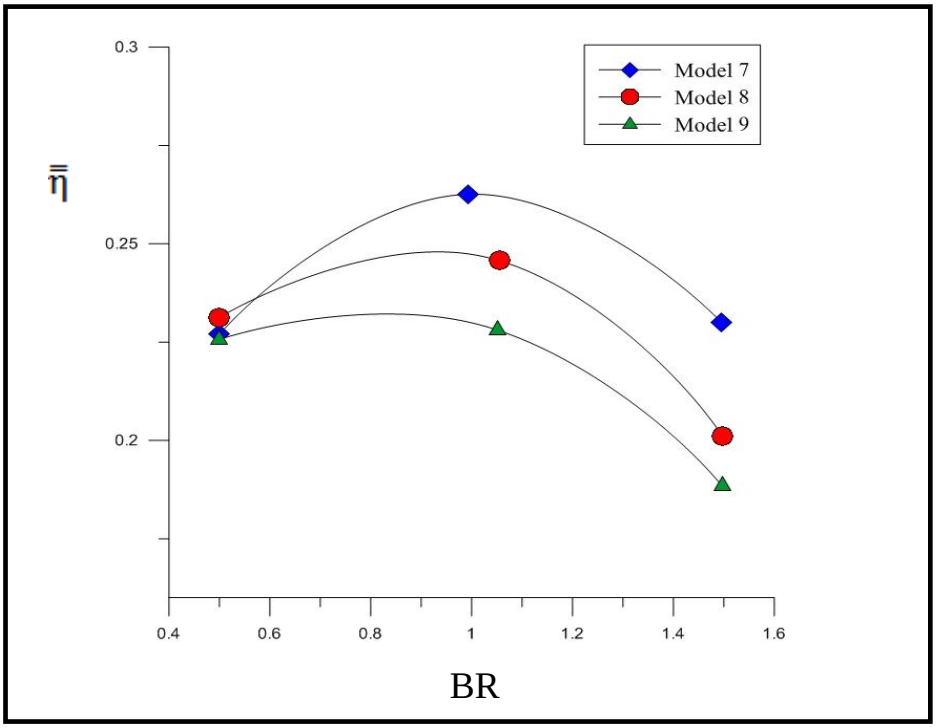

Figure (5-29): Effect of blowing ratio on the overall area-averaged film cooling effectiveness ($\bar{\bar{\eta}}$) for model 7, model 8, and model 9

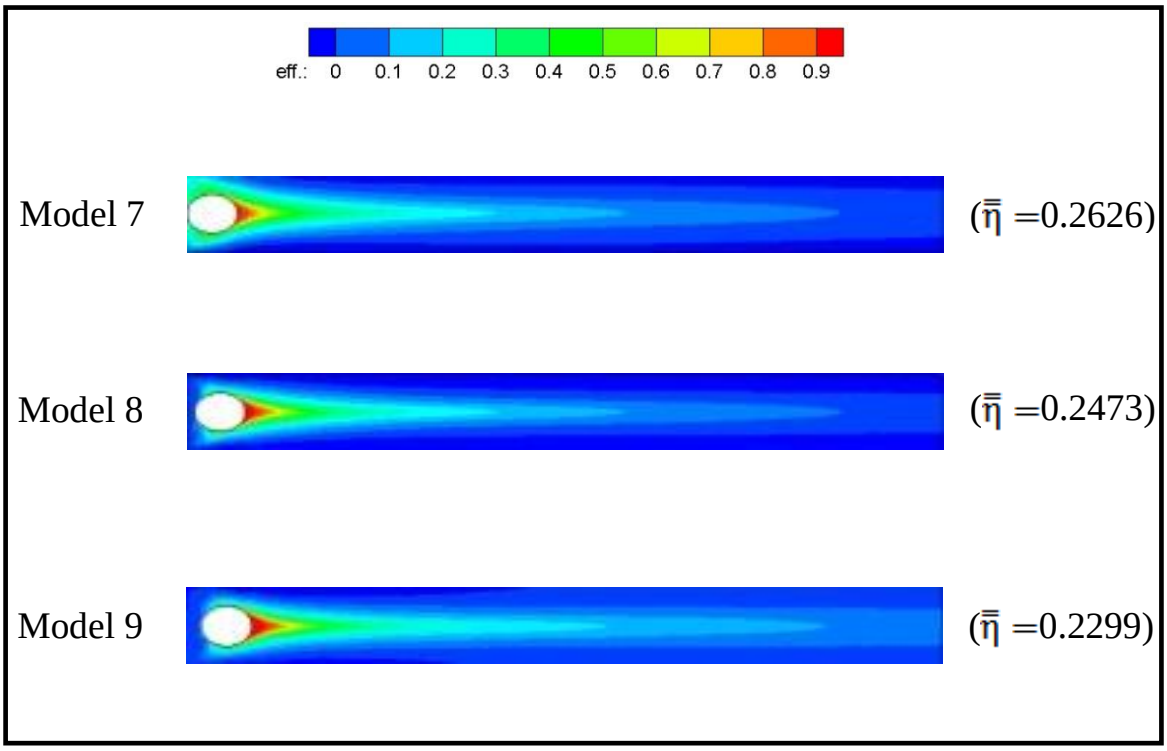

Figure (5-30): Comparison of film effectiveness contour and ($\bar{\bar{\eta}}$) for model 7, model 8, and model 9 at BR=1

5.2.3.4 Effect of Using Upstream-Downstream Ramps (Double-Ramps) with Cylindrical and Conical Holes

Figure (5-31) shows the predicted pressure distribution on plate surface of double ramps models, it can be observed that the pressure around the hole is reduced significantly, particularly for double-ramped cylindrical hole model (model 4). The reduction in pressure is due to the mainstream flow being diverted upward by the ramp and interacted with the film-cooling jet. Also, it can be seen that the ramp increases the pressure upstream step and decreases the pressure downstream in the backward-facing step. The coolant penetrated laterally around the hole since the low pressure zone counteracted behind the ramp backward-facing.

Figures (5-32 a & b) depict the vortex propagation at different (Y-Z) planes downstream model 4 and model 10 at different blowing ratios. These figures show clearly counter rotating vortex pairs generate at hole rim at X/D=0. At (X/D=2), this vortex dissipated, the jet entrained with the mainstream and the coolant jet has been lifted off from the surface. At X/D=4, behind the ramp backward-facing step, a (CVP) and a pair of anti-kidney vortices are generated ,both vortices united to form a horseshoe vortex, as shown at X/D=8. These vortices disappeared gradually downstream, therefor the mixed stream following close toward the plate surface and penetrated laterally in the presence of low pressure zone, and this was confirmed by figure (5-33). Coolant from both double-ramped cylindrical and conical holes cases enters a space between the ramps before they issued into the mainstream, and provides more cooling effects; as compared with the baseline case of two-dimensional film that spreads laterally, thus the spanwise penetration of the coolant results in higher spanwise averaged film cooling effectiveness.

Figure (5-34) shows the temperature contours at different (Y-Z) planes (X/D=0, 2, 4, 6, 8, and 10) for model 4 and model 10. It is clear that in the way downstream distance, the vortices are lifted off from the surface promote, lesser coolant to be following under the jet core which results in increasing the temperature along the surface and leads to lower film effectiveness.

Figure (5-35) manifests the variation of ($\bar{\eta}$) with (X/D) for model 1, model 4 and model 10. It is clear that the double-ramped holes case improved the adiabatic film cooling effectiveness, and a larger surface is protected laterally in the hole area. Film cooling is found to be more effective at blowing ratio of 1 than other blowing ratios.

Figure (5-36) shows the effect of blowing ratio on the overall area-averaged film cooling effectiveness ($\bar{\bar{\eta}}$), it is seen clearly from the

plot that model 10 (double-ramped conical hole) shows much higher ($\bar{\bar{\eta}}$) than other models, there is an slight increase in film cooling effectiveness as blowing ratio increased.

Figure (5-37) gives the summary of the film cooling effectiveness contours for different models with the values of overall area-averaged effectiveness ($\bar{\bar{\eta}}$). At different blowing ratios, model (10) gives better performance than the other models. The overall area-averaged film cooling effectiveness ($\bar{\bar{\eta}}$) for model 4 enhanced by (44.3%, 213%, and 367.8%) over that of the baseline at (BR= 0.5, 1.0, and 1.5), respectively. For model (10), the overall area-averaged film cooling effectiveness ($\bar{\bar{\eta}}$) enhanced by (142.8%, 373%, and 667.5%) over that of the baseline at (BR= 0.5, 1.0, and 1.5), respectively. All details of the above results are given in Table (5-1).

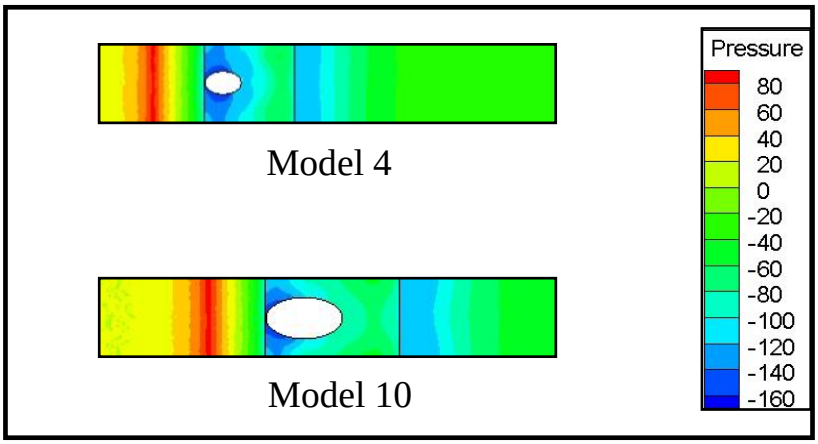

Figure (5-31) Pressure distribution on flat plate surface for double-ramped holes

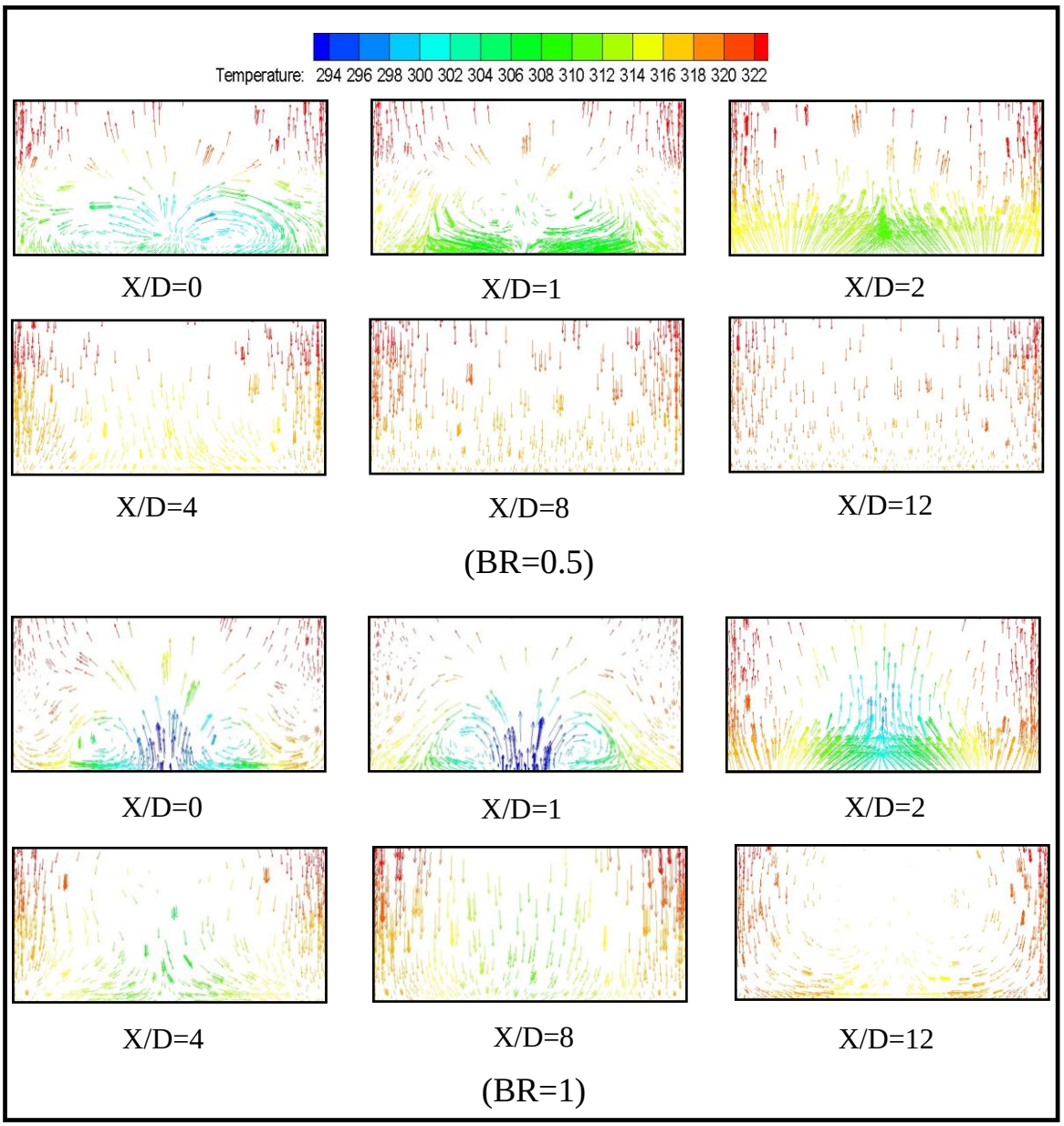

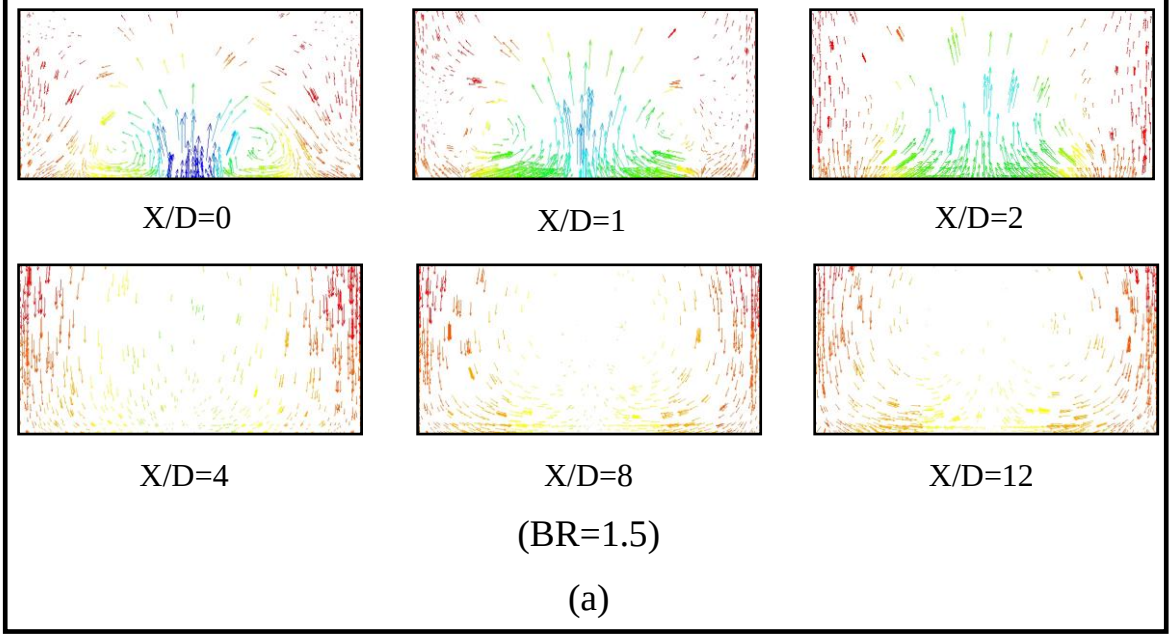

(BR=1.5)

(a)

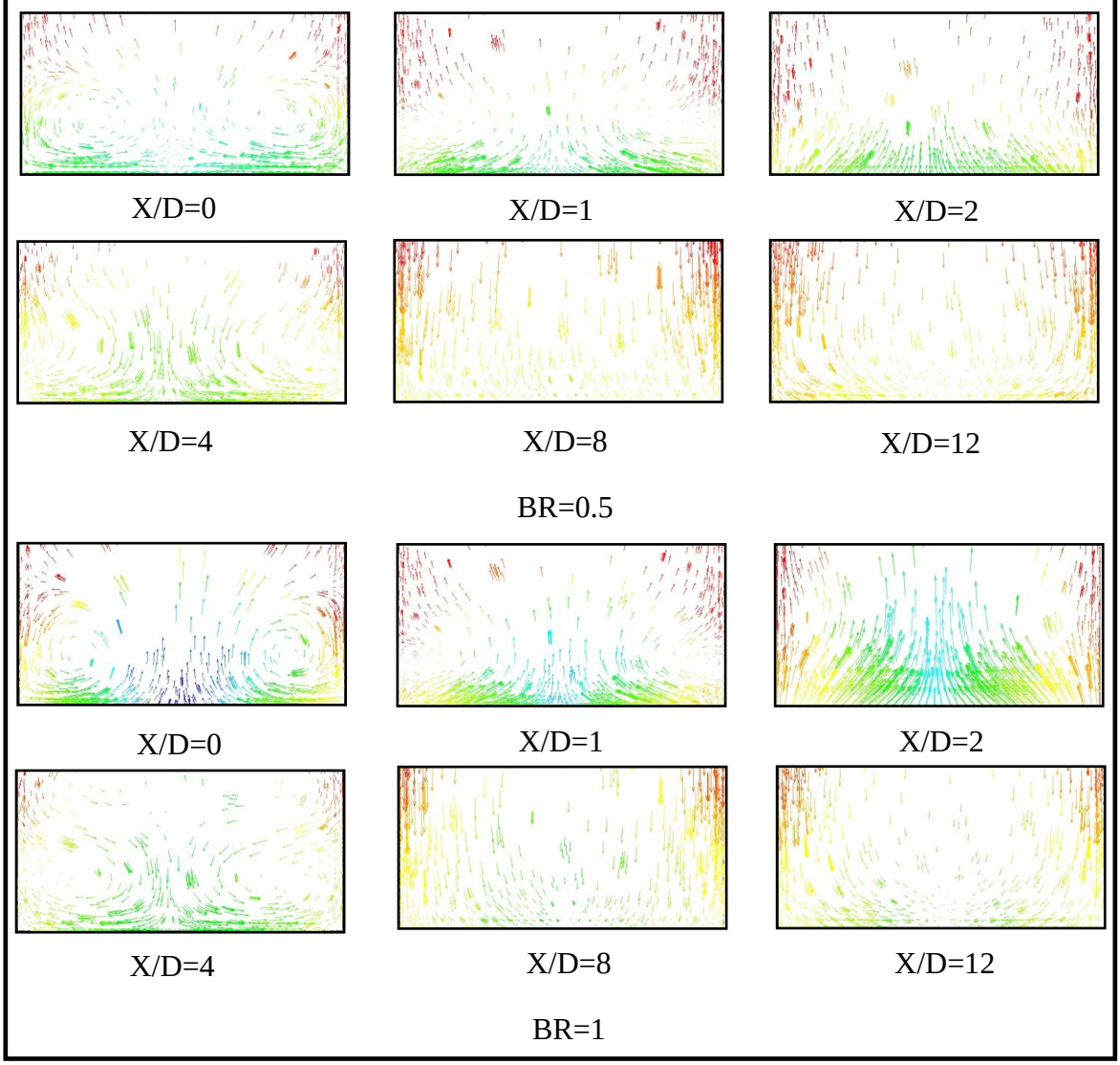

BR=0.5

BR=1

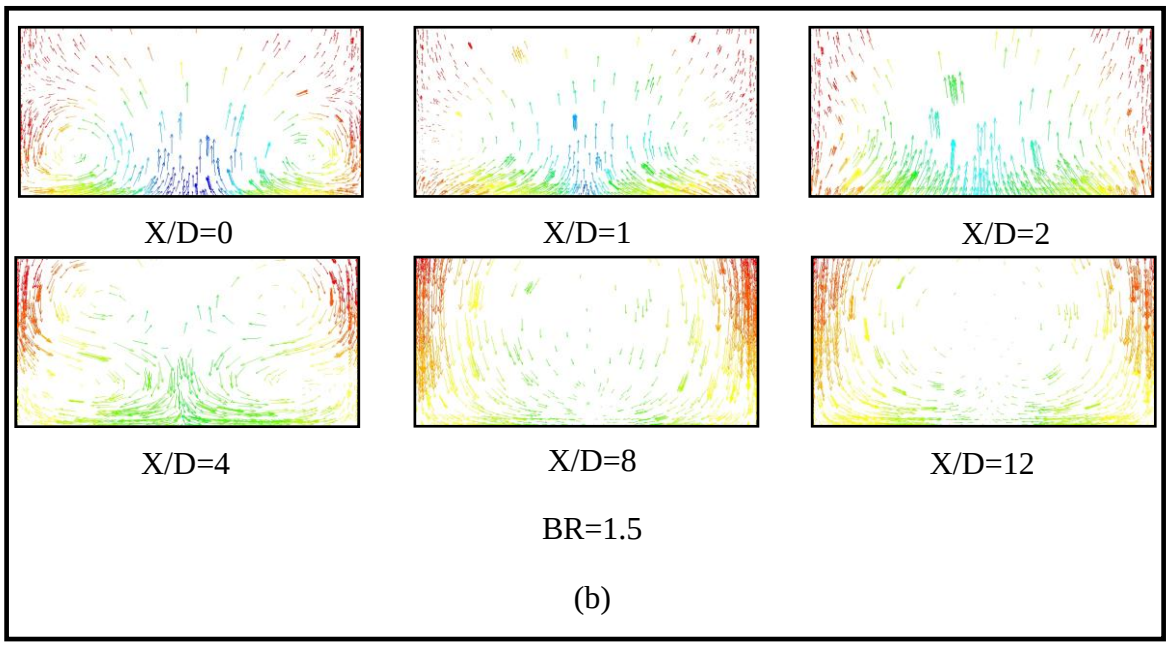

Figure (5-32): Vortex propagation colored by temperature for (a) model 4 (b) model 10 at different (Y-Z) planes

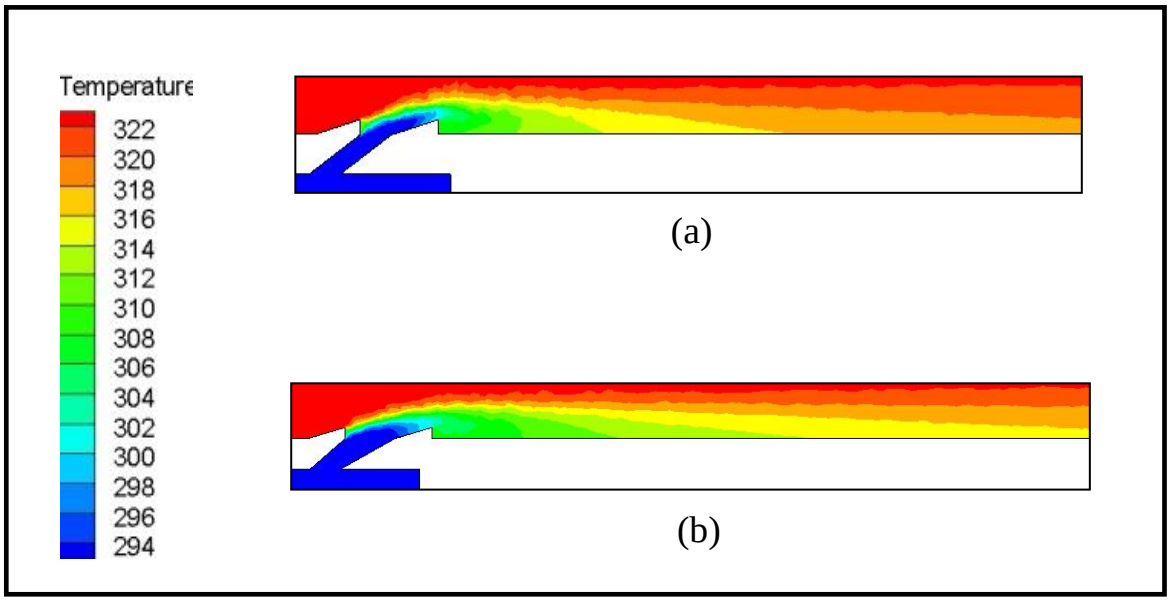

Figure (5-33): Mainstream and coolant jet interaction contour colored by temperature distribution at center (X-Y) plane for (a) model 4, (b) model 10 at BR=1

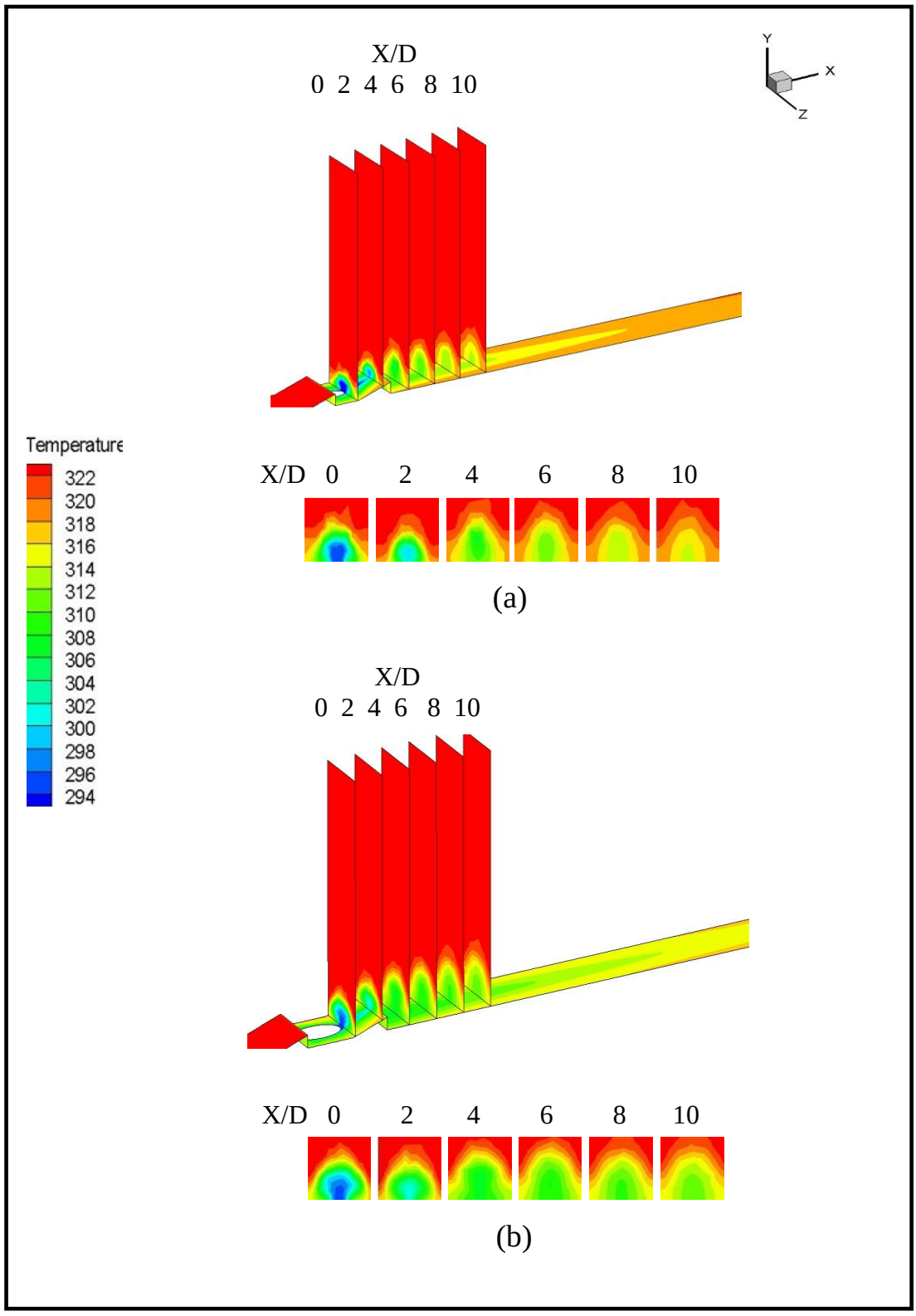

Figure (5-34): Temperature contours at different (Y-Z) planes (X/D=0, 2, 4, 6, 8, and 10) for (a) model 4 (b) model 10 at BR=1

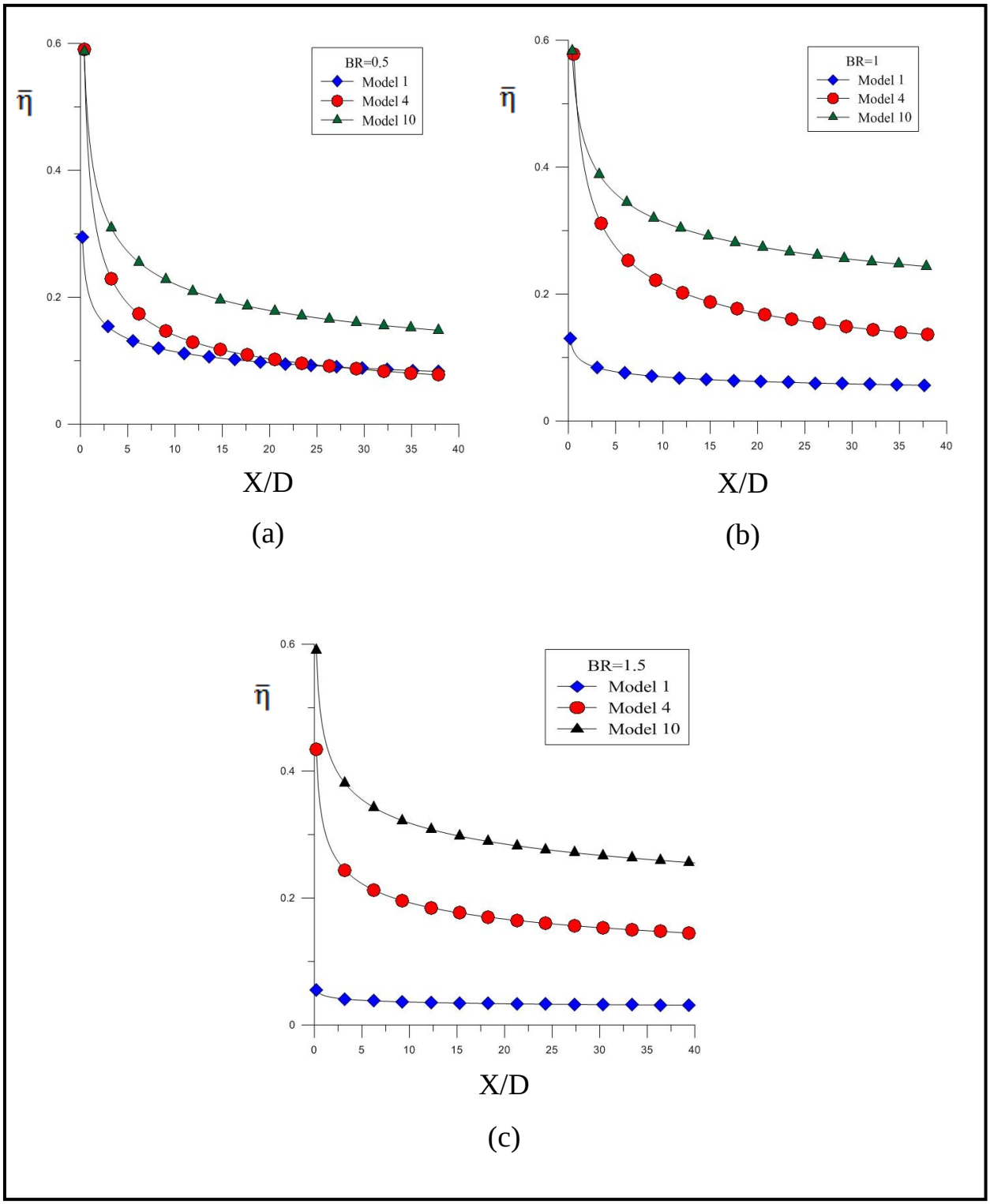

Figure (5-35): Comparison of ($\bar{\eta}$) versus (X/D) between model 1, model 4, model 10 at (a) BR=0.5 (b) BR=1 (c) BR=1.5

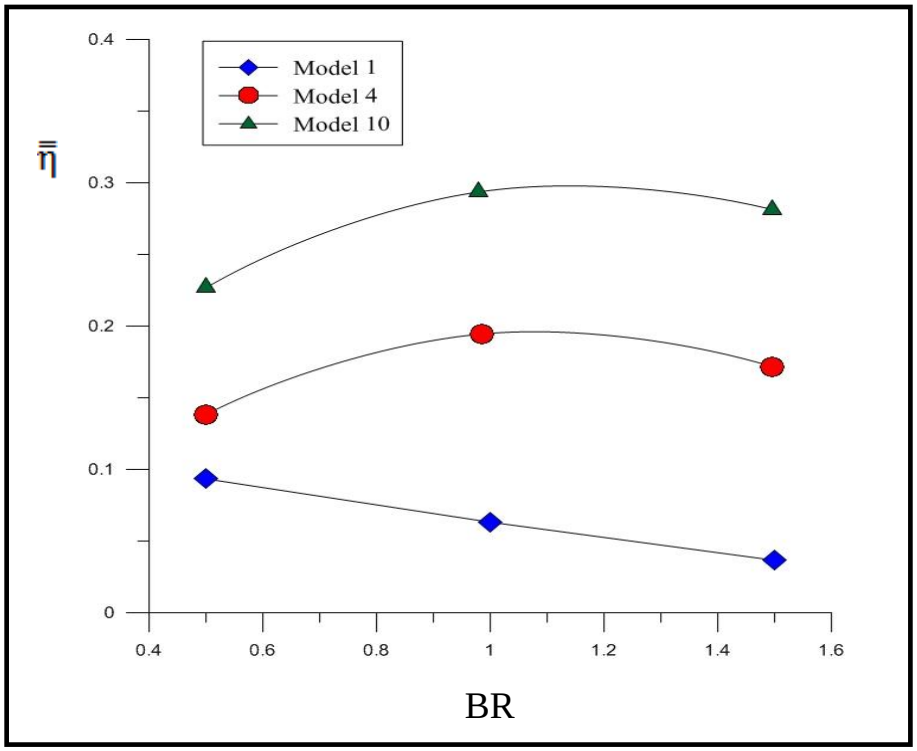

Figure (5-36): Effect of blowing ratio on the overall area-averaged film cooling effectiveness ($\bar{\bar{\eta}}$) for model 1, model 4, and model 10

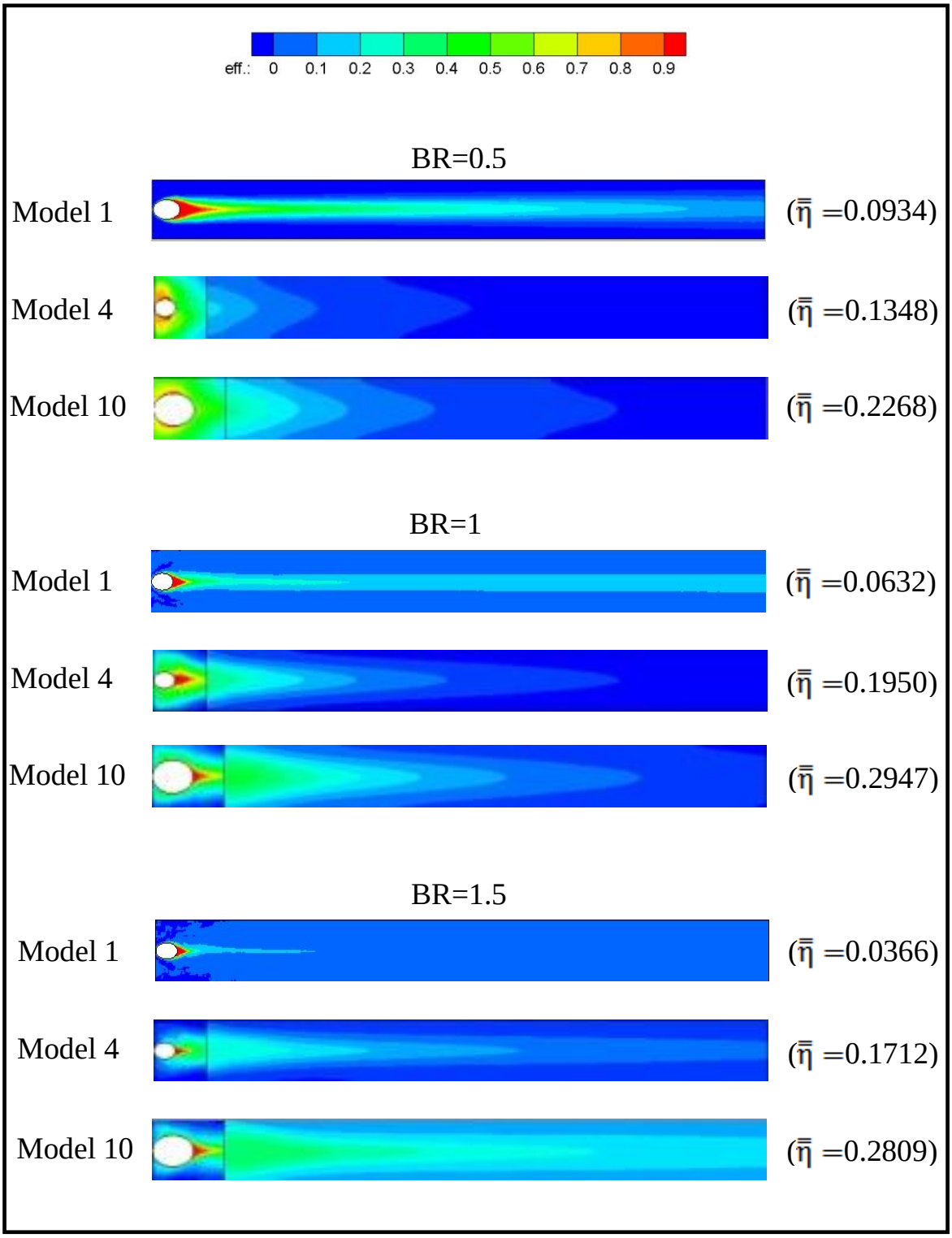

Figure (5-37): Comparison of film effectiveness contours and ($\bar{\bar{\eta}}$) between model 4 and model 10 with model 1 (baseline) at different BRs

5.3 Experimental Results

Six models have been selected according to the computational results, as given in Table (5-2), these models gives a highest adiabatic film cooling effectiveness, so they considered in the experimental test program.

The adiabatic film cooling effectiveness for all models was obtained experimentally at three blowing ratios (BR= 0.5, 1.0, and 1.5), the IR images for models surface at each investigated test was captured and stored by thermal camera at the reached steady-state condition, as shown in figure (5-38). These images were transferred to PC smart view software program supplied with camera; this program can be used to limit the selected area to avoid the effect of the test section walls. The IR images were converted to corresponding temperature digital values and then saved as Excel sheet data. Finally, the values of the adiabatic film cooling effectiveness (η) were computed and tabulated in the Excel sheet data.

To calculate the local heat transfer coefficient ratios and the local net heat flux ratios based on the transient experimental measuring data, the IR images for plate surface of each model at each investigated test were captured at successive time steps and stored by thermal camera. The IR images were converted to corresponding temperature digital values by Smart View Software Program supplied with camera, then exported as a text document and saved as data in Excel sheet. MATLAB program software are prepared by using a semi-infinite solid assumption presented in chapter four in order to introduce the local heat transfer coefficient ratios and local net heat flux ratios based on those temperature, then the heat transfer coefficient ratio and heat flux ratio saved as data in Excel sheet, the spanwise averaged heat transfer coefficient ratios $(\overline{h}/h_o)$, the

spanwise averaged heat flux ratios ($\bar{q}/q_o$), and the overall values were calculated and tabulated in the Excel sheet data.

Table (5-2): Geometry models to be tested experimentally.

Model Number	**Ramp dimensions**	
	γ	β
Model 1 Baseline case	-	-
Model 2 Single ramped-cylindrical hole	16.7^o	0
Model 3 Double ramped-cylindrical hole	16.7^o	0
Model 4 conical hole without ramp	-	-
Model 5 Single ramped-conical hole	16.7^o	0
Model 6 Double ramped-conical hole	16.7^o	0

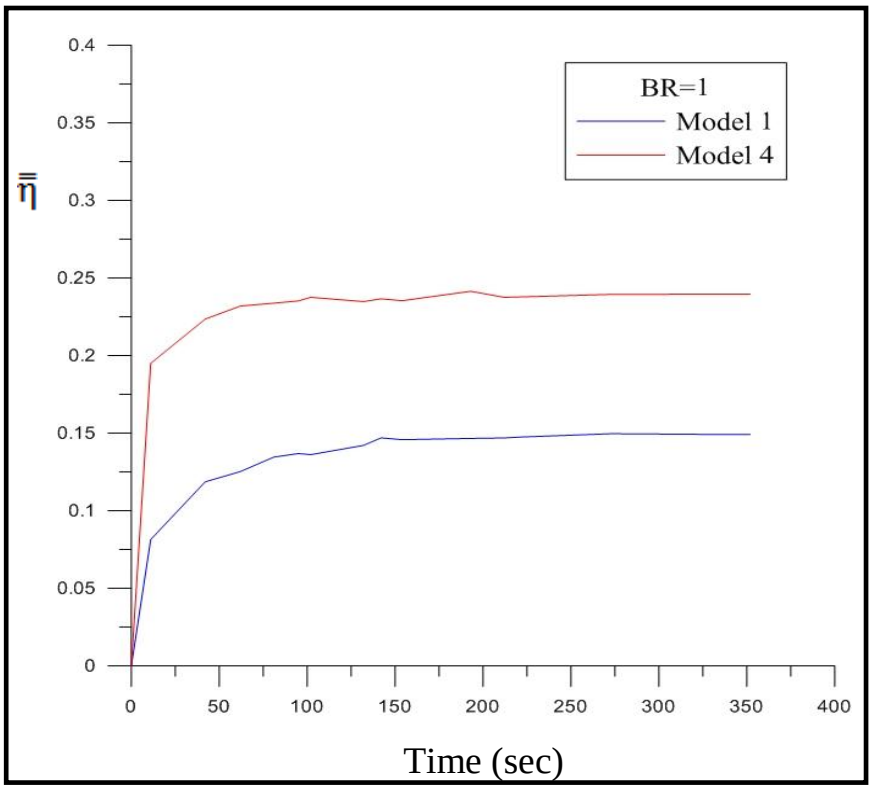

Figure (5-38): Overall area-averaged effectiveness ($\bar{\bar{\eta}}$) history for film cooling system

5.3.1 Adiabatic Film Cooling Effectiveness

The verification of the current experimental approach, the test results of the baseline case (model 1), was made by comparison with the experimental results of the similar case study of baseline case of Yuen et al.[[26]. Sample of results at blowing ratios of 0.5 and 1 of the spanwise averaged film cooling effectiveness distribution along the X/D together with that of Yuen et al.[26] experimental results are presented early in figure (5-1). The results showed approximately similar levels of (η) with slightly difference in local values. It is fair to say that the results obtained from the present experiments are in a good agreement with experimental results of Yuen et al.[[26].

Experimental results of the present investigation are in the thermal aspect in the form of distribution and contour plots of various

variables, including the film cooling effectiveness, heat transfer coefficient ratio, and heat flux ratio.

5.3.1.1 Cylindrical Hole Models (Models 1, 2, and 3)

Figure (5-39) presents a sample of image captured by IR camera for model 1. Figure (5-40) show the comparison of the spanwise averaged film cooling effectiveness ($\bar{\eta}$) versus normalized streamwise distance (X/D) of models 1, 2, and 3 at BR= 1 and 1.5. The spanwise averaged film cooling effectiveness ($\bar{\eta}$) was calculated as the averaged values taken from the local reading of 20 pixels in spanwise direction for eighteen locations downstream the hole exit (from X/D=0 to X/D=40), the spanwise averaged film effectiveness was plotted against the normalized streamwise distance downstream of the film hole (X/D). Both ramped models (2 and 3) showed a rapid decaying in effectiveness downstream distance. At blowing ratio of 1, there is no significant difference in film cooling effectiveness between model 2 and model 3. At blowing ratio of 1.5, the ramped hole provided better cooling effectiveness than model 1. Model 3 provided the highest and significant improvement in the spanwise averaged film cooling effectiveness.

Figure (5-41) depicts the test results of film cooling effectiveness contours for different cylindrical hole models at different BRs. At low blowing ratio, film cooling in model 1 was extended for a long distance downstream but with weak spanwise penetration. At moderate and high blowing ratios, there is a poor film cooling effectiveness. Ramped models provided a wide spanwise penetration of film cooling giving good improvement in film cooling effectiveness, significantly at BR=1.5.

Figure (5-42) presents the effect of blowing ratio on the overall area-averaged film effectiveness ($\bar{\bar{\eta}}$) for the three cylindrical hole models. Model 2 shows higher values of overall film cooling effectiveness than model 1, while model 3 enhanced the ($\bar{\bar{\eta}}$) more than other models (1 and 2), particularly at high blowing ratio. The maximum film cooling effectiveness for both ramped cases is achieved at blowing ratio of 1.

The overall averaged film cooling effectiveness ($\bar{\bar{\eta}}$) for model 2 enhanced by (40.2%, 175.8%, and 234.9%) and for model 3 enhanced by (45.3%, 185.8%, and 368.9%) over that of the conventional single jet holes row at (BR= 0.5, 1.0, and 1.5), respectively.

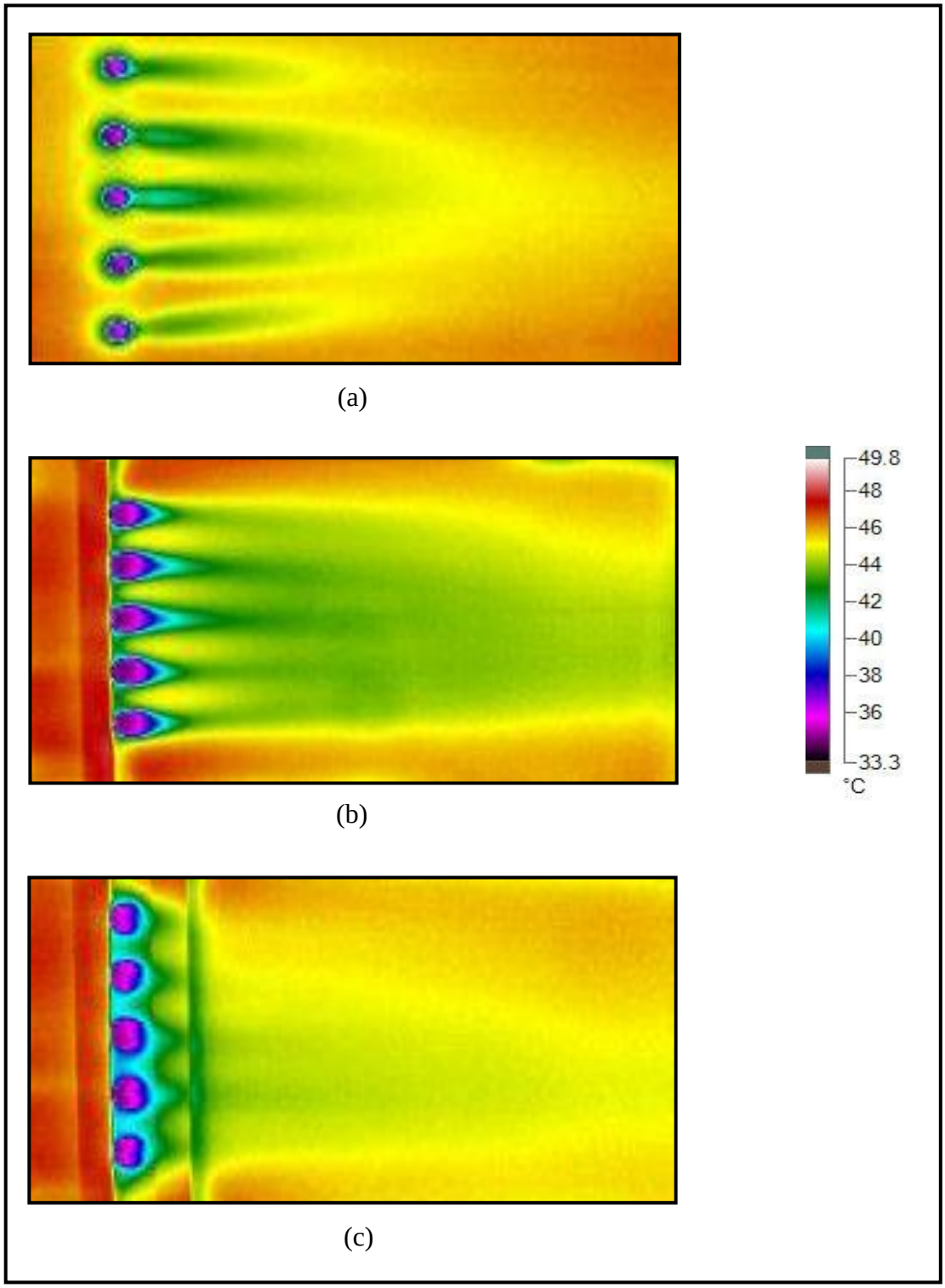

Figure (5-39): Samples of experimental surface image captured by IR camera at BR=1 (a) holes without ramp (b) upstream ramped-holes (c) upstream-downstream ramped-holes

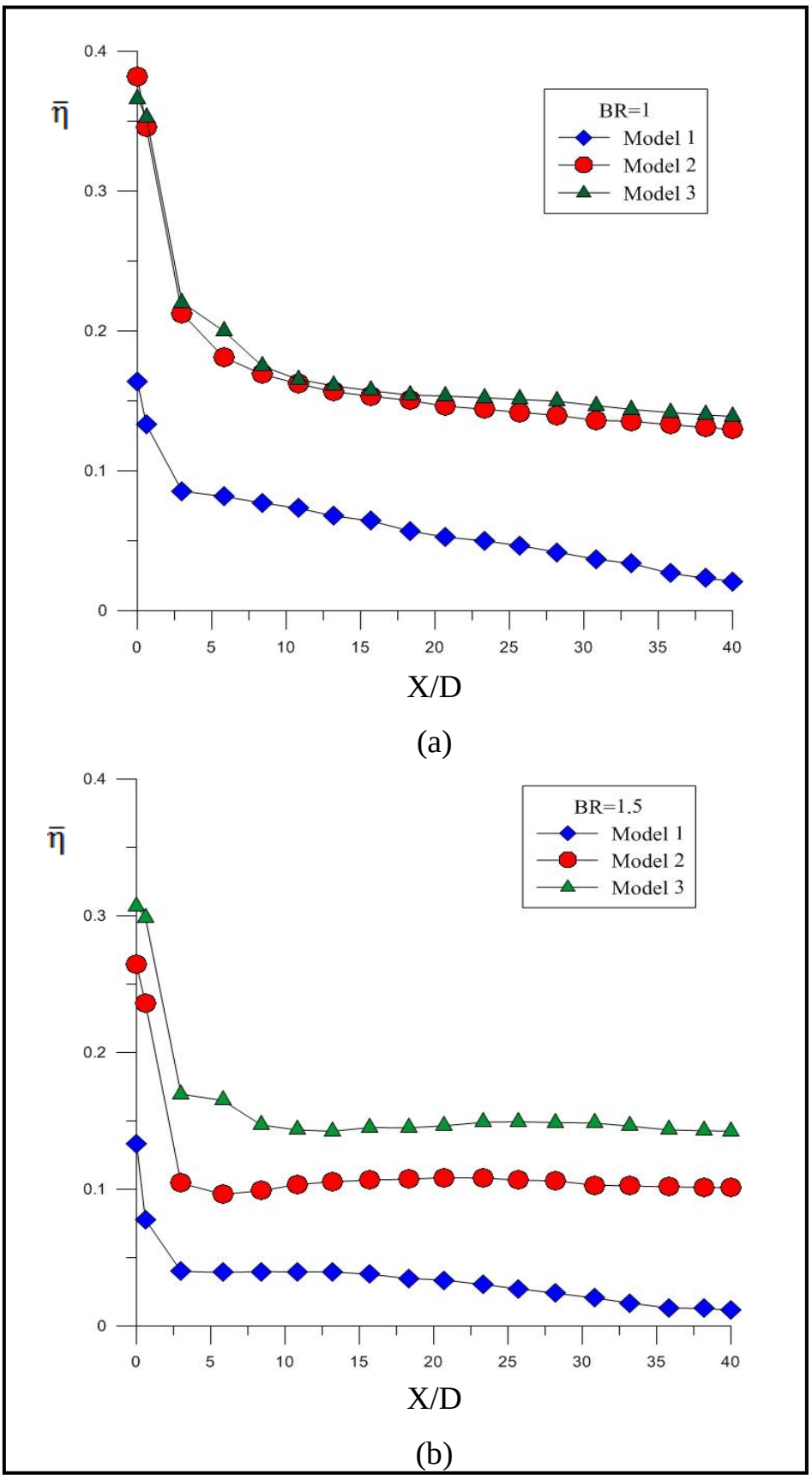

Figure (5-40): Experimental comparison of ($\bar{\eta}$) versus (X/D) for cylindrical hole models at BRs of 1and 1.5

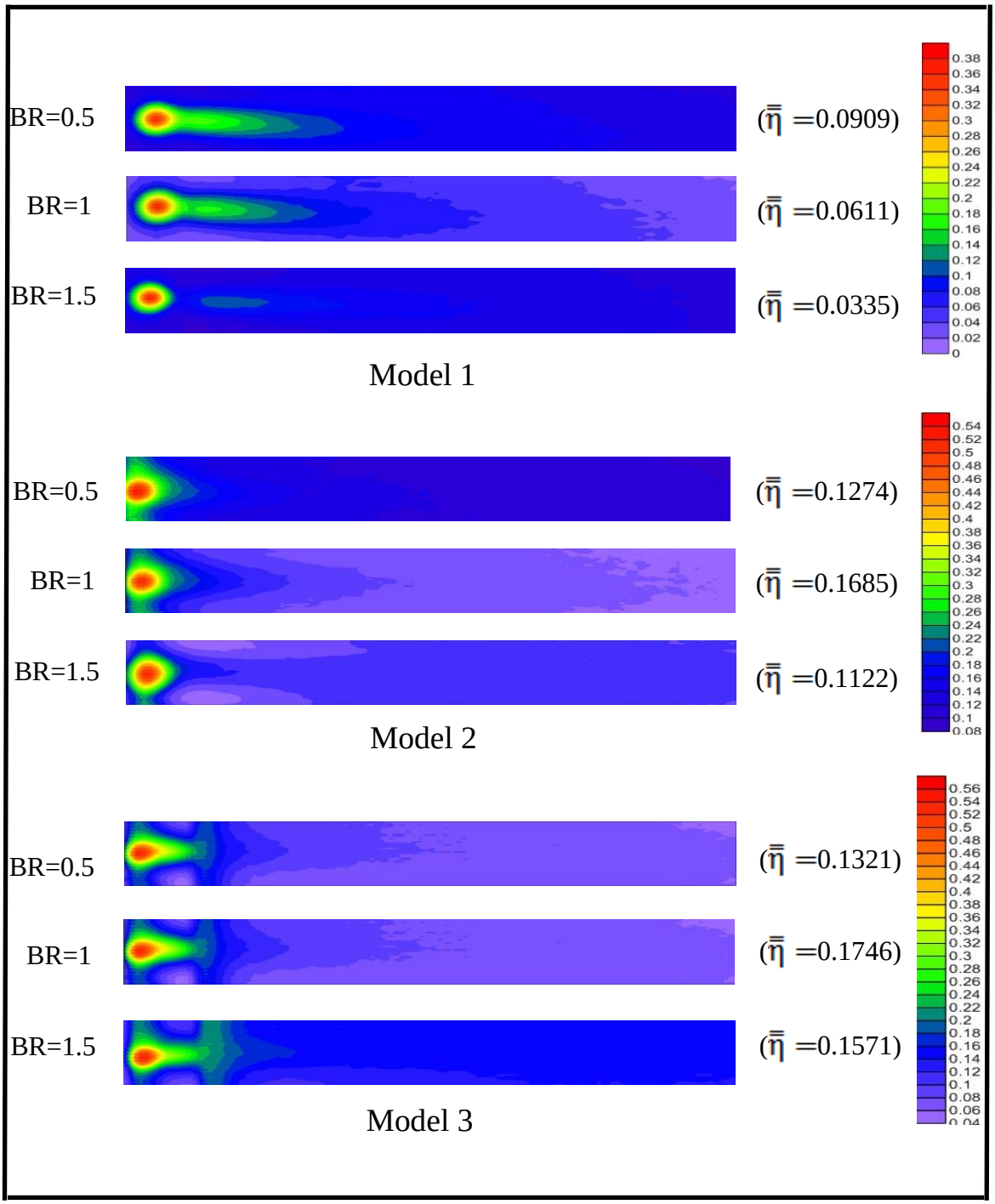

Figure (5-41): Experimental comparison of film effectiveness contours for different cylindrical hole models at different BRs.

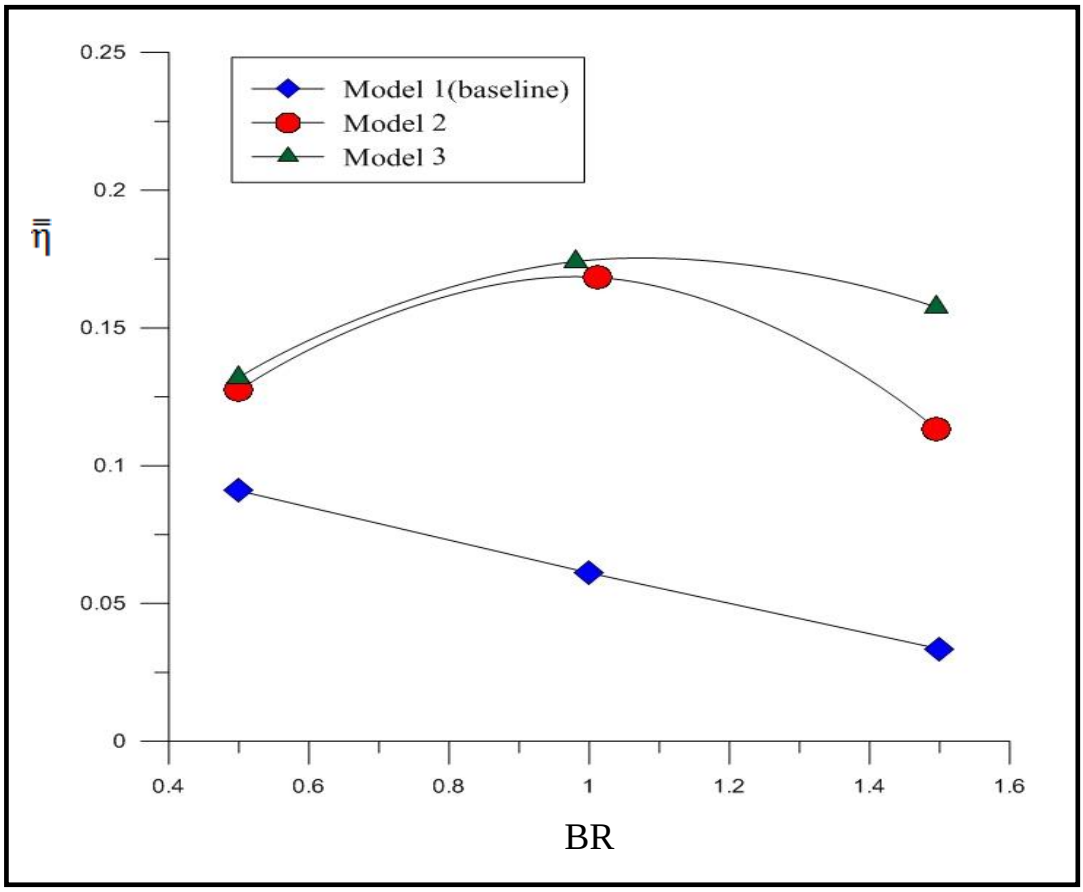

Figure (5-42): Effect of (BR) on ($\bar{\bar{\eta}}$) for model 1 (baseline), model 2, and model 3

5.3.1.2 Conical Hole Models (Models 4,5, and 6)

Figure (5-43) compares the distribution of spanwise averaged film cooling effectiveness along the normalized streamwise distance (X/D) for models (4, 5, and 6). For moderate and high blowing ratios (1 and 1.5), model 6 provides better film cooling effectiveness than model 4, in which model 4 regarded as the baseline case of the conical models generation (models 4, 5, and 6). The effectiveness distribution for model 5 and model 6 are seemed to be very close to each other, and there is a significant difference between them and model 4. The ramped-conical

holes improved the film cooling effectiveness significantly at blowing of 1.5, as shown clearly in figure (5-43).

Figure (5-44) shows the film cooling effectiveness contours for models (1, 4, 5, and 6). For single-ramped case (model 5), the film cooling effectiveness contours showed good protection at all blowing ratios especially at BR=1. The double ramped-hole model (model 6) the best protection specially, at blowing ratios of 1 and 1.5. These remarkable results are verified by the results presented in figure (5-45). Effect of blowing ratios on the overall area-averaged film cooling effectiveness is presented in this figure for models (1, 4, 5, and 6). The conical hole cases (models 4, 5, and 6) gave higher values of the overall area-averaged film cooling effectiveness than that of baseline case (model 1). The double-ramped conical hole (model 6) seems to work better than other cases, especially at blowing ratio greater than 0.5, and there is a slight difference between model 5 and model 6 in film cooling effectiveness values at all blowing ratios.

The overall area-averaged film cooling effectiveness ($\bar{\bar{\eta}}$) for single ramped-holes (model 5) enhanced by (134%, 292.6%, and 554.6%) and for double ramped-holes (model 6) enhanced by (130.3%, 343.7%, and 679.4%) over that of the conventional single cylindrical holes row at (BR= 0.5, 1.0, and 1.5), respectively.

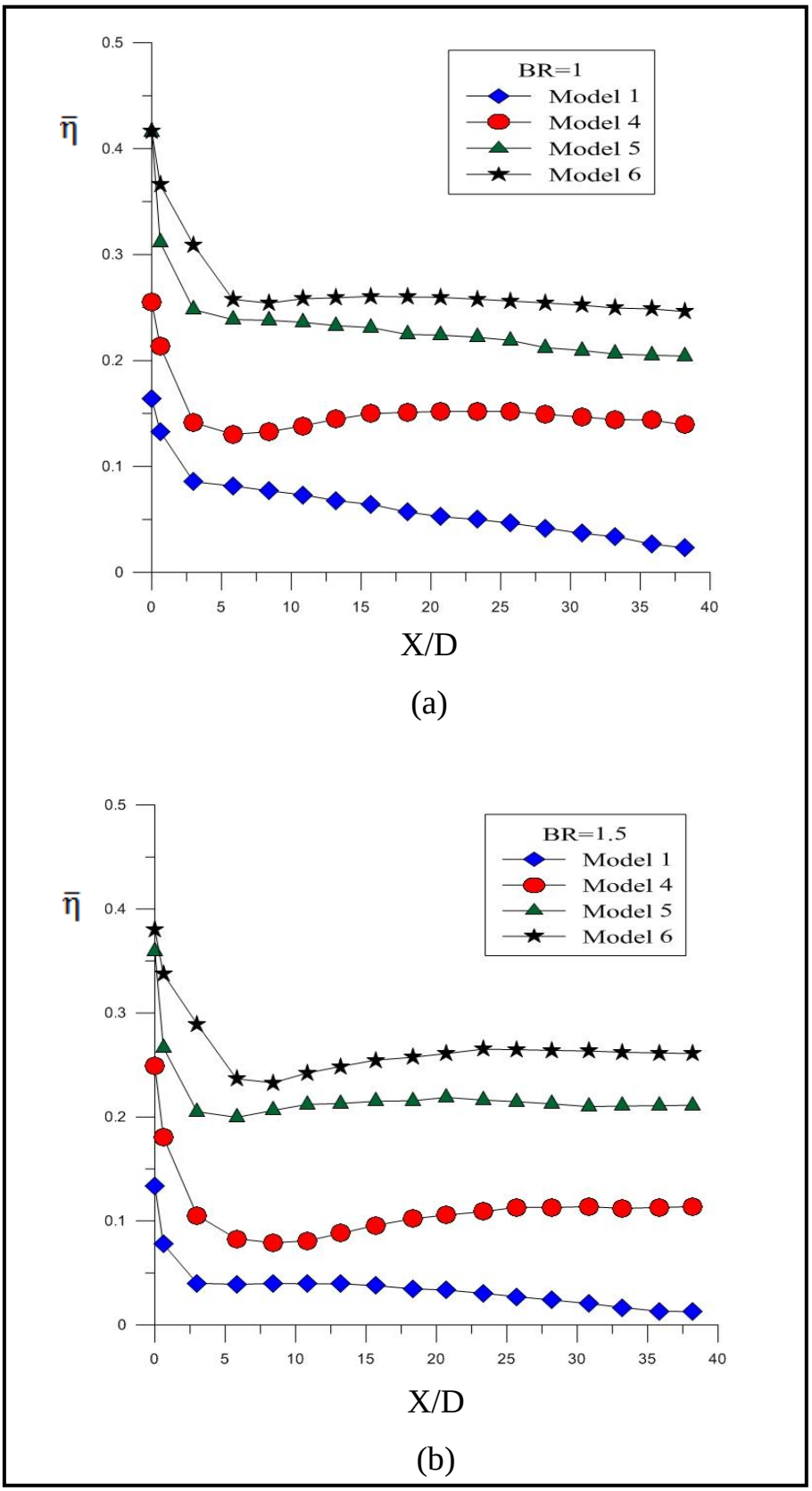

Figure (5-43): Experimental comparison of ($\bar{\eta}$) versus (X/D) for conical hole cases at (a) BR=1 (b) BR=1.5

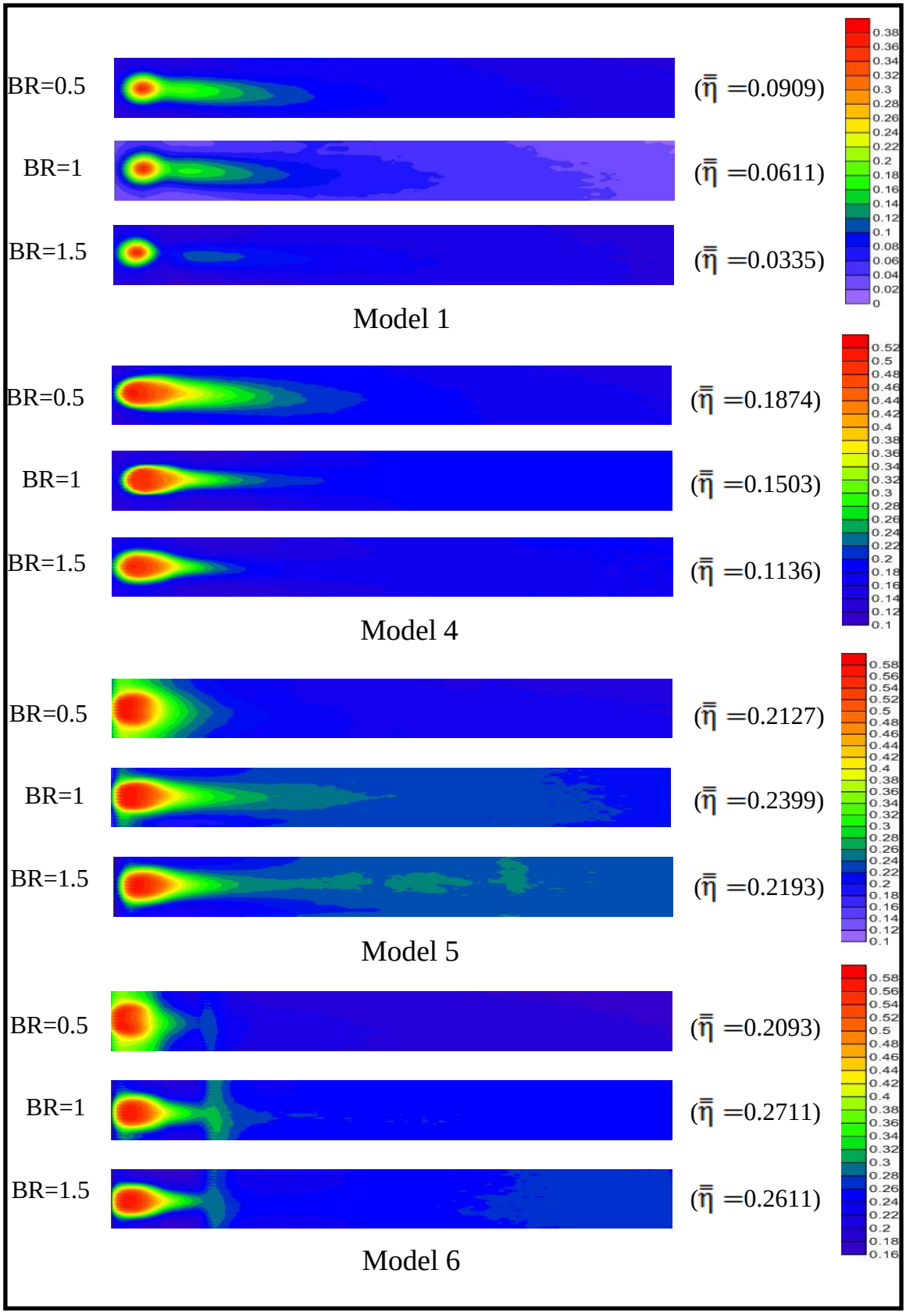

Figure (5-44): Experimental comparison of film effectiveness contours for different conical hole models with baseline at different BRs.

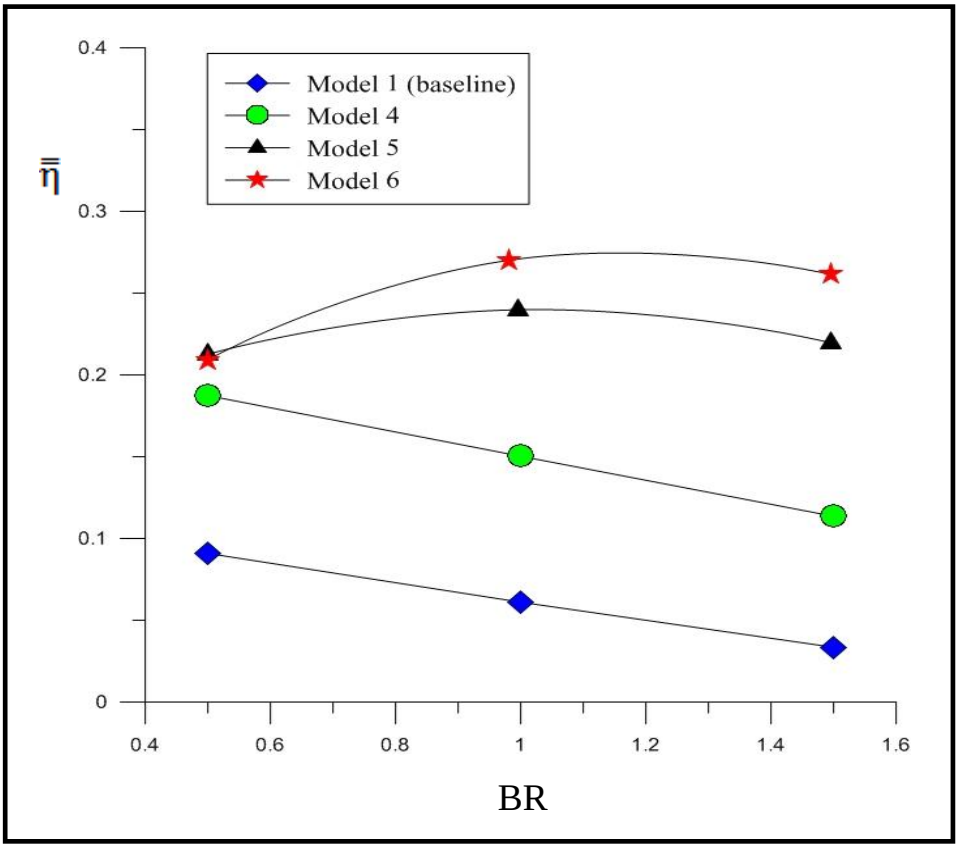

Figure (5-45): Effect of (BR) on ($\bar{\bar{\eta}}$) for baseline, model 4, model 5, and model 6

5.3.2 Heat Transfer Coefficient

The local heat transfer coefficient with film cooling (h) is normalized by the heat transfer coefficient without film holes on a flat surface (h_0). The verification of the current calculation method of spanwise averaged heat transfer coefficient ratio ($\bar{h}/h_o$) is made by comparison with the experimental results of Lu et al. [36]. Sample of the test results of the heat transfer coefficient ratio ($\bar{h}/h_o$) distribution along the nondimensional distance (X/D) for model (1) at BR=1 together with the experimental results of the similar model of Lu et al.[36] are presented in figure (5-46). It is fair to say that the present experimental results are in a good agreement with that of Lu et al. [36].

Figures (5-47) and (5-48) present the ramp geometry effect on the detailed spanwise averaged heat transfer coefficient ratio ($\bar{h}/h_o$) distributions for both cylindrical and conical holes cases at BR=1. The heat transfer coefficient ratio for ramped-hole cases was increased compared to the baseline case, such phenomena were due to the interaction between the coolant jet and the mainstream flow, and this interaction produced high turbulence region. This phenomenon was explained by Nasir et al. [72], in which they showed that the jet injection increased the turbulence level inside the boundary layers due to the shear layer mixing, and this is the main reason that the heat transfer coefficient increased in the hole downstream region. As shown in figures (5-47) and (5-48) in the downstream region, especially at (X/D >10), the heat transfer coefficients have higher values and remain in the same level up to the end of the test surface. It is clear in the ramped-holes case, the heat transfer coefficient increased over that of the baseline case.

5.3.3 Heat Load

The heat load can be simulated by combining the film cooling effectiveness (η) and heat transfer coefficient ratio (h/h_o), therefore the ratio (q/q_o) can be introduced to present the reduction in heat flux at the test surface with the presence of coolant air. A net heat flux ratio is used to measure the combined effect of film effectiveness and heat transfer coefficient. The relation between (η) and (q/q_o) given in equation (4-14) may be used to explain the heat load transfer to the plate, the heat flux ratio (q/q_o) indicates the reduction in heat flux on the test surface from the hot stream, if the value of the net heat flux ratio is less than 1.0, then the introduction of film cooling has beneficial effect. If the value is greater than 1.0, it can be said that the film cooling did not serve its purpose of cooling. In the practical application, turbine designers are concerned with the reduction of heat load to the film protected surface. The ratio (q/q_o) are calculated at every pixel point, averaged, and tabulated in Excel data sheet.

Figures (5-49) and (5-50) present the effect of blowing ratio on the overall area-averaged heat flux ratio ($\bar{\bar{q}}/q_o$) for both cylindrical and conical holes models. It is clear from the plot that the cylindrical holes with or without ramps have a positive result except at high blowing ratio when it's provided a heat flux ratio more than unity. Also, the conical hole cases provided positive result at all blowing ratios (i.e., ($\bar{\bar{q}}/q_o$) < 1).

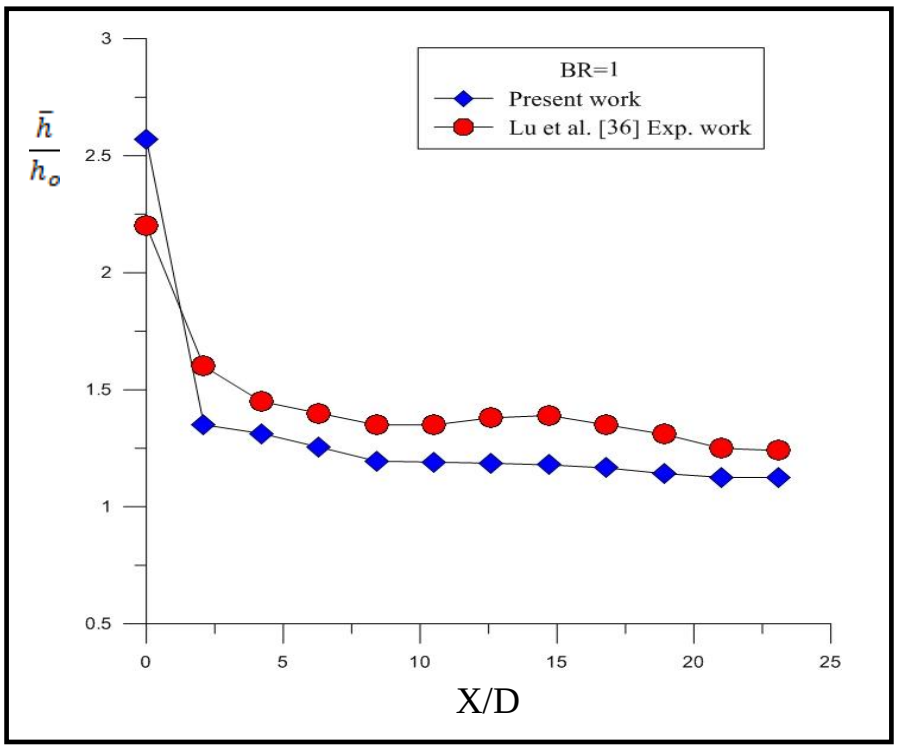

Figure (5-46): Verification of experimental results of heat transfer coefficient ratio ($\bar{h}/h_o$) of the present study with the experimental results of Lu et al. [36]

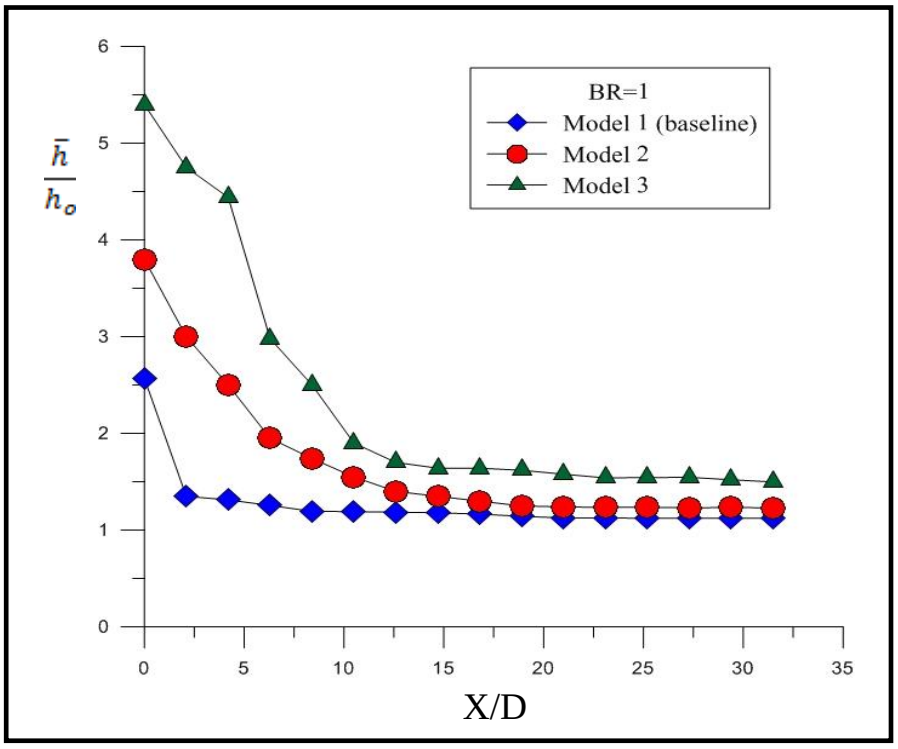

Figure (5-47): Effect of ramped cylindrical hole on the spanwise averaged heat transfer coefficient ratio ($\bar{h}/h_o$) distributions

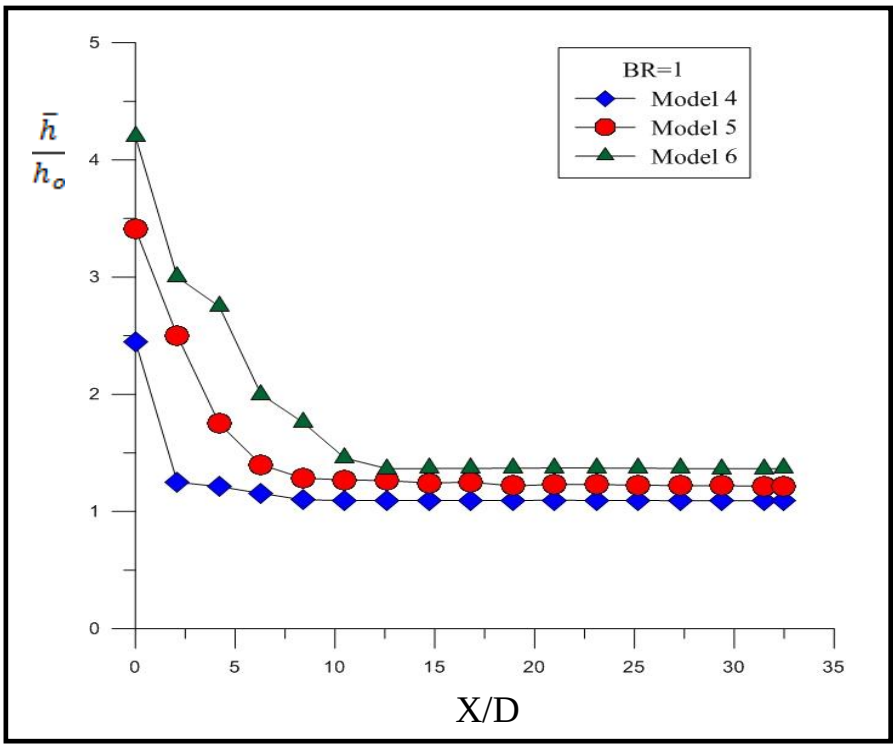

Figure (5-48): Effect of ramped conical hole on the spanwise averaged heat transfer coefficient ratio ($\bar{h}/h_o$) distributions

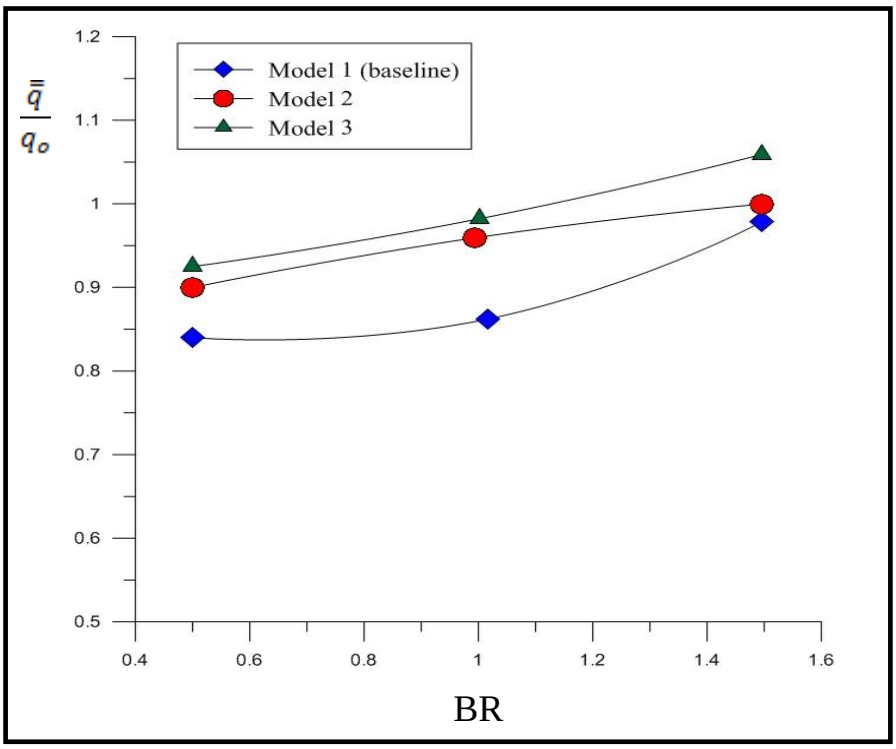

Figure (5-49): Effect of blowing ratio on the overall area-averaged heat flux ratio ($\bar{\bar{q}}/q_o$) for cylindrical hole models

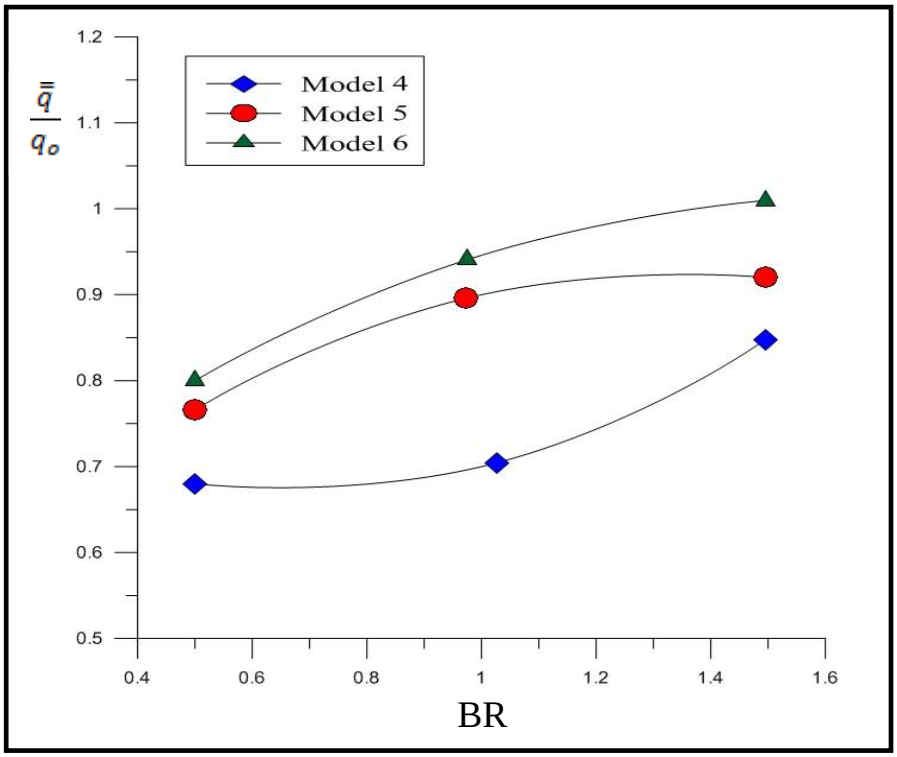

Figure (5-50): Effect of blowing ratio on the overall area-averaged heat flux ratio ($\bar{\bar{q}}/q_o$) for conical hole models

Chapter Six

Conclusions and Recommendations

Chapter Six
Conclusions and Recommendations

This chapter is providing the most important results obtained throughout this study either experimentally or theoretically in order to evaluate the film cooling performance when using ramped- holes injection holes.

6.1 Conclusions

The present work has reached to the following conclusions:

1. Numerical prediction of the flow field structure for holes arrangement showed that the vortices (counter pair kidney vortex and horseshoe vortex) both have major effects on the cooling performance, in which as the strength of the kidney vortex decreases and the horseshow vortex is lifting up, leading to an improvement in the coolant performance.
2. The conical hole shows much higher film cooling effectiveness than cylindrical hole in all blowing ratios; both showed a decrease of the film cooling effectiveness with increasing the blowing ratio.
3. A detailed study on two recent ramped-holes configurations enhanced the film cooling effectiveness and kept the heat flux ratios in rang of accepted values.
4. The film cooling effectiveness increased as the ramp height backward-facing step increased (large ramp angle).
5. Placing ramp at the hole edge gives the best film cooling effectiveness.

6.2 Futuristic Recommendations

According to the fields covered by the present investigation, the following lines of investigation are recommended for future works;

- Study the effect of using ramped-holes with curved surface.
- Study the effect of using ramps on the aerodynamic losses.
- Study the effect of using ramps with other holes shape.
- Study the effect of using ramps with more than one row of holes at different orientation angles on the film cooling performance.
- Study the effect of using ramps with the staggered hole arrangement.
- Study the performance of film cooling when using different ramp shapes.

References

REFERENCES

[1] William W. Bathie, "Fundamentals of Gas Turbines", second edition, John Wiley & Sons,Inc , 1996.

[2] Airplane Flying Handbook, U.S. Department of Transportation Federal Aviation Administration, FAA-H-8083-3A, 2004.

[3] Cohen H., Rogers G.F.C., Saravanamuttoo H.I.H., "Gas Turbine Theory", 4th edition, Longman House, Burnt Mill, England, 1996.

[4] Friedrichs, S., "End wall Film-Cooling in Axial Flow Turbines", PhD thesis, Cambridge University, 1997.

[5] Lakshminarayana, B., "Fluid Dynamics and Heat Transfer of Turbomachinery", John Wiley & Sons Inc., 1996.

[6] Jones, T.V., "Definition of Heat Transfer Coefficient in the Turbine Situation", IMechE 1991-3, C423/046, Turbomachinery: Latest Developments in a Changing Scene, pp. 201-206, 1991.

[7] Haven, B.A. and Kurosaka, M., "Improved Jet Coverage through Vortex Cancellation", AIAA Journal Vol.34, No. 11, pp. 2443-2444, 1996.

[8] Haven, B.A., Yamagata, D.K., Kurosaka, M., Yamawaki, S. and Maya, T., "Anti-kidney Pair of Vortices in Shaped Holes and Their Influence on Film Cooling Effectiveness" ASME Paper 97-GT-45, 1997.

[9] Han, J. C., Sandip D. and Srinath, V. Ekkad. "Gas Turbine Heat Transfer and Cooling Technology", Taylor & Francis Group, 2001.

[10] Goldstein, R. J., Eckert, E. R. G., Eriksen, V. L. and Ramsey, J. W., "Film Cooling Following Injection through Inclined Circular Tubes", Israel Journal of Technology, Vol. 8, No. 1-2, pp. 145-154, 1970.

[11] Goldstein, R.J. , Eckert, E.R.G. and Burggraf, R. , "Effects of Hole Geometry and Density on Three Dimensional Film Cooling",

International Journal of Heat and Mass Transfer, Vol.17, pp.595-606, 1974.

[12] Brown, A. and Saluja, C.L., "Film Cooling from a Single Hole and a Row of Holes of Variable Pitch to Diameter Ratio", International Journal of Heat and Mass Transfer, Vol. 22, pp. 525-533, 1978.

[13] Foster, N.W. and Lampard, D., "The Flow And Film Cooling Effectiveness Following Injection Through a Row of Holes", ASME Journal of Engineering Power, Vol.102, pp. 584-588, 1980.

[14] Makki, Y. and G. Jakubowski, "An Experimental Study of Film Cooling from Diffused Trapezoidal Shaped Holes", AIAA Paper No. 86-1326, 1986.

[15] Honami, S., Shizawa, T. and Uchiyama, A., "Behavior of the Laterally Injected Jet in Film Cooling: Measurements of Surface Temperature and Velocity/Temperature Field Within the Jet", ASME Journal of Turbomachinery, Vol. 116, pp. 106-112, 1994.

[16] Sen, B., Schmidt, D.L. and Bogard, D.G., "Film Cooling with Compound Angle Holes: heat transfer", ASME Journal of Turbomachinery, Vol.118, pp. 800-806, 1996.

[17] Schmidt, D.L., Sen, B. and Bogard, D.G., "Film Cooling with Compound Angle Holes: Adiabatic effectiveness", ASME Journal of Turbomachinery, Vol. 118, pp. 807-813, 1996.

[18] Kohli, A. and Bogard, D.G., "Adiabatic Effectiveness, Thermal Fields, and Velocity Fields for Film Cooling with Large Angle Injection", ASME Journal of Turbomachinery, Vol.119, pp.352-358, 1997.

[19] Ekkad, S. V., Zapata, D., and Han, J. C., "Film Effectiveness Over a Flat Surface with Air and CO_2 Injection Through Compound Angle Holes Using a Transient Liquid Crystal Image Method", ASME Journal of Turbomachinery, Vol.119, pp. 587-593, 1997.

[20] In Sung Jung and Joon Sik Lee, "Effects of Orientation Angles on Film Cooling over a Flat Plate: Boundary Layer Temperature Distributions and Adiabatic Film Cooling Effectiveness", ASME Journal of Turbomachinery, Vol.122, pp.153-160, 2000.

[21] Baldauf, S., Schulz, A. and Wittig, S., "High-Resolution Measurements of Local Effectiveness from Discrete Hole Film Cooling", ASME Journal of Turbomachinery, Vol. 123, pp. 758-765, 2001.

[22] Takahashi, H., Nuntadusit, C., Kimoto, H., Ishida, H., Ukai, T. and Takeishi, K., "Characteristics of Various Film Cooling Jets Injected in a Conduit", Annals New York Academy of Sciences, pp. 345-352, 2001.

[23] Lee, H.W., Park, J.J. and Lee, J.S., "Flow Visualization and Film Cooling Effectiveness Measurements Around Shaped Holes with Compound Angle Orientations", International Journal of Heat and Mass Transfer, Republic of Korea, Vol. 45, PP. 145-156, 2002.

[24] Yu, Y., Yen, C.-H., Shih, T.I.-P., Chyu, M.K., and Gogineni, S., "Film Cooling Effectiveness and Heat Transfer Coefficient Distributions Around Diffusion Shaped Holes", ASME Journal of Heat Transfer, Vol. 124, pp. 820-827, 2002.

[25] Rhee, D.H., Lee, Y.S., Kim, Y.B. and Cho, H.H., "Film Cooling and Thermal Field Measurements for Staggered Rows of Rectangular-Shaped Film Cooling Holes", ASME Paper No. GT2003-38608, Proceedings of ASME Turbo Expo, 2003.

[26] Yuen, C. H.N. and Botas, R.F.M., "Film Cooling Characteristics of a Single Round Hole at Various Stream Wise Angles in a Cross Flow: Part I Effectiveness", International Journal of Heat and Mass Transfer, Vol. 46, pp. 221-235, 2003.

[27] Hasan N., Sumanta A. and Ekkad,S.V., "Improved Film Cooling from Cylindrical Angled Holes with Triangular Tabs: Effect of Tab

Orientations", International Journal of Heat and Fluid Flow, Vol. 24, pp. 657-668, 2003.

[28] Barigozzi, G., Franchini, G. and Perdichizzi, A., "The Effect of an Upstream Ramp on Cylindrical and Fan-Shaped Hole Film Cooling – Part II: Adiabatic Effectiveness Results", ASME Turbo Expo, Paper No. GT2007-27079, 2007.

[29] Mohamad J. Hyder and Mansor A. Khan, "Study of Effect of Hole Shape on Film Cooling Effectiveness", Proceedings of International Bhurban Conference on Applied Sciences & Technology, Islamabad, Pakistan, 2011.

[30] Shuping P. Chen, Minking K. Chyu and Tom I.-P. Shih,"Effects of Upstream Ramp on the Performance of Film Cooling", International Journal of Thermal Sciences, Vol.50, pp. 1085-1094, 2011.

[31] Assim H.Yousif, Amer M. Al-Dabagh and Muwafag S. Alwan ,"Thermal Performance of Film Cooling for Two Staggered Rows Circular Jet", Engineering & Technology Journal, Vol.31, No.1, pp. 66-80, 2013 .

[32] Hyams, D., McGovern, K. and Leylek, J., "Effects of Geometry on Slot-Jet Film Cooling Performance", ASME Paper No. 96-GT-187, 1996.

[33] Cho, H.H, Rhee, D.H., Lee, and Kim, B. G., "Enhancement of Film Cooling Performance Using a Shaped Film Cooling Hole with Compound Angle Injection" , JSME International Journal, series B, Vol.44, NO.1, 2001.

[34] Bunker, R.S., "Film Cooling Effectiveness Due to Discrete Holes within a Transverse Surface Slot", ASME Paper GT2002-30178, 2002.

[35] Sargison, J. E., Guo, S. M., Oldfield, M. L.G., Lock, G. D. and Rawlinson, A. J., "Flow Visualization of a Converging Slot-Hole Film Cooling Geometry", ASME Paper GT 2002-30177, 2002.

[36] Lu, Y., Nasir, H. and Ekkad, S.V. , "Film Cooling From a Row Of Holes Embedded in Transverse Slots", ASME Paper IGTI2005-68598, 2005.

[37] Lu, Y., Dhungel, A., Ekkad, S.V. and Bunker, R.S., "Effect of Trench Width and Depth on Film Cooling from Cylindrical Holes Embedded in Trenches", ASME Paper GT 2007-27388, 2007.

[38] Walters, D.K. and Leylek, J.H., "A Detailed Analysis of Film-Cooling Physics: Part I—Streamwise Injection with Cylindrical Holes", ASME Journal of Turbomachinery, Vol. 122, pp. 102-112, 2000.

[39] Hyams, D. and Leylek, J.H., "A Detailed Analysis of Film Cooling Physics: part III- Streamwise Injection with Shaped Holes", ASME Journal of Turbomachinery, Vol. 122, pp. 122-132, 2000.

[40] Heidmann, J.D. and Hunter, S.D., "Coarse Grid Modeling of Turbine Film Cooling Flows Using Volumetric Source Terms", ASME Paper No. 2001-GT-0138, 2001.

[41] Abbe`s Azzi and Bassam A. Jubran, "Numerical Modeling of Film Cooling from Converging Slot-Hole", Heat Mass Transfer, Vol. 43, pp. 381–388, 2007.

[42] Sangkwon, Na. and Shih, T. I-P. , "Increasing Adiabatic Film-Cooling Effectiveness by Using an Upstream Ramp", Journal of Heat Transfer, Vol.129, pp. 464-470, 2007.

[43] Kanani, H., Shams M., Ebrahimi, R. and Ahmadian, T., "Numerical Simulation of Film Cooling Effectiveness on a Flat Plate", International Journal of Numerical Methods in Fluids, Vol. 56, Issue 8, pp. 1329-1336, 2008.

[44] Baheri, S., Alavi T. , S.P. and Jubran, B.A., "Film Cooling Effectiveness From Trenched Shaped and Compound Holes", Heat and Mass Transfer Journal, Vol. 44, pp. 989-998, 2008.

[45] Silieti, H., Kassab, A.J. and Divo, E., "Film cooling effectiveness: Comparison of Adiabatic and Conjugate Heat Transfer CFD Models", International Journal of Heat and Mass Transfer, Vol. 48, pp. 2237- 2248, 2009.

[46] Fayyaz H. A. and Muhammad J. H., "Computational Study of Film Cooling Effectiveness for a Comparison of Cylindrical, Square and Triangular Holes of Equal Cross-Sectional Area", Mehran University Research Journal of Engineering and Technology, Vol. 29, pp. 541-555, 2010.

[47] Dia, P. and Lin, F., "Numerical Study on Film Cooling Effectiveness from Shaped and Crescent Holes", Heat and Mass Transfer Journal, Vol. 47, pp. 147-154, 2011.

[48] Lee, K.D. and Kim, K.Y., "Surrogate Based Optimization of a Laidback Fanshaped Hole for Film Cooling", International Journal of Heat and Mass Transfer, Republic of Korea, Vol. 32, pp. 226-238, 2011.

[49] "Fluent 12 User's Guide, Programing and Tutorial Guide" Fluent, Version 12, ANSYS Inc, 2009.

[50] Versteeg, H.K. and Malalasekera, W., "An Introduction to Computational Fluid Dynamics the Finite Volume Method", Longman Group, London, 1996.

[51] Roy, D.N., " Applied Fluid Mechanics", Affiliated East-West Private LTD, New Delhi, 1987.

[52] Launder B.E. and Spalding D.B., "The Numerical Computation of Turbulent Flows", Computer Methods in Applied Mechanics and Engineering, Vol. 3, pp. 269-289, 1974.

[53] Launder, B. E. and Spalding, D. B., "Lectures in Mathematical Models of Turbulence", Academic Press, London, England, 1972.

[54] Theodoridis G.S., Lakhel D. and Rodi W., "Three-Dimensional Calculations of the Flow Field around a Turbine Blade with Film Cooling

Injection near the Leading Edge", Institute for Hydromechanics, University of Karlsruhe, Kaiserstrasse 12, D-76128 Karlsruhe, Germany, 2001.

[55] Chi Zhang, Bo Song,Yuzhen Lin, Quanhong Xu, and Gaoen Liu, " Cooling Effectiveness of Effusion Walls with Deflection Hole Angles Measured by Infrared Imaging" , Applied Thermal Engineering, Vol. 29, pp. 966-972, 2009.

[56] Jones, D.A. and Clarke, D.B., "Simulation of a Wind-body Junction Experiment Using the Fluent Code", DSTD-TR-1731, Australia, 2005.

[57] Barth, T. J. and Jespersen, D., "The Design and Application of Upwind Schemes on Unstructured Meshes", Technical Report AIAA-89-0366, AIAA 27th Aerospace Science Meeting, Reno, Nevada, 1989.

[58] Rhie, C. M. and Chow, W. L., "Numerical Study of the Turbulent Flow Past an Airfoil with Trailing Edge Separation", AIAA Journal, Vol. 21, No. 11, pp. 1525-1532, 1983.

[59] Patankar, S. V., "Numerical Heat Transfer and Fluid Flow", Hemisphere Publishing, Washington DC, 1980.

[60] Assim H.Y., Jawad, T.S. and Kadhim, J.A., "Design Study of a Low Speed Wind Tunnel", MTC Journal, No. 6, 1991.

[**6**1] Muwafaq S. Alwan, " Experimental and Numerical Investigation of Film Cooling Thermal Performance for Staggered Rows of Circular Jet", PhD thesis, University of Technology, Baghdad, 2012.

[62] Humam K. Jalghaf, "A Study into the Effect of Round Shaped Holes with Compound Angles Orientations on Film Cooling Effectiveness", MSc. thesis, University of Technology, Baghdad, 2013.

[63] BS1042 Standard, "Method of Measurement of Fluid Flow in Closed Conduits", Part 1, Section 1.1, 1980.

[64] BS1042 Standard, "Method for the Measurement of Fluid Flow in Pipes", Part 2A, 1974.

[65] FLUKE Ti32, Thermal Imagers, User's Manual, USA, 2009.

[66] Incropera, F. P. and DeWitt, D. P., *"*Fundamentals of Heat and Mass Transfer,*"* Fifth Edition, New York, John Wiley & Sons, 2002.

[67] Vedula, R. P. and Metzger, D. E., "A Method for the Simultaneous Determination of Local Effectiveness and Heat Transfer Distributions in a Three Temperature Convective Situations," ASME Paper 91-GT-345, 1991.

[68] Ekkad, S. V., Ou, S. and Rivir, R. V., "A Transient Infrared Thermography Method for Simultaneous Film Cooling Effectiveness and Heat Transfer Coefficient Measurements from a Single Test", GT2004-54236, Proceedings of ASME Turbo Expo, Vienna, Austria, 2004.

[69] Ekkad, S.V. and Zapata, D. , " Heat Transfer Coefficients Over a Flat Surface with Air and CO2 Injection Through Compound Angle Holes Using a Transient Liquid Crystal Image Method", ASME Journal of Turbomachinery, Vol. 119, pp. 580-586, 1997.

[70] Kline, S.J. and McClintock, F.A., "Describing Uncertainties in Single Sample Experiments", Mechanical Engineering, Vol. 75, pp. 3-8, 1953.

[71] Bunker, R. S., "Gas Turbine Heat Transfer: 10 Remaining Hot Gas Path Challenges", Proceedings of GT2006, ASME Turbo Expo: Power for Land, Sea and Air, Barcelona, SPAIN, May 2006.

[72] Nasir H., Acharya S., and Ekkad S. V. , "Improved Film Cooling from Cylindrical Angled Holes with Triangular Tabs: Effect of Tab Orientations", International Journal of Heat and Fluid Flow Vol.24 , pp.657-668, 2003.

[73] FILR System, Incorporated, Therma CAMTM P65, "User's Manual", North Billerica, MA. , 2006.

Appendices

Appendix A

The temperature measuring system calibration

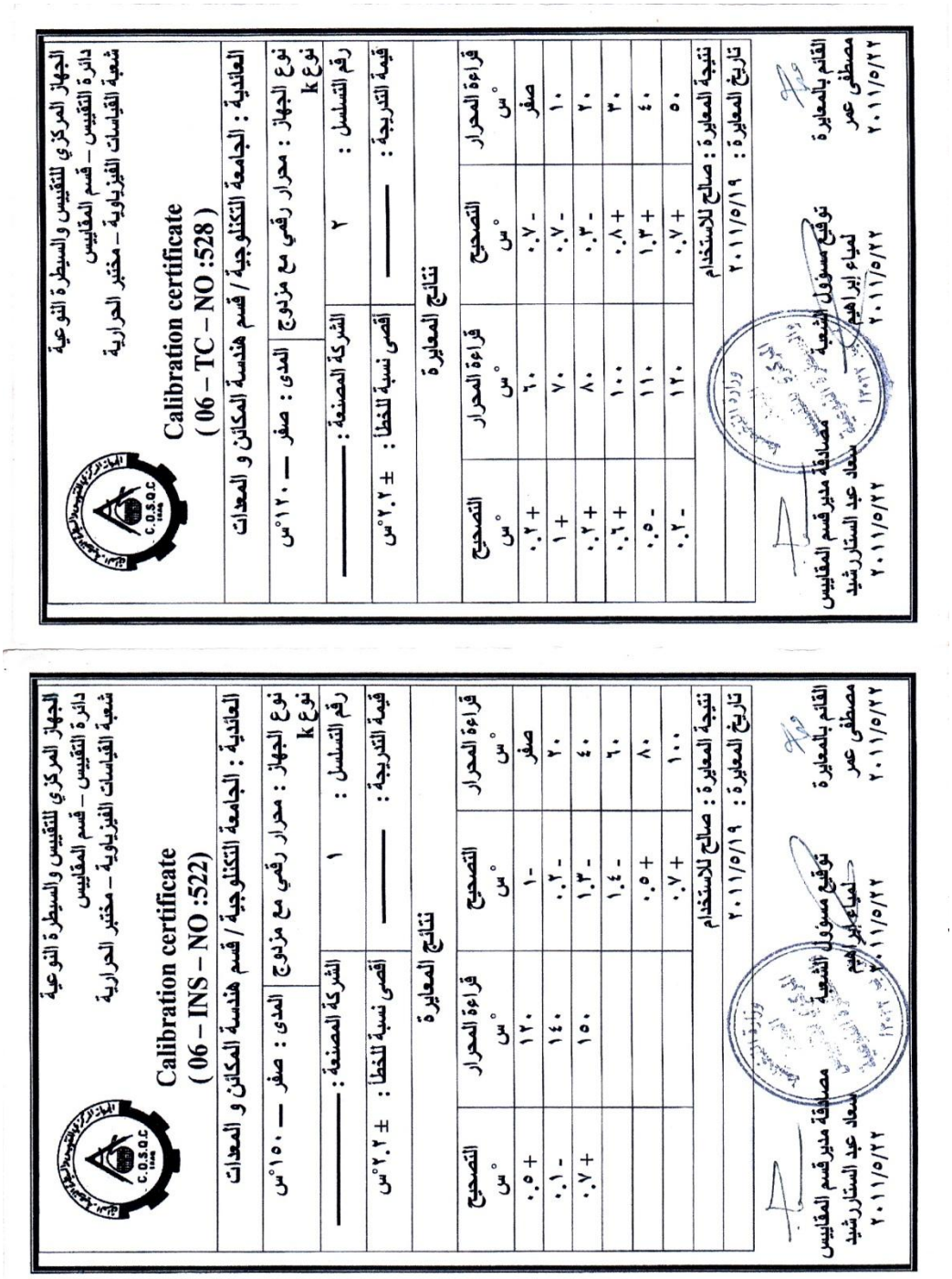

الجهاز المركزي للتقييس والسيطرة النوعية
دائرة التقييس – قسم المقاييس
شعبة القياسات الفيزياوية – مختبر الحرارية

Calibration certificate
(06 – TC – NO :528)

العائدية : الجامعة التكنلوجية / قسم هندسة المكائن و المعدات

نوع الجهاز : محرار رقمي مع مزدوج نوع k | المدى : صفر — ١٢٠°س | الشركة المصنعة : _____

رقم التسلسل : ٢ | قيمة التدريجة : _____ | أقصى نسبة للخطأ : ± ٢.٢°س

نتائج المعايرة

قراءة المحرار °س	التصحيح °س	قراءة المحرار °س	التصحيح °س
صفر	-٠.٧	٦٠	+٠.٢
١٠	-٠.٧	٧٠	+١
٢٠	-٠.٣	٨٠	+٠.٢
٣٠	+٠.٨	١٠٠	+٠.٦
٤٠	+١.٣	١١٠	-٠.٥
٥٠	+٠.٧	١٢٠	-٠.٢

نتيجة المعايرة : صالح للاستخدام

تاريخ المعايرة : ٢٠١١/٥/١٩

القائم بالمعايرة
مصطفى عمر
٢٠١١/٥/٢٢

توقيع مسؤول الشعبة
لمياء إبراهيم
٢٠١١/٥/٢٢

مصادقة مدير قسم المقاييس
سعاد عبد الستار رشيد
٢٠١١/٥/٢٢

الجهاز المركزي للتقييس والسيطرة النوعية
دائرة التقييس – قسم المقاييس
شعبة القياسات الفيزياوية – مختبر الحرارية

Calibration certificate
(06 – INS – NO :522)

العائدية : الجامعة التكنلوجية / قسم هندسة المكائن و المعدات

نوع الجهاز : محرار رقمي مع مزدوج نوع k | المدى : صفر — ١٥٠°س | الشركة المصنعة : _____

رقم التسلسل : ١ | قيمة التدريجة : _____ | أقصى نسبة للخطأ : ± ٢.٢°س

نتائج المعايرة

قراءة المحرار °س	التصحيح °س	قراءة المحرار °س	التصحيح °س
صفر	-١	١٢٠	+٠.٥
٢٠	-٠.٢	١٤٠	-٠.١
٤٠	-١.٣	١٥٠	+٠.٧
٦٠	-١.٤		
٨٠	+٠.٥		
١٠٠	+٠.٧		

نتيجة المعايرة : صالح للاستخدام

تاريخ المعايرة : ٢٠١١/٥/١٩

القائم بالمعايرة
مصطفى عمر
٢٠١١/٥/٢٢

توقيع مسؤول الشعبة
لمياء إبراهيم
٢٠١١/٥/٢٢

مصادقة مدير قسم المقاييس
سعاد عبد الستار رشيد
٢٠١١/٥/٢٢

Figure (A-1): Thermometer reader

Resolution/ ranges	0.1°C 0.1 °F	– 20 °C to 400 °C –4 °F to 752 °F
Accuracy	± 3 % of reading or ± 3°C (5 °F), which ever is greater. * ***Accuracy test under the measurement range within – 10 °C to 350 °C .*** * *Meter operating temp. within 23 ± 5 °C and the emissivity value of measurement target set to 0.95.* * *Spec. tested under the 20 cm dia. black body, the measuring distance from the probe sensing Head is 30 cm.* * *Spec. tested environment : RF Field Strength less than 3 V/M and frequency less than the 30 MHz.*	
Temp. Sensor	Thermocouple pie.	
Emissivity Setting	* *By push button. Setting range : 0.20 to 1.00.* * *The default emissivity value is 0.95, which will cover 90% of a typical application.*	
Measurement Wave length Region	6 to 12 micro meter.	
Distance Factor	D/S : Approx. 7:1. D – Distance, S – Spot.	

Figure (A-2): Thermometer reader specifications

Appendix B
Flow Rate Calculation

The coolant air flow rate through the orifice meter was calculated and corrected according to BS1042 [63]. The basic flow rate equation is given by:

$$\dot{m} = C \frac{\pi}{4} d_2^2 \sqrt{2g\rho_{air}\Delta h_w(\frac{\rho_w}{\rho_{air}} - 1)}$$

Where:

$C = C_d\, E\, \epsilon$

C_d = Discharge coefficient = 0.6182

E = Velocity of approach factor = $(1 - \beta^4)^{-\frac{1}{2}}$ = 1.163, where

$\beta = \frac{d_2}{d_1}$

d_2 = Orifice diameter = 0.014 m

d_1 = Pipe diameter = 0.02m

ϵ = Expansibility (expansion) factor = 0.947

$C = 0.67158$

$$\dot{m} = 0.67158 * \frac{\pi}{4} * (0.014)^2 \sqrt{2g\rho_{air}\Delta h_w(\frac{\rho_w}{\rho_{air}} - 1)}$$

Δh_w: obtained from U tube manometer.

Appendix C
The Pitot-tube correction

The reading of the tube is determined according to Ref. **[64]** as follows:

$\Delta P = (\rho H)_{water}.g = P_t - P_s = \frac{1}{2} E \rho u^2{}_\infty$

$E = E_o + w + \Omega$, where

E = Correction Coefficient,

E_0= Effect of static pressure holes distance equal to 0.9975. (For current study)

w = Viscosity coefficients= 0.0 (Fully developed flow), and

Ω = Distance effect from tube to wall which was found from figure below;

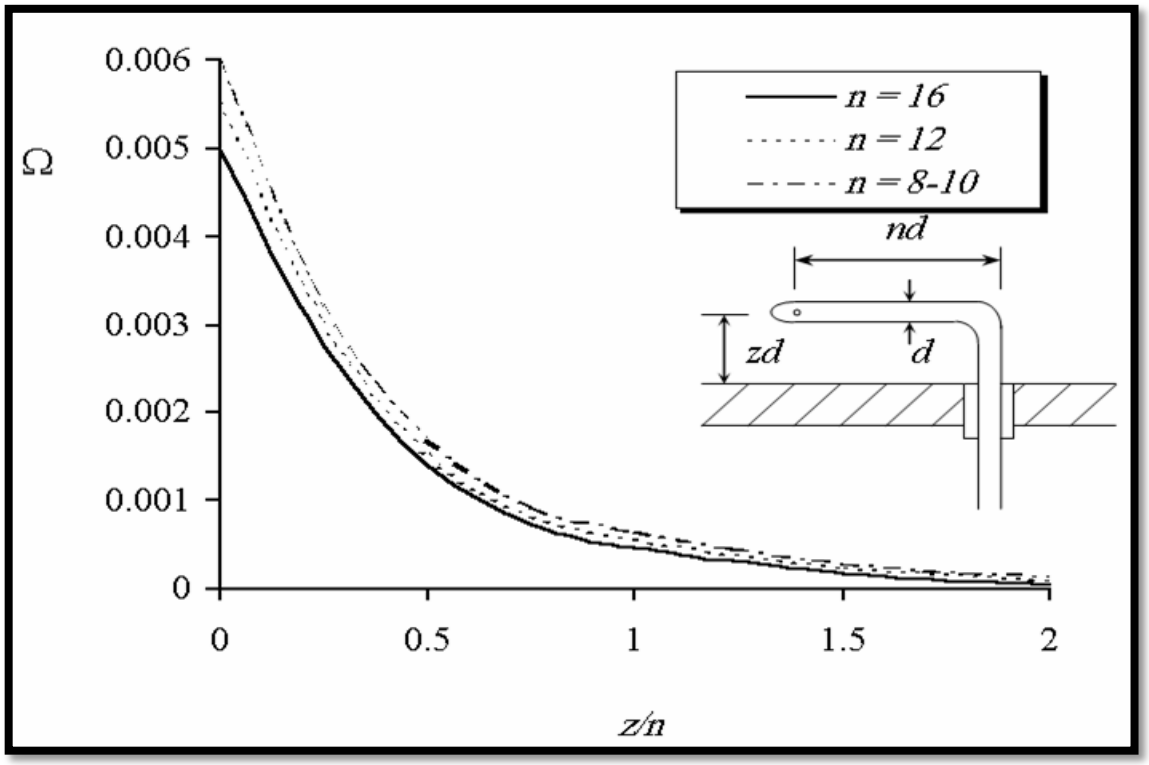

Correction of Pitot- static tube distance **[64]**

Appendix (D)

Principle of thermography measurement technique

All bodies at a temperature above the absolute zero emit thermal radiation in all wavelengths in all possible directions into space. Thermal radiation refers to radiation energy emitted by bodies because of their temperature. According to Maxwell's electromagnetic theory, radiation is treated as electromagnetic waves. The electromagnetic spectrum is divided arbitrarily into a number of wavelength regions, called bands. Figure (1) shows such subdivisions of the electromagnetic wave spectrum.

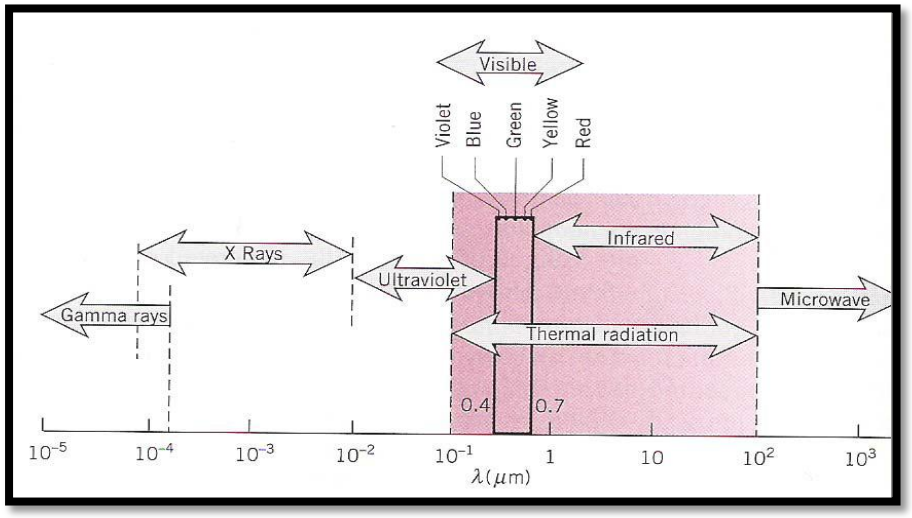

Figure (1) Electromagnetic spectrum of radiation [66]

There is no fundamental difference between radiations in the different bands of the electromagnetic spectrum. They are all governed by the same laws, and the only differences are those due to differences in wavelength.

Infrared Thermography makes use of the infrared spectral band. At the short-wavelength end, the boundary lies at the limit of visual perception. Whereas, at the long wavelength, it merges as microwave radio wavelengths. The infrared band is often further subdivided into four smaller bands, the boundaries of which are also arbitrarily chosen. They include: the near infrared (0.75-3 μm), the middle infrared (3-6 μm), the far infrared (6-15 μm) and the extreme infrared (15-100 μm).

Thermography is the use of an infrared imaging and measurement camera to "see" and "measure" thermal energy emitted from an object. Thermal, or infrared radiation, is electromagnetic radiation that is not visible, because its wavelength is longer than that of visible light. Unlike visible light, in the infrared world, everything with a temperature above zero emits heat. It is observed that the higher the object's temperature, the greater the IR radiation emitted. Infrared allows us to see what our eyes cannot. Infrared thermography cameras produce images of invisible infrared or "heat" radiation and provide precise non-contact temperature measurement capabilities. When viewing an object, the camera receives radiation not only from the object itself, but also collects radiation from the surroundings reflected via the object surface. Both these radiation contributions become attenuated to some extent by the atmosphere in the measurement path. Also, radiation contribution comes from the atmosphere itself.

IR CAMERA MEASUREMENT FORMULA

Figure (2) represents the description of the measurement situation in real conditions.

What has been neglected could for instance be sun light scattering in the atmosphere or stray radiation from intense radiation sources outside the field of view. Fortunately, in most cases, they are small enough to be neglected. Assume that the received radiation power (W) from a blackbody at source temperature (T_S) generates a camera output signal (U_S) which is proportional to the power input (power linear camera). The following equation can be written to represent the camera output signal as [73]:

$$U_s = C \times W(T_s) \;\; or \;\; U_s = CW_s \tag{1}$$

Where, (C) is constant. If the source be a gray body with emittance (ε), the received radiation will be (εW_S).

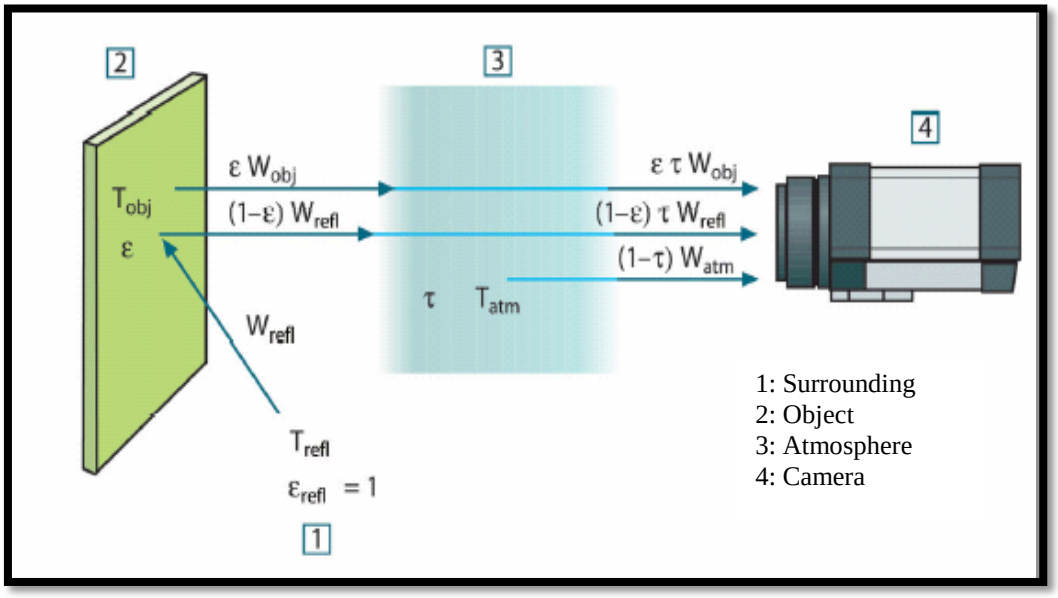

Figure (2) Schematic representation of the general thermography measurement situation [73].

From figure (2), the three collected radiation power terms can be written as:

1- Emission from the object = $\varepsilon\ \tau\ W_{obj}$ (2)

Where, (ε) is the emittance of the object, and (τ) is the transmittance of the atmosphere. The object temperature is (T_{obj}).

2-Reflected emission from the ambient source =$(1-\varepsilon)\ \tau\ W_{ref}$ (3)

Where, (1-ε) is the reflectance of the object. The ambient sources have the temperature (T_{ref}). It is assumed that the temperature (T_{ref}) is the same for all emitting surfaces within the half sphere seen from a point on the object surface. This is a necessary simplification in order to derive a workable formula.

The emittance for the surroundings is equal to 1 according to Ref. [73], and this is correct in accordance with Kirchhoff's law: "All radiation impinging on the surrounding surfaces will be absorbed by the same surfaces".

3-Emission from the atmosphere = $(1-\tau)\tau W_{atm}$ (4)

Where, $(1-\tau)$ is the emittance of the atmosphere. The temperature of the atmosphere is (T_{atm}). The total radiation power received can be written as:

$$W_{tot} = \varepsilon\ \tau\ W_{obj} + (1-\varepsilon)\tau W_{ref} + (1-\tau)\tau W_{atm} \quad (5)$$

Then, multiply each term by the constant (C) of equation (4-5) and replacing the (*CW*) products by the corresponding (*U*) according to the same equation to get the following equation:

$$U_{tot} = \varepsilon\ \tau\ U_{obj} + (1-\varepsilon)\tau U_{ref} + (1-\tau)\tau U_{atm} \quad (6)$$

Solving the above equation for (U_{obj})

$$U_{obj} = \frac{1}{\varepsilon\tau} U_{tot} - \frac{1-\varepsilon}{\varepsilon} U_{ref} - \frac{1-\tau}{\varepsilon} U_{atm} \quad (7)$$

This is the general measurement formula used in the Infrared (IR) camera used for the measurement, where:

U_{obj} = Calculated camera output voltage for a blackbody of temperature, T_{obj} , i.e., a voltage that can be directly converted into true requested object temperature.

U_{tot} = Measured camera output voltage for the actual case.

U_{ref} = Theoretical camera output voltage for a blackbody of temperature, T_{ref} according to the calibration.

U_{atm} = Theoretical camera output voltage for a blackbody of temperature, T_{atm} according to the calibration.

It is necessary to compensate for the effect of a number of different radiation sources to obtain temperature accurately. This is done on-line automatically by the camera. However, the following object parameters must be supplied to the camera:

- The emissivity.
- The transmissivity of the atmosphere, (If the atmosphere is air like in our case, is equal to 1).
- The temperature of the atmosphere.
- Object distance.

The test surface was painted with mat black to increase the emissivity of the test surface.

Appendix E

Matlab program flow chart

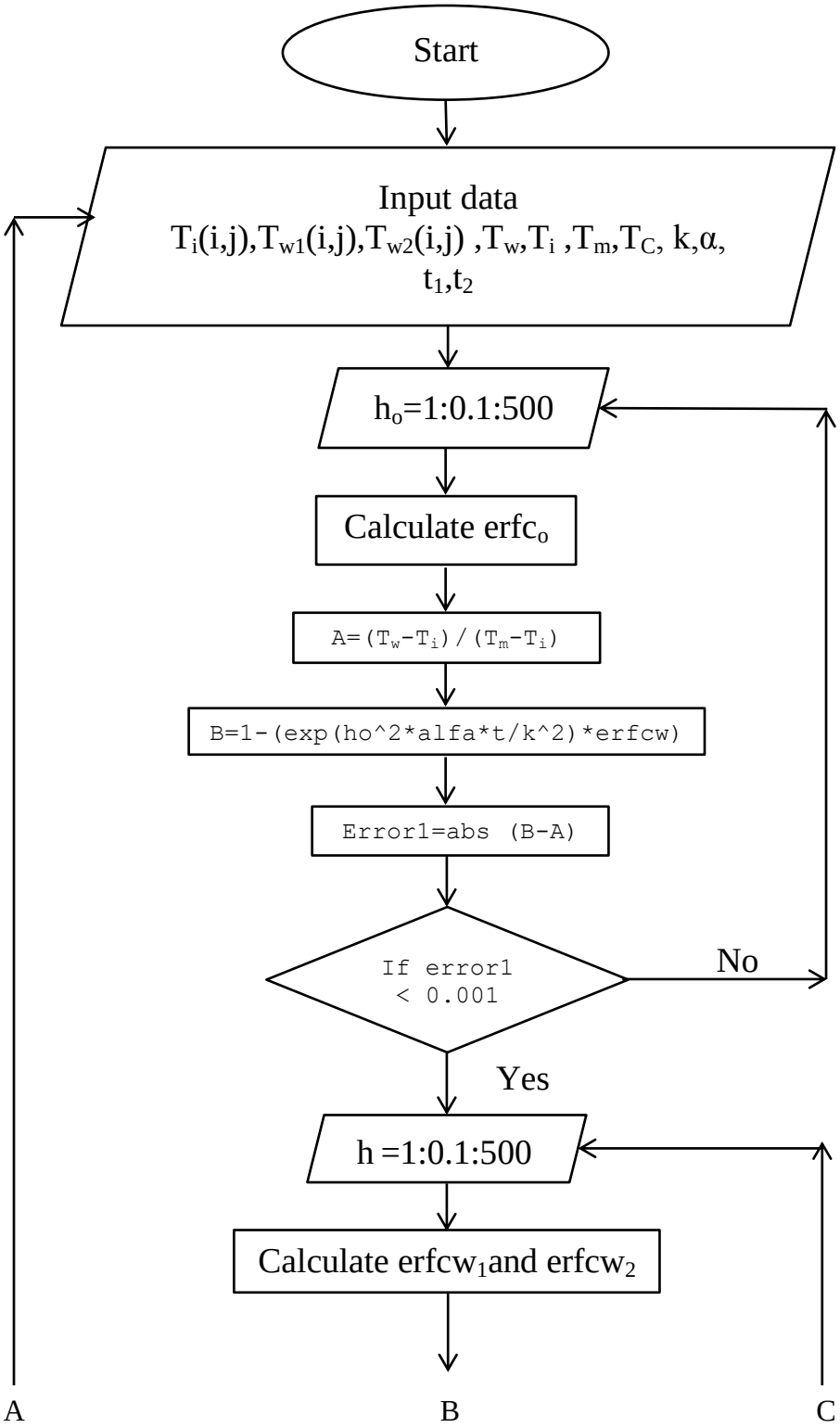

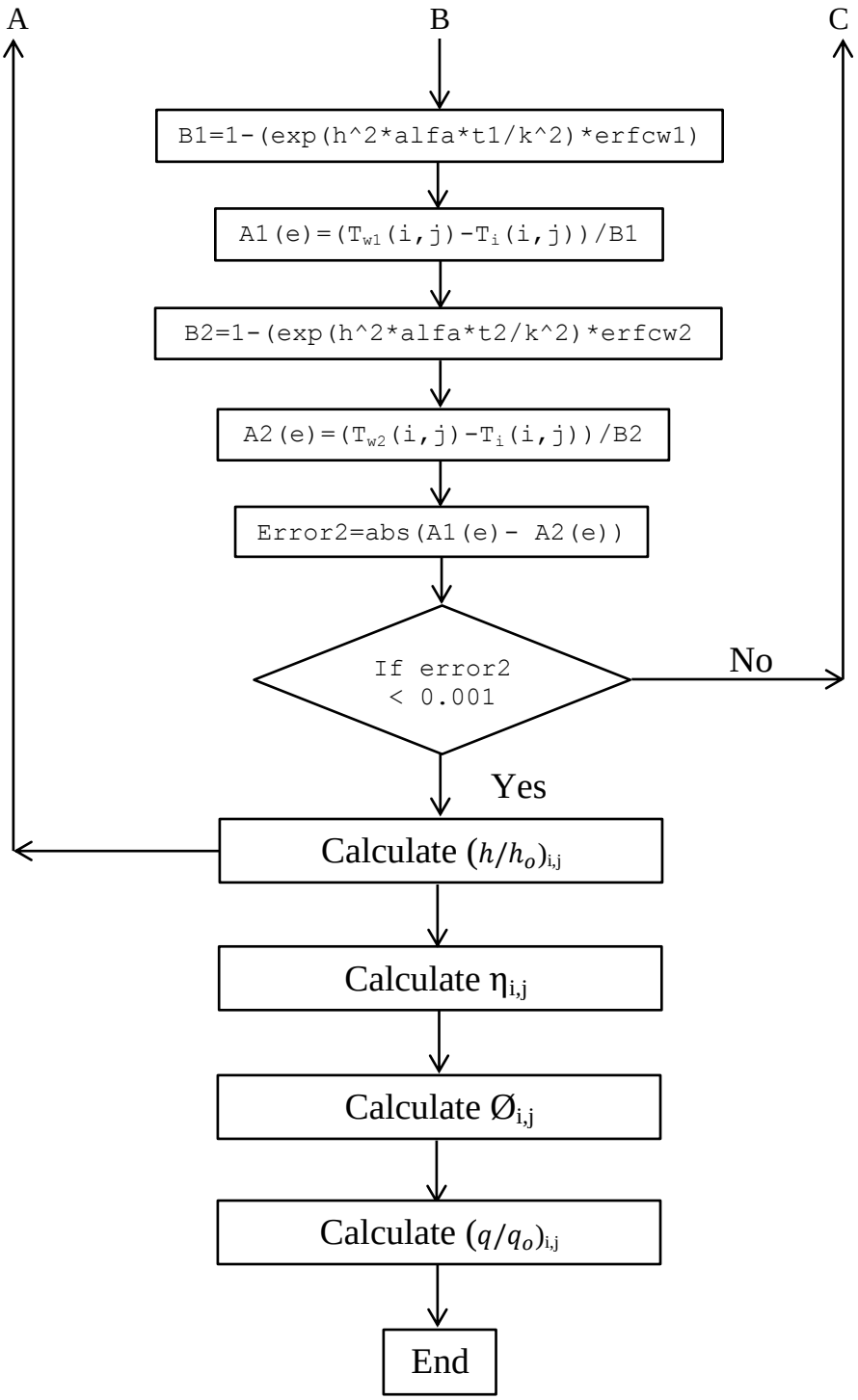
A
B
C
B1=1-(exp(h^2*alfa*t1/k^2)*erfcw1)
A1(e)=(Tw1(i,j)-Ti(i,j))/B1
B2=1-(exp(h^2*alfa*t2/k^2)*erfcw2
A2(e)=(Tw2(i,j)-Ti(i,j))/B2
Error2=abs(A1(e)- A2(e))
If error2 < 0.001
No
Yes
Calculate (h/ho)i,j
Calculate ηi,j
Calculate Øi,j
Calculate (q/qo)i,j
End

Appendix F

Author's Published Research

F-1
"Enhancement of adiabatic film cooling effectiveness by using conical shape hole"

Presented at the Anbar University-College of engineering
Anbar journal for engineering since

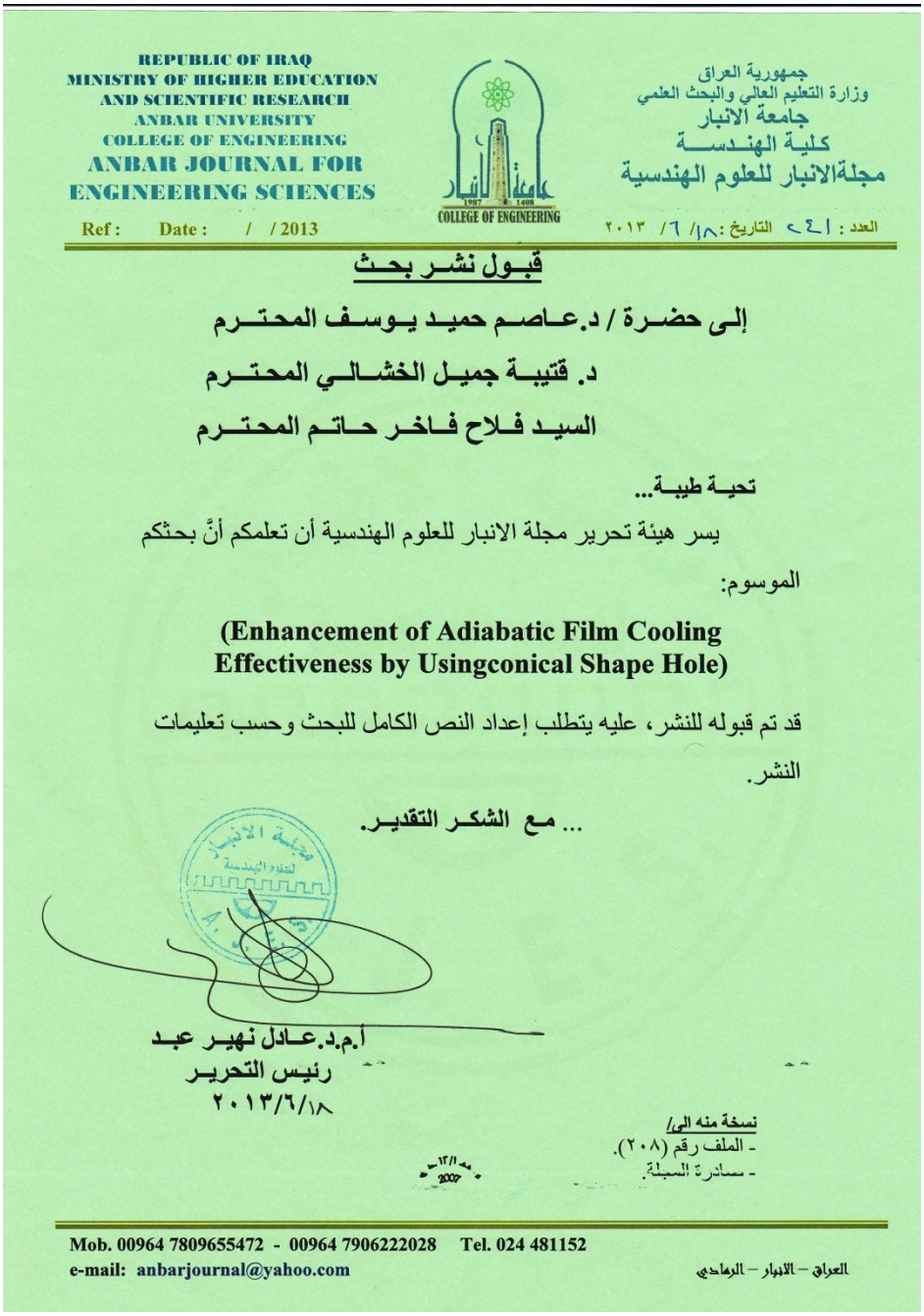

REPUBLIC OF IRAQ
MINISTRY OF HIGHER EDUCATION AND SCIENTIFIC RESEARCH
ANBAR UNIVERSITY
COLLEGE OF ENGINEERING
ANBAR JOURNAL FOR ENGINEERING SCIENCES

جمهورية العراق
وزارة التعليم العالي والبحث العلمي
جامعة الانبار
كلية الهندسة
مجلة الانبار للعلوم الهندسية

COLLEGE OF ENGINEERING

Ref : Date : / /2013

العدد : ٤١ التاريخ : ١٨/ ٦/ ٢٠١٣

قبول نشر بحث

إلى حضرة / د.عاصم حميد يوسف المحترم

د. قتيبة جميل الخشالي المحترم

السيد فلاح فاخر حاتم المحترم

تحية طيبة...

يسر هيئة تحرير مجلة الانبار للعلوم الهندسية أن تعلمكم أنَّ بحثكم

الموسوم:

(Enhancement of Adiabatic Film Cooling Effectiveness by Usingconical Shape Hole)

قد تم قبوله للنشر، عليه يتطلب إعداد النص الكامل للبحث وحسب تعليمات النشر.

... مع الشكر التقدير.

أ.م.د.عادل نهير عبد
رئيس التحرير
٢٠١٣/٦/١٨

نسخة منه الى/
- الملف رقم (٢٠٨).
- مسادرة السيلة.

Mob. 00964 7809655472 - 00964 7906222028 Tel. 024 481152
e-mail: anbarjournal@yahoo.com

العراق – الانبار – الرمادي

Enhancement of adiabatic film cooling effectiveness by using conical shape hole

Dr. Assim. H. Yoosif **Dr. Kutaeba J. M. AL-Khishali** **Falah F. Hatem**

assem_yousif20000@yahoo.com **falahhatem59@yahoo.com**

Mechanical Engineering Dep.

University of technology, Baghdad

ABSTRACT

Film cooling is one of the methods used to protect the surfaces exposed to high-temperature flows, such as those exist in gas turbines. It involves the injection of coolant fluid (at a lower temperature than that of the main flow) to cover the surface to be protected. This injection is through holes that can have various shapes; simple shapes, such as those with straight cylindrical or shaped holes (included many holes geometry, like conical holes). The computational results show that immediately downstream of the hole exit, a horseshoe vortex structure consisting of a pair of counter-rotating vortices is generated. This vortex generation affected the distribution of film coolant over the surface being protected. The fluid dynamics of these vortices are dependent upon the shape of the film cooling hole, and blowing ratio, therefore the film coolant coverage which determines the film cooling effectiveness distribution and also has an effect on the heat transfer coefficient distribution. Differences in horseshoe vortex structures and in resultant effectiveness distributions are shown for cylindrical and conical hole cases for blowing ratios of 0.5 and 1. The computational film cooling effectiveness values obtained are compared with the existing experimental results. The conical hole provides greater centerline film cooling effectiveness immediately at the hole exit, and better lateral film coolant coverage away of the hole exit. The conical jet hole enhanced the average streamwise adiabatic film cooling effectiveness by 11.11% and 123.2% at BR= 0.5 and 1.0, respectively, while in the averaged lateral adiabatic in the spanwise direction, the film cooling effectiveness enhanced by 61.75% and 192.6% at BR= 0.5 and 1.0, respectively .

Keywords: Film cooling, effectiveness, conical holes, Enhancement

1-INTRODUCTION

The thermal efficiency and specific power of gas turbine can be improved by increasing the turbine inlet temperature, operation a high-temperature caused a thermal failure to prevent that risk film cooling is commonly used. Film cooling involved injection of coolant from film holes to form a thin thermal barrier layer to protect the blade surface from the hot gases flow.

The objective of film cooling is to achieve low heat transfer from the surrounding hot mainstream to the turbine blades, and large effectiveness on the blade surface. In the recent years, several studies have focused on developing the holes shape to enhance film cooling effectiveness. Film cooling research on flat surface is common, flat surface models can be used to study the effects of individual parameters with relative ease and are less expensive. Studies have proved that the results obtained on simple flat surface models can be applied to real engine designs with slight corrections **[1]**. The definition of film cooling effectiveness is given in the dimensionless form, this effectiveness represents the efficiency of a cooling film; the maximum value of unity is achieved when the adiabatic wall temperature is the same as the coolant temperature. Studies on film cooling effectiveness in the hole streamwise direction on a flat are presented in **Fig. (1)**, for several existing researchers, such as, Eriksen and Goldstein **[2]**, Goldstein and Yoshida **[3]**, Goldstein et al. **[4]**, Bergeles **[5]**, Brown and Saluja **[6]**, Sinha et al. **[7]**, and Schmidt et al. **[8]**. From the literature, one can conclude that the optimum injection angle is found to be as (30º-35º) according to Bunker**[9]**, in which the flow pattern of the 30^o and 35^o jet(s) can take different forms, depending on the blowing ratio, the jet(s) can remain attached, detach and reattach, or lift off completely. From the cited references above, it was suggested for a single jet and a row of jets of a given streamwise inclination, the effectiveness near the holes increased with increasing blowing ratio, until a certain value beyond which the jets started to lift off, and the effectiveness decreased, and this ratio is often referred as the optimum blowing ratio. The optimum blowing ratio for a single 30^o to 35^o jet is usually between a blowing ratio of 0.4 and 0.6, and slightly less for a single vertical jet around 0.5, and relatively less for a row of 60^o jets. It is well known that significant improvement can be achieved in cooling characteristics of the film by using cooling holes with appropriately designed expanded exits. Goldstein et al. **[10]** were among the first to pioneer the use of shaped film holes for improved film cooling performance. The performance of inclined holes with 10° laterally flared exit was compared with the performance of streamwise inclined cylindrical film holes. Effectiveness data showed that the shaped film hole provides better lateral coverage and better centerline effectiveness. Hyung et al. **[11]** investigated experimentally and numerically the film cooling performance around a conical-shaped film cooling hole with compound angle orientations. The result shows that the shaped holes reduced the penetration of jet, and more uniform cooling performance is obtained even at relatively high blowing rates, because the conically expanded hole exit reduces the momentum of the lateral spreading. The better cooling performance is obtained with shaped holes expands 4^o in all direction from the hole middle to the exit. Schmidt et al **[8]** and Sen et al. **[12]** presented two companion papers in which the effect of adding a 15° forward diffusion exit to a streamwise oriented hole was investigated. They found that the exit diffused film hole demonstrated better spread of adiabatic effectiveness than the cylindrical counterpart. From the heat transfer coefficient standpoint, the forward expanded hole performed poorly, presumably because of the increased interaction between the jet and mainstream. Kohli and Bogard **[13]** examined the film cooling effectiveness of the shaped holes on a flat plate using 35^o and 55^o injection angles, the result shows shaped holes with large injection angle has better cooling performance than cylindrical holes. They also report on the thermal and velocity fields in the region around the injection holes. Sargison et al. **[14]** Studied a converging slot-hole geometry (console) in which the hole transitions from circular to slot with convergence in the axial direction and divergence laterally. The attempt was to make the three-dimensional nature of the jet into a two-dimensional slot film. The results were aimed at improving effectiveness. Yuen and Martinez-Botas **[15]** studied the film cooling effectiveness using a cylindrical hole at an angle of 30^o, 60^o, and 90°. A

hole length of L=4D was used, the free-stream Reynolds number based on the free-stream velocity and hole diameter was 8563, and the blowing ratio was varied from 0.33-2. For a single 30° hole, in the region immediately downstream of the hole, the maximum effectiveness occurred for a blowing ratio less than 0.5. Downstream of this immediate region, centerline effectiveness and lateral spread increased up to a blowing ratio of 0.5, then decreased with increasing blowing ratio due to jet penetration into the free stream. Also, the region with effectiveness greater than 0.2 did not extend beyond X/D=13. Baheri et al. **[16]** presented a comparative-numerical investigation on film cooling from a row of simple and compound angle holes injected at 35º on a flat plate with four film cooling configurations: (a) cylindrical film hole; (b) 15º forward diffused film hole; (c) trenched cylindrical film hole; and (d) trenched 15º forward diffused film hole. All simulations are at fixed blowing ratio of 1.25 and pitch to diameter ratio of 3. The mathematical film cooling model consists of the RANS, the energy equation and the standard (k-ε) model using a finite volume method. They found that the trenched compound angle injection shaped hole produces much higher film cooling protection than the other configurations. Fayyaz and Muhammad **[17]** compared computationally using CFD Fluent the film cooling effectiveness of cylindrical, square and two types of equilateral triangular holes with an inclination of 30^o with streamwise direction, theoretical results of the cylindrical hole compared with experimental results by Yuen and Martinez-Botas **[15]** showing well in agreement even for high blowing ratio. They also observed that triangular hole having lateral straight edge on leeward side shows much higher effectiveness values than circular film cooling hole case in the near hole region and almost similar coolant jet height as that in case of circular film cooling. Also, it is observed that triangular hole having lateral straight edge on windward side and converging corner on leeward side shows lesser coolant jet height and higher film cooling effectiveness in the region X/D>10, especially at blowing ratios greater than 1.0.

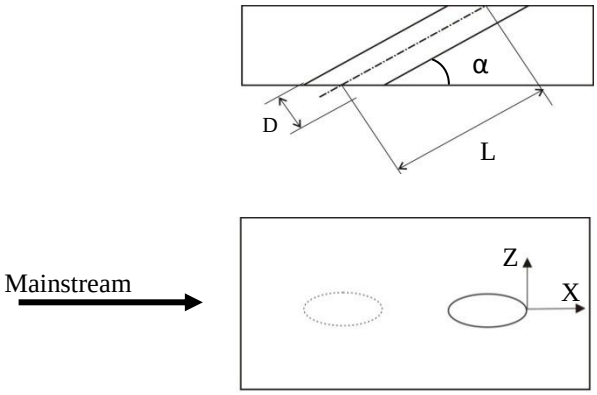

Figure (1) Hole at a streamwise angle, α

2- PROBLEM DESCRIPTION

The film cooling performance of conical hole geometry is compared with cylindrical hole geometry numerically by using a commercial CFD package (FLUENT from ANSYS). The computational results of cylindrical holes are compared with the existing experimental results given by Durham **[18]**, Kohli **[13]**, and Sinha **[7]**. The problem is treated as steady state, three dimensions, incompressible, and turbulent flow. Schematic diagram (with dimensions in millimeters) of the side view of the computational domain and both holes of the film cooling problem is shown in **Fig.(2)**, the cooling jet emerged from a plenum through one row of cylindrical or conical holes, each cylindrical hole has a diameter D of 5 mm, a length of 3.5D and an inclination angle of 35^{o} relative to the plane tangent to the flat plate. The spacing between the centers of the film-cooling holes in the spanwise direction is 3D.The conical hole has a diameter of 5 mm at plenum edge diverged by 4^{o} to the flat plate exit and an inclination angle(α) of 35^{o} between hole centerline and plane tangent to the flat plate. The exact dimensions and parameters have been chosen, so that the results can be compared to those discussed in references.

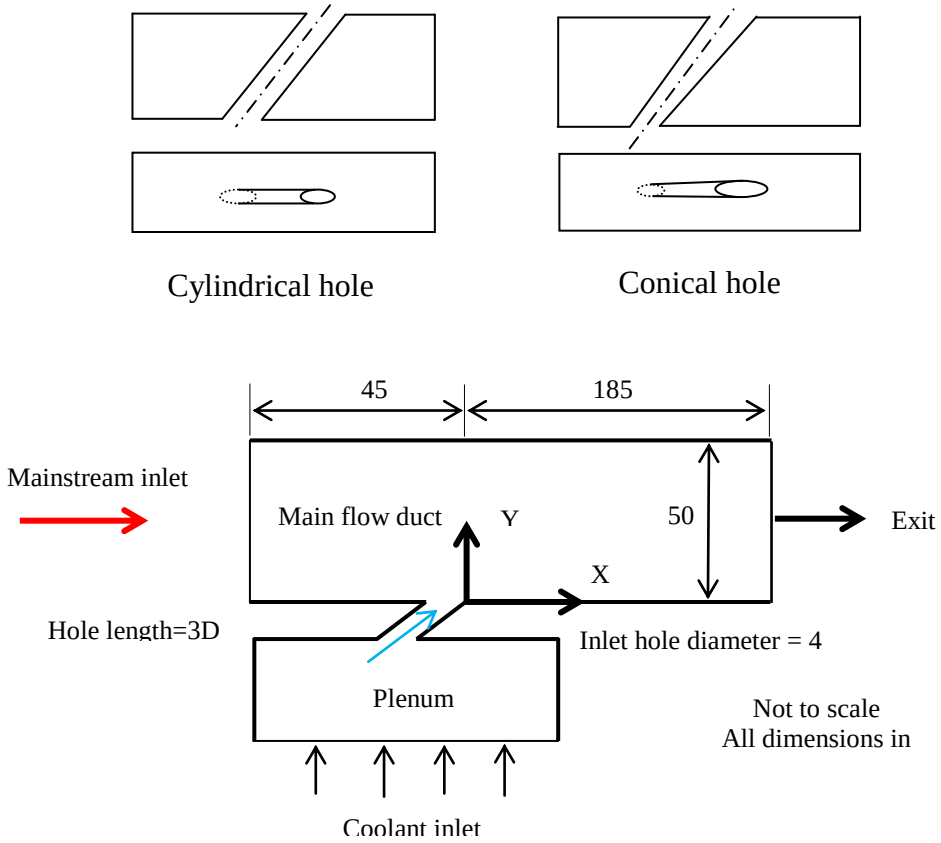

Figure (2) Schematic of the film-cooling configuration studied

3- GOVERNING EQUATIONS

The time-averaged, steady state Navier-Stokes equations as well as equations for mass and energy are solved. The governing equations for conservation of mass, momentum, and energy are given as:

$$\frac{\partial}{\partial x}(\rho u_i) = S_m \tag{1}$$

$$\frac{\partial}{\partial x}(\rho u_i u_j) = \rho\overline{g_j} - \frac{\partial p}{\partial x_i} + \frac{\partial}{\partial x_i}(\tau_{ij} - \rho\overline{\acute{u}_i\acute{u}_j}) + F_j \tag{2}$$

$$\frac{\partial}{\partial x}(\rho u c_p u_i T) = \frac{\partial}{\partial x_i}\left(\lambda\frac{\partial T}{\partial x_i} - \rho c_p\overline{\acute{u}_i\acute{T}}\right) + \mu\phi + S_h \tag{3}$$

Where τ_{ij} is the symmetric stress tensor defined as:

$$\tau_{ij} = \mu\left(\frac{\partial u_j}{\partial x_i} + \frac{\partial u_i}{\partial x_j} - \frac{2}{3}\delta_{ij}\frac{\partial u_k}{\partial x_k}\right) \tag{4}$$

$(\mu\phi)$ Is the viscous dissipation, and λ is the thermal conductivity. The terms of $\rho\overline{\acute{u}_i\acute{u}_j}$ and $\rho c_p\overline{\acute{u}_i\acute{T}}$ represent the Reynolds stresses and turbulent heat fluxes, respectively which should be modeled properly for a turbulent flow.

Two additional transport equations for the turbulence kinetic energy (k) and the turbulence dissipation rate (ε) are solved. The standard (k –ε) model **[19]** is a semi-empirical model based on model transport equations for the turbulent kinetic energy (k) and its dissipation rate (ε). Assumed that the flow is fully turbulent, and the effects of molecular viscosity are negligible, the turbulence kinetic energy (k) and its dissipation rate (ε) are obtained from the following equations **[20]**:

$$\frac{\partial}{\partial x_i}\rho k u_i = \frac{\partial}{\partial x_j}\left[\left(\mu + \frac{\mu_t}{\sigma_k}\right)\frac{\partial K}{\partial x_j}\right] + G_k + G_b - \rho\varepsilon + Y_M + S_k \tag{5}$$

$$\frac{\partial}{\partial x_i}\rho\varepsilon u_i = \frac{\partial}{\partial x_j}\left[\left(\mu + \frac{\mu_t}{\sigma_\varepsilon}\right)\frac{\partial \varepsilon}{\partial x_j}\right] + C_{1\varepsilon}\frac{\varepsilon}{k}(G_k + C_{3\varepsilon}G_b) - C_{2\varepsilon}\rho\frac{\varepsilon^2}{k} + S_\varepsilon \tag{6}$$

Turbulent viscosity (μ_t) is computed as a function of (k) and (ε).

$$\mu_t = \rho C_\mu\frac{k^2}{\varepsilon} \tag{7}$$

The generation of turbulence kinetic energy due to the mean velocity gradients (G_k) is computed by:

$$G_k = -\rho\acute{u}_i\acute{u}_j\frac{\partial u_j}{\partial x_i} \tag{8}$$

The generation of turbulence kinetic energy due to the buoyancy (G_b) can be neglected. Y_M represents the contribution of the fluctuating dilatation in compressible turbulence to the overall dissipation rate, ($C_{1\varepsilon}$) , ($C_{2\varepsilon}$) , and (C_μ) are taken as the default values ($C_{1\varepsilon}$ =1.44, $C_{2\varepsilon}$=1.92, and C_μ=0.09) in FLUENT **[21]**. (σ_k) and (σ_ε) are the turbulent Prandtl numbers for (k) and (ε) taken as 1 & 1.3, respectively. (S_k) and (S_ε) are user-defined source terms **[21]**.
The term (λ) in the energy equation (3) is the effective thermal conductivity which is given by:

$$\lambda = k + \frac{c_p u_t}{Pr_t} \tag{9}$$

The cooling effectiveness is defined as:

$$\eta = \frac{T_m - T_w}{T_m - T_c} \tag{10}$$

4- BOUNDRY CODITIONS

At all boundaries except those denoted as "main inlet", "coolant inlet", "exit", and symmetry boundary conditions shown in **Fig.2**, an adiabatic wall boundary condition is used. At the "main inlet," a velocity-inlet boundary condition is specified with x-velocity equal to 20 m/s, and all other components equal to zero. The temperature is given as 323K at the main inlet. The turbulence intensity and hydraulic diameter (which is used to determine the turbulence length scales) are specified as 2% and 24 mm, respectively. The plenum inlet mass flow rate was adjusted to produce the blowing ratio desired and the inlet temperature of the coolant is 298K to match the coolant to freestream density ratio (DR) of 1.09 with experiments. The turbulence intensity and hydraulic diameter are specified as 3% and 23mm, respectively. At the "exit", a pressure-outlet boundary condition is specified with a gage pressure equal to zero (giving an absolute pressure of 101.325 Pa).

5- SOLVER

A 3D segregated, steady state solver is used for linearization of governing equations, implicit method is used. For turbulence modeling, (k-ε) model with standard wall functions is used **[19, 20]**.To avoid use of enhanced wall treatment the mesh was kept fine enough to have wall Y+ in the range 0-10. Discretization scheme used is 2nd order upwind for momentum as given by **[22]**, turbulence kinetic energy, turbulence dissipation rate and energy, whereas for pressure standard, discretization scheme is used as given by **[23]**. For pressure-velocity coupling, a simple algorithm is used as given by **[24]**.

6- RESULTS AND DISCUSSION

For two geometries, two values of the blowing ratio which is defined as BR=$\rho_c U_c$ / $\rho_m U_m$ are considered, namely BR=0.5 and BR=1.0. For comparison purposes, the averaged centerline (streamwise) adiabatic film cooling effectiveness and the averaged lateral (spanwise) adiabatic

film cooling effectiveness are used as the main comparison parameters. In the first part of present work, the experimental data given by **[7, 18 &13]** are used to confine the present CFD results for the case of cylindrical hole shape. Results presented in **Figs. (3, 4 and 5)** are for averaged centerline film cooling effectiveness and averaged lateral film cooling effectiveness. These results reveal that the centerline effectiveness is in excellent agreement with the experimental results, **Fig. (3)**, in the entire region except in the near hole region when (X/D < 5). Immediate decrease of centerline effectiveness is due to either the mainstream penetration in to coolant jet or due to coolant jet lift-off from the adiabatic test surface, For low blowing ratios (0.5), as the coolant velocities are smaller as compared to mainstream velocity, so jet lift-off is low as clear from higher centerline effectiveness in the near hole region, the immediate decrease of effectiveness for these low blowing ratios in near hole region is due to the penetration of mainstream fluid into the coolant jet. For blowing ratios greater than 0.5, centerline effectiveness decreases to very low values in the near hole region, this is due to the jet lifting-off from the surface, as shown in **Fig.(4)**. CFD results for averaged lateral film cooling effectiveness are in a well agreement with the experimental results for low blowing ratios of 0.5, as shown in **Fig.(5)**, while **Fig.(6)** illustrates the main flow features of a single (cylindrical and conical) hole injected air in the mainstream direction at two blowing ratios of 0.5 and 1. The amount of central spreading of coolant far downstream of the hole is better for conical holes, especially at high blowing ratio. Comparisons of cylindrical and conical holes cases of effectiveness on the downstream test surface of the hole for blowing ratios of 0.5 and 1.0 are presented in **Fig. (7)**. Immediately downstream the holes exit, a so-called horseshoe vortex structure consisting of a pair of counter-rotating vortices is generated. This vortex generation has an effect on the distribution of film coolant over the surface being protected. The fluid dynamics of these vortices is dependent upon the shape of the film cooling holes and blowing ratio, therefore so is the film coolant coverage which determines the film cooling effectiveness distribution. In general, multiple vortex structures are produced where two large vortex structures have been detected, the pair of counter rotating vortices, and horseshoe vortices. The counter rotating vortex are the largest vortex appeared in the flow structure, which occurs at the interaction of coolant jet and hot mainstream, as shown in **Fig. (8)**. The vortex main structures are originated from the holes rims as shown in a front view direction, which agree with most literature **[25, 26]**. As the vortex propagates downstream the hole, the vortex grows continually downstream, as shown in **Fig. (8)**. Kidney-vortices have sense of rotation that acts as the coolant lifter. The jet lift-off phenomenon typically occurs at a high momentum ratio (i.e., BR> 0.5). For low blowing ratio (i.e., BR=0.5) the momentum ratio is also very low, the mainstream flow departs upward flow pushing the coolant jet towards the surface. This occurs in the cylindrical and conical hole producing low jet vortices levels, and the coolant stays attached to the surface, providing good film coolant effectiveness. But, at high blowing ratio (i.e., BR=1), the jet has high jet vortices levels in the cylindrical hole then the coolant lifted-off from the surface providing bad film cooling effectiveness, but in the conical hole and due to the divergent passage, the coolant jet has no high vortices levels, so it's providing a good film coolant effectiveness, as shown in **Fig.(7)**. The comparison was made between the numerical results of cylindrical and conical holes, at blowing ratio of 0.5 and 1are made in **Figs. (9 to12)**, the streamwise and spanwise film cooling effectiveness provided by the conical hole is better than that of the cylindrical hole, particularly at blowing ratio of 1. The cylindrical hole provides an averaged centerline film cooling effectiveness of 0.3653 and area-averaged film cooling effectiveness for whole surface of 0.1145, while the conical hole provides 0.4059 for the averaged centerline film cooling

effectiveness and 0.1852 for the area-averaged one. The enhancement for averaged centerline cooling effectiveness is 11.11% and 61.75% for the area-averaged film cooling effectiveness. At blowing ratio of 1, the cylindrical hole provides a centerline film cooling effectiveness of 0.2309 and area-averaged film cooling effectiveness for whole surface of 0.0787, while the conical hole provides 0.5153 for the centerline film cooling effectiveness and 0.2303 for the area-averaged one. The enhancement for centerline film cooling effectiveness is 123.32% and 192.63% for the area-averaged film cooling effectiveness.

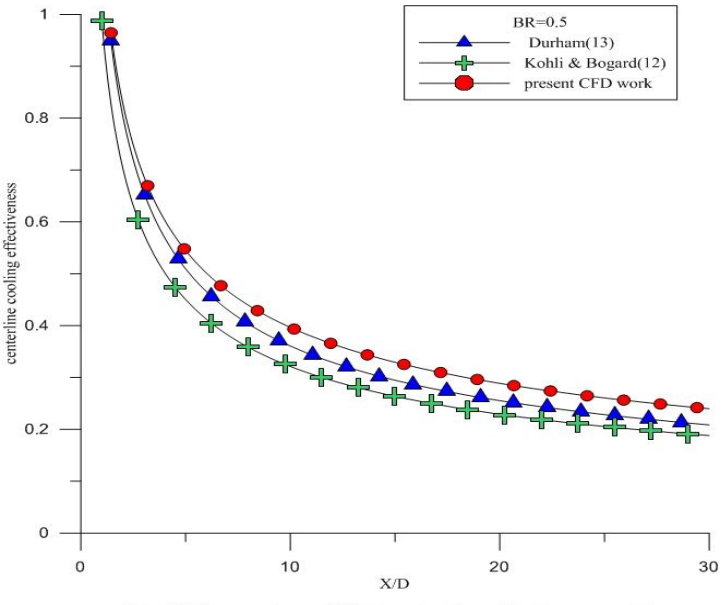

Figure (3) comparison of CFD centerline effectiveness with experiment (BR=0.5)

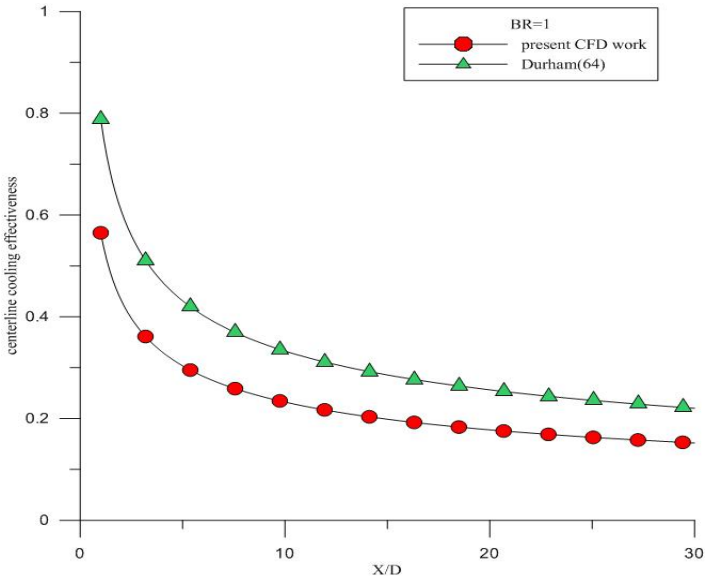

Figure (4) comparison of CFD centerline effectiveness with experiment (BR=1)

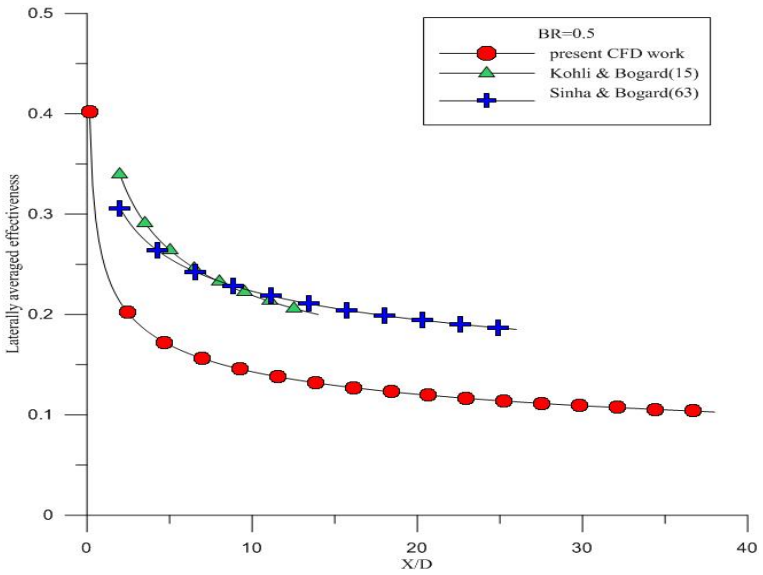

Figure (5) comparison of CFD laterally averaged effectiveness with experiment (BR=0.5)

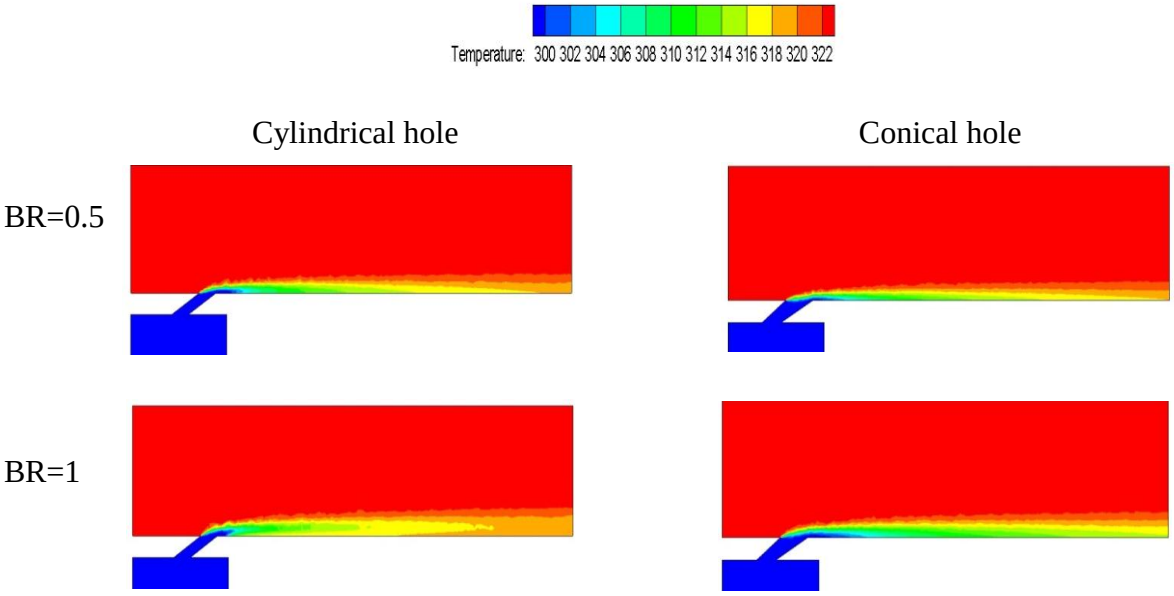

Figure (6) Mainstream and coolant jet interaction contour distribution for cylindrical & conical holes at different BRs

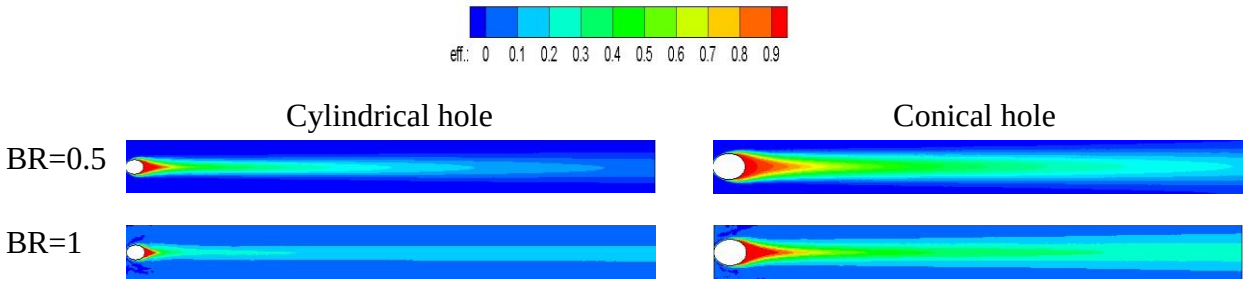

Figure (7) Effectiveness distribution for cylindrical & conical holes at different BRs

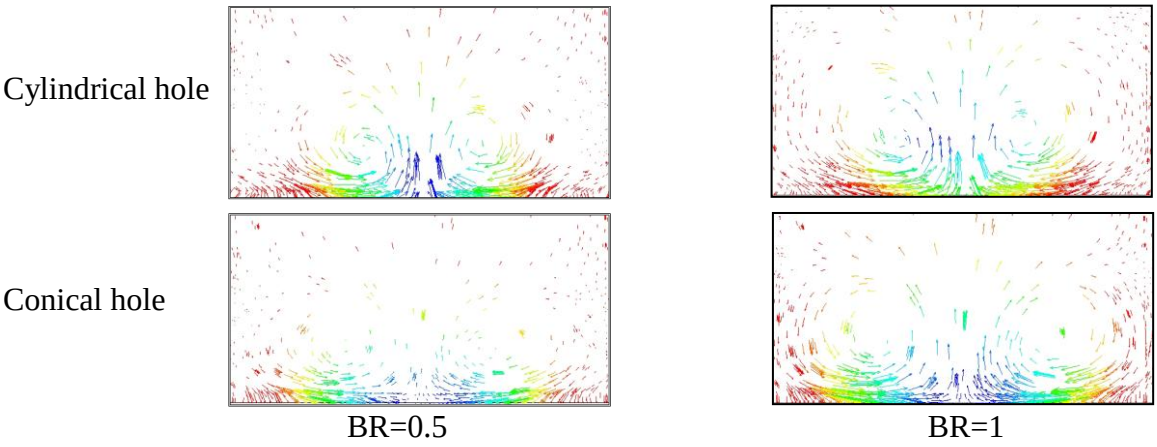

Figure (8) Flow vectors colored by temperature at X/D=3 for single hole forward injection at different BRs

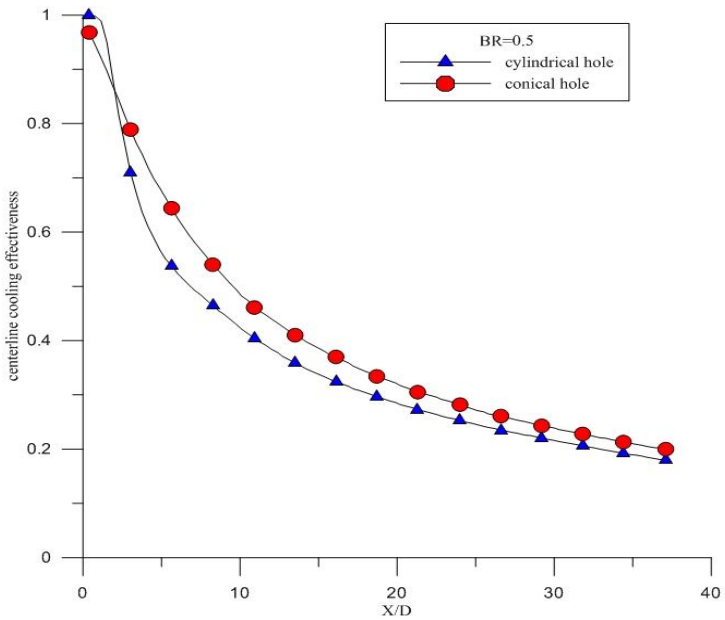

Figure (9) comparison of centerline effectiveness versus nondimensional position between cylindrical & conical hole (BR=0.5)

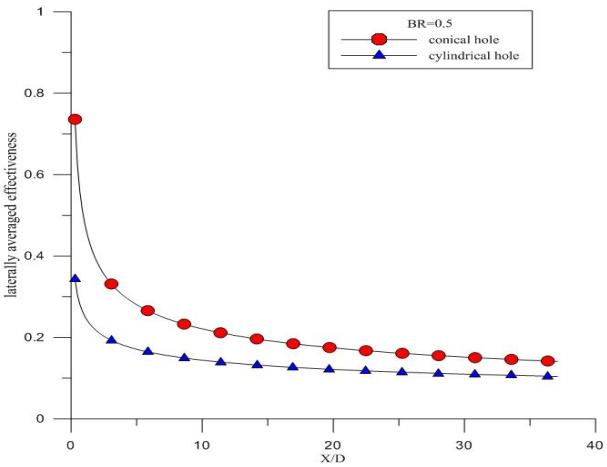

Figure (10) Comparison of laterally averaged effectiveness versus nondimensional position between cylindrical & conical hole (BR=0.5)

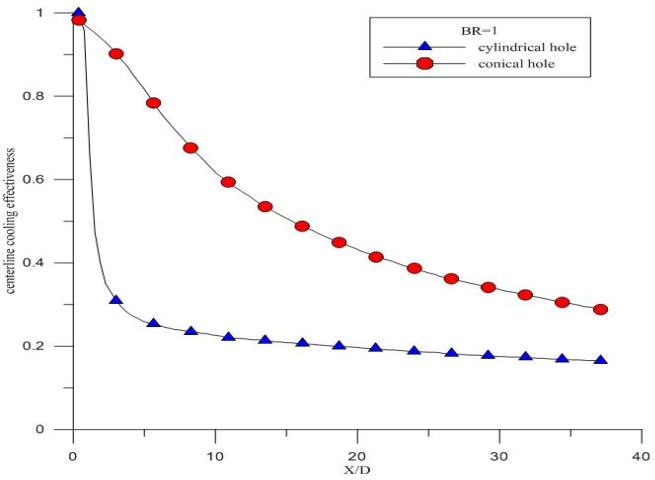

Figure (11) Comparison of centerline effectiveness versus nondimensional position between cylindrical & conical hole (BR=1)

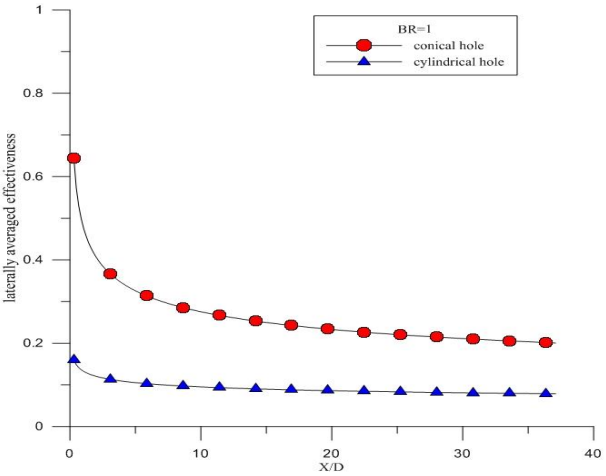

Figure (12) Comparison of laterally averaged effectiveness versus nondimensional position between cylindrical & conical hole (BR=1)

8- CONCLUSION

1- Bench mark cylindrical film cooling hole case is successfully modeled, the CFD results of present work show a good agreement with the experimental work.
2- It was found that the conical hole gave a greater lateral separation of the kidney vortices immediately downstream of the hole that resulted in increased film cooling effectiveness immediately downstream of the hole and improved lateral distribution of coolant far downstream of the hole.
3- The film cooling effectiveness of conical hole is better than that of the cylindrical hole particularly at high blowing ratio.

9-REFRANCESE

[1] Han, J. C., Sandip, D., and Ekkad, S. V., "Gas Turbine Heat Transfer and Cooling Technology", Taylor & Francis Group, 2001 .

[2] Eriksen, V.L., Goldstein, R.J., " Heat transfer and Film Cooling Following Injection Through Inclined Circular Tubes", ASME J. Heat Transfer, PP. 239–245, 1974.

[3] Goldstein, R.J., Yoshida, T., "Boundary Layer and Laminar Injection on Film Cooling Performance", ASME J. Heat Transfer Vol.104, pp.355–362, 1982.

[4] Goldstein, R.J. , Jin, P. , and Olson, R.L. ," Film Cooling Effectiveness and Mass/Heat Transfer Coefficient Downstream of One Row of Discrete Holes", ASME Paper No. 98-GT- 174, 1998.

[5] Bergeles, G., "Three-dimensional Discrete Hole Cooling Processes : An Experimental and Theoretical Study", Ph.D. thesis, University of London, Imperial College of Science, Technology and Medicine, London, 1976.

[6] Brown, A. , Saluja, C.L., " Film Cooling From a Single Hole and a Row of Holes of Variable Pitch to Diameter Ratio ", Int. J. Heat Mass Transfer,Vol. 22, PP. 525–533, 1979.

[7] Sinha, A.K., Bogard, D.G., and Crawford, M.E. " Film-cooling Effectiveness Downstream of a Single Row of Holes with Variable Density Ratio " , ASME J. Turbomach., Vol.113, pp. 442–449,1991.

[8] Schmidt, D.L., Sen, B. , Bogard, D.G. , " Film Cooling with Compound Angle Holes: adiabatic effectiveness", ASME J. Turbomach., Vol.118, pp. 807–813, (1996).

[9] Bunker, R. S., 2006, "Gas Turbine Heat Transfer: 10 Remaining Hot Gas Path Challenges," Proceedings of GT2006, ASME Turbo Expo 2006: Power for Land, Sea and Air, May 8-11, 2006, Barcelona, SPAIN.

[10] Goldstein, R.J., Eckert, E.R.G., and Burggraf, F.,"Effects of Hole Geometry and Density on Three Dimensional Film Cooling", Int. J. Heat Mass Transfer, Vol. 17, pp. 595-607,1974.

[11] Hyung Hee CHO, Dong Ho RHEE, and Byung Gi KIM, "Enhancement of Film Cooling Performance Using a Shaped Film Cooling Hole with Compound Angle Injection" JSME international Journal, series B, Vol.44, NO.1, 2001 .

[12] Sen, B., Schmidt, D.L. , and Bogard, D.G., "Film Cooling with Compound Angle Holes: heat transfer". ASME Journal of Turbomach. ,Vol.118, PP. 800-806, 1996.

[13] Kohli, A., Bogard, D.G., "Adiabatic Effectiveness, Thermal Fields, and Velocity Fields for Film Cooling with Large Angle Injection" , ASME Journal of Turbomach. , Vol.119 , pp. 352–358, 1997.

[14] Sargison, J. E.,Guo, S. M.,Oldfield, M. L.G.,Lock, G. D.,and Rawlinson,A. J.,"Flow Visualization of a Converging Slot-Hole Film Cooling Geometry", ASME Paper GT-30177,2002.

[15] Yuen, C.H.N., and Martinez-Botas, R.F., "Film Cooling Characteristics of Rows of Round Holes at Various Streamwise Angles in a Cross flow : Part II. Heat Transfer Coefficient", International. Journal of Heat and Mass Transfer, Vol.48, pp. 5017-5035, 2005.
[16] Baheri, S.,Alavi Tabrizi,S.P. and Jubran, B.A.,"Film Cooling Effectiveness from Trenched Shaped and Compound holes", Heat Mass Transfer, Vol. 44, PP. 989-998, 2008.
[17] Fayyaz, H. A. and Muhammad, J. H., "Computational Study of Film Cooling Effectiveness for a Comparison of Cylindrical, Square and Triangular Holes of Equal Cross-Sectional Area", Mehran university research journal of Eng. & tech. ,Vol. 29, pp. 541-555,2010
[18] Durham, M.G. , "Comparison of Square-hole and Round-hole of Film Cooling : A Computational Study", MSc. thesis, Orlando, Florida, University of central Florida ,2004.
[19] Launder B.E., and Spalding D.B., "The Numerical Computation of Turbulent Flows" , Computer Methods in Applied Mechanics and Engineering, Vol. 3, pp. 269-289, 1974.
[20] Launder, B. E., and Spalding, D. B., "Lectures in Mathematical Models of Turbulence", Academic Press, London, England, 1972.
[21] Fluent 12 User's Guide, programing and Tutorial Guide, Version 12, Ansys Inc, 2009.
[22] Barth, T. J., and Jespersen, D., "The Design and Application of Upwind Schemes on Unstructured Meshes" , Technical Report AIAA-89-0366, AIAA 27th Aerospace Science Meeting, Reno, Nevada, 1989.
[23] Rhie, C. M., and Chow, W. L., "Numerical Study of the Turbulent Flow Past an Airfoil with Trailing Edge Separation", AIAA Journal, Vol. 21, No. 11, pp. 1525-1532, 1983.
[24] Patankar, S. V., "Numerical Heat Transfer and Fluid Flow", Hemisphere Publishing, Washington DC, 1980.
[25] Friedrichs, S., "End Wall Film-Cooling in Axial Flow Turbines", PhD thesis, Cambridge University, 1997.
[26] Haven, B.A., Kurosaka, M., "Kidney and anti-kidney vortices in cross flow jets", J. Fluid Mech., 352:27-64, USA ,1997.

Nomenclature

BR Blowing ratio [$BR=\rho_c U_c / \rho_m U_m$]
C_p Specific heat
D Film hole diameter
DR Density ratios [$DR= \rho_c/\rho_m$]
k Turbulence kinetic energy
h_d Hydraulic diameter
Re Free stream Reynolds number
T Temperature
U Velocity
x Streamwise distance along the test plate
y Coordinate normal to surface

Greek Symbols

η Film effectiveness,
μ Viscosity of air
ε Turbulent kinetic energy dissipation rate
ρ Density
α Injection angle

Subscripts

c coolant
m mainstream
w wall

تحسين فعالية التبريد الغشائي باستخدام فتحات مخروطية الشكل

أ.د.عاصم حميد يوسف أ.م.د. قتيبة جميل الخشالي م.م. فلاح فاخر حاتم

الجامعة التكنولوجية / قسم هندسة المكائن والمعدات / بغداد

الخلاصة

يعتبر التبريد الغشائي احد الطرق المستخدمة لحماية السطوح التي تتعرض لدرجات حرارة عالية كتلك الموجودة في التوربينات الغازية. هذه الطريقة عبارة عن نفث مائع التبريد ليكون غطاء يحمي السطح المراد حمايته تتم عملية نفث مائع التبريد عن طريق ثقوب باشكال متعددة . نتائج استخدام الحل العددي بينت انه نتيجة لتداخل المائعين البارد والساخن تتكون دوامة تعرف بدوامة حدوة الحصان horseshoe vortex تحوي على زوج من الدوامات المتعاكسة counter-rotating vortices تؤثر على توزيع غشاء التبريد فوق السطح المراد حمايته .ان عملية تكون هذه الدوامات تعتمد على شكل الثقب المستخدم لنفث المائع البارد وهذه بدورها تؤثر على توزيع فعالية التبريد ومعامل انتقال الحرارة للسطح. تمت مقارنة النتائج التحليلة لفعالية التبريد وشكل الدوامات لثقب اسطواني عند نسب نفخ 0.5 و 1 مع النتائج العملية الموثقة سابقا، اذ تم مقارنة اداء شكل الثقب المخروطي مع الشكل الاسطواني ووجد ان الثقب المخروطي يعطي فعالية اكبر على امتداد مركز الثقب وعرضيا باتجاه الباع. ان استخدام الثقوب المخروطية يؤدي الى زيادة فعالية التبريد الادياباتي عند منطقة اسفل الثقب بنسبة 11.11% و 123.2% لنسب نفخ 0.5 و 1 على التوالي، بينما كانت الزيادة في معدل فعالية التبريد الادياباتي على امتداد الباع بنسبة 61.75% و 192.6% لنسب نفخ 0.5 و 1 على التوالي.

الكلمات الرئيسية: تبريد الغشاء ، الفعالية ،الفتحات المخروطية ، تحسين الفعالية

F-2

"Film cooling experimental investigation for ramped-conical holes geometry"

Presented at the International Journal of Scientific & Engineering Research, Volume 4, Issue 10, October-2013

International Journal of Scientific and Engineering Research (IJSER)

PUBLICATION CERTIFICATE

Paper Number: I029901
Paper Title: Flim Coolometrying Experimental Investigation for Ramped-Conical Holes Ge
Authors: Dr. Assim H. yoosif , Dr. Kutaeda J. , Falah f.

Type of the paper: (Please highlight)

☐ Research ☐ Application ☐ Case Study ☐ Survey ☐ On-going ☐ Other

Evaluation: (Please highlight)

	Low				High
Significance of Contribution:	1	2	3	4	5
Originality of Content:	1	2	3	4	5
Technical Quality:	1	2	3	4	5
Clarity of Presentation:	1	2	3	4	5

Overall recommendation (Please highlight)

Accept in current state
Accept with minor revision
Major Revision needed, recommend resubmission
Reject

Any additional comments: Paper Published in IJSER Volume 4, Issue10, October 2013 Edition (ISSN 2229-5518).

IJSER

Digitally signed by IJSER
DN: cn=IJSER, c=FR, o=IJSER Publishing, ou=Research, email=ijser.editor@ijser.org

Film cooling experimental investigation for ramped-conical holes geometry

Dr. Assim. H. Yousif, Dr. Kutaeba J. M. AL-Khishali, Falah F. Hatem

Abstract— The effect of introducing ramped-conical holes on film cooling performance has been investigated experimentally. Four models have been considered; model 1 consists of one row of cylindrical film cooling holes acting as the baseline case, model 2 consists of one row of single conical film cooling holes, model 3 consists of one row of single conical ramped-holes (upstream ramp with a backward-facing step), and model 4 consists of one row of double conical ramped-holes (upstream and downstream ramped-holes both with a backward-facing step. Detailed heat transfer coefficient and film effectiveness measurements are obtained simultaneously using a single test transient IR thermography technique. The study is performed at a single mainstream Reynolds number based on free-stream velocity and film hole diameter of 13000 at three different coolant-to-mainstream blowing ratios of 0.5, 1.0, and 1.5. The results show that film effectiveness is greatly enhanced when using ramp due to improved two dimensional natures of the film and lateral spreading, the distribution of laterally average film cooling effectiveness along the x-axis show that the double ramped-holes model provides promising film cooling performance particularly at moderate and high blowing ratios

Index Terms— Film cooling, effectiveness, conical, ramp, Enhancement

1 Introduction

Film cooling is one of the methods used to protect surfaces exposed to high-temperature such as, that exist in gas turbines by injection of coolant fluid (at a lower temperature than that of the main flow) to flood the surfaces to be protected. Bathie [1] stated that the advanced gas-turbine stages are designed to operate at increasingly higher inlet temperatures to increase thermal efficiency and specific power. This increase is made possible by advances in materials such as super alloys and thermal-barrier coatings and by cooling technology such as internal, impingement cooling. The inlet temperatures can far exceed allowable material temperatures by using cooling. Film cooling involved injection of coolant from film holes to forms a thin thermal barrier layer to protect the blade surface from the hot gases flow. The objective of film cooling is to achieve low heat transfer from the surrounding hot mainstream to the turbine blades, and large effectiveness on the blade surface. In the recent years several studies have been focused on developing the holes shape to enhance film cooling effectiveness. Film cooling research on flat surface is common, flat surface models can be used to study the effects of individual parameters with relative ease and are less expensive. Studies have proved that the results obtained on simple flat surface models can be applied to real engine designs with slight corrections Han et al. [2].

2 Film cooling operating parameters

Many investigators studied the effects of design and operating parameters on film cooling at which the cooling jets injected from one or two rows of inclined cylindrical holes. The studied parameters include film-cooling hole inclination, length-to-diameter ratio, spacing between holes, turbulence and embedded vortices in the hot-gas flow. The vortex system generated when cold jet injected in the hot main stream was described in details by Haven et al. [3] and Hyams et al. [4]. They showed the important role played by vortices in the evolution of film-cooling jets. The effects of hole geometry on the vortices dynamics of hot-gas/film-cooling jet interactions were investigated by Haven et al. [3], Hyams et al. [4], Kim and Kim [5]. Bunker [6] provided a comprehensive review of the research on hole shape. Haven and Kurosaka [7] examined the effects of placing vanes inside film-cooling holes that produce vortices in the same sense as the anti-kidney vortices. Zaman and Foss [8] and Zaman [9] steadied the effects of tabs placed at the film-cooling-hole exit were steadies. Ekkad et al. [10] showed that placing tabs on the upstream side of the film-cooling-hole exit can improve film-cooling effectiveness. Proposal was made by Shih et al. [11] to place a strut or obstruction within each film-cooling hole that do not necessarily generate appreciable vortices but can cause vortices inside film-cooling holes to be stretched and tilted in a way that would change the magnitude and direction of the vortices in the CRVs and the anti-kidney pair. Bunker [12] proposed creating a trench about a row of film cooling holes to modify the boundary-layer/cooling jet interactions. Holes embedded in trench were found quite useful in improving film-cooling effectiveness as investigated by Altorairi [13].

3 PAST STUDIES OF RAMPED- HOLES

The vortex system generates when cold jet injected in the hot main stream was described in details by Haven et al. [3] and Kelso et al. [14]. They showed the important role played by vortices in the evolution of film-cooling jets. One pair, referred to as the counter-rotating vortex pair (CRVs), was found to lift the jet off the surface that it is intended to protect and to entrain hot gas underneath it. The other pair, referred to an anti-kidney pair, was shown to have a sense of rotation opposite to that of the CRVs, and so can counteract the undesirable effects of the CRVs in entraining hot gas. Thus, it is of interest to develop strategies to control the formation and strength of these vortices in a way that leads to more effective film cooling. There are many ways to alter the structure of these vortices. Since the vortices in the cooling jet originates from the flow in the film-cooling hole, the boundary layer upstream of the film cooling hole, and the boundary-layer/cooling jet interactions, most investigators have focused on the geometry of the film-cooling hole. The boundary layer upstream of the film cooling hole can be altered by using ramped-holes concept to increase the adiabatic effectiveness of film cooling from row of film cooling holes. Sangkwon and Shih [15] proposed a geometry modification upstream of the holes to approach boundary layer flow and its interaction with the film cooling jets; this was done by making the surface just upstream of the holes row into a ramp with a backward-facing step. They showed numerically that an upstream ramp with a backward-facing step can greatly increase surface adiabatic effectiveness. The laterally averaged adiabatic effectiveness with a

ramp can be two or more times higher than without the ramp by increasing upstream and lateral spreading of the coolant. Shuping et al [16] examined experimentally on a concept for enhancing the film cooling performance by placing an upstream ramp in front of a row of cylindrical film cooling holes. They tested the upstream ramp with different angles (γ = 8.5°, 15°, and 24°) and blowing ratios *of (*0.3, 0.4, 0.6, 0.9, and 1.4). In general, a relatively large ramp angle with a high blowing ratio leads to more effective film protection. Since extended surfaces such as a ramp could increase surface heat transfer and this is undesirable on the hot-gas side, it is noted that the ramp can be constructed in the thermal-barrier coating (TBC) system by using the ceramic top coat, which has very low thermal conductivity.

4 EXPERIMENTAL SETUP AND PROCEDURE

The experimental facilities consist of a low speed hot air supplier system with attached cold jet in the test section, as shown in Fig.1. The settling chamber of the test rig contains series rows of electrical heaters, row of honeycomb, and screens to ensure adequate hot air of uniform velocity and temperature throughout the test rig. The hot air routed through a convergent-divergent contraction having a rectangular cross-section before flowing through the test section. The bottom wall of the test section considered as testing plat, four plate models are considered, each model made of (234x123mm) Perspex plate of 0.8cm thickness. Fig.2 shows ramped-holes configurations with double ramped-holes arrangement. In order to allow the air to reach the desired temperature, the air is initially routed out away from the test section by using a by-bass gate passage. The temperature of the air is continuously monitored at the exit of the gate and when the desired temperature is reached, the gate is gradually fully opened.

Centrifugal air blower was used to supply the coolant air to the plenum. The plenum is located below the test model as shown in Fig.3**.** The coolant air enters a plenum then injected through holes into the test section. The coolant air pressure was measured at the inlet of the test section. Digital calibrated thermometers are used to measure the mainstream and coolant air temperatures. Pre-testing shows that all holes injected constant desired flow rate and temperature. The mainstream hot air temperature adjusted with a laboratory temperature (ambient air drawn by a blower) to give highest limit of (T_c/T_h=0.4). There are four models to be tested each model having one row of five holes, considered here; model 1 consists of one row of cylindrical film cooling holes, model 2 consists of one row of conical film cooling holes without upstream ramp, model 3 consists of one row of conical film cooling holes with upstream ramp of backward-facing step, and model 4 consists of one row of conical film cooling holes with upstream and downstream ramps both of backward-facing step. Fig.3 shows the frontal views of models 3 and 4 configurations.

5 SURFACE TEMPERATURES MEASUREMENTS

The infrared thermograph system (Fluke Ti32) is used to measure surface temperatures. The thermal image can be displayed using standard color palettes or Ultra Contrast TM color palettes. The IR system is greatly affected by both background temperature and local emissivity. The test surface was sprayed with mat black color to increase the emissivity as a perfect black body. The temperature measurement taken is not accurately recorded unless the IR system is calibrated. The system is calibrated by measuring the temperature of the test surface using thermocouple type K and the reading of IR camera. The test surface is heated by mainstream hot air. The measured of temperatures obtained by both ways and they are recorded and stored during the heating process until achieving a steady state condition. Due to the emissivity of the test surface the temperature is obtained by IR camera is different from the temperature obtained by the thermocouple; therefore IR camera reading is adjusted until both temperatures reading are matched. The system calibration of the temperature range in present work is taken between -10^{o}C and +80^{o}C. The test surface was modeled as a semi-infinite solid medium imposed by a sudden transient heating. The entire solid medium was initially at a uniform temperature before the transient test. During the transient heating test, each point on the surface will respond with different temperature at different time due to different heat transfer coefficient. The test surface is modeled as undergoing 1-D transient conduction with convective boundary conditions at the wall. Fig. (4) shows a schematic diagram of flow over a flat plate.

The test plate is initially at a uniform temperature, (T_i), and the convective boundary condition is suddenly applied on the plate at time, t >0, (the hot stream of air provides a heat flux to the surface of

the plate and convective heat transfer phenomena occurs). The 2-D transient conduction equation is given by:

$$\frac{\partial^2 T}{\partial x^2}+\frac{\partial^2 T}{\partial y^2}=\frac{1}{\alpha}\frac{\partial T}{\partial t} \quad (1)$$

Neglecting the lateral conduction equation (1) becomes:

$$\frac{\partial^2 T}{\partial x^2}=\frac{1}{\alpha}\frac{\partial T}{\partial t} \quad (2)$$

Solving equation (1) need two boundary conditions and an initial condition:

Initial condition at $t = 0$, $T = T_i$ (3)

At $x = 0$ and $t \geq 0$ $-K\frac{\partial T}{\partial x} = h(T_w - T_m)$ (4)

At $x = \infty$ and $t \geq 0$, $T = T_i$ (5)

The main approximation often applied to analyze transient conduction shown in Fig. (4) is the semi-infinite approximation. Semi-infinite solids can be visualized as very thick walls with one side exposed to some fluid, the other side remains unaffected by the fluid temperature since the wall is very thick. Solving the partial equation (1) with the prescribed initial condition and boundary conditions at x = 0 gives the transient response of the test plate wall due to the convective heat load applied by the hot mainstream air. The solution is given by the flowing equation [17].

$$\frac{T_w-T_i}{T_m-T_i}=1-\exp\left[\frac{h^2\alpha t}{k^2}\right]erfc\left[\frac{h\sqrt{\alpha t}}{k}\right] \quad (6)$$

Where h is the unknown quantity in the equation with T_w is the wall temperature at time t after the initiation of the transient test. The material properties, α (1.0752 x 10^{-7} m^2/s) and k (0.1873 W/m.K) [17] dictate the applicability of the semi-infinite solid solution.

The assumptions of semi-infinite solid are valid for this work because the transient test duration is small, usually less than 60 seconds and also because of the test surface is made of Perspex which has low thermal conductivity, low thermal diffusivity and low lateral conduction, combinations of the above facts make sure that heat is conducted only in the x-direction and it does not reach the bottom of the test surface.

In film cooling case, the film should be treated as a mixture of air mainstream and the coolant air. The mainstream temperature (T_m) in equation (6) has to be replaced by the film temperature (T_f). Equation (6) has two unknowns (h and T_f). To solve this equation, two sets of data points are required to obtain the unknowns. In this case, a transient infrared thermograph technique will be used to obtain both h and η from a single test as described by Ekkad et al. [18]. Thus, two images with surface temperature distributions are captured at two different times during the transient test.

The IR images for models test surface at each test are captured and stored by the memory of the thermal camera. These images are transferred to PC. The IR images are converted to corresponding temperature digital values and then saved as data in Excel sheet. MATLAB programs Software are prepared by using a semi-infinite solid assumption to introduce the film cooling effectiveness and heat transfer coefficient contours.

6 Film cooling effectiveness

A non-dimensional temperature term is known as the film cooling effectiveness (η), and is defined as:

$$\eta=\frac{T_f-T_m}{T_c-T_m} \quad (7)$$

The term blowing ratio (BR) is used to study the effect of the amount of coolant flow to mainstream flow. It is defined as the ratio of the mass flux of the coolant to the mass flux of the mainstream ($BR=\rho_c U_c/\rho_m U_m$).

The verification of the current experimental approach, the test results of the baseline case (model 1) is made by comparison with the experimental results of the similar case study of baseline case of Yuen [19]. Sample of results at BR= 1 of adiabatic spanwise averaged film cooling effectiveness distribution along the X/D together with that of Yuen [19] experimental results are presented in Fig.(6). The results show approximately similar levels of (η) with slightly different in local values. It is fair to say that the results obtained from the present experiments are in good agreement with experimental results of Yuen [19].

Experimental results of the present investigation are in the thermal aspect in the form of distribution and contour plots of various variables including the film cooling effectiveness and heat transfer coefficient.

The ramped-holes models geometry are design from holes inclined at θ = 35°, the hole spacing between adjacent holes was 3.5D, in both ramped-holes models, the configurations are taken as ramps (length = 2.5D and γ=16.7°) located at a distance (β=0) from the hole edge.

Fig.7 shows the comparison of spanwise averaged film cooling effectiveness distribution along the normalized streamwise distance (X/D). The present average value covers one pitch distance of -1.75< Z/D <1.75. Both ramped-holes cases (models 3 and 4) show rapid decaying particularly with increasing downstream distance from the hole. For blowing ratios of 0.5 & 1 the ramped-hole case provided better cooling effectiveness than (model 1 and2). At BR=1.5 double ramped-holes provide highest and significant improvement in the laterally averaged film cooling effectiveness. In general better performance at moderate and high blowing ratios (BR = 1.0 and 1.5) is contributed by the existing of double ramps. The double ramps contribute to lesser penetration of coolant jet into mainstream allowing the coolant air to remain close to the wall compared with the three other cases. Also from this figure it can be seen that for single ramp case (Model 3), the adiabatic film cooling effectiveness is enhanced in the lateral area at BR=1 and this is confirmed by the film cooling effectiveness contours presented in Fig.8.

The overall area averaged film cooling effectiveness ($\bar{\eta}$) for single ramped-holes (model 3) is enhanced by (134%, 292.6%, and 554.6%) at (BR= 0.5, 1.0, and 1.5) respectively. All enhancements are calculated with reference to the conventional single cylindrical holes row (model 1). Results of double ramped-holes case (model 4) show that the overall area averaged film cooling effectiveness is enhanced greatly by (130.3%, 343.7%, and 679.4%) at (BR= 0.5, 1.0, and 1.5) respectively. In general, the results clearly show the benefits of adding double ramps to the conventional single conical holes row, in which there is almost a 679.4% increase in overall area averaged film cooling effectiveness at BR =1.5.

7 Heat load

In the practical application, turbine designers are concerned with the reduction of heat load to the film protected surface. The heat load can be simulated by combining the film cooling effectiveness (η) and heat transfer coefficient ratio (h/h_o), therefore the ratio (q/q_o) can be introduced to present the reduction in heat flux at the test surface with the presence of coolant air. A net heat flux ratio is used to measure the combined effect of film effectiveness and heat transfer coefficient. The following relation between (η) and (q/q_o) as given by Ekkad and Zapata [20] may be used to estimate (q/q_o):

$$\frac{q}{q_o} = \frac{h}{h_o}\left(1 - \frac{\eta}{\phi}\right) \quad (8)$$

The verification of the current calculation method of spanwise averaged heat transfer coefficient ratio ($\bar{h}/h_o$) is made by comparison with the experimental results of Lu [21] for the baseline case (model 1). Sample of comparison results of ($\bar{h}/h_o$) at BR=1 along the normalized streamwise distance (X/D) are presented in Fig.9, both results are in good agreement.

Fig.10 presents detailed spanwise averaged heat transfer coefficient ratio ($\bar{h}/h_o$) at BR=1. The heat transfer coefficient ratio for ramps cases is increased compared to the baseline case. Such increase are due to the interaction between the coolant jet and the mainstream flow, this interaction produced high turbulence region. Several studies have shown that jet injection produces increased turbulence level inside the boundary layers due to the shear layer mixing and this is the main reason that (h) downstream of hole show higher values according to Nasir et al. [22] . At present test at the downstream region (X/D>10) the heat transfer coefficients have higher values and remain in the same level up to the end of the test surface. It is clear in the ramped-holes case, the heat transfer coefficient increased over that of (models 1 and 2).

Heat flux ratio indicates the reduction in heat flux on the test surface from the film injection. As indicated by Akkad and Zapata [20], if the value of the net heat flux ratio is less than 1.0, then the introduction of film cooling has beneficial effect. If the value is greater than 1.0, it can be said that the film cooling did not serve its purpose of cooling.

Fig.11 represents the effect of (BRs) on overall area-averaged heat flux ratio($\bar{\bar{q}}/q_o$). All models show good results of ($\bar{\bar{q}}/q_o$) except for(model 1 and) at blowing ratio of 1.5 the values of ($\bar{\bar{q}}/q_o$) is exceed unity.

8 Conclusion

Double ramped- conical holes are recently proposed to improve the two dimensional natures and lateral spreading of the film cooling. Film

cooling effectiveness, heat transfer coefficients, and heat flux ratio were evaluated by using semi-infinite solid assumption with the aid of the measurements of model surface temperatures by transient infrared thermography technique. The film cooling performance was found to be enhanced greatly by introducing single and double ramped holes compared to baseline (conventional single jet holes row). Accepted performance is obtained at moderate and high blowing ratios for double ramped-holes. The ramped-holes increase film effectiveness over that of the baseline by (554.6%) for single ramped-holes and by (679.4%) for double ramped-holes at BR=1.5. The heat transfer coefficient ratio increased as compared to the baseline case, this is due to the interaction between the jet and the main stream which produces a region of high turbulence.

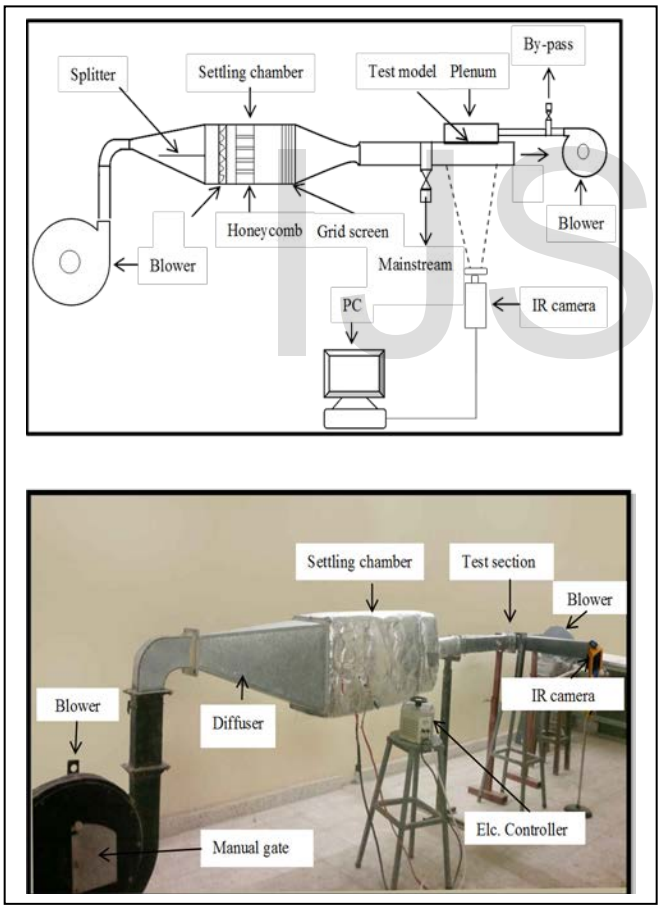

Figure (1) Photography and schematic of the experimental test rig

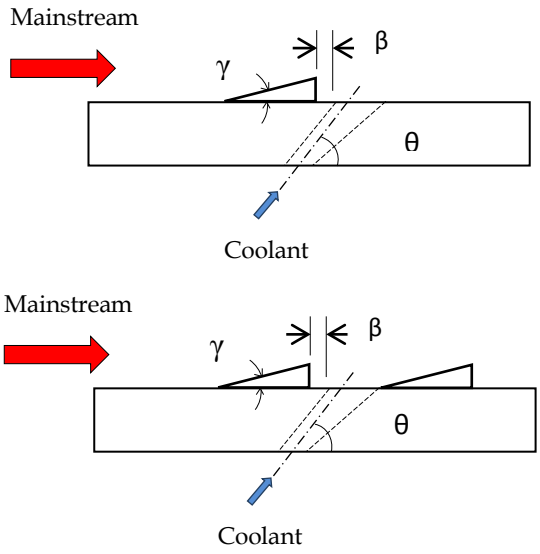

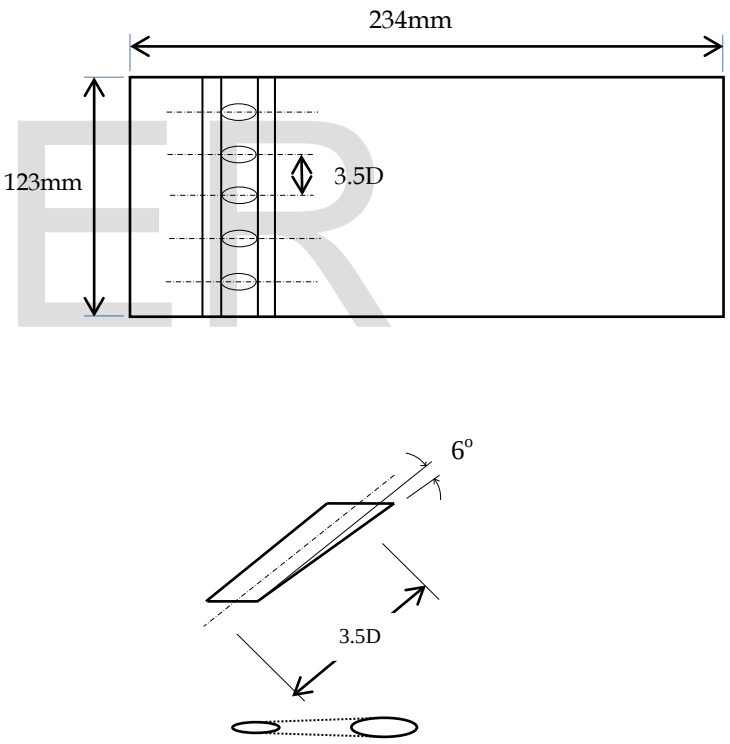

Figure (2) Schematic of ramped-holes configurations

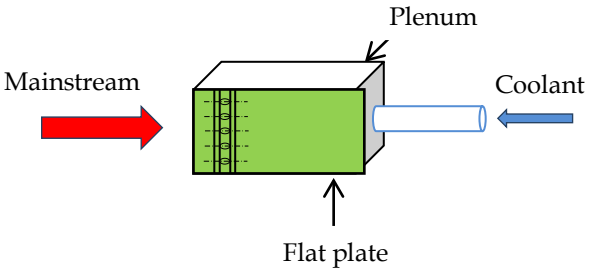

Figure (3) Schematic of test section

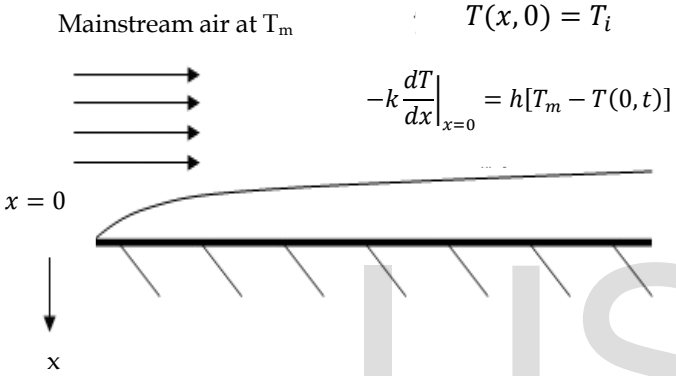

Figure (4) Flow over a flat plate

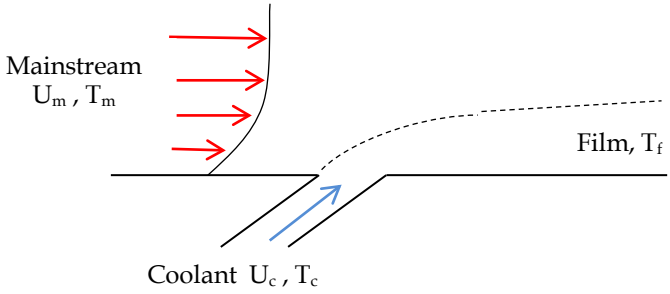

Figure (5) Film cooling over a flat plate

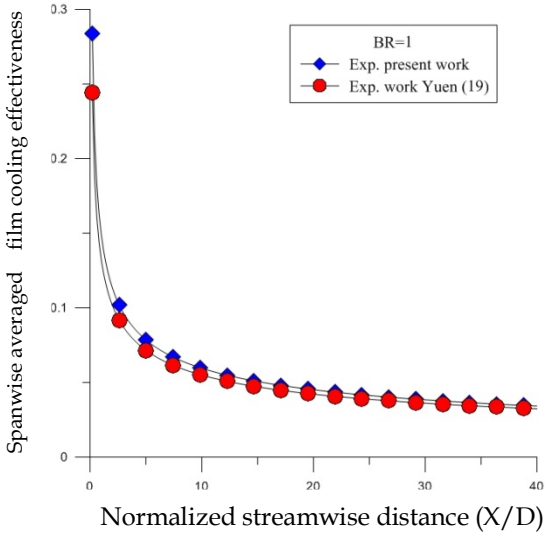

Figure (6) Verification of the present study with the experimental results of Yuen [19]

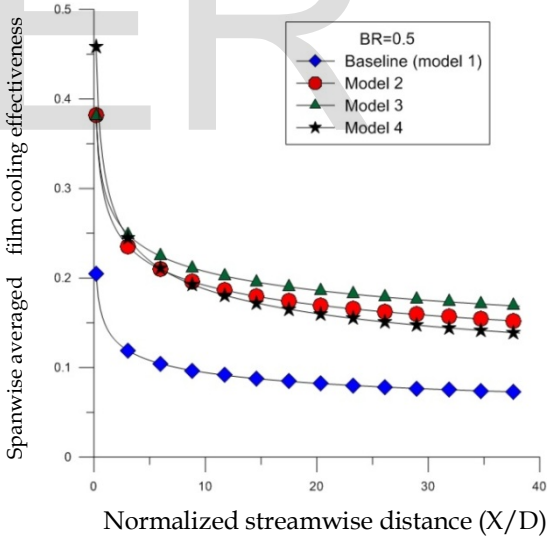

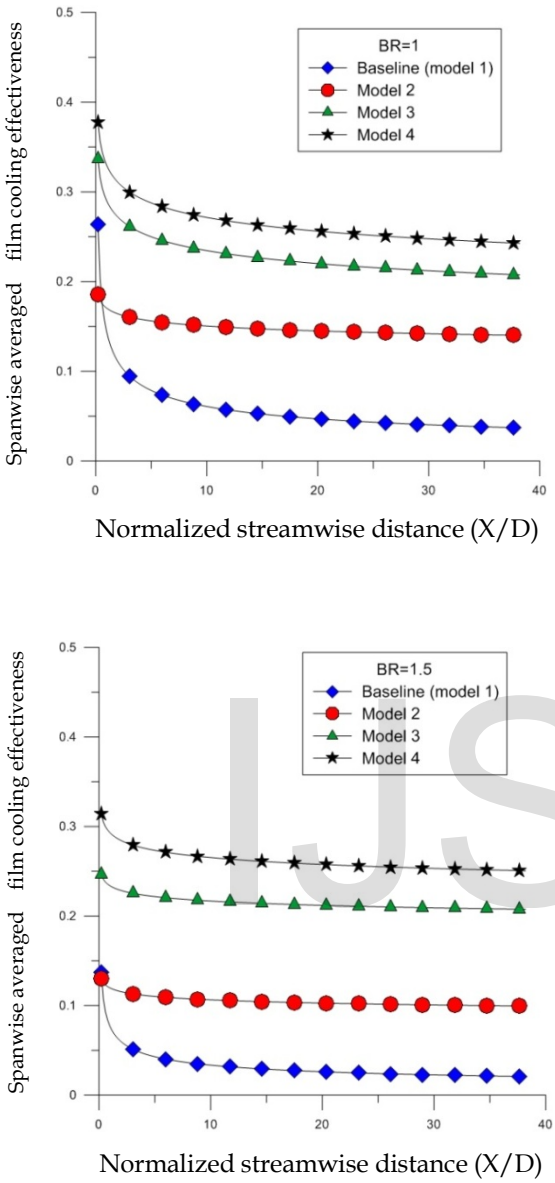

Figure (7) Comparison of spanwise averaged film cooling effectiveness ($\bar{\eta}$) distribution along the normalized streamwise distance (X/D) for different models at different BRs.

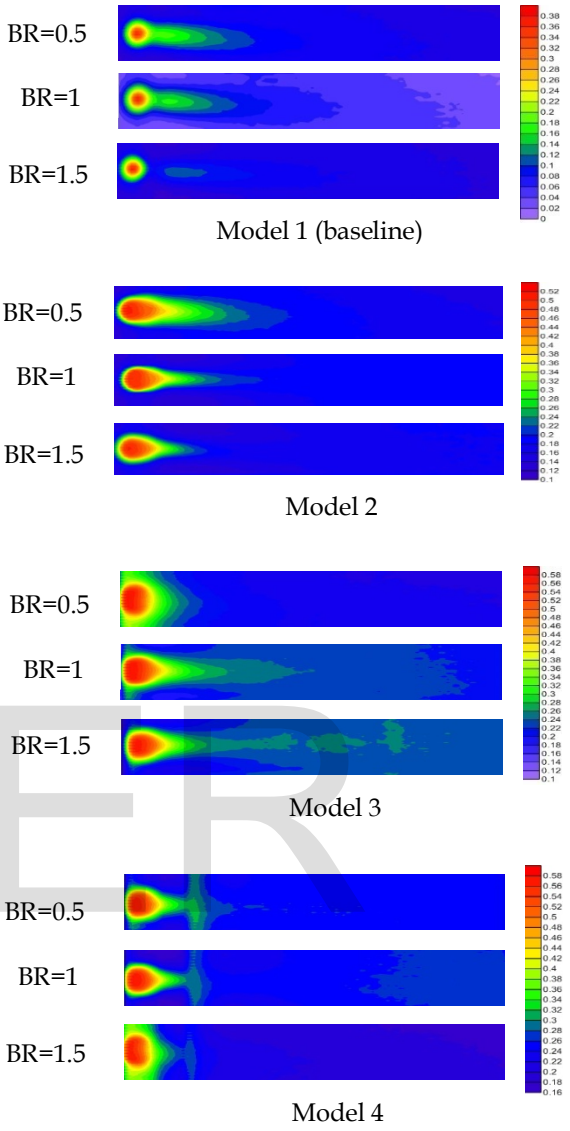

Figure (8) Film cooling effectiveness contours for different models

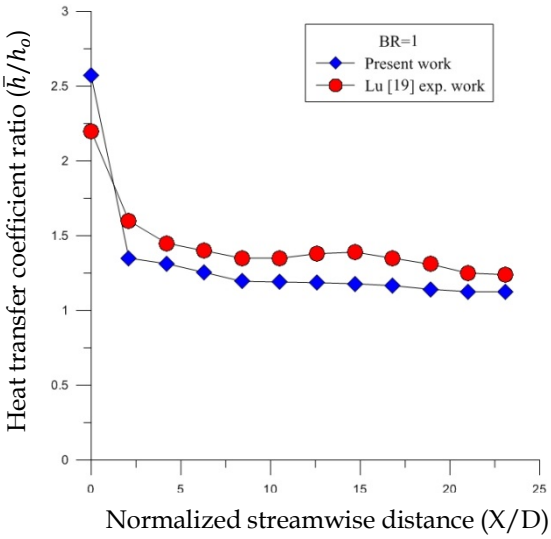

Figure (9) Verification of experimental results of heat transfer coefficient ratio $(\bar{h}/h_o)$ of the present study with the experimental results of Lu [20]

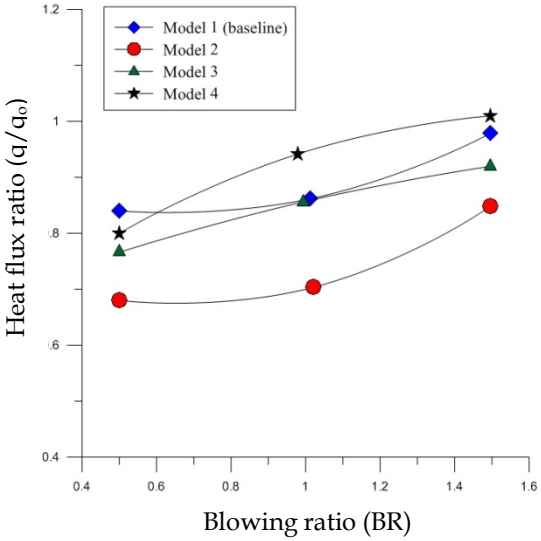

Figure (11) Effect of blowing ratio on overall area-averaged heat flux ratio for conical hole cases

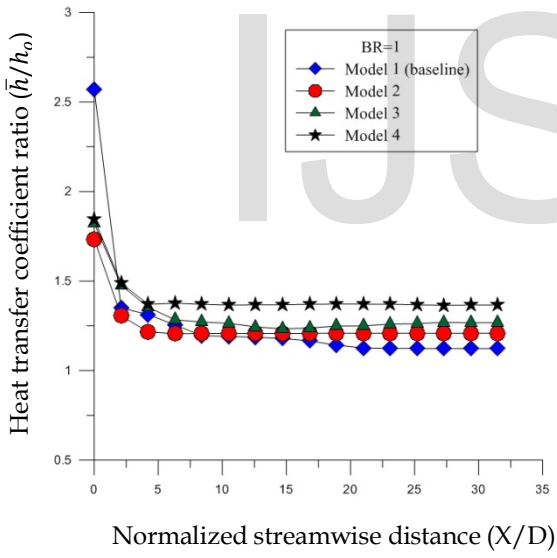

Figure (10) Effect of hole configuration on spanwise averaged heat transfer coefficient ratio for different models

REFERENCES

[1] W. W. Bathie, Fundamentals of gas turbines. Second edition, John Wiley &Sons, Inc (1996).

[2] J. C. Han, H. Du, S.V. Ekkad. "Gas turbine heat transfer and cooling technology". Taylor & Francis Group (2001).

[3] Haven, B.A., Yamagata, D.K., Kurosaka, M., Yamawaki, S., Maya, T., 1997, "Anti-kidney Pair of Vortices in Shaped Holes and their Influence on Film Cooling Effectiveness" ASME Paper 97-GT-45.

[4] D. G. Hyams, K. T. McGovern, J. H, Leylek. Effects of geometry on slot-jet film cooling performance. ASME Paper No. 96-GT-187 (1997).

[5] J. K. Kim, S. -M. Kim. Influence of shaped injection holes on turbine blade leading edgefilm cooling. Int. J. Heat and Mass Transfer 47 (2004) 245-256.

[6], R. S. Bunker. A review of shaped hole turbine cooling technology. ASME J. Heat Transfer, 127 (2005) 441–453.

[7] B. A. Haven, M. Kurosaka, Improved jet coverage through vortex cancellation. AIAA J., 34(11) (1996) 2443–2444.

[8] K. B. M. Q. Zaman, J. K. Foss. The effects of vortex generators on a jet in a cross-flow. Phys. Fluids, **9**(1), (1997) 106–114.

[9] K. B. M. Q. Zaman. Reduction of a get penetration in a cross-flow by using tabs. AIAA Paper No. 98–3276 (1998).

[10] S. V. Ekkad, H. Nasir, S Acharya. Flat surface film cooling from cylindrical holes with discrete tabs. J. Thermophys. Heat Transfer 17(3) (2003) 304–312.
[11], T. I.-P. Shih, Y.-L. Lin, M. K. Chyu, S. Gogineni, Computations film cooling from holes with struts. ASME paper No. 99-GT-282 (1999).
[12], R. S. Bunker. Film cooling effectiveness due to discrete holes within transverse surface slots. Proceedings IGTI Turbo Expo, Amsterdam, the Netherlands, ASME Paper No. GT-2002–30178 (2002).
[13] M. S. Altorairi. Film cooling from cylindrical holes in transverse slots, MSc. thesis, Louisiana State University (2003), Baton Rouge, LA, USA.
[14] R. M. Kelso, T. T. Lim, A. E. Perry. An experimental study of round jets in cross-flow. J. Fluid Mech. 306(1996) 111–144.
[15] Na. Sangkwon, T. I-P. Shih. Increasing adiabatic film-cooling effectiveness by using an upstream ramp. Journal of Heat Transfer Vol.129 (2007) 464-470.
[16] S. P. Chen, M. K. Chyu, T. I.-P. Shih, Effects of upstream ramp on the performance of film cooling, Int. J. Thermal Sciences Vol. 50, Issue 6 (June 2011) 1085–1094.
[17] F.P. Incropera, D. Dewitt. Fundamentals of heat transfer, Wiley & Sons, New York, NY . (2006),.
[18] Ekkad, S. V., Ou, S. and Rivir, R. V., 2004, "A Transient Infrared Thermography Method for Simultaneous Film Cooling Effectiveness and Heat Transfer Coefficient Measurements from a Single test," GT2004-54236, Proceedings of ASME Turbo Expo 2004, Vienna, Austria.
[19] Yuen, C. H.N. and Botas, R.F.M., 2003, "Film cooling characteristics of a single round hole at various stream wise angles in a cross flow: Part I effectiveness", International Journal of Heat and Mass Transfer, Vol. 46, PP. 221-235.
[20] S.V. Ekkad, D. Zapata. Heat transfer coefficients over a flat surface with air and CO2 injection through compound angle holes using a transient liquid crystal image method. ASME J. Turbomachinery 119 No. 3 (1997) 580-586.
[21] Lu, Y., Dhungel, A., Ekkad, S.V., and Bunker, R.S., 2007, "Effect of Trench Width and Depth on Film Cooling from Cylindrical Holes Embedded in Trenches", ASME Paper GT 2007-27388.
[22] H. Nasir, S. Acharya, S. Ekkad. Improved film cooling from cylindrical angled holes with triangular tabs: effect of tab orientations. Int. J. Heat and Fluid Flow 24 (2003) 657-668.

F-3

"Effect of ramped-cylindrical holes on film cooling effectiveness"

Presented at the Al-Mustasirya University-College of engineering-International Conference of Engineering Sciences 26-27 March 2014

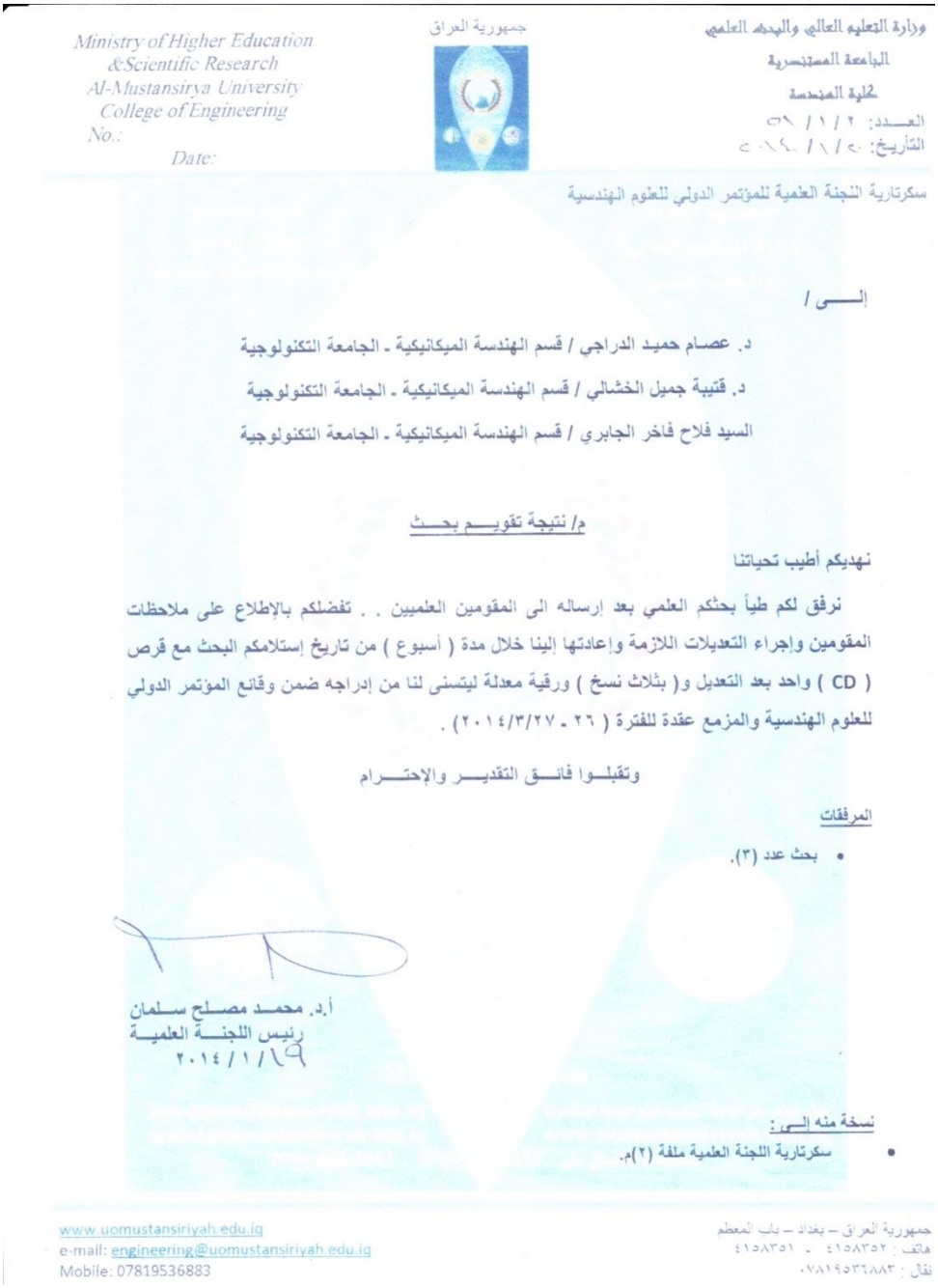

وزارة التعليم العالي والبحث العلمي
الجامعة المستنصرية
كلية الهندسة
العـــدد: ٢ / ١ / ٥٨
التاريخ: ٢٠ / ١ / ٢٠١٤

جمهورية العراق

Ministry of Higher Education &Scientific Research
Al-Mustansirya University
College of Engineering
No.:
Date:

سكرتارية اللجنة العلمية للمؤتمر الدولي للعلوم الهندسية

إلـــــى /

د. عصام حميد الدراجي / قسم الهندسة الميكانيكية ـ الجامعة التكنولوجية

د. قتيبة جميل الخشالي / قسم الهندسة الميكانيكية ـ الجامعة التكنولوجية

السيد فلاح فاخر الجابري / قسم الهندسة الميكانيكية ـ الجامعة التكنولوجية

م/ نتيجة تقويـــم بحـــث

نهديكم أطيب تحياتنا

نرفق لكم طياً بحثكم العلمي بعد إرساله الى المقومين العلميين . . تفضلكم بالإطلاع على ملاحظات المقومين وإجراء التعديلات اللازمة وإعادتها إلينا خلال مدة (أسبوع) من تاريخ إستلامكم البحث مع قرص (CD) واحد بعد التعديل و(بثلاث نسخ) ورقية معدلة ليتسنى لنا من إدراجه ضمن وقائع المؤتمر الدولي للعلوم الهندسية والمزمع عقدة للفترة (٢٦ ـ ٢٠١٤/٣/٢٧) .

وتقبلـــوا فائـــق التقديـــر والإحتـــرام

المرفقات

- بحث عدد (٣).

أ.د. محمـد مصـلح سـلمان
رئيس اللجنـــة العلميـــة
٢٠١٤ / ١ / ١٩

نسخة منه إلـــى :

- سكرتارية اللجنة العلمية ملفة (٢)م.

www.uomustansiriyah.edu.iq
e-mail: engineering@uomustansiriyah.edu.iq
Mobile: 07819536883

جمهورية العراق – بغداد – باب المعظم
هاتف : ٤١٥٨٣٥٢ - ٤١٥٨٣٥١
نقال : ٠٧٨١٩٥٣٦٨٨٣

Effect of ramped-cylindrical holes on film cooling effectiveness

Dr. Assim. Hameed AL-Daraje ***Dr. Kutaeba Jameel AL-Khishali***
Falah Fakher AL-Jabery
falahhatem59@yahoo.com

د.عاصم حميد الدراجي ***د.قتيبة جميل الخشال*** ***فلاح فاخر الجابري***

Mechanical Engineering Dep. / University of technology, Baghdad

Abstract:

Gas turbine parts require better cooling technique to face the increase in the operating temperature with each new engine model. Film cooling is one of the most efficient cooling methods used to protect the gas turbine parts from the hot gases. Holes arrangement offers reliable technique to improve the film cooling performance. The effect of using ramps with cylindrical holes on the film cooling performance has been investigated experimentally. Three models have been considered; one of these models is row of cylindrical holes works as a baseline model, model 2 consists of one row of single ramped-holes (upstream ramp with a backward-facing step), and model 3 consists of one row of double ramped-holes (upstream and downstream ramps both with a backward-facing step). Detailed heat transfer coefficient and film cooling effectiveness measurements are obtained simultaneously using a single test transient IR thermography technique. A test study is performed at a single mainstream of Reynolds number 76600 at three different coolant-to-mainstream blowing ratios 0.5, 1.0, and 1.5. Test results showed that the double ramped-holes model provides promising film cooling performance particularly at moderate and high blowing ratios.

Keywords: adiabatic, effectiveness, film cooling, inclination, ramp, row.

Nomenclature

D Hole diameter (mm)
k Thermal conductivity of test surface material(W/(mK))
h Heat transfer coefficient (W/m^2K)
($\bar{h}/h_o$) The local heat transfer coefficient with film cooling (h) is normalized by the heat transfer coefficient without film holes on a flat surface (h_0)
Re Mainstream Reynolds′ number based on hole diameter
t Time (s)

T Temperature (K)

q Heat flux to the surface with film cooling (W/m^2)

$\bar{\bar{q}}/q_o$ Total area-averaged heat flux ratio

U Velocity (m/s)

x, *y* and *z* Cartesian coordinate axes

X Streamwise distance along the test plate (mm)

Y Distance normal to the test plate surface (mm)

Z Pitch wise distance (mm)

Greek Symbols

α Thermal diffusivity of the test surface material (m^2/s)

γ Ramp inclination angle with respect to plate surface (degree)

β Ramp upstream distance from hole (mm)

η Local adiabatic film cooling effectiveness

$\bar{\eta}$ Laterally averaged film cooling effectiveness

$\bar{\bar{\eta}}$ Overall area- averaged film cooling effectiveness

θ Streamwise injection angle from stagnation (degree)

ϕ Overall cooling effectiveness

ρ Density (kg/m^3)

Subscripts

c Coolant

i Initial

f Film

m Mainstream

o Without film cooling

aw Adiabatic wall

Abbreviations

BR Blowing Ratio

CFD Computational Fluid Dynamics

CPVs Counter rotating vortex pair

DR Density Ratio

TBC Thermal Barrier Coatings

1-Introduction

Film cooling is one of the methods used to protect surfaces exposed to high-temperature such as that exist in gas turbines, by injection of coolant fluid (at a lower temperature than that of the main flow) to flood the surfaces to be protected. Bathie [1] stated that the advanced gas-turbine stages are designed to operate at increasingly higher inlet temperatures to increase thermal efficiency and specific power. This increase is made possible by advances in materials such as super alloys and thermal-barrier coatings and by cooling technology such as internal, impingement cooling. The inlet temperatures can far exceed allowable material temperatures by using cooling. Film cooling involved injection of coolant from film holes to forms a thin thermal barrier layer to protect the blade surface from the hot gases flow. The objective of film cooling is to achieve low heat transfer from the surrounding hot mainstream to the turbine blades, and large effectiveness on the blade surface. In the recent years several studies have been focused on developing the holes shape to enhance film cooling effectiveness. Film cooling research on flat surface is common, flat surface models can be used to study the effects of individual parameters with relative ease and are less expensive. Studies have proved that the results obtained on simple flat surface models can be applied to real engine designs with slight corrections (Han et al. [2]).

Many investigators studied the effects of design and operating parameters on film cooling at which the cooling jets injected from one or two rows of inclined cylindrical holes. The studied parameters include film-cooling hole inclination, length-to-diameter ratio, spacing between holes, turbulence and embedded vortices in the hot-gas flow. The vortex system generated when cold jet injected in the hot main stream was described in details by Haven et al. [3] and Hyams et al. [4], they showed the important role played by vortices in the evolution of film-cooling jets, and the effects of hole geometry on the vortices dynamics of hot-gas/film-cooling jet interactions were investigated by Haven et al. [3]. Bunker [5] provided a comprehensive review of the research on hole shape. Haven and Kurosaka [6] examined the effects of placing vanes inside film-cooling holes that produce vortices in the same sense as the anti-kidney vortices. Zaman and Foss [7] and Zaman [8] steadied the effects of tabs placed at the film-cooling-hole exit were steadies. Ekkad et al. [9] showed that placing tabs on the upstream side of the film-cooling-hole exit can improve film-cooling effectiveness. Proposal was made by Shih et al. [10] to place a strut or obstruction within each film-cooling hole that do not necessarily generate appreciable vortices but can cause vortices inside film-cooling holes to be stretched and tilted in a way that would change the magnitude and direction of the vortices in the CRVs and the anti-kidney pair. Bunker [11] proposed creating a trench about a row of film cooling holes to modify the boundary-layer/cooling jet interactions. Holes embedded in trench were found quite useful in improving film-cooling effectiveness as investigated by Altorairi [12].

The vortex system generates when cold jet injected in the hot main stream was described in details by Haven et al. [3] and Kelso et al. [13]. They showed the important role played by vortices in the evolution of film-cooling jets. One pair, referred to as the counter-rotating vortex pair (CRVs), was found to lift the jet off the surface that it is intended to protect and to entrain hot gas underneath it. The other pair, referred to an anti-kidney pair, was shown to have a sense of rotation opposite to that of the CRVs, and so can counteract the undesirable effects of the CRVs in entraining hot gas. Thus, it is of interest to develop strategies to control the formation and strength of these vortices in a way that leads to more effective film cooling. There are many ways to alter the structure of these vortices. Since the vortices in the cooling jet originates from the flow in the film-cooling hole, the boundary layer upstream of the film cooling hole, and the boundary-layer/cooling jet interactions, most investigators have focused on the geometry of the film-cooling hole. The boundary layer upstream of the film cooling hole can be altered by using ramped-holes concept to increase the adiabatic effectiveness of film cooling from row of film cooling holes. Sangkwon and Shih [14] proposed a geometry modification upstream of the holes to approach boundary layer flow and its interaction with the film cooling jets; this was done by making the surface just upstream of the holes row into a ramp with a backward-facing step. They showed numerically that an upstream ramp with a backward-facing step can greatly increase surface adiabatic effectiveness. The laterally averaged adiabatic effectiveness with a ramp can be two or more times higher than without the ramp by increasing upstream and lateral spreading of the coolant. Chen et al [15] examined experimentally on a concept for enhancing the film cooling performance by placing an upstream ramp in front of a row of cylindrical film cooling holes. They tested the upstream ramp with different angles (γ = 8.5°, 15°, and 24°) and blowing ratios of (0.3, 0.4, 0.6, 0.9, and 1.4). In general, a relatively large ramp angle with a high blowing ratio leads to more effective film protection. Since extended surfaces such as a ramp could increase surface heat transfer and this is undesirable on the hot-gas side, it is noted that the ramp can be constructed in the thermal-barrier coating (TBC) system by using the ceramic top coat, which has very low thermal conductivity. The present work objectives are to predict the film cooling performance for different novel ramped-cylindrical holes combinations.

2- Experimental setup and procedure

The experimental facilities consist of a low speed hot air supplier system with attached cold jet in the test section, as shown in **Fig.1**. The settling chamber of the test rig contains series rows of electrical heaters, row of honeycomb, and screens to ensure adequate hot air of uniform velocity and temperature throughout the test rig. The hot air routed through a convergent-divergent contraction having a rectangular cross-section before flowing through the test section. The bottom wall of the test section considered as testing plat, three plate models are considered, each model made of (234x123mm)

Perspex plate of 0.8cm thickness. **Fig.2** shows ramped-holes configurations with double ramped-holes arrangement (model 3). In order to allow the air to reach the desired temperature, the air is initially routed out away from the test section by using a by-bass gate passage. The temperature of the air is continuously monitored at the exit of the gate and when the desired temperature is reached, the gate is gradually fully opened. Centrifugal air blower was used to supply the coolant air to the plenum. The plenum is located below the test model as shown in **Fig.3.** The coolant air enters a plenum then injected through holes into the test section. Digital calibrated thermometers are used to measure the mainstream and coolant air temperatures. Pre-testing shows that all holes injected constant desired flow rate and temperature. The mainstream hot air temperature adjusted with a laboratory temperature (ambient air drawn by a blower) to give highest limit of (T_c/T_h=0.4). There are three models to be tested each model having one row of five holes, considered here; model 1 consists of one row of cylindrical film cooling holes, model 2consists of one row of cylindrical film cooling holes with upstream ramp of backward-facing step, and model 3 consists of one row of cylindrical film cooling holes with upstream and downstream ramps both of backward-facing step. The infrared thermograph system (Fluke Ti32) ^{TM} is used to measure surface temperatures. The thermal image can be displayed using standard color palettes or Ultra Contrast color palettes. The IR system is greatly affected by both background temperature and local emissivity. The test surface was sprayed with mat black color to increase the emissivity as a perfect black body. The temperature measurement taken is not accurately recorded unless the IR system is calibrated. The system is calibrated by measuring the temperature of the test surface using thermocouple type (K) and the reading of IR camera. The test surface is heated by mainstream hot air. The measured of temperatures obtained by both ways and they are recorded and stored during the heating process until achieving a steady state condition. Due to the emissivity of the test surface the temperature is obtained by IR camera is different from the temperature obtained by the thermocouple; therefore IR camera reading is adjusted until both temperatures reading are matched. The system calibration of the temperature range in present work is taken between -10ºC and +80ºC.

The test surface was modeled as a semi-infinite solid medium imposed by a sudden transient heating. The entire solid medium was initially at a uniform temperature before the transient test. During the transient heating test, each point on the surface will respond with different temperature at different time due to different heat transfer coefficient. The test surface is modeled as undergoing 1-D transient conduction with convective boundary conditions at the wall. **Fig. (4)** shows a schematic diagram of flow over a flat plate.

3- Mathematical calculation

The test plate is initially at a uniform temperature, (T_i), and the convective boundary condition is suddenly applied on the plate at time, t >0, (the hot stream of air provides a

heat flux to the surface of the plate and convective heat transfer phenomena occurs). The 2-D transient conduction equation is given by:

$$\frac{\partial^2 T}{\partial x^2} + \frac{\partial^2 T}{\partial y^2} = \frac{1}{\alpha}\frac{\partial T}{\partial t} \quad (1)$$

Neglecting the lateral conduction equation (1) becomes:

$$\frac{\partial^2 T}{\partial x^2} = \frac{1}{\alpha}\frac{\partial T}{\partial t} \quad (2)$$

Solving equation (1) need two boundary conditions and an initial condition:

Initial condition at $t = 0$, $T = T_i$

At $x = 0$ and $t \geq 0$, $-k\frac{\partial T}{\partial x} = h(T_w - T_m)$

At $x = \infty$ and $t \geq 0$, $T = T_i$

The main approximation often applied to analyze transient conduction shown in **Fig. (4)** is the semi-infinite approximation. Semi-infinite solids can be visualized as very thick walls with one side exposed to some fluid, the other side remains unaffected by the fluid temperature since the wall is very thick. Solving the partial equation (1) with the prescribed initial condition and boundary conditions at $x = 0$ gives the transient response of the test plate wall due to the convective heat load applied by the hot mainstream air. The solution is given by the flowing equation [16].

$$\frac{T_w - T_i}{T_m - T_i} = 1 - \exp\left[\frac{h^2 \alpha t}{k^2}\right] erfc\left[\frac{h\sqrt{\alpha t}}{k}\right] \quad (3)$$

Where h is the unknown quantity in the equation with T_w is the wall temperature at time t after the initiation of the transient test. The material properties, α (1.0752 x 10^{-7} m^2/s) and k (0.1873 W/m.K) [16] dictate the applicability of the semi-infinite solid solution.

The assumptions of semi-infinite solid are valid for this work because the transient test duration is small, usually less than 60 seconds and also because of the test surface is made of Perspex which has low thermal conductivity, low thermal diffusivity and low lateral conduction, combinations of the above facts make sure that heat is conducted only in the x-direction and it does not reach the bottom of the test surface.

In film cooling case, the film should be treated as a mixture of air mainstream and the coolant air as shown in **Fig. (5)**. The mainstream temperature (T_m) in equation (3) has to

be replaced by the film temperature (T_f). Equation (3) has two unknowns (h and T_f). To solve this equation, two sets of data points are required to obtain the unknowns. In this case, a transient infrared thermograph technique will be used to obtain both h and η from a single test as described by Ekkad et al. [17]. Thus, two images with surface temperature distributions are captured at two different times during the transient test.

A non-dimensional temperature term is known as the film cooling effectiveness (η), and is defined as:

$$\eta = \frac{T_f - T_m}{T_c - T_m} \tag{4}$$

The term blowing ratio (BR) is used to study the effect of the amount of coolant flow to mainstream flow. It is defined as the ratio of the mass flux of the coolant to the mass flux of the mainstream:

$$BR = \frac{\rho_c u_c}{\rho_m u_m} \tag{5}$$

In the practical application, turbine designers are concerned with the reduction of heat load to the film protected surface. The heat load can be simulated by combining the film cooling effectiveness (η) and local heat transfer coefficient ratio (h/h_o), therefore the local ratio (q/q_o) can be introduced to present the reduction in heat flux at the test surface with the presence of coolant air. A net heat flux ratio is used to measure the combined effect of film effectiveness and heat transfer coefficient. The following relation between (η) and (q/q_o) as given by Ekkad and Zapata [18] may be used to estimate (q/q_o):

$$\frac{q}{q_o} = \frac{h}{h_o}\left(1 - \frac{\eta}{\phi}\right) \tag{6}$$

The IR images for models test surface at each test are captured and stored by the memory of the thermal camera. These images are transferred to PC. The IR images are converted to corresponding temperature digital values and then saved as data in Excel sheet. MATLAB programs Software are prepared by using a semi-infinite solid assumption to introduce the film cooling effectiveness, heat transfer coefficient ratio, and heat flux ratio.

4- Results and discussion

The verification of the current experimental approach, the test results of the baseline case (model 1) is made by comparison with the experimental results of the similar case study of baseline case of Yuen and Botas [19]. Sample of results at BR= 1 of adiabatic spanwise averaged film cooling effectiveness distribution along the X/D together with that of Yuen [19] experimental results are presented in **Fig.(6)**. The results show approximately similar levels of (η) with slightly different in local values. It is fair to say

that the results obtained from the present experiments are in good agreement with experimental results of Yuen and Botas [19].

Experimental results of the present investigation are in the thermal aspect in the form of distribution and contour plots of various variables including the film cooling effectiveness, heat

transfer coefficient ratio, and heat flux ratio. The ramped-holes models geometry are design from holes inclined at $\theta = 35^{o}$, the hole spacing between adjacent holes was 3.5D, in both ramped-holes models, the configurations are taken as ramps (length = 2.5D and γ=16.7°) located at a distance (β=0) from the hole edge.

Fig.7 shows the comparison of spanwise averaged film cooling effectiveness distribution along the X/D. The present average value covers one pitch distance of -1.75< Z/D <1.75. Both ramped-holes cases (models 2 and 3) show rapid decaying particularly with increasing downstream distance from the hole. For blowing ratios of 0.5 & 1 the ramped-hole case provided better cooling effectiveness than (model 1). At BR=1.5 double ramped-holes provide highest and significant improvement in the spanwise averaged film cooling effectiveness. In general better performance at moderate and high blowing ratios (BR = 1.0 and 1.5) is contributed by the existing of double ramps. The double ramps contribute to lesser penetration of coolant jet into mainstream allowing the coolant air to remain close to the wall compared with the two other cases; this is confirmed by the film cooling effectiveness contours presented in Fig.8.

The overall area averaged film cooling effectiveness ($\bar{\bar{\eta}}$) for single ramped-holes (model 2) is enhanced by (40.2%, 175.8%, and 234.9%) at (BR= 0.5, 1.0, and 1.5) respectively. All enhancements are calculated with reference to the conventional single cylindrical holes row (model 1). Results of double ramped-holes case (model 3) show that the overall area averaged film cooling effectiveness is enhanced greatly by (45.3%, 185.8%, and 369%) at (BR= 0.5, 1.0, and 1.5) respectively. In general, the results clearly show the benefits of adding double ramps to the conventional single cylindrical holes row, in which there is almost a 369% increase in overall area averaged film cooling effectiveness at BR =1.5.

The verification of the current calculation method of spanwise averaged heat transfer coefficient ratio ($\bar{h}/h_o$) is made by comparison with the experimental results of Lu et al. [20] for the baseline case (model 1). Sample of comparison results of ($\bar{h}/h_o$) at BR=1 along the X/D distance are presented in **Fig.9**, both results are in good agreement.

Fig.10 presents detailed spanwise averaged heat transfer coefficient ratio ($\bar{h}/h_o$) at BR=1. The heat transfer coefficient ratio for ramps cases is increased compared to the baseline case. Such increase are due to the interaction between the coolant jet and the mainstream flow, this interaction produced high turbulence region. Several studies have shown that jet injection produces increased turbulence level inside the boundary layers due to the shear layer mixing and this is the main reason that (h) downstream of hole show higher values

according to Nasir et al. [21]. At present test at the downstream region (X/D>10) the heat transfer coefficients have higher values and remain in the same level up to the end of the test surface. It is clear in the ramped-holes case, the heat transfer coefficient increased over that of (models 1).

Heat flux ratio indicates the reduction in heat flux on the test surface from the film injection. As indicated by Akkad and Zapata [18], if the value of the net heat flux ratio is less than 1.0, then the introduction of film cooling has beneficial effect. If the value is greater than 1.0, it can be said that the film cooling did not serve its purpose of cooling.

Fig.11 represents the effect of (BRs) on overall area-averaged heat flux ratio ($\bar{\bar{q}}/q_o$). All models show good results of ($\bar{\bar{q}}/q_o$) except for model 3 at blowing ratio of 1.5 the values of ($\bar{\bar{q}}/q_o$) is exceed unity.

5- Conclusion

1. A detailed study on two recent ramped-holes configurations enhanced the film cooling effectiveness and kept the heat flux ratios in rang of accepted values.
2. The film cooling performance was found to be enhanced greatly by introducing single and double ramped holes compared to baseline (conventional single jet holes row).
3. The ramped-holes increase film effectiveness over that of the baseline by (234.9%) for single ramped-holes and by (369%) for double ramped-holes at BR=1.5.
4. The heat transfer coefficient ratio increased as compared to the baseline case, this is due to the interaction between the jet and the main stream which produces a region of high turbulence.

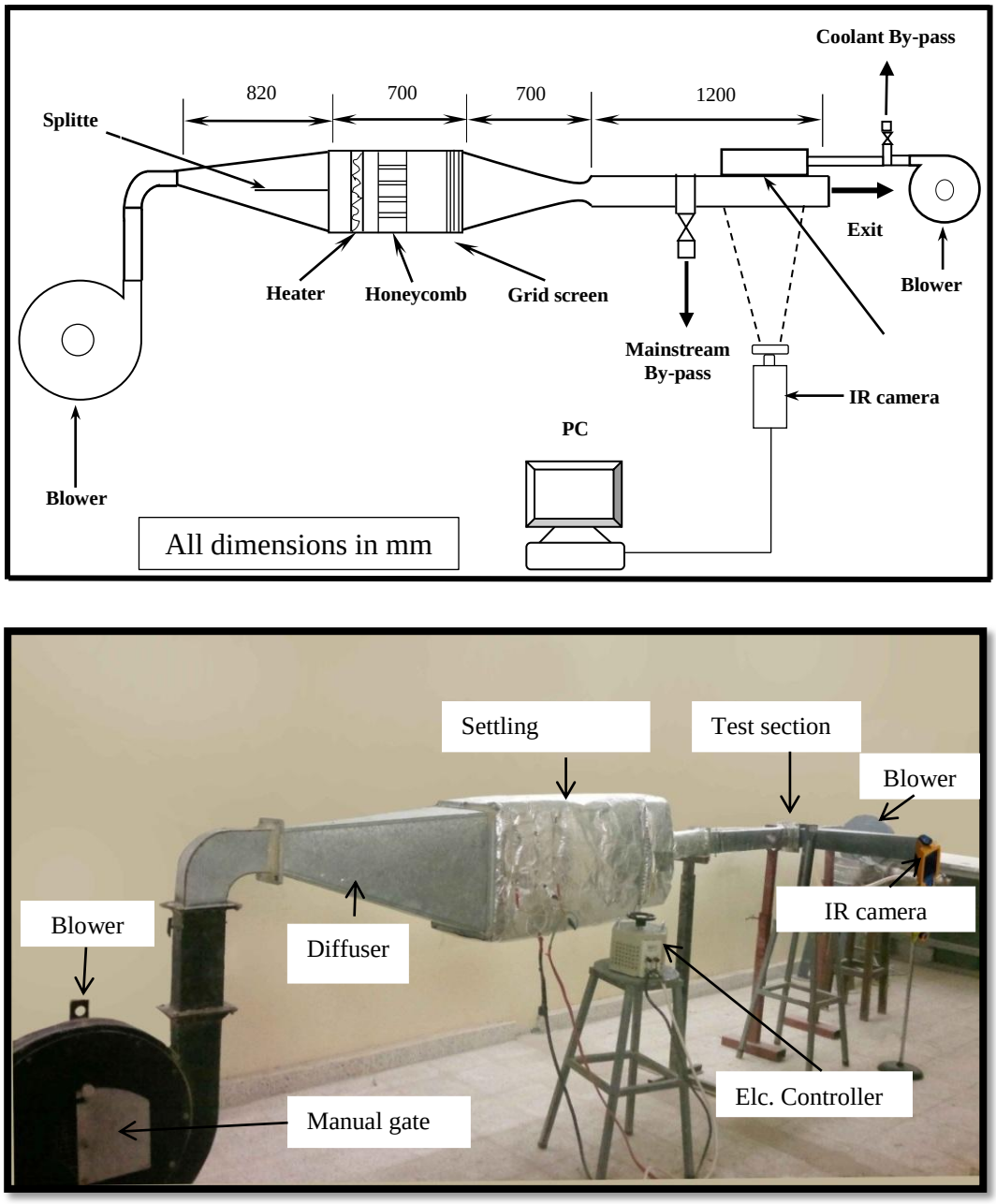

Figure (1) Photography and schematic of the experimental test rig

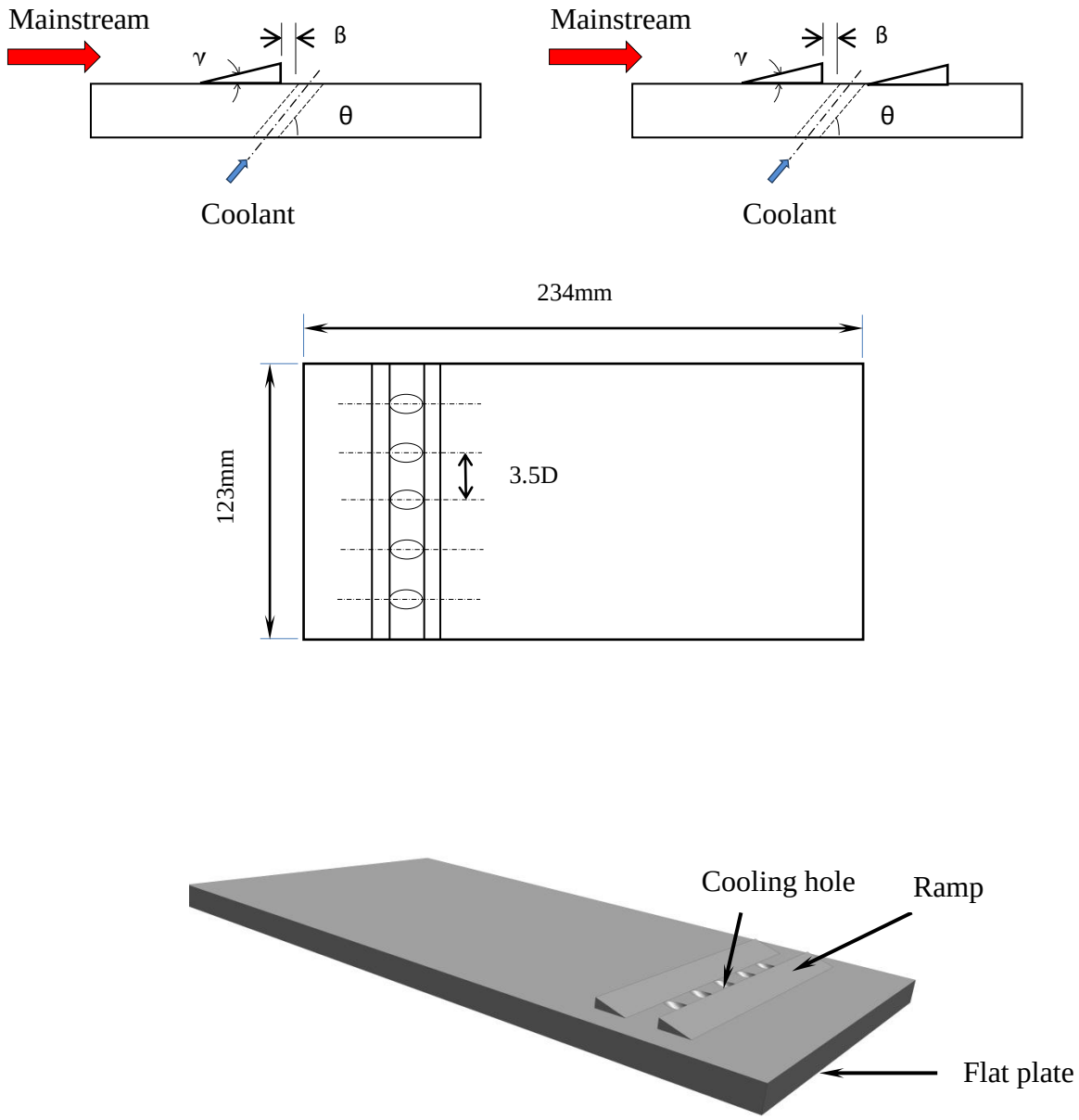

Figure (2) Schematic of ramped-holes configurations (side & top views), and Solid model for double-ramped film hole configuration

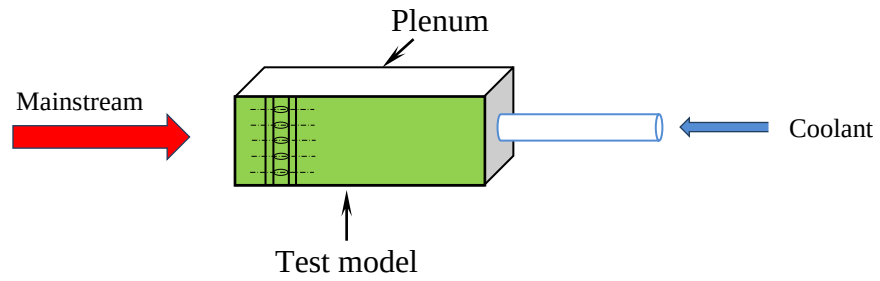

Figure (3) Schematic diagram of test section

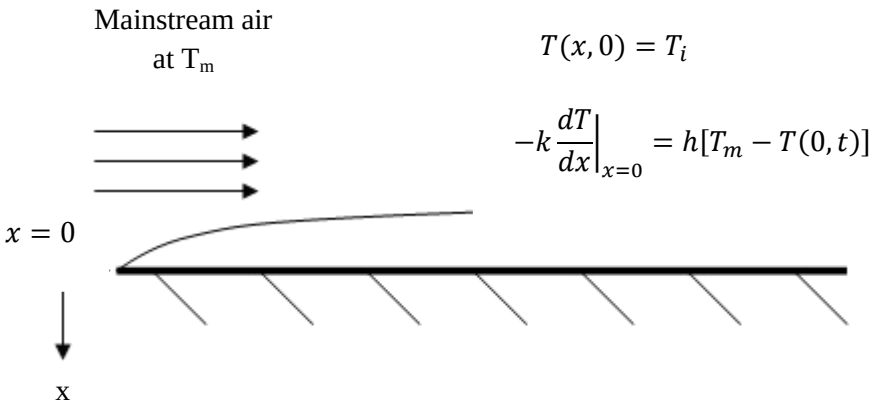

Figure (4) Flow over a flat plate

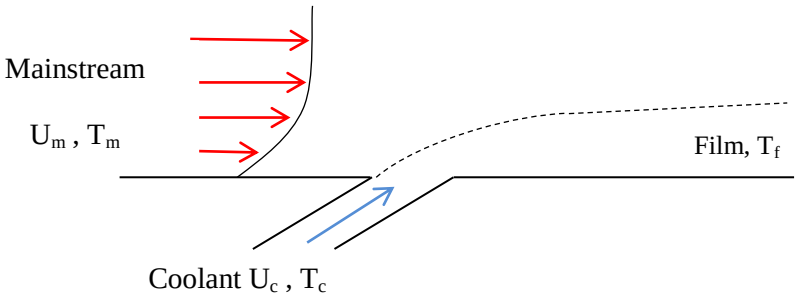

Figure (5) Film cooling over a flat plate

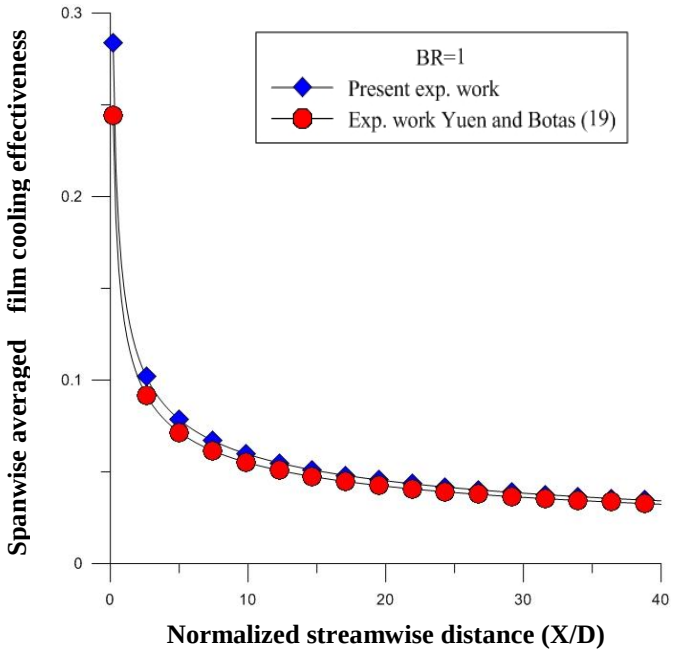

Figure (6) Verification of the present study with the Yuen [19] experimental results

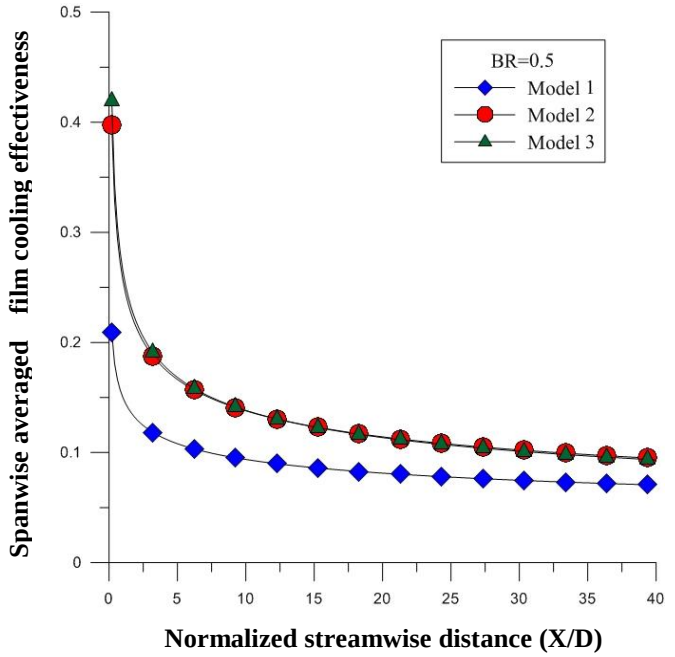

(A)

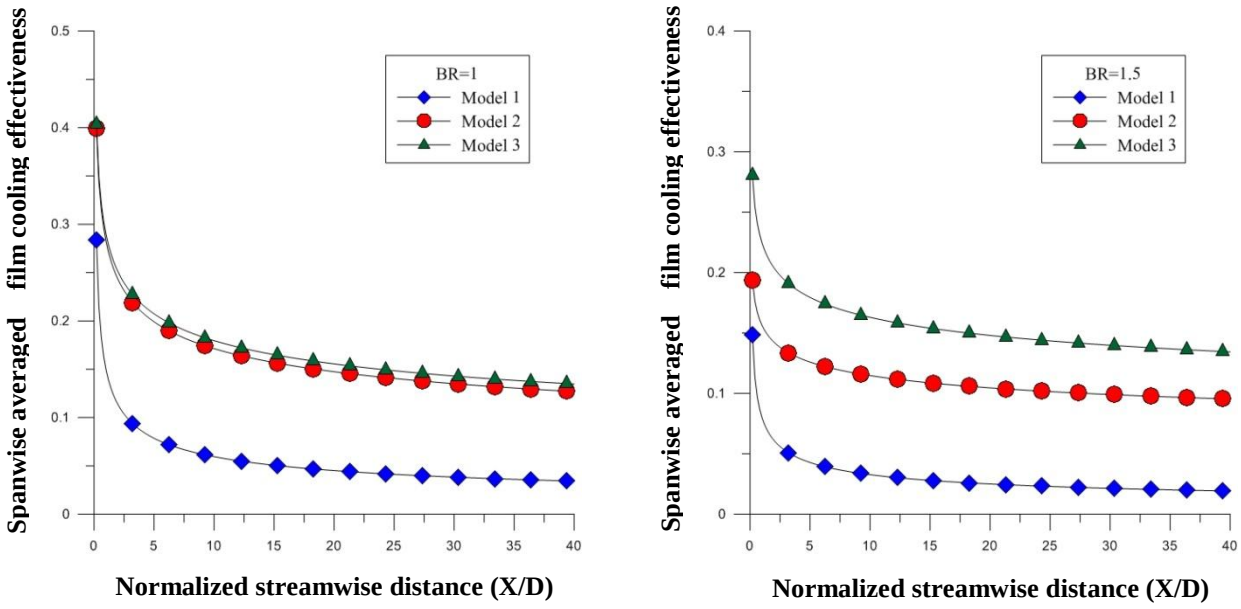

(B) **(C)**

Figure (7) Experimental comparison of ($\bar{\eta}$) versus (X/D) for different models at different BRs.

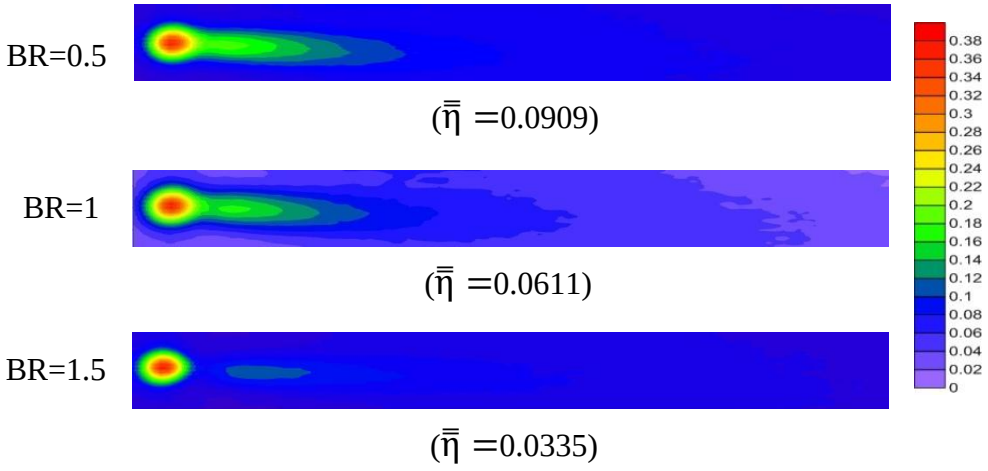

Model 1

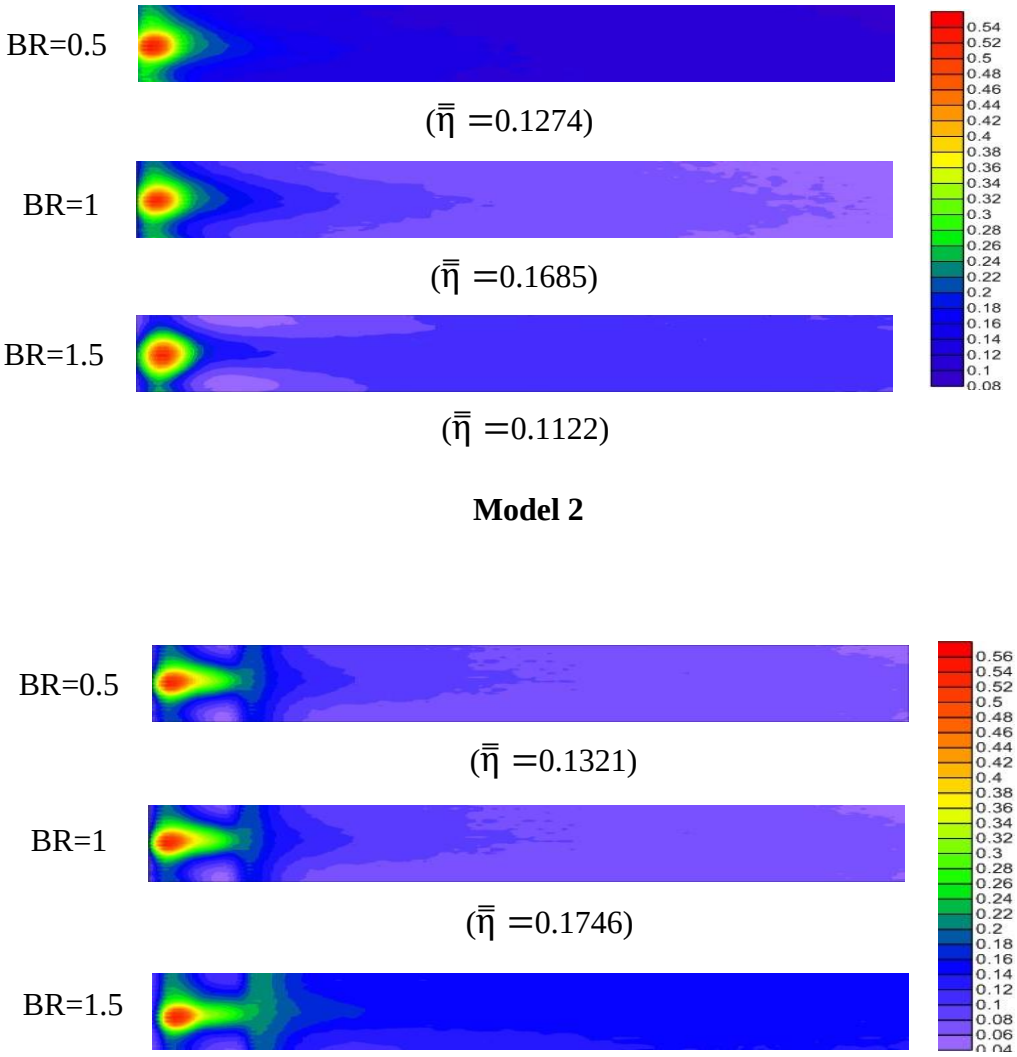

Figure (8) Experimental comparison of film effectiveness contours with ($\bar{\bar{\eta}}$) for different models at different BRs

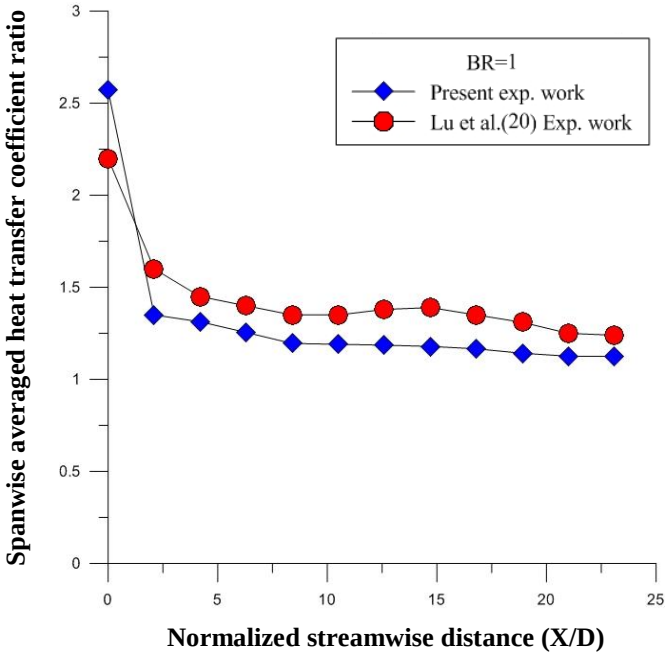

Figure (9) Verification of experimental results of heat transfer coefficient ratio ($\overline{h}/h_o$) of the present study with the experimental results of Lu et al. [20]

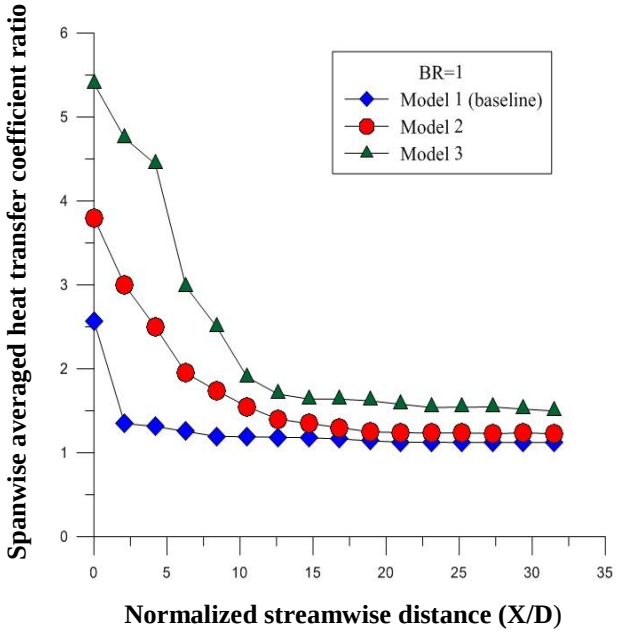

Figure (10) Effect of ramped cylindrical hole on spanwise averaged heat transfer coefficient ratio ($\overline{h}/h_o$) distributions

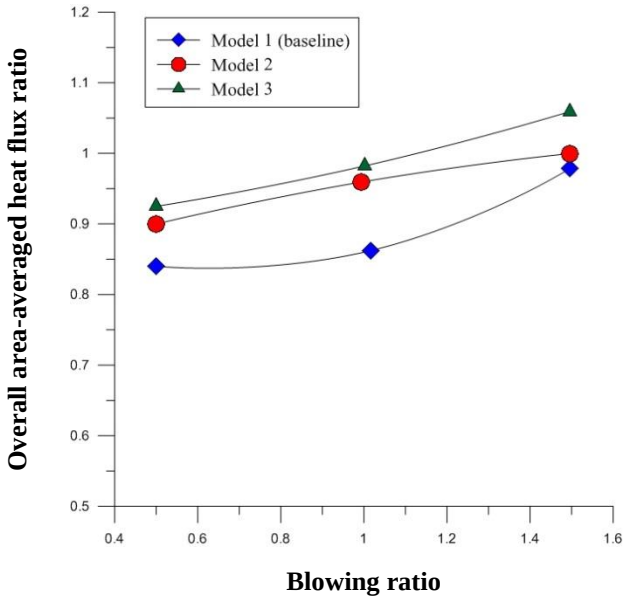

Figure (11) Effect of blowing ratio on overall area-averaged heat flux ratio ($\overline{\overline{q}}/q_o$) for all models

References

[1] W. W. Bathie, "Fundamentals of gas turbines", Second edition, John Wiley &Sons, Inc (1996).

[2] J. C. Han, H. Du, S.V. Ekkad "Gas turbine heat transfer and cooling technology", Taylor & Francis Group (2001).

[3] B.A. Haven, Yamagata, D.K., Kurosaka, M., Yamawaki, S., Maya, T., 1997, "Anti-kidney Pair of Vortices in Shaped Holes and their Influence on Film Cooling Effectiveness", ASME Paper 97-GT-45.

[4] D. G. Hyams, K. T. McGovern, J. H, Leylek, "Effects of geometry on slot-jet film cooling performance", ASME Paper No. 96-GT-187 (1997).

[5], R. S. Bunker, "A review of shaped hole turbine cooling technology", ASME J. Heat Transfer, 127 (2005) 441–453.

[6] B. A. Haven, M. Kurosaka, "Improved jet coverage through vortex cancellation", AIAA J., 34(11) (1996) 2443–2444.

[7] K. B. M. Q. Zaman, J. K. Foss,"The effects of vortex generators on a jet in a cross-flow", Phys. Fluids, 9(1), (1997) 106–114.

[8] K. B. M. Q. Zaman, " Reduction of a get penetration in a cross-flow by using tabs", AIAA Paper No. 98–3276 (1998).

[9] S. V. Ekkad, H. Nasir, S Acharya," Flat surface film cooling from cylindrical holes with discrete tabs", J. Thermophys. Heat Transfer 17(3) (2003) 304–312.
[10], T. I.-P. Shih, Y.-L. Lin, M. K. Chyu, S. Gogineni, "Computations film cooling from holes with struts", ASME paper No. 99-GT-282 (1999).
[11], R. S. Bunker, "Film cooling effectiveness due to discrete holes within transverse surface slots", Proceedings IGTI Turbo Expo, Amsterdam, the Netherlands, ASME Paper No. GT-2002–30178 (2002).
[12] M. S. Altorairi, "Film cooling from cylindrical holes in transverse slots", MSc. thesis, Louisiana State University (2003), Baton Rouge, LA, USA.
[13] R. M. Kelso, T. T. Lim, A. E. Perry, "An experimental study of round jets in cross-flow", Journal of Fluid Mech. Vol.306(1996) 111–144.
[14] Na. Sangkwon, T. I-P. Shih. "Increasing adiabatic film-cooling effectiveness by using an upstream ramp", Journal of Heat Transfer Vol.129 (2007) 464-470.
[15] S. P. Chen, M. K. Chyu, T. I.-P. Shih," Effects of upstream ramp on the performance of film cooling", Int. J. Thermal Sciences Vol. 50, Issue 6 (June 2011) 1085–1094.
[16] F.P. Incropera, D. Dewitt, "Fundamentals of heat transfer", Wiley & Sons, New York, NY . (2006),.
[17] S. V Ekkad, Ou, S. and Rivir, R. V., 2004, "A Transient Infrared Thermography Method for Simultaneous Film Cooling Effectiveness and Heat Transfer Coefficient Measurements from a Single test" , GT2004-54236, Proceedings of ASME Turbo Expo 2004, Vienna, Austria.
[18] S.V. Ekkad, D. Zapata, "Heat transfer coefficients over a flat surface with air and CO2 injection through compound angle holes using a transient liquid crystal image method", ASME J. Turbomachinery 119 No. 3 (1997) 580-586.
[19] Yuen, C. H.N. and Botas, R.F.M., 2003, "Film cooling characteristics of a single round hole at various stream wise angles in a cross flow: Part I effectiveness", International Journal of Heat and Mass Transfer, Vol. 46, PP. 221-235.
[20] Lu, Y., Dhungel, A., Ekkad, S.V., and Bunker, R.S., 2007, "Effect of Trench Width and Depth on Film Cooling from Cylindrical Holes Embedded in Trenches", ASME Paper GT 2007-27388.
[21] H. Nasir, S. Acharya, S. Ekkad, "Improved film cooling from cylindrical angled holes with triangular tabs: effect of tab orientations", Int. J. Heat and Fluid Flow 24 (2003) 657-668.

دراسة عملية لاداء غشاء التبريد لثقوب اسطوانية مزودة بمنحدرات

د.عاصم حميد الدراجي *د.قتيبة جميل الخشالي* *فلاح فاخر الجابري*

قسم هندسة المكائن والمعدات / الجامعة التكنولوجية

الخلاصة

تحتاج اجزاء التوربينات الغازية الحديثة لتقنية تبريد جيدة لمواجهة درجات حرارة التشغيل العالية ، تقنية غشاء التبريد واحدة من اكفأ الطرق المستخدمة لحماية اجزاء التوربين الغازي من الغازات الحارة. يؤثر ترتيب وشكل الثقوب على أداء غشاء التبريد . تم عمليا" دراسة تأثير وضع منحدرات مع الثقوب الأسطوانية على أداء غشاء التبريد، اختبرت ثلاث نماذج مختلفة، احد هذه النماذج هو صف من الثقوب الاسطوانية الذي يعمل كنموذج اساسي لغرض المقارنة. يتكون النموذج الثاني من صف واحد من الثقوب مزود بمنحدر امامي واحد ، ويتكون النموذج الثالث من صف واحد من الثقوب مزود بزوج من المنحدرات . قطرالثقب الاسطواني هو 4 mm، نسبة طول الثقب الى قطره هي 3.5 و المسافة بين كل اثنين من الثقوب المتجاورة 3.5D، زاوية الحقن (θ) هي35^{o} لجميع النماذج . تم تحديد فعالية غشاء التبريد ومعامل انتقال الحرارة على عينة الاختبار بأجراء تجارب عملية بأستخدام تقنية الصورة الحرارية تحت الحمراء (IR thermography technique) بآلية الفحص الحراري الانتقالي الواحد. أجريت التجارب لعدد رينولدز للجريان الرئيسي مقداره 76600 ولثلاث نسب نفخ (0.5 و1.0 و1.5). اظهرت النتائج العملية تحسنا" كبيرا" في فعالية غشاء التبريد عند استخدام المنحدرات مع ثقوب النفث بسبب تحسن الانتشار العرضي لغشاء التبريد واظهر نموذج الثقوب مزدوجة المنحدرات تحسنا" واعدا" في توزيع المعدل العرضي لفعالية غشاء التبريد خصوصا" لنسب النفخ المتوسطة والعالية.

الخلاصه

التبريد الغشائي (Film cooling) هو احد الطرق المستخدمة لحماية الأسطح المعرضة لدرجات حرارة عالية ، كتلك التي تكون في التوربينات الغازية . التبريد الغشائي هوعبارة عن نفث لهواءالتبريد ذي درجات الحرارة الأقل من درجة حرارة الجريان الحار الرئيسي ليكون مائع التبريد غشاءا" سطحيا" يحمي السطح من التعرض لدرجات الحرارة العالية . تتم عملية النفث من خلال الثقوب التي تكون لها أشكال هندسية مختلفة ؛ كالأشكال البسيطة (مثل الثقوب الاسطوانية) ، أو ثقوب باشكال هندسية اخرى (مثل الثقوب المخروطية) .تم دراسة تأثير وضع منحدرات مع الثقوب الأسطوانية والمخروطية على أداء تقنية غشاء التبريد عدديا" و تجريبا" ، وقد تم استخدام برانامج (FLUENT) للتنبؤ بسلوك جريان التداخل حول منطقة ثقوب النفث ، مع اجراء محاكاة تحاكي التجارب العملية حيث تم اختبار ستة نماذج مختلفة اختيرت بالاعتماد على نتائج التحليل العددي ، اول هذه النماذج هو صف من الثقوب الاسطوانية يعمل كنموذج اساسي للمقارنة . وكان قطرالثقب الاسطواني هو 4 mm ونسبة طول الثقب الى قطره هي 3.5 والمسافة بين كل ثقبين متجاورين هو 4D ، وتتألف نماذج الثقب المخروطي من صف من الثقوب قطر كل منها 4 mm في جهة دخول هواء التبريد وينفرج باتجاه المخرج بزاوية مقدارها 6^o ، وكانت زاوية حقن هواء التبريد باتجاه اسفل انسياب جريان الهواء الحار (θ) هي 35^o لجميع النماذج . وتم تحديد فعالية التبريد الغشائي ومعامل انتقال الحرارة ونسبة الفيض الحراري على عينة الاختبار بأستخدام تقنية الصورة الحرارية تحت الحمراء (IR thermography technique) بآلية الفحص الحراري الانتقالي الواحد حيث كان مقدارعدد رينولدز هو 5100 محسوبا" على اساس سرعة الجريان الرئيسي وقطر ثقب التبريد ، وبأستعمال ثلاث نسب من النفخ (0.5 و1.0 و1.5) . تم مقارنة النتائج العملية للنموذج الاساسي مع نتائج عملية لبحوث سابقة بنفس الظروف عند نسب نفخ 0.5 و 1 وكان هناك تطابق جيد ، وكذلك تم مقارنة النتائج النظرية مع النتائج العملية للبحث الحالي ، وقد تبين بان النتائج النظرية لفعالية التبريد تعطي سلوك مشابه تقريبا مع اختلاف طفيف عن النتائج العملية.

اظهرت النتائج العملية تحسنا" كبيرا" في فعالية التبريد الغشائي عند استخدام المنحدرات مع ثقوب النفث بسبب تحسن الانتشار العرضي لغشاء التبريد واظهر نموذج الثقوب بمنحدرين (امامي وخلفي) تحسنا" واعدا" للمعدل العرضي لفعالية التبريد الغشائي على امتداد

محور اسفل الانسياب سيما لنسب النفث المتوسطة والعالية ، كما زادت بمعدلات مقبولة نسب معامل انتقال الحرارة ونسب الفيض الحراري عند استخدام المنحدرات مع جميع انواع الثقوب .

بلغت نسب التحسين في المعدل الكلي لفعالية التبريد الغشائي للثقوب الاسطوانية المزودة بمنحدر امامي واحد (40.2% و 175.8% و 234.9%) وبلغت نسب التحسين في المعدل الكلي لفعالية التبريد الغشائي للثقوب الاسطوانية المزودة بمنحدرين (امامي وخلفي) (45.3% و 185.8% و 369%) عند المقارنة بالنموذج الاساسي عند نسب نفخ (0.5 و 1 و 1.5) على التوالي ، وكانت نسبة التحسين في المعدل الكلي لفعالية التبريد الغشائي للثقوب المخروطية المزودة بمنحدر امامي واحد (134% و 292.6% و 554.6%) وللثقوب المخروطية المزودة بمنحدرين (امامي وخلفي) (130.3% و 343.7% و 679.4%) عند المقارنة بالنموذج الاساسي عند نسب نفخ (0.5 و1.0 و1.5) على التوالي ، لذا يمكن القول ان استخدام الثقوب المخروطية المزودة بمنحدرات يمثل احد الحلول في تقنية التبريد الغشائي لا سيما في غرف الاحتراق .

جمهورية العراق
وزارة التعليم العالي والبحث العلمي
الجامعة التكنولوجية
قسم هندسة المكائن والمعدات

تحسين أداء التبريد الغشائي لثقوب النفث باستخدام المنحدرات

أطروحة مقدمة إلى
قسم هندسة المكائن والمعدات
في الجامعة التكنولوجية
كجزء من متطلبات نيل درجة الدكتوراه في الهندسة الميكانيكية

من قبل

فلاح فاخر حاتم الجابري
(بكلوريوس 1981، ماجستير 1987)

إشراف

الاستاذ الدكتور المهندس
عاصم حميد يوسف الدراجي

الاستاذ المساعد الدكتور المهندس
قتيبة جميل مهدي الخشالي

ربيع الأول 1435 كانون الثاني 2014
بغداد - العراق